NASA TECHNICAL MEMORANDUM NASA TM 75732

SOLUTION OF A FEW NONLINEAR PROBLEMS IN AERODYNAMICS BY THE FINITE ELEMENTS AND FUNCTIONAL LEAST SQUARES METHODS

Jacques Periaux

Translation of "Résolution de quelques problèmes non linéaires en aerodynamique par des méthodes d'éléments finis et de moindres carrés fonctionnels," Doctoral Dissertation, University of Paris, June 19, 1979, 280 pages

NATIONAL AERONAUTICS AND SPACE ADMINISTRATION
WASHINGTON, D.C. 20546 DECEMBER 1979

ACKNOWLEDGMENTS

This thesis is the result of two years of applied research under the direction of Professor R. GLOWINSKI and is the fruit of a research collaboration between the LABORIA/IRIA and the AMD/BA industries. 1*

I should like to thank Professor J.L. LIONS whose instruction made it possible to undertake this research.

I am deeply indebted to Professor R. GLOWINSKI who directed and encouraged this research, and who gave me the honor of presiding over the examining committee.

I should like to acknowledge my deepest gratitude to MR. O. PIRONNEAU, who together with MR. GLOWINSKI, originated the optimal control methods presented, and who lavished me with advice and encouragement throughout this research.

I thank Professor P.A. RAVIART for giving me the honor of being a member of the examining committee.

Special thanks to Mr. P. BOHN, director of the Advanced Studies Division (Division des Etudes Avancées), and to Mr. P. PERRIER, Chief of the Department of Aerodynamic Theory (Département d'Aérodynamique Théorique), and to the AMD/BA for participating on the examining commitee and for their knowledge of numerical methods and of powerful computer centers which was shared with me.

I should like to acknowledge other debts: the discussions with Mr. PERRIER and his helpful suggestions in the field of Fluid Mechanics, and the discussions with Mrs. M.O. BRISTEAU du LABORIA and Mr Mr. B. MANTEL and Mr. G. POIRIER from AMD/BA. I should also like to thank them for their friendly collaboration throughout this study.

My thanks go also to Mrs. F. WEBER and Mr. HUBERT for the careful typing and drawings of this document.

Finally, this thesis is dedicated to my wife and to the memory of her father.

---

* Numbers in the margin indicate pagination in the foreign text.

SUMMARY /6

The objective of this study is to provide the numerical simulation of the transsonic flows of idealized fluids and of incompressible viscous fluids, by the non linear least squares methods of R. GLOWINSKI and O. PIRONNEAU. The complexity of the geometries studied in industrial aerodynamics explains the preference given to the finite elements for the approximation of the equations.

Chapters 1, 2, 3, 4 describe the non linear equations, the boundary conditions and the various constraints controlling the two types of flow. The standard iterative methods for solving a quasi elliptical non linear equation with partial derivatives (E.D.P.) are briefly reviewed in Chapter 5 with emphasis placed on two examples : the fixed point method applied to the Gelder functional in the case of compressible subsonic flows and the Newton method used in the technique of decomposition of the lifting potential.

Chapter 6 presents the new abstract least squares method. It consists of substituting the non linear equation by a problem of minimization in a H^{-1} type Sobolev functional space, which is itself equivalent to an optimal control problem and solved by a conjugate gradient algorithm with metric H^1. The application of this methodology to transsonic equations is presented in Chapter 7. We show how to include within the optimal control formulation two constraints of aerodynamics: the condition of entropy, on the one hand, treated either by penalization or by artificial viscosity, and the Joukowski condition, on the other hand, taken into account by a fixed point method on circulation.

The Navier-Stokes equations are reduced to a problem of minimization in H^{-1} in the same manner in Chapter 8. Accordingly, we show that the state systems of the mixed optimal control problem are generalized Stokes problems in steady and unsteady cases, after quantification in time with the use of implicit Crank-Nicholson (for example) type schemes. To solve them, a mixed formulation proposed by GLOWINSKI-PIRONNEAU and based on certain decomposition properties of the biharmonic operator, is used. The Stokes algorithm is substitued by a sequence of Dirichlet problems coupled with an integral equation (E) conditioned on the pressure trace, defined on the boundary of the domain occupied by the fluid. /7

Chapters 9 and 10 are devoted to the approximation of a transsonic and Navier-Stokes optimal control formulation by P_k Lagrange conform finite elements, with degree k=1 or 2. The numerical implementation of the conjugate gradient algorithms is developed and presented in the form of flow charts. The numerical implementation of the Stokes algorithm (E_h) is described and the choice of a direct (Choleski) or iterative (preconditioned conjugate gradient) method for solving it is discussed.

The large amounts of computations, due to complex tridimensional configurations (nacelle, vehicle, air-inlet, airplane),

stored in the main core of the computer, require an incomplete Choleski factorization of the discrete Dirichlet matrices shown on the inside of the control loop. The use of auxiliary operators $\tilde{L}\tilde{L}^t$ in the solution of an optimal control problem is presented in Chapter 11 through comparisons of research results of J.A. MEIJERINK-M.A. VAN DER VORST and O. AXELSSON.

The numerical experiments are described in Chapter 12. The transsonic calculations obtained from the finite elements-optimal control codes are compared with those obtained from the finite differences codes of A. JAMESON on a NACA 0012 airfoil and a Korn airfoil.

More complex transsonic configurations of industrial aerodynamics such as multi-bodies or air inlets are analyzed.

The feasibility of optimal control conjugate gradient algorithms is verified on bi and tridimensional Navier-Stokes calculations, requiring considerable data processing resources (memory and CPU). Separated flows around/in an air inlet and around an swept-back wing with high incidence, are simulated numerically by following at various time cycles the evolution of the field of velocities, the field of pressures, the streamlines and the vorticity.

Finally, the last paragraph of Chapter 12 is devoted to the data processing efficiency of the auxiliary operators. It shows, through examples taken from the two flow families, how it is possible, by using preconditioned optimal control algorithms, to calculate entirely in the main core of the computer, with small percentages of Dirichlet matrices $\tilde{A}_{d/100}$ $(5 \leq d < 20)$ without reducing the convergence velocity of the algorithm.

TABLE OF CONTENTS

4

SOLUTION OF A FEW NON LINEAR PROBLEMS IN AERODYNAMICS BY THE FINITE ELEMENTS AND FUNCTIONAL LEAST SQUARES METHODS

Jacques Periaux
Pierre and Marie Curie University

0. INTRODUCTION

0.1. APPLICATIONS OF NON LINEAR AERODYNAMICS TO THE AERONAUTICS INDUSTRY

The calculation of pressures in aeronautics plays an essential role in the optimization of aerodynamic shapes. The appearance of more and more powerful computers, over the past decade, both with respect to calculation speed and to memory capacity, has made it possible for the aviator to simulate numerically flows which approximate more and more the flight conditions. To accomplish this it was necessary to define theoretically and numerically two families of non linear equations : irrotational compressible idealized fluids, on the one hand, in order to study the transonic domain of the airplane, and incompressible viscuous fluids, on the other hand, modeled by the Navier-Stokes equations to provide a robust tool required for the study of separated laminar flows in a first phase, then of turbulent flows in a second phase.

The domaines occupied by the fluid are bi and tridimensional. They belong either to <u>external</u> aerodynamics when relating to airfoils (P) or to wings (V), or to <u>internal</u> aerodynamics when relating to pipes (T), cavities (CA) or conduits (C). Finally, air inlets belong to a third category : <u>mixed</u> aerodynamics. The common denominator of these domaines is the <u>complexity</u> of the boundaries (one region surrounding a multibody, or one 3-D air inlet composed of extremely complicated geometries, making it difficult to reduce it by conform conversion to a standard rectangular (or cubical) domain !). Furthermore, the final selection of the physical space as calculation domain was subjected to a numerical method by taking into account the boundary conditions with fine accuracy : <u>THE FINITE ELEMENTS</u>.

0.2. <u>Difficulties</u> with respect to industrial configurations /10

The numerical analysis of flows around industrial obstacles points up 3 types of difficulties :

1 - <u>geometrical</u> difficulties: the configurations studied are extremely complex and require a delicate collection of data (description of a 2-D multi-body, or a wing + fuselage + air inlet + empennage type airplane configuration).

2 - <u>theoretical</u> difficulties : the equations to be solved are non linear and their solutions may be composed of discontinuities. Furthermore, the following constraints must be satisfied simultaneously :

- constraint of aerodynamic reaction or Joukowski condition for perfect fluids,
- constraint of physical shock or condition of entropy for transonic perfect fluids,
- constraint of incompressiblity for viscuous fluids.

3 - <u>numerical</u> difficulties : the volume of tridimensional calculations (several thousands of unknowns) make it necessary to use algorithms which are both <u>rapid</u> for convergence and <u>robust</u> for stability.

Figure 1 summarizes the situation in industry and describes the solution selected.

1. - FEASIBLE MODELING OF AN INCOMPRESSIBLE IDEALIZED FLOW /12

1.1. 2-D Non Lifting Case

If Ω and Γ designate respectively the domain and boundary of the region occupied by the fluid, as the latter is incompressible and irrotational, it obeys the following equations and boundary conditions (1)

$$\begin{aligned} &\vec{\nabla}\cdot\vec{u} = 0 \; ; \; \vec{u} \text{ continuous} \\ &\vec{\nabla}\wedge\vec{u} = 0 \qquad\qquad (\Omega) \\ &\vec{u}\cdot\vec{n} = g \quad (\Gamma), \quad \Gamma = \Gamma_\infty \cup \Gamma_p \end{aligned} \tag{1}$$

where, in (1), $\vec{u}$ designates the fluid velocity and g the normal component of velocity on Γ; on Γ_∞ boundary sufficiently removed from the obstacle to ensure that the latter does not perturb the flow, $g = \vec{u}_\infty\cdot\vec{n}$ where $\vec{n}$ is the external standard of the domain, whereas on Γ_p wall of the obstacle (P) $g=0$ and $\vec{u}\cdot\vec{n} = 0$ means then that the fluid <u>slides</u> over the wall.

A - NON LINEAR GEOMETRIES/FINITE ELEMENTS   B - COMPLEX INDUSTRIAL CONFIGURATIONS
C - NON LINEAR EQUATIONS/ OPTIMAL CONTROL   D - VOLUME OF CALCULATIONS/PRECONDITIONED CONJUGATE GRADIENT

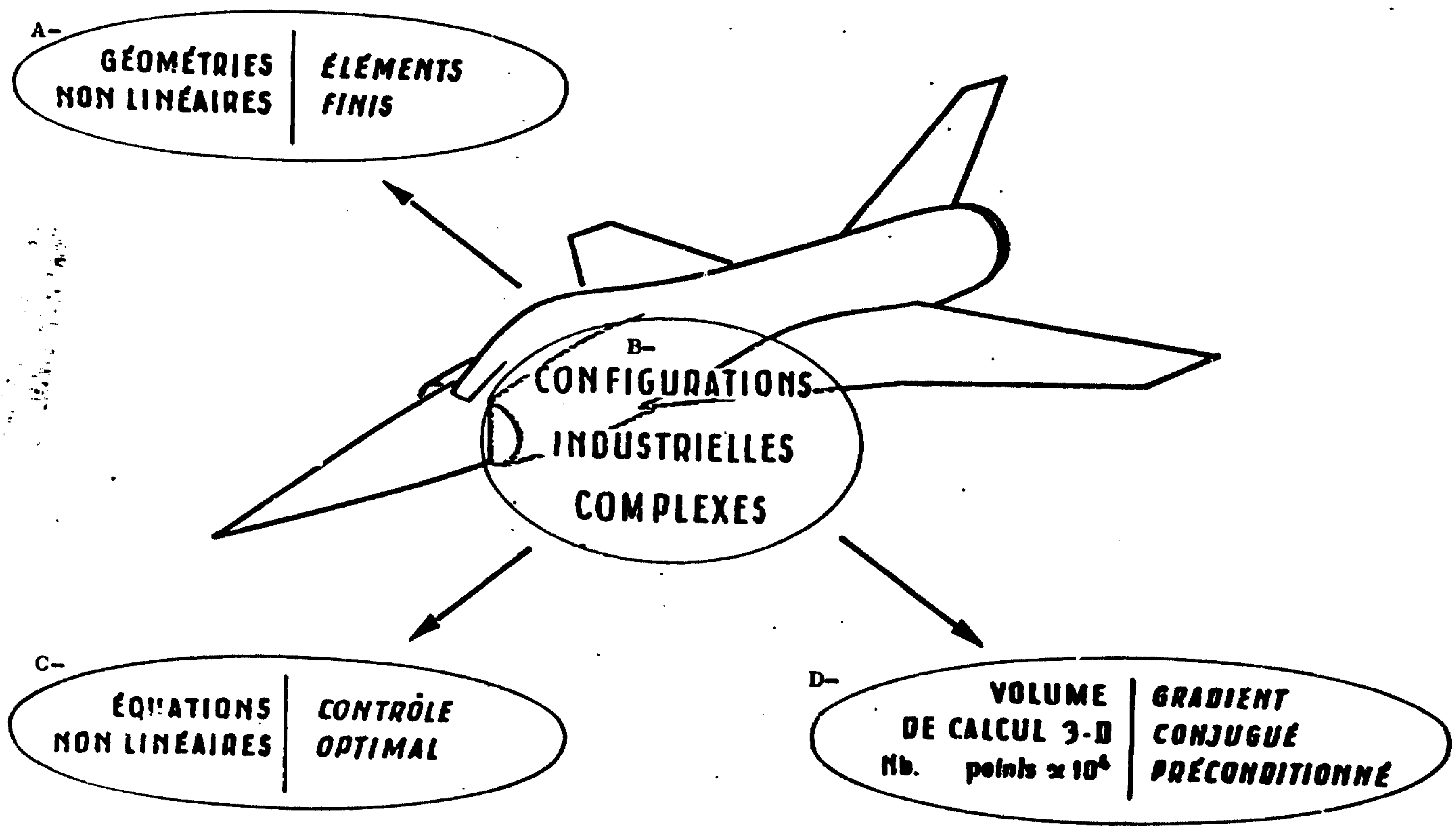

Figure 1

The irrotational condition is expressed in a standard manner by the existence of a <u>velocity potential</u> ϕ such that $\vec{u} = \vec{\nabla}\phi$.

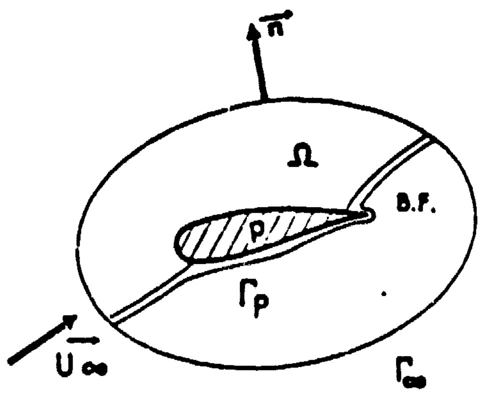

Figure 2

It is therefore possible to reformulate (1) as a problem with elliptical type linear boundaries (figure 3)

$$\Delta\phi = 0 \quad (\Omega) \quad ; \qquad (2)$$
$$\frac{\partial\phi}{\partial n} = g \quad (\Gamma)$$

ϕ <u>continuous</u>

$\vec{u}$ <u>continuous</u>

Note: As the boundary conditions are the Neumann type, it is practical to determine the potential at a defined point of the trailing edge

$$\phi = 0 \quad (BF)$$

13

1.2. Lifting Case 2-D

An obstacle brought to light and the boundary of which may not be differentiated (point of reflection) can lift.

The lift (C_z) is introduced artificially by the Joukowski condition $\vec{u}_{BF} = 0$ (refer to GERMAIN (1)). In this case, (1) should be added to an additional scalar equation at the trailing edge

$$J(\vec{u}) = 0 \quad (BF)$$

This constraint makes it possible for a circulation ℓ to be induced around the obstacle, depending on the velocity at infinity and the shape of the body.

A feasible modeling of the Joukowski condition imposes the equality of the pressures on both sides of the singular geometrical point (weakening of the condition $\vec{u}=0$ which is impossible to calculate numerically). By applying the law of Bernoulli

$p = f(|\vec{u}|^2) = 1 - \dfrac{|\vec{u}|^2}{|\vec{u}_\infty|^2}$ the condition of Joukowski is written

$$|\vec{u}^+|^2_{BF} = |\vec{u}^-|^2_{BF} \qquad (3)$$

If (3) is added to (2), then a cut should be made (C) originating at the trailing edge (BF) up to infinity Γ_∞ (Figure 3)

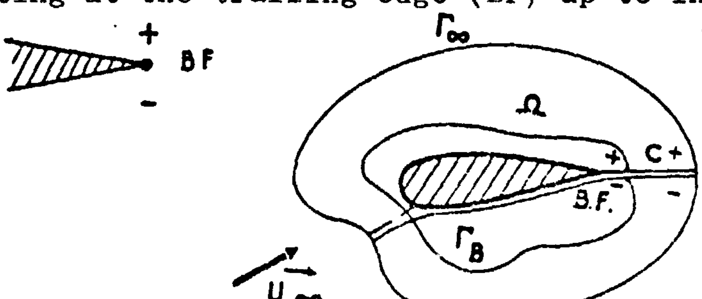

Important Note : On figure 2 the second stop-point is not located at the trailing edge : the fluid by-passes the obstacle, whereas in figure 3, the condition of Joukowski necessitates that the fluid does not by-pass the obstacle.

On the other hand, if by starting at a point $P^+ \in C^+$ the obstacle is by-passed and we return to point $P^- \in C^-$ which is geometrically mixed, then we have the relationship (4)

$$\phi(P^+) = \phi(P^-) + \ell \quad , \forall P \in (C) \qquad (4)$$

where ℓ designates the unkown circulation.

Taking (3) and (4) into account, the formulation of the lifting problem analogous to (2) is written

$$
\begin{array}{lllll}
(5.1) & \Delta\phi = 0 \quad (\Omega) \quad ; & \phi \ \text{discontinuous} & & \\
(5.2) & \phi^{+} = \phi^{-} + \ell \quad (C) & & & \\
(5.3) & |\vec{\nabla}\phi^{+}|^{2} = |\vec{\nabla}\phi^{-}|^{2} \quad (BF) & \vec{u} \ \underline{\text{continuous}} & & (5) \\
(5.4) & \dfrac{\partial\phi}{\partial n} = g \quad (\Gamma) \quad \Gamma = \Gamma_p \cup \Gamma_\infty & & & \\
(5.5) & \phi = 0 \quad (BF) & & &
\end{array}
$$

It may be noted that the non linearity of (5) is due to the Joukowski condition and that the solution of the problem (5) is the $\underline{(\phi,\ell)}$ couple where ϕ is a function and ℓ is scalar.

In the tridimensional lifting case, a discontinuous sheet (ND) should be introduced at the beginning of the trailing edge line, following the bisecting plane up to boundary Γ_∞ and generated by the variations of the circulation in enlargement. (Figure 4).

$$ND = \bigcup_{j=1}^{N} (ND)_j$$

$$LBF = \sum_{j=1}^{N} (BF)_j$$

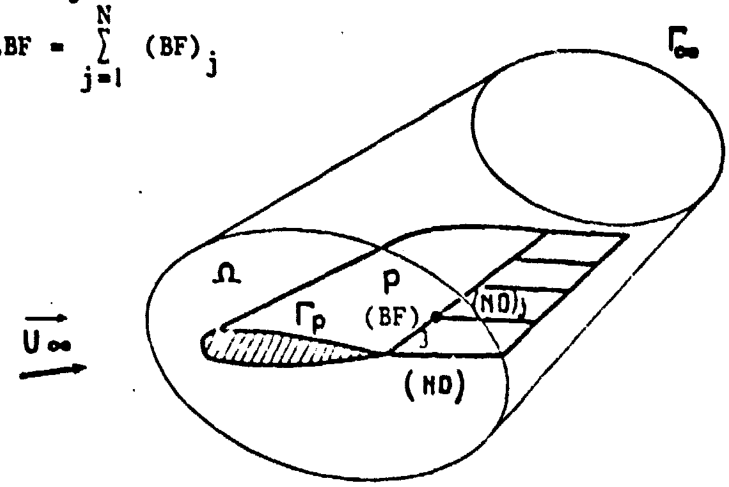

Figure 4

The coiling of this sheet for reasons of calculation time is left out and the formulation of the 3-D problem analogous to (5) is expressed :

$$\begin{aligned}
&\Delta\phi = 0 \qquad (\Omega)\ ; \qquad \phi \text{ discontinuous on (ND)}, \ |\vec{u}| \text{ continuous}\\
&\phi^+(P_j) = \phi^-(P_j) + \ell(y_j) \qquad \forall\, P_j \in (ND)_j\\
&|\vec{\nabla}\phi(Q_j^+)|^2 = |\vec{\nabla}\phi(Q_j^-)|^2 \qquad \forall\, Q_j \in (LBF)\\
&\frac{\partial\phi}{\partial n} = g \qquad (\Gamma)
\end{aligned} \tag{6}$$

It may be noted that the solution of problem (6) is the <u>couple</u> <u>(ϕ,ℓ)</u> where ϕ is a function and ℓ is a function of the enlargment. Finally, the formulation (5) is generalized in the case of a lifting flow around a multi-body (MC), by introducing K cuts originating at the trailing edges of the K-bodies up to infinity Γ_∞ as is shown on figure 5 (Example of a hyper lifting force (leading edge + primary + flap)).

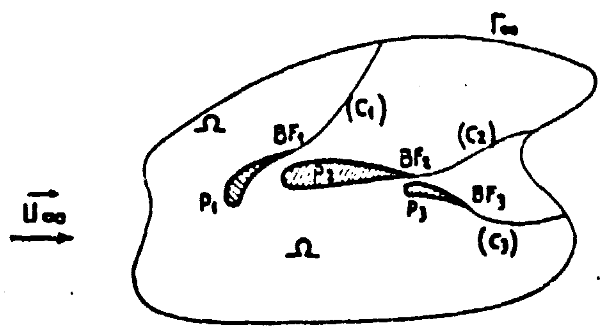

<u>Figure 5</u>

The problem at the boundaries to be solved is then:

Find ϕ & $\vec{\ell} = (\ell_1, \ell_2, \ell_3, \ldots)$ solution of

$$\begin{aligned}
&\Delta\phi = 0 \quad \Omega \quad ;\ \phi \text{ discontinuous } |\vec{u}| \text{ continuous}\\
&\phi(P^+) = \phi(P^-) + \ell_i \qquad \forall\, P \in C_i \quad i = 1,2,3,\ldots\\
&|\vec{\nabla}\phi(Q^+)|^2 = |\vec{\nabla}\phi(Q^-)|^2 \qquad \forall\, Q \in (BF)_i \quad i = 1,2,3,\ldots\\
&\frac{\partial\phi}{\partial n} = g \quad (\Gamma)
\end{aligned} \tag{5$_M$}$$

2. - FEASIBLE MODELING OF A SUBSONIC COMPRESSIBLE IDEALIZED FLUID /15

2.1. 2-D Non Lifting Case

As the flow is assumed to be irrotational, the compressibility model is the *isentropic* type (refer to LANDAU-LIPSCHITZ (2) and the flow is controlled by the equation and the boundary conditions (7)

$$
\left.
\begin{aligned}
&\vec{\nabla}\cdot\rho\vec{u} = 0 \quad ; \ \vec{u} \text{ continuous} \\
&\rho = \rho_o\left(1 - \frac{\gamma-1}{\gamma+1}\,\frac{|\vec{u}|^2}{C_*^2}\right)^{1/(\gamma-1)} && (\Omega) \\
&\vec{\nabla}\wedge\vec{u} = 0 \\
&\rho\vec{u}\cdot\vec{n} = g && (\Gamma)
\end{aligned}
\right\} \qquad (7)
$$

/16

where ρ designates the fluid density

γ the ratio of specific heats ($\gamma = 1.4$ in the atmosphere)

C_* the critical velocity

so that if we set

$$\rho_o = 1 \ ; \ k = \frac{\gamma-1}{\gamma+1}\,\frac{1}{C_*^2} \ ; \ \alpha = \frac{1}{\gamma-1}$$

then the law of compressibility is written

$$\rho = (1-k|\vec{u}|^2)^\alpha$$

If we introduce the velocity potential ϕ by using $\vec{\nabla}\wedge\vec{u} = 0$, it is possible to reformulate (7) as a quasi-elliptical type NON LINEAR boundary problem (8)

$$
\begin{aligned}
&(8.1) \quad \vec{\nabla}\cdot\rho\vec{\nabla}\phi = 0 \ ; \ \phi - * \qquad \vec{u} - * \qquad *\text{continuous} \\
&(8.2) \quad \rho = (1-k|\vec{\nabla}\phi|^2)^\alpha \qquad (\Omega) \\
&(8.3) \quad \rho\,\frac{\partial\phi}{\partial n} = g \qquad (\Gamma_1) \\
&(8.4) \quad \phi|_{\Gamma_2} = 0 \qquad (\Gamma_2) \ ; \ \Gamma = \Gamma_1 \cup \Gamma_2
\end{aligned}
\qquad (8)
$$

In the compressible case, it is interesting to add the local Mach number given by

$$M^2 = \frac{2}{\gamma+1}\left[\frac{|\vec{\nabla}\phi|^2}{1-\frac{\gamma-1}{\gamma+1}|\vec{\nabla}\phi|^2}\right].$$

Furthermore, in the subsonic case, we have at every point of the fluid occupying the domain, the relationship $M^2 < 1$.

2.2. 2-D Lifting Case /17

Extension to the compressible lifting case does not present any particular problem with respect to the incompressible fluid. The formulation is given directly by

$$\begin{aligned}
&\vec{\nabla}\cdot(\rho\vec{\nabla}\phi) = 0 \quad ; \ \phi \text{ discontinuous} \quad \vec{u} \text{ continuous} \\
&\rho = (1-k|\vec{\nabla}\phi|^2)^\alpha \qquad (\Omega) \\
&\phi^+ = \phi^- + \ell \qquad (C) \\
&|\vec{\nabla}\phi^+|^2 = |\vec{\nabla}\phi^-|^2 \qquad (BF)
\end{aligned} \qquad (10)$$

3. - MODELING OF THE POTENTIAL TRANSONIC FLOW FROM A COMPRESSIBLE IDEALIZED FLUID

3.1. Equations

A characteristic of transonic flows is in the presence of shocks. The condition of irrotation necessitates that their intensity is small: $M^2 < 1.5$ where M is given by (9).

If the local Mach variation is observed in a transonic case, it may be seen that there are what is called supersonic zones where the local Mach is higher than 1 $(M > 1)$ and subsonic zones where the local Mach is less than 1 $(M < 1)$. Example : flow around a circle at $M_\infty = .45$

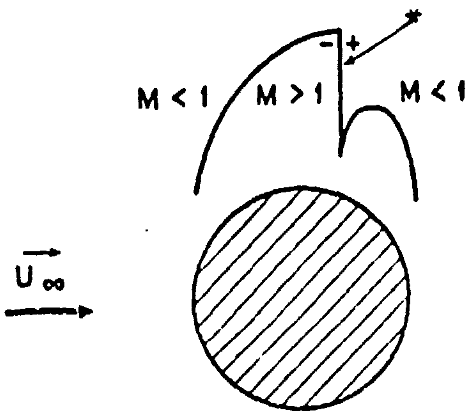

Figure 6

*physical shock

In a transonic state through shock, the flow must satisfy the RANKINE-HUGONIOT conditions (2)

$$[\rho\vec{u}\cdot\vec{n}]^{+} = [\rho\vec{u}\cdot\vec{n}]^{-}$$

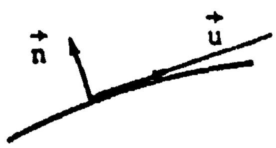

Figure 6-b

with
$\vec{u}\cdot\vec{s}$ continuous
$+$ the region **after** the shock, $-$ region **before** shock
$\vec{s}$, unit vector of flow direction
$\vec{n}$, orthogonal at $\vec{s}$ or in the direct sense of figure 6-b.

A characteristic of the transonic flow is that the fluid velocity may be locally discontinuous when passing through a shock. 18

Let us now consider the equations and boundary conditions of a transonic compressible fluid. They are the same as those for a subsonic compressible fluid.

$$\begin{array}{ll} \vec{\nabla}\cdot\rho\vec{u} = 0 \quad \vec{\nabla}\wedge\vec{u} = 0\,; & \vec{u} \text{ may be discontinuous} \\ \rho = (1-k|\vec{u}|^2)^{\alpha} \quad (\Omega) & \\ [\rho\vec{u}\cdot\vec{n}]^{+} = [\rho\vec{u}\cdot\vec{n}]^{-} & \\ \rho\dfrac{\partial\phi}{\partial n} = g \quad (\Gamma) & \end{array} \qquad (12)$$

The introduction of ϕ, however, by using $\vec{\nabla}\wedge\vec{u} = 0$ leads to a mixed elliptical type non linear (13) boundary problem $(M<1)$. -hyperbolic $(M>1)$.

$$\begin{array}{lll} (13.1) & \vec{\nabla}\cdot\rho\vec{\nabla}\phi = 0 & \phi \text{ continuous} \\ (13.2) & \rho = (1-k|\vec{\nabla}\phi|^2)^{\alpha} \quad (\Omega) & \\ (13.3) & [\rho\vec{\nabla}\phi\cdot\vec{n}]^{+} = [\rho\vec{\nabla}\phi\cdot\vec{n}]^{-} & \\ (13.4) & \rho\dfrac{\partial\phi}{\partial n} = g \quad (\Gamma) & \vec{u} \text{ discontinuous} \end{array} \qquad (13)$$

Fundamental Remarks

1) There is no uniquity theorem for the solution of (13) in the transonic case.
2) The conditions of discontinuity through the shock shall be implicitely satisfied in the variational formulation of (13.1).

Figures 7, 8 show two possible Mach solutions in the case of a flow around a circle for $M_\infty = .45$

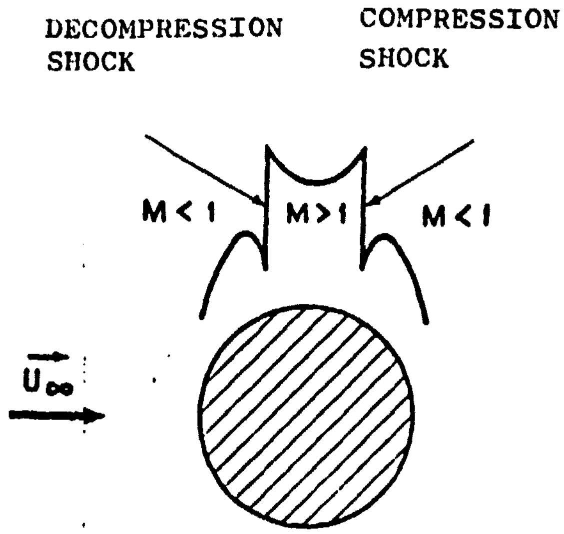

Figure 7

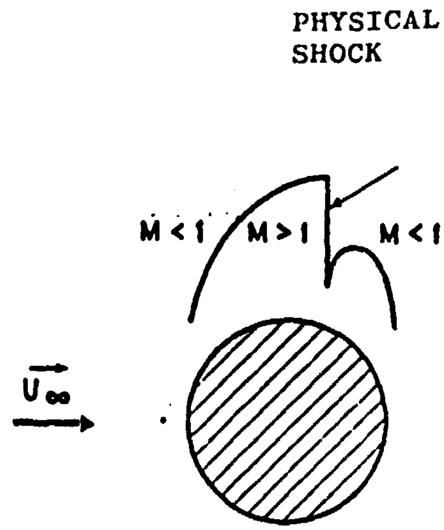

Figure 8

19

The equation (13.1), where ρ is given by (13.2), is elliptical (hyperbolic resp.) in the regions of Ω where the flow is subsonic $(M<1)$ (supersonic resp. $(M>1)$). The solution of figure 7 contains 2 shocks whereas the one on figure 8 only contains one. The latter is physically acceptable, whereas the solution with a double shock, including a decompress. shock, violates the laws of thermodynamics. (refer to LANDAU-LIPCHITZ (2)).

Accordingly, the formulation (12) or (13) is physically inadequate. In order to prevent the appearance of non physical shocks, a condition of <u>entropy</u> must be added to 13. In the methods of finite differences, the condition of entropy is satisfied by introducing $(M>1)$ of decentered differences or an artificial viscosity (see MURMAN-COLE (3), JAMESON (5), BAUER-GARABEDIAN-KORN (4) into the supersonic zone $(M>1)$.

In the finite elements techniques, the condition of entropy is treated as an added constraint to (13) or by a technique of artificial viscosity, similar to the finite differences, by modifying the equation locally in the supersonic zone (13.1).

3.2. The condition of entropy formulated as a constraint

During the passage of a shock wave, entropy increases and we show that in the case of a potential flow, this condition may be translated by a decrease in velocity through the transonic shocks. This characteristic applied to a monodimensional flow is translated by

$$u^{+} - u^{-} < 0 \tag{14}$$

where u^{+} designates the velocity after shock,
u^{-} designates the velocity before shock,
(Figure 9)

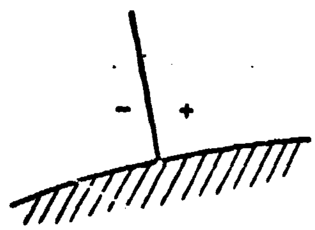

Figure 9

If $u = \dfrac{d\phi}{dx}$ then (14)

$$\frac{d^{2}\phi}{dx^{2}} < +\infty \tag{15}$$

By analogy (15) in bi and tridimensional becomes

$\Delta\phi < +\infty$ or $\Delta\phi < K$ with constant K to be selected (16)

In the variational formulation of the transonic problem, we shall consider a small shape of (16) given in (17) obtained by integrating (16) by parts. /20

$$- \int_{\Omega} \vec{\nabla}\phi \cdot \vec{\nabla}\omega \, d\Omega \le K \int_{\Omega} \omega \, d\Omega \quad \forall \, \hat{\omega} \in \mathcal{D}^{+}(\Omega)$$

$$\text{where} \quad \mathcal{D}^{+}(\Omega) = \{\omega | \omega \in (\Omega) \; ; \; \omega \ge 0\} \tag{17}$$

$$\mathcal{D}(\Omega) = \{\omega | \omega \in C^{\infty}(\bar{\Omega}), \text{ supp } \omega \text{ compact}\}$$

It is important to note that in (17) only the derivates of first order, more accessible in a finite elements approach, are shown.

The transonic formulation selected in this case is:

$$\boxed{\begin{array}{l} \vec{\nabla} \cdot \rho \, \vec{\nabla}\phi = 0 \\ \rho = (1 - k|\vec{\nabla}\phi|^{2})^{\alpha} \\ [\rho\vec{\nabla}\phi \cdot \vec{n}]^{+} = [\rho\vec{\nabla}\phi \cdot \vec{n}]^{-} \\ \rho \dfrac{\partial\phi}{\partial n} = g \\ \Delta\phi < K \end{array}} \tag{18}$$

3.3 The Condition of Entropy Formulated by the Artificial Viscosity

In reference to M.O. BRISTEAU (6) and to JAMESON (5), (13.1) may be rewritten in $(13)_\ell$ in a local reference marked $(\vec{n},\vec{s})$ or $|\vec{n}|$ is the unit vector of the flow direction $\vec{u}$ and $\vec{s}$ the perpendicular orientated in the standard direction on figure 10. $\frac{\vec{n}}{} = \vec{s}$

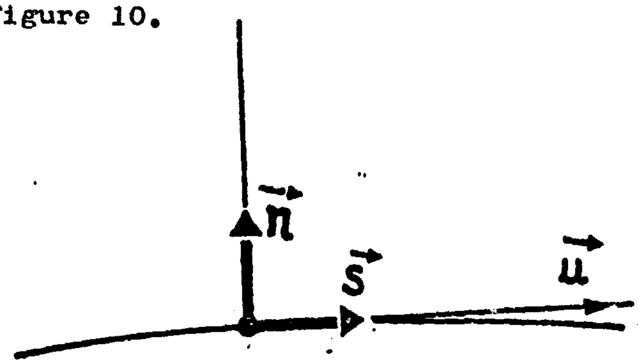

Figure 10

$$\boxed{\rho \frac{\partial^2\phi}{\partial n^2} + \frac{\rho}{1-kV^2}(1-V^2)\frac{\partial^2\phi}{\partial s^2} = 0} \qquad (13)_\ell$$

$$V^2 = u^2+v^2$$

$$\frac{\partial}{\partial n} = -\frac{v}{V}\frac{\partial}{\partial x} + \frac{u}{V}\frac{\partial}{\partial y} \;;\; \frac{\partial}{\partial s} = \frac{u}{V}\frac{\partial}{\partial x} + \frac{v}{V}\frac{\partial}{\partial y} \;;\; (\vec{\nabla})_\ell = \left(\frac{\partial}{\partial s}, \frac{\partial}{\partial n}\right)$$

In this form, the elliptical or hyperbolic characteristic of the equation appears, depending on whether or not V is smaller or larger than 1. In a similar manner to the decentering practiced in the finite differences, the operator of artificial viscosity is added to (13.1) /21

$$E(\phi) = -\frac{\partial}{\partial s}\left((|\vec{u}|^2-1)^+ \frac{\rho}{1-K|\vec{u}|^2}\frac{\partial^2\phi}{\partial s^2}\right) \qquad (19)$$

with $(|\vec{u}|^2-1)^+ = \sup(0, |\vec{u}|^2-1)$ and the transonic formulation selected in this case is given by

$$\boxed{\begin{array}{ll} -\vec{\nabla}\cdot(\rho\vec{\nabla}\phi) + \nu E(\phi) = 0 \;;\; \nu > 0 & \\ \rho = (1-k|\nabla\phi|^2)^\alpha & (\Omega) \\ [\rho\vec{\nabla}\phi\cdot\vec{n}]^+ = [\rho\vec{\nabla}\phi\cdot\vec{n}]^- & \\ \frac{\partial\phi}{\partial n} = g \quad (\Gamma) & \end{array}} \qquad (20)$$

Note : ν parameter of viscosity >0 depends on step h of the triangulation of the domain in numerical applications.

Other artificial viscosity operators mentioned in (5), (37) as $\tilde{E}$ in (21) have been tested numerically and give very close solutions

$$\tilde{E}(\phi) = -\frac{\partial}{\partial s}\left(\left(|\vec{u}|^2-1\right)^+|\Delta\phi|\Delta\phi\right) \quad (21)$$

3.4 Lifting case

Extension to the transonic lifting case does not present any problem with respect to the compressible subsonic fluid. The formulation is given in (22) from (18)

$$\boxed{\begin{array}{ll}
\vec{\nabla}\cdot\rho\vec{\nabla}\phi = 0 \;;\; \phi \text{ discontin.} \;;\; \vec{u} \text{ discontin.} & \\
\rho = (1-k|\vec{\nabla}\phi|^2)^\alpha & \\
[\rho\vec{\nabla}\phi\cdot\vec{n}]^+ = [\rho\vec{\nabla}\phi\cdot\vec{n}]^- & (\Omega) \\
\Delta\phi < K & \\
\phi^+ = \phi^- + \ell & (C) \\
|\vec{\nabla}\phi^+|^2 = |\vec{\nabla}\phi^-|^2 & (BF) \\
\frac{\partial\phi}{\partial n} = g & (\Gamma) \\
\phi = 0 & (BF)
\end{array}} \quad (22)$$

4. - MODELING OF AN UNSTEADY INCOMPRESSIBLE VISCUOUS FLUID

If Ω and Γ designate respectively the domain occupied by the fluid and its boundary, the latter obeys the Navier Stokes equations without dimensions, increased by boundary and initial conditions, i.e. /22

$$
\left.
\begin{array}{lll}
(23.1) & \dfrac{\partial \vec{u}}{\partial t} - \nu\Delta\vec{u} + (\vec{u}\cdot\vec{\nabla})\vec{u} + \vec{\nabla}p = 0 & \\
(23.2) & \vec{\nabla}\cdot\vec{u} = 0 & (\Omega) \\
(23.3) & \vec{u} = \vec{z} & \\
(23.4) & \vec{u}(\vec{x},0) = \vec{u}^{o} &
\end{array}
\right\} \quad (23)
$$

where $\vec{u}$ is the fluid velocity

p is the pressure

ν is the fluid viscosity ($\nu = 1/Re$ with Re = Reynolds number)

$\vec{z}$ and $\vec{u}_0$ specified; $\vec{z}=0$ if $\Gamma=\Gamma_p$ represent a wall (condition of adherence

$\vec{z}=\vec{u}_\infty$ if $\Gamma=\Gamma_\infty$ represent "infinity"

An example of external flow around an airfoil is given on figure 11.

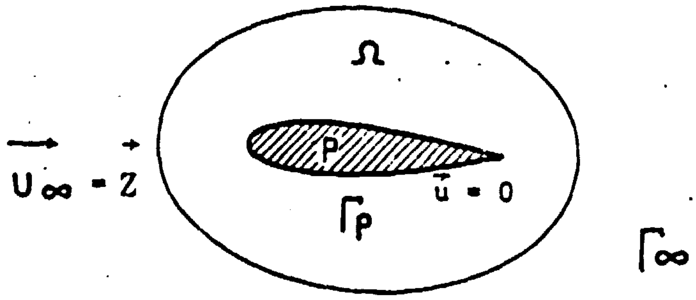

Figure 11

In the steady case (23) is reduced to

$$
\left.
\begin{array}{ll}
- \nu\Delta\vec{u} + (\vec{u}\cdot\vec{\nabla})\vec{u} + \vec{\nabla}p = 0 & \\
\vec{\nabla}\cdot\vec{u} = 0 & (\Omega) \\
\vec{u} = \vec{z} & (\Gamma)
\end{array}
\right\} \quad (23)_s
$$

In the unsteady case, the fluid is controlled by a system of equations with parabolic type non linear partial derivatives, whereas in the steady case, it obeys a system of equations with elliptical type non linear partial derivatives. In

(23) and $(23)_s$ the main numerical difficulties are the condition of incompressiblity, the Reynolds and the non linear convection.

5. - THE STANDARD ITERATIVE METHODS FOR SOLVING EQUATIONS WITH QUASI-ELLIPTICAL NON LINEAR PARTIAL DERIVATIVES 224

5.1. The Model Problem

For reasons of simplicity, we are interested in the solution of the non linear Dirichlet problem (24)

$$\boxed{\begin{array}{ll} -\Delta\phi - T(\phi) = 0 & (\Omega) \\ \phi = 0 & (\Gamma) = (\partial\Omega) \end{array}} \qquad (24)$$

with T non linear operator and (Ω) a boundary of R^2.

5.2. The Fixed Point Methods

The simplest algorithm to solve (24) is

$$n=0 \; ; \; \phi^o \text{ given so that } \phi^o|_\Gamma = 0 \qquad (25)$$

For $n \geq 0$ compute ϕ^{n+1} knowing ϕ^n by solving (26)

$$\begin{array}{ll} -\Delta\phi^{n+1} = T(\phi^n) & (\Omega) \\ \phi^{n+1} = 0 & (\Gamma) \end{array} \qquad (27)$$

(25) (26) (27) is a converging algorithm for <u>subsonic</u> compressible flows (refer to GELDER (7), NORRY-DEVRIES (8), PERIAUX (9)).

<u>The Gelder algorithm</u> in the case of a 2-D pipe. In this case, (Ω) is represented by figure 12.

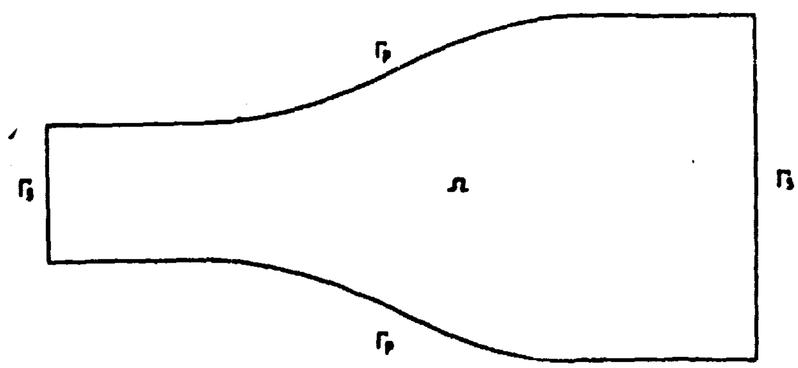

2-D Diverging Pipe

Figure 12

In this case $(\Gamma) = (\Gamma_s \cup \Gamma_p)$ and (8) is expressed

$$
\begin{array}{lll}
(28.1) & \vec{\nabla}\cdot\rho\,\vec{\nabla}\phi = 0 & (\Omega) \\
(28.2) & \rho = (1-k|\vec{\nabla}^2\phi|)^{\alpha} & (\Omega) \\
(28.3) & \dfrac{\partial\phi}{\partial n} = 0 & (\Gamma_p) \\
(28.4) & \phi|_{\Gamma_s} = h(\vec{x}) & (\Gamma_s)
\end{array}
\qquad (28)
$$

The variational formulation (29) is obtained by multiplying (28.1) by a test function $\omega \in H^1(\Omega)$ and by integrating by sections where 25

$H^1(\Omega) = \{\omega \in L^2(\Omega) | \nabla\omega \in L^2(\Omega)$

$$\int_\Omega (1-k\vec{\nabla}^2\phi)^{\alpha}\vec{\nabla}\phi\cdot\vec{\nabla}\omega\, dx = 0,\ \forall\omega \in H^1(\Omega)\ ,\ \omega|_{\Gamma_s} = 0\ ,\ \phi|_{\Gamma_s} = h \qquad (29)$$

Let us introduce the functional (30) $G_o(\phi)$ and the space

$H^1_{os}(\Omega) = \{\psi \in H^1(\Omega) | \psi|_{\Gamma_s} = 0\}$

$$G_o(\phi) = -\frac{1}{2k(\alpha+1)}\int_\Omega (1-k|\vec{\nabla}\phi|^2)^{\alpha+1}\, dx \qquad (30)$$

Let us calculate, in the meaning of Gâteaux (refer to VAINBERG (10)), the derivative of G_o at a point ϕ^* of H^1_{os}

$$\lim_{\lambda\to 0}\frac{d}{d\lambda}G_o(\phi^*+\lambda\delta\phi^*) = \langle G'_o(\phi^*),\delta\phi^*\rangle$$

The steady state of G_o in ϕ^* is expressed in (31)

$$\delta G_o = G_o(\phi^*+\delta\phi^*) - G_o(\phi^*) = \langle G'_o(\phi^*),\delta\phi\rangle + 0(\delta\phi^*) \quad \forall(\delta\phi^*)\in H^1_{os}(\Omega) \qquad (31)$$

By using (28.2) and (30), (31) is written (32)

$$\delta G_o = \int_\Omega (1-k|\vec{\nabla}\phi|^2)^{\alpha}\vec{\nabla}\phi^*\cdot\vec{\nabla}\delta\phi^*\, dx + 0(\delta\phi^*) \qquad (32)$$

and therefore ϕ^* is a <u>steady point</u> of G_o in $H^1_{os}(\Omega)$ if it satisfies (33)

$$\boxed{\int_\Omega (1-k|\vec{\nabla}\phi^*|^2)^{\alpha}\vec{\nabla}\phi^*\cdot\vec{\nabla}\omega\, d\vec{x} = 0\ ,\ \forall\omega\in H^1_{os}(\Omega)} \qquad (33)$$

By approximating (33) from (29) : all the steady points ϕ^* in $H^1_{os}(\Omega)$ satisfying $\phi^*-h|_{\Gamma_s} = 0$ are solutions of (28).

We can now prove the uniquity of (34)

$$\min_{\phi} G_o(\phi) \tag{34}$$

in the case of the subsonic state by demonstrating that in this particular case G_o is convex. We have only to calculate for that in (33)

$$G_o'' = \lim_{\lambda\to 0} \frac{d^2}{d\lambda^2} (G_o(\phi+\lambda\delta\phi))$$

$$G_o''(\phi) = -\int_\Omega (1-k|\vec\nabla\phi|^2)^\alpha \{\vec\nabla\delta\phi\vec\nabla\delta\phi - \frac{2k\alpha}{(1-k|\vec\nabla\phi|^2)} (\vec\nabla\phi\cdot\vec\nabla\delta\phi)^2\} dx \tag{35}$$

By refering to (9) $M^2 = 2k\alpha\,(1-k|\vec\nabla\phi|^2)^{-1}|\vec\nabla\phi|^2$ with M local mach /26
and using the identity $|\vec a\cdot\vec b| = |a||b| \cos\theta$, (35) is written (36)

$$G_o''(\phi) = -\int_\Omega \rho(1-M^2 \cos^2 \theta)|\vec\nabla\delta\phi|^2 dx \tag{36}$$

It is now easy to verify that if $M<1$ in Ω -subsonic case) G_o'' is convex and that

$$\phi^* = \operatorname{Arg} \min_{\phi-h\in H^1_{os}} G_o(\phi) \qquad \text{is the solution of (28)}$$

whereas if $M>1$ in Ω (transonic case) G_o'' is no longer convex and that is only a saddle point of G_o.

A fixed point algorithm or <u>quasi linearization</u> is described in (37)

i) $n=0$ ϕ^o initialisé en $-\Delta\phi^o = 0$ $\phi^o-h|_{\Gamma_s} = 0$

the continuation $\{\phi_n\}_{n\geq 1}$ is constructed by solving for $\phi^{n+1} \in H^1(\Omega)$

$$\text{ii)}\ \boxed{\begin{array}{l}\displaystyle\int_\Omega \rho^n\, \vec\nabla\phi^{n+1}\cdot\vec\nabla\omega\, d\Omega = 0\ ,\ \forall\omega\in H^1_{os}(\Omega)\\ (\phi^{n+1}-h)|_{\Gamma_s} = 0\end{array}} \tag{37}$$

The convergence of (37) in the hardest subsonic cases is obtained in 10 maximum iterations.

Note : The fixed point methods (37) are related to the gradient methods. In fact, (27) is a special case of (38) with $\rho = 1$

$$\begin{aligned} &\phi^o \text{ given} \\ &n \geq 0 \\ &-\Delta\ \phi^{n+1/2} = T(\phi^n) \quad \text{in } \Omega \\ &\phi^{n+1/2} = 0 \qquad \text{on } \Gamma \\ &\phi^{n+1} = \phi^n + \rho(\phi^{n+1/2} - \phi^n) \end{aligned} \tag{38}$$

but (38) by eliminating $\phi^{n+1/2}$ is expressed (38)'

$$\phi^{n+1} = \phi^n - \rho(-\Delta)^{-1}\ (-\Delta\phi^n - T(\phi^n)) \qquad (38)'$$

(38)' is a gradient method if T is the derivative a functional. An example of (38)' described in (41), consists of minimizing the functional G_o by a gradient method in the metric adapted to standard H^1_{os} written out $\|\cdot\|_1$, where $\ll f_1, f_2 \gg = \int_\Omega \vec\nabla f_1 . \vec\nabla f_2\ d\Omega$ designates the scalar product of the space of Sobolev H^1_{os}.

Generally, if $\delta\phi \in L^2(\Omega)$; $G_o'(\phi)$ defined by (39) is a dual element of $L^2(\Omega)' = L^2(\Omega)$

$$\langle G_o'(\phi), \delta\phi \rangle = \int_\Omega \rho\vec\nabla\phi\vec\nabla\delta\phi\ d\Omega\ . \tag{39}$$

/27

Let us introduce $g \in H^1_{os}$ solution of (40)

$$\int_\Omega \vec\nabla g . \vec\nabla\delta\phi\ d\Omega = \int_\Omega \rho\vec\nabla\phi . \vec\nabla\delta\phi d\Omega \quad , \forall\delta\phi \in H^1_{os} \tag{40}$$

Then (41) consists of

41.1. ϕ^o initialized in $\Delta\phi^o = 0\ ,\ \phi^o - h|_{\Gamma_s} = 0$

$$g^o \in H^1_{os}(\Omega) \quad \text{calculated by} \quad -\Delta g^o = G'(\phi^o) \tag{41}$$

we set $h^o = g^o$

41.2. $- n \geq 1$ knowing ϕ^n and $g^n \in H^1_{os}$, $\{\phi^{n+1}\}\ \{g^{n+1}\} \in H^1_{os}$ is constructed in two phases :

Phase 1 : Calculate $\lambda^* = \arg\min_\lambda G_o(\phi^n - \lambda h^n)$
set $\phi^{n+1} = \phi^n - \lambda^* h^n$

Phase 2 : Construct the new direction of descent
To accomplish that solve

Solve $\quad -\Delta g^{n+1} = J'(\phi^{n+1})\ ,\ g^{n+1} \in H^1_{os}(\Omega)$

Calculate $\quad \gamma^{n+1} = \dfrac{\int_\Omega \vec{\nabla} g^{n+1} \cdot \vec{\nabla}(g^{n+1} - g^n)}{\int_\Omega |\vec{\nabla} g^n|^2 dx}\, dx$

ans set $\quad h^{n+1} = g^{n+1} + \gamma^{n+1} h^n\ ;\ n=n+1$, and go to 1.

(41) is the version of the POLAK-RIBIERE conjugate (1) in the metric adapted H^1_{os}. The rapidity of the convergence of (41) is comparable to the one of the fixed point described in (37).

The gradient method with metric adapted to the preconditioning shall play a fundamental role in the case of transonic fluids.

5.3. The Newton Methods /28

Assuming this time T differentiable (24) may be solved by the algorithm (42)

$$
\begin{array}{ll}
(42.1) & \phi^o \text{ given} \\
(42.2) & n \geq 1\ ,\ \phi^{n+1} \text{ is calculated from } \phi^n \text{ by} \\
 & -\Delta\phi^{n+1} - T'(\phi^n)\phi^{n+1} = T(\phi^n) - T'(\phi^n)\cdot\phi^n \text{ in } \Omega \\
(42.3) & \phi^{n+1} = 0 \text{ on } \Gamma
\end{array}
\qquad (42)
$$

(42) is a special case $(\rho=1)$ of (43) used for the hardest cases

$$
\begin{array}{ll}
(43.1) & \phi^o \text{ given} \\
(43.2) & n \geq 1\ ,\ \phi^{n+1} \text{ is calculated from } \phi^n \text{ by} \\
 & -\Delta\phi^{n+1/2} - T'(\phi^n)\phi^{n+1/2} = T(\phi^n) - T'(\phi^n)\cdot\phi^n \text{ in } \Omega \\
 & \phi^{n+1/2} = 0 \text{ on } \Gamma \\
(43.3) & \phi^{n+1} = \phi^n + \rho(\phi^{n+1/2} - \phi^n)\ ,\ \rho>0
\end{array}
\qquad (43)
$$

The treatment of the Joukowski condition, differentiable non linear constraint, is an application of (42).

Example of the Flow Around an Airfoil

(5) may be solved directly by using the discontinuous velocity potential in the form of an iterative procedure (A1) including the Joukowski condition, the technique of decomposition

of the potential (A2) (refer to NORRIE-DEVRIES (8)).

A1 - If (C) designates an arbitrary lifting cut of the trailing edge $\overline{(BF)}$ up to infinity (Γ_∞), the velocity potential ϕ is a discontinuous function along (C).

Let us introduce $\Omega_c = \overset{\circ}{\widehat{\tilde{\Omega} - (C)}}$. If $H^1(\Omega)$ designates the standard Sobolev space

$$H^1(\Omega) = \{v \in L^2(\Omega) \; ; \; \vec{\nabla} v \in L^2(\Omega)\}$$

then it is possible to give a variational formulation of (5) in $H^1_\ell(\tilde{\Omega}_c)$ under the space of $H^1(\tilde{\Omega}_c)$ defined in (44).

$$H^1_\ell(\tilde{\Omega}_c) = \{v \in H^1(\tilde{\Omega}_c) \; |v|_{(BF)} = 0 \; ; \; v|_{C^+} - v|_{C^-} = \ell\}. \tag{44}$$

29

Account taken of the continuity of the velocities along (C) which is expressed in (45)

$$\begin{aligned} \vec{u}^+ \cdot \vec{n}^+ \Big|_{C^+} &= \vec{u} \cdot \vec{n}^- \Big|_{C^-} \\ \frac{\partial \phi}{\partial n^+} \Big|_{C^+} &= \frac{\partial \phi}{\partial n^-} \Big|_{C^-} \end{aligned} \tag{45}$$

By multiplying 5.1 by a test function and by integrating in parts by taking into account (45)-(5.2), the equation (5.1) is written in the variational form (4.6)

$$\int_{\tilde{\Omega}_c} \vec{\nabla}\phi \cdot \vec{\nabla}\omega \, dx = 0 \quad \forall \omega \in H^1_\ell(\tilde{\Omega}_c) \quad , \; \phi \in H^1(\tilde{\Omega}_c) \tag{46}$$

Assuming $JK(\ell) = |\vec{\nabla}\phi_\ell|^2_{(C^+)} - |\vec{\nabla}\phi_\ell|^2_{(C^-)}$, the Joukowski condition is expressed in (47)

$$JK(\ell)\Big|_{BF} = 0 \tag{47}$$

The algorithm (42) applied to this example is expressed in (48)

i) Assuming ℓ^o given ; ϕ^o is solution of (46) in $H^1_{\ell^o}(\Omega)$

ii) For $n \geq 0$ $\{\phi^n, \ell^n\}$ being known, $\{\ell^{n+1}, \phi^{n+1}\}$ are calculated by the equation

$$\ell^{n+1} = \ell^n - JK'^{-1}(\ell^n) \circ JK(\ell^n) \tag{48}$$

with $JK' = 2($[illegible]$\cdot \vec{\nabla}\delta\phi^+ - \vec{\nabla}\phi \cdot \vec{\nabla}\delta\phi^-)$, ϕ^{n+1} solution of (46) in $H^1_{\ell^{n+1}}(\tilde{\Omega}_c)$.

iii) stop test on ℓ^n satisfied, otherwise n=n+1, go to ii).
The convergence is ensured in several iterations (5 maximum).

<u>A2</u> - The velocity potential ϕ is the linear combination (50) of two potentials ϕ_{NP} and ϕ_R, ϕ_{NP} <u>continuous</u> potential and ϕ_R <u>discontinuous</u> potential, solution of $(49)_{NP}$ and $(49)_R$

$$\begin{array}{lll} \Delta\phi_{NP} = 0 & \Omega & \\ \dfrac{\partial \phi}{\partial n}NP = g & \Gamma & \qquad (49)_{NP} \\ \phi_{NP} = 0 & (BF) & \end{array}$$ /30

$$\left.\begin{array}{lll} \Delta\phi_R = 0 & (\Omega) \\ \dfrac{\partial \phi}{\partial n} R = 0 & (\Gamma) \\ \phi_R\Big|_{C^+} - \phi_R\Big|_{C^-} = 1 & (C) \\ \dfrac{\partial \phi}{\partial n^+}R\Big|_{C^+} - \dfrac{\partial \phi}{\partial n^-}R\Big|_{C^-} = 0 & \\ \phi_R = 0 & (BF) \end{array}\right\} \qquad (49)_R$$

$$\phi = \phi_{NP} + \ell\phi_R \tag{50}$$

If ℓ is selected so that (51) occurs

$$JK(\ell) = |\vec{\nabla}\Phi|^2_{BF^+} - |\vec{\nabla}\Phi|^2_{BF^-} = 0 \qquad (51)$$

it is then easy to verify that $\{\phi,\ell\}$ solution of (49), (50), (51) is the solution of (5).

Assuming $H^1_{BF}(\Omega) = \{\omega \in H^1(\Omega) | \omega|_{BF} = 0\}$ and $H^1(\tilde{\Omega}_c)$ is the subset of $H^1(\tilde{\Omega}_c)$ of the verifying functions on the cut (C)

$$\omega|_{C^+} - \omega|_{C^-} = 1.$$

Then the variational formulation of the equation '49)$_{NP}$ is expressed in (52)

$$\int_\Omega \vec{\nabla}\phi_{NP} \cdot \vec{\nabla}\omega \, dx = \int_\Gamma g\omega \, d\Gamma \quad \forall \omega \in H^1_{BF} \qquad (52)$$

$$\phi_{NP} \in H$$

whereas the one of equation $(49)_R$ is given in (53)

$$\int_{\tilde{\Omega}_c} \vec{\nabla}\phi_R \cdot \vec{\nabla}\omega \, dx = 0 \quad \forall \omega \in H^1_\ell(\tilde{\Omega}_c) \qquad (53)$$

$$\phi_R \in H^1_1(\tilde{\Omega}_c)$$

The solution of (5) is then given by algorithm (54)

i) ϕ_{NR} and ϕ_R solutions of (52) (53) ; ℓ^o initializes; $\phi^o = \phi_{NP} + \ell^o \phi_R$

ii) For $n \geq 0$; $\{\ell^n, \phi^n\}$ being known $\{\ell^{n+1}, \phi^{n+1}\}$ is calculated by the equation

$$\ell^{n+1} = \ell^n - JK'^{-1}(\ell^n) JK(\ell^n) \qquad (54)$$

with

$$JK(\ell^n) = |\vec{\nabla}\phi^n|^2_{BF^+} - |\vec{\nabla}\phi^n|^2_{BF^-}$$

$$JK'(\ell^n) = 2\{\vec{\nabla}\phi^n . \vec{\nabla}\phi_R|_{BF^+} - \vec{\nabla}\phi^n . \vec{\nabla}\phi_R|_{BF^-}\}$$

$$\phi^{n+1} = \phi_{NR} + \ell^{n+1}\phi_R$$

iii) If a stop test is not satisfied by ℓ^{n+1} ; n=n+1 we return to ii

The convergence of (54) is ensured in 3 or 4 iterations.

Remarks : (48) and (54) are generalized in the two following directions :

-compressible subsonic and transonic equations
-complex geometries : 2-D multi-bodies and 3-D airfoils.

Example : Expansion of (54) to a multi-body in subsonic state. The domain (Ω) is shown on figure 13.

If ρ is eliminated in 8.1 by using 8.2, the problem with boundaries to be solved is given in (55)

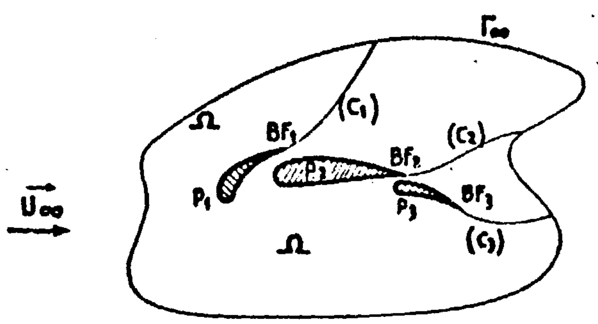

Figure 13

$$(\phi_x^2-a^2)\phi_{xx} + (\phi_y^2-a^2)\phi_{yy} + 2\phi_x\phi_y\phi_{xy} = 0 \tag{55.1}$$

$$\phi|_{C_i^+} - \phi|_{C_i^-} = \ell_i \quad i=1,3 \tag{55.2}$$

(55)

$$JK(\ell) = |\vec{\nabla}\phi|^2_{BF_i^+} - |\vec{\nabla}\phi|^2_{BF_i^-} = 0 \quad i=1,3 \tag{55.3}$$

$$\frac{\partial\phi}{\partial n} = g \text{ on } \Gamma_1 = \Gamma_\infty \cup (\bigcup_i P_i) \quad , \phi = 0 \text{ on } \Gamma_2 = \{BF_3\} \tag{55.4}$$

(55.1) may be reformulated in (55.4) in the form (55.5)

$$-\Delta\phi + T(\phi) = 0 \tag{55.5}$$

with $T(\phi) = \dfrac{\phi_x^2\phi_{xx} + \phi_y^2\phi_{yy} + 2\phi_x\phi_y\phi_{xy}}{a^2}$

$$a^2 = A+B|\vec{\nabla}\phi|^2 \qquad A = a_\infty^2 + \frac{1}{2}(\gamma-1)|\vec{u}_\infty|^2 \qquad B = \frac{1}{2}(1-\gamma)$$

The method of quasi-linearization developed in (37) is used in (56) to construct a continuation $\{\phi^n\} \in H^1(\Omega)$ verifying

$$\begin{aligned}&\int_\Omega \vec{\nabla}\phi^{n+1}\cdot\vec{\nabla}\omega\, dx - \int_\Gamma g\,\omega\, dx + \int_\Omega T(\phi^n)\,\omega\, dx = 0\\ &\phi^{n+1} \in H^1_{02}(\Omega)\\ &\forall\omega \in H^1_{o2} = \{\omega \in H^1(\Omega)\,|\,\omega|_{\Gamma_2} = 0\}\end{aligned} \tag{56}$$

If ϕ^{n+1} designates the <u>discontinuous</u> potential of the velocities and $(\ell_i)^n$ the circulations around bodies (P_i) with iteration n, ϕ^{n+1} is expressed in (57)

$$\phi^{n+1} = \phi^{n+1}_{NP} + \sum_{i=1}^{3} \ell_i\,\phi_{Ri} \tag{57}$$

where ϕ^{n+1}_{NP} and ϕ_{Ri} are solutions of (58) (59)

$$\left.\begin{aligned}&\int_\Omega \vec{\nabla}\phi^{n+1}_{NP}\cdot\vec{\nabla}\omega dx - \int_\Gamma g\,\omega\, dx + \int_\Omega T(\phi^n)\omega\, dx = 0\\ &\phi^{n+1}_{NP} \in H^1_{02}(\Omega)\ ;\ \forall\omega \in H^1_{o2}(\Omega)\end{aligned}\right\} \tag{58}$$

$$\left.\begin{aligned}&\int_\Omega \vec{\nabla}\phi_{R_i}\cdot\vec{\nabla}\omega\, dx = 0 \quad \forall\omega \in H^1_1(\tilde{\Omega}_{c_i})\\ &\phi_{R_i} \in H^1_{\ell_i}(\tilde{\Omega}_{c_i}) \quad i=1,3\end{aligned}\right\} \tag{59}$$

The expansion of (54) is the shown by algorithm (60).

$$\begin{array}{lll}(\phi_{R_i})_{i=1,3} & \text{solutions of (59)} & \text{(i)}\\ (\phi^o_{NP}) & \text{solution of (58) with } T \equiv 0 & \\ \vec{\ell}^o & \text{solution of } JK_o(\ell^o) = 0 & \\ \phi^o \text{ initialized} & \phi^o = \phi^o_{NP} + \sum_1^3 \ell^o_i\phi_{R_i} & (60)\end{array}$$

(ii) $n \geq 1$ $\{\phi^n\}$ and $\{\ell^n\}$ being known $\{\phi^{n+1}\}$ $\{\ell^{n+1}\}$ are calculated by first using (58) providing ϕ_{NP}^{n+1}, then by solving the equation

$$JK_{n+1}(\ell^{n+1}) = 0 \qquad \phi^{n+1} = \phi_{NP}^{n+1} + \sum_i \ell_i^{n+1} \phi_{R_i}$$

(iii) if a stop test is not satisfied for ℓ^{n+1} ; $n=n+1$ and go to ii.

The method of decomposition at phase n+1 is reviewed on figure 14.

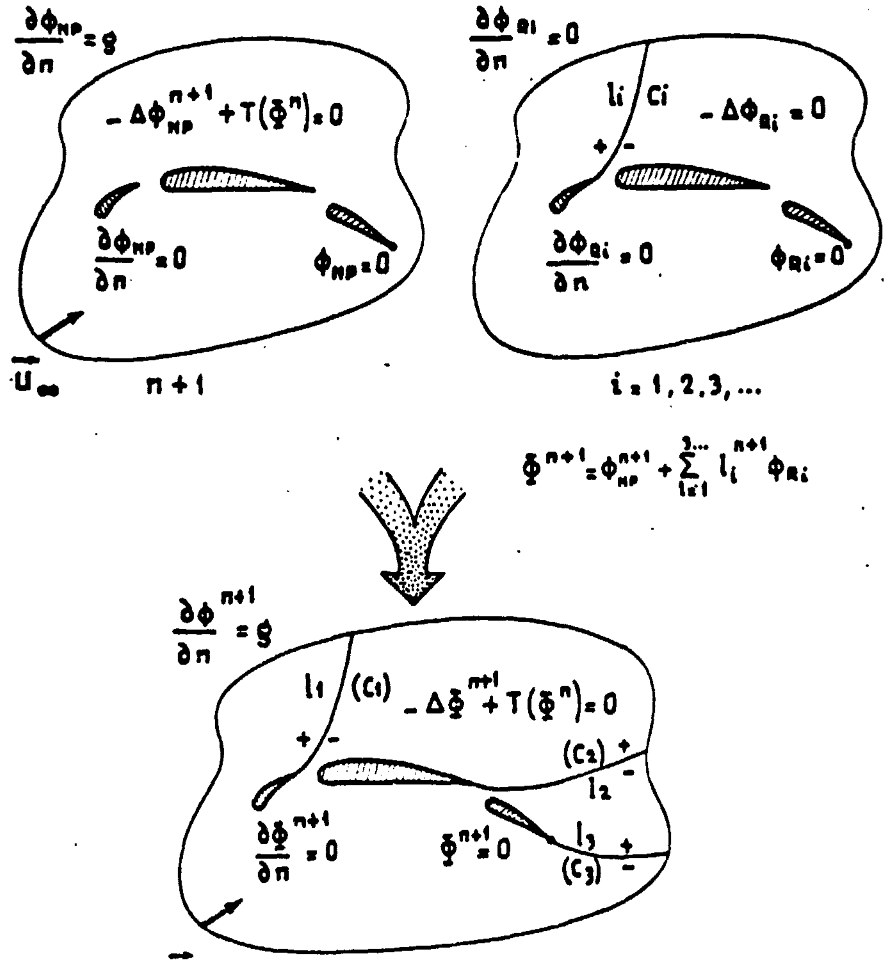

Figure 14

5.4. The Pseudo-unsteady Methods

They consist of associating to problem (24) a problem depending on time (61)

$$
\begin{aligned}
&\frac{\partial\phi}{\partial t} - \Delta\phi - T(\phi) = 0 && (\Omega)\\
&\phi|_{\Gamma} = 0 && (\Gamma) \qquad\qquad (61)\\
&\phi(x,0) = \phi_o(x)
\end{aligned}
$$

The solution of (61) : boundary $\underset{t\to\infty}{\phi(t,x)}$ is obtained by using a spatial approximation, substituting for (61) a system of normal differential equations integrated numerically on interval $(0,T($, T large.

In the case of an undifficult problem, an explicite scheme described in (62) is adequate to integrate numerically (61)

$$
\begin{aligned}
&\text{i)}\quad \phi^o = \phi_o\\
&\text{ii)}\quad n \geq 0 \quad \frac{\phi^{n+1}-\phi^n}{\Delta t} - \Delta\phi^n - T(\phi^n) = 0 && (\Omega) \qquad (62)\\
&\qquad\qquad\quad \phi^{n+1} = 0 && (\Gamma)
\end{aligned}
$$

Examples of the Pseudo-unsteady Approach :

1. - Solution of the Navier-Stokes equations (refer to FORTIN (14)) by the Arrow-Hurwi z algorithm

The variational formulation of $(23)_s$ is given in (63).

$$
\nu a(\vec{u},\vec{v}) + b(\vec{u},\vec{u},\vec{v}) = (\vec{f},\vec{v}) \quad \forall\ \vec{v}\in J_o\ ,\ \vec{f}\in L^2(\Omega) \qquad (63)
$$

where $J_o = \{\vec{v}\in [H_o^1(\Omega)]^N | \vec{\nabla}\cdot\vec{v} = 0\}$ (for simplicity we have assumed) $\vec{u}|_{\Gamma} = 0$)

with $a(\vec{u},\vec{v}) = \int_\Omega \vec{\nabla}\vec{u}\cdot\vec{\nabla}\vec{v}\ dx$

$b(\vec{u},\vec{u},\vec{v}) = \int_\Omega (\vec{u}\cdot\vec{\nabla})\vec{u}\cdot\vec{v}\ dx$

$(\vec{f},\vec{v}) = \int_\Omega \vec{f}\cdot\vec{v}\ dx$ N, dimension of space

Let us now consider the discrete problem $(63)_d$ associated with $\vec{u}_h \in (P_2)^N$, $\vec{w}_h \in (P_2)^N$, $p_h \in P_1$ and $q_h \in P_1$ where P_k designates tho polygons with degree k

$$\nu a(\vec{u}_h,\vec{w}_h)+b(\vec{u}_h,\vec{u}_h,\vec{w}_h)-(p_h,\vec{\nabla}\cdot\vec{w}_h) = (\vec{f},\vec{w}_h) \qquad (63)_d$$
$$(\vec{\nabla}\cdot\vec{u}_h,q_h) = 0$$

The Arrow-Hurwicz discrete algorithm substituted for $(62)_d$ may be described in (64) in the form of an <u>explicite scheme.</u>

135

i) $\vec{u}_h^o, p_h^o$ initialized

ii) $n \geq 1$, $\{\vec{u}_h^n, p_h^n\}$ known, $\{\vec{u}^{n+1}\}$ is calculated in (64.1)

$$(\vec{u}_h^{n+1}-\vec{u}_h^n,\vec{w}_h) + K\nu a(\vec{u}_h^n,\vec{w}_h)+Kb(\vec{u}_h^n,\vec{u}_h^n,\vec{w}_h)-K(p_h^n,\vec{\nabla}\cdot\vec{w}_h) = K(\vec{f},\vec{w}_h) \quad (64.1)$$
$$\forall\, w_h \in P^2 \; ; \; K = \Delta t$$

(iii) $n \geq 1$, $\{p_h^n\}$ & $\{\vec{u}_h^{n+1}\}$ known, p_h^{n+1} is computed in (64.2)

$$(p_h^{n+1}-p_h^n,q_h) + K(\vec{\nabla}\cdot\vec{u}_h^{n+1},q_h) = 0 \quad , \forall\, q_h \in P^1 \qquad (64.2)$$

(iv) Convergence test on $(\vec{u}_h^{n+1}, p_h^{n+1})$ not satisfied, do n=n+1, go to ii).

<u>Note</u> : The explicit numerical scheme described in (63) is relatively easy to program and economical to place in the computer core. Nevertheless, the conditions of <u>stability</u> connecting <u>ν ,K and h</u> has an industrial constraint. Furthermore, the numerical simulation of separated flows, relatively hard case, requires several <u>hundreds</u> of iterations.

2-<u>Solution of Potential of Small Perturbations in Transonic State by Finite Differences</u> (Refer to I.A. ESSER (13)).

To the non linear system (63')

$$F_1 = \vec{\nabla}\wedge\vec{u} \; ; \; \vec{u} = (u,v) \qquad (63)'$$
$$F_2 = \alpha u_{,x} + v_{,y} \; ; \; \alpha = (1-M_\infty^2 - (\gamma+1)M_\infty u)$$

we relate the hyperbolic system (63") with suitably chosen boundary conditions.

$$\frac{\partial u}{\partial t} = F_1$$
$$\frac{\partial v}{\partial t} = bF_2 \quad ; \quad b > 0 \qquad (63)"$$

where b equal to the initial unity in H. YOSHIHARA (12) is optimized by taking $b = |\alpha|$ to accelerate the convergence velocity of an explicit scheme of second order of the Lax-Wendroff type.

In the case of a very "hard" problem, it is better to use an implicit integration scheme to solve (61) described in algorithm (65) /35

i) $\phi^o = \phi_o$

ii) $n \geq 0$ (65)

$$\frac{\phi^{n+1}-\phi^n}{\Delta t} - \Delta\phi^{n+1} - T(\phi^{n+1}) = 0 \qquad (\Omega)$$
$$\phi^{n+1} = 0 \qquad (\Gamma)$$

at each step Δt a non linear (66) type (24), but better conditioned, non linear problem must be solved.

$$\left(\frac{Id}{\partial t} - \Delta\right)\phi^{n+1} - T(\phi^{n+1}) = \frac{\phi^n}{\Delta t} \qquad (\Omega) \qquad (66)$$
$$\phi^{n+1}_{|\Gamma} = 0 \qquad (\Gamma)$$

6. - THE FUNCTIONAL LEAST SQUARES METHODS

6.1. Relationships between a Least Squares Method and an Optimal Control Problem

A least squares type formulation related to a model problem (24) is given in (67)

$$\min_{v \in V} \int_\Omega |\Delta v + T(v)|^2 \, d\Omega = \min_{v \in V} ||\Delta v + T(v)||_2^2 \qquad (67)$$
$$||f||_2^2 = \int_\Omega |f|^2 \, d\Omega$$

and V a functional space $L^2(\Omega)$ for example.

Assuming ξ now the solution of the boundary problem (68)

$$\begin{aligned} -\Delta\xi &= T(v) \\ \xi|_\Gamma &= 0 \end{aligned} \tag{68}$$

(67) is then equivalent to (69)

$$\min_{v \in V} \int_\Omega |\Delta(v-\xi)|^2 \, d\Omega$$

with $\xi = \xi(v)$ via (68).

By referring to J.L. LIONS (15), it is obvious that (68)-(69) has the structure of an optimal control problem where

- α) v designates the CONTROL vector
- β) ξ designates the STATE vector
- γ) (68) is the STATE EQUATION
- δ) the functional (69) is the function of cost or criterion

From (68) (69), it may be seen that other formulas are possible by selecting a different cost function. We may, for example, consider the optimal control problem (68), (70) /32

$$\min_{v \in V} \int_\Omega |v-\xi|^2 \, d\Omega \tag{70}$$

with $\xi \equiv \xi(v)$ via (68).

(68 (69) and (68) (70) shall give a solution identical to the solution of the model problem (24), but with <u>different converging velocities</u>. Furthermore, the choice of a least squares method is very important on the numerical level. In fact, a standard which is inappropriate for the state equation (69) appearing in the cost function may lead to a <u>slow</u> convergence. A sound choice of the cost function with respect to non linear Dirichlet problems of the second order is discussed in paragraph 6.2.

6.2. <u>The Least Squares Method in a Particular Functional Space H^{-1}</u>

Let us introduce in (71) (72) the Sobolev spaces required for the study of the model problem (24)

$$H^1(\Omega) = \{\phi \in L^2(\Omega) \ , \ \vec{\nabla}\phi \in L^2(\Omega)\} \tag{71}$$

$$H^1_0(\Omega) = \{\phi \in H^1(\Omega), \ \phi|_\Gamma = 0\} \tag{72}$$

$$(\phi_1,\phi_2)_{H^1(\Omega)} = \int_\Omega \phi_1\phi_2 d\Omega + \int_\Omega \vec{\nabla}\phi_1\cdot\vec{\nabla}\phi_2\, d\Omega \tag{73}$$

$$\|\phi\|_{H^1(\Omega)} = \int_\Omega \phi^2 d\Omega + \int_\Omega |\vec{\nabla}\phi|^2 d\Omega \tag{74}$$

$H^1(\Omega)$ s a sub-space of $H^1(\Omega)$. Consequently, if Ω is limited, $H^1(\Omega)$ is a Hilbert space with scalar product (75) and corresponding standard (76) /38

$$(\phi_1,\phi_2)_{H_0^1(\Omega)} = \int_\Omega \vec{\nabla}\phi_1\cdot\vec{\nabla}\phi_2\, d\Omega \tag{75}$$

$$\|\phi\|_{H_0^1(\Omega)} = (\int_\Omega |\vec{\nabla}\phi|^2\, d\Omega)^{1/2}. \tag{76}$$

Assuming $H^{-1}(\Omega) = (H_0^1(\Omega))'$ the dual topolocial space of $H_0^1(\Omega)$. By observing that $(L^2(\Omega))' = L^2(\Omega)$ the inclusion (77) is permissible

$$H_0^1(\Omega) \subset L^2(\Omega) \subset H^{-1}(\Omega) \tag{77}$$

Furthermore, the application $\Delta = \vec{\nabla}^2$ is an isomorphism of $H_0^1(\Omega)$ in $H^{-1}(\Omega)$ If $<\cdot,\cdot>$ designates the bilinear shape of the duality between $H^{-1}(\Omega)$ and $H_0^1(\Omega)$ defined in (78) by

$$<f,\phi> = \int_\Omega f\ \phi\ dx \quad \forall\ f \in L^2(\Omega)\ ;\ \forall\ \phi \in H_0^1(\Omega) \tag{78}$$

then the topology of $H^{-1}(\Omega)$ is defined by $\|\cdot\|_{-1}$ in (79) by using (76) (78)

$$\|f\|_{-1} = \sup_{\phi\in H_0^1(\Omega)-\{0\}} \frac{|<f,\phi>|}{\|\phi\|_{H_0^1(\Omega)}} \tag{79}$$

Refer to LIONS-MAGENES (16), NECAS (17) for more results and characteristics relating to Sobolev spaces.

By using (79) the best formulation in the direction of least squares for solving the model problem (24) is given in (80)

$$\boxed{\min_{v\in H_0^1(\Omega)} \|\Delta v+T(v)\|_{-1}} \tag{80}$$

By introducing $\xi \in H_o^1(\Omega)$ solution of (68), then (80) takes the form (81)

$$\boxed{\underset{v \in H_o^1(\Omega)}{\text{Min}} \|\Delta(v-\xi)\|_{-1}} \tag{81}$$

By expanding $\|\Delta(v-\xi)\|_{-1}$ into (82)

$$\|\Delta(v-\xi)\|_{-1} = \sup_{\phi \in H_o^1(\Omega)-\{0\}} \frac{|\langle\Delta(v-\xi),\phi\rangle|}{\|\phi\|_{H_o^1}} \tag{82}$$

and by applying the Green formula to (82), we have

$$|\langle\Delta(v-\xi),\phi\rangle| = \left|\int_\Gamma \frac{\partial}{\partial n}(v-\xi)\phi \, d\Gamma - \int_\Omega \vec{\nabla}(v-\xi)\cdot\vec{\nabla}\phi \, d\Omega\right| = \left|\int_\Omega \vec{\nabla}(v-\xi)\cdot\vec{\nabla}\phi \, d\Omega\right| \tag{83}$$

and (82) takes then the final form (84)

$$\|\Delta(v-\xi)\|_{-1} = \sup_{\phi \in H_o^1(\Omega)-\{0\}} \frac{\left|\int_\Omega \vec{\nabla}(v-\xi)\cdot\vec{\nabla}\phi \, d\Omega\right|}{\|\phi\|_{H^1}} = \|v-\xi\|_{H_o^1(\Omega)} \tag{84}$$

The least squares method in H^{-1} (80) is, then, equal to an optimal control problem

$$\left|\begin{array}{l}\underset{v \in H_o^1(\Omega)}{\min} \{J(v) = \frac{1}{2}\int_\Omega |\vec{\nabla}(v-\xi)|^2 d\Omega \,|\, \xi \in H_o^1(\Omega) \text{ solution } -\Delta\xi = T(v)\}\end{array}\right. \tag{85}$$

6.3. Iterative Solution of an Optimal Control Problem by a Conjugate Gradient Algorithm

The Polak-Ribière (11) version of the conjugate gradient is used to solve (85), the algorithm of which is composed of 3 steps.

i) Initialization

$v^o \in H_o^1(\Omega)$ given (for example solution of $-\Delta v^o = 0$, $v^o|_\Gamma = 0$)
$g^o \in H_o^1(\Omega)$ gradient of $J(v)$ in $H^1(\Omega)$

is calculated in (87)

$$-\Delta g^o = J'(v^o)$$
$$g^o|_\Gamma = 0 \tag{87}$$

We set :

$$z^o = g^o \tag{88}$$

Then for $n \geq 0$, assuming v^n, g^n, z^n known, calculate v^{n+1}, g^{n+1}, z^{n+1} by

ii) descent

Calculate $\lambda^* = \arg\min_{\lambda \geq 0} J(v^n - \lambda z^n)$ (89)

and set (90)

$$v^{n+1} = v^n - \lambda^* z^n$$

iii) Construction of the new descent direction

Define $g^{n+1} \in H_0^1(\Omega)$ solution of problem (91) /39

$$-\Delta g^{n+1} = J'(v^{n+1}) \qquad (91)$$

$$g^{n+1}|_\Gamma = 0$$

then calculate ϕ^{n+1} in (92)

$$\gamma^{n+1} = \frac{\int_\Omega \vec{\nabla} g^{n+1} \cdot \vec{\nabla}(g^{n+1} - g^n)\, d\Omega}{\int_\Omega |\vec{\nabla} g^n|^2\, d\Omega} \qquad (92)$$

and define z^{n+1} in (93) /40

$$z^{n+1} = g^{n+1} + \gamma^{n+1} z^n \qquad (93)$$

do n=n+1 and go in ii)

The two important points of the algorithm (86)-(93) are :

1) - The problem of minimization to one variable (89) solved by dichotomy, or the Fibonnacci method (refer to "GOLDEN SEARCH" in POLAK (11)).

2) - The calculation of g^{n+1} from v^{n+1} requires the solution of two Dirichlet problems at each iteration (68) with $v = v^{n+1}$, and (91).

The point (91) is detailed below. $J'(v)$ is calculated in a standard way (derived from a functional in the meaning of Gateaux (refer to VAINBERG (10)) in (94).

Assuming $\delta v \in H_0^1(\Omega)$

$$\langle J'(v), \delta v\rangle = \lim_{\substack{t \to 0 \\ t \neq 0}} \frac{J(v + t\delta v) - J(v)}{t} \qquad (94)$$

(94) is expressed by using (85)

$$\langle J'(v), \delta v\rangle = \int_\Omega \vec{\nabla}(v - \xi)\vec{\nabla}\delta(v - \xi)\, d\Omega \qquad (95)$$

By differentiating (68) $\delta\xi \in H_0^1(\Omega)$ satisfies (96) $-\Delta\delta\xi = T'(v)\cdot\delta v$

$$\delta\xi|_\Gamma = 0 \qquad (96)$$

Using (95) and (96) the final calculation of $J'(v)$ is given in (97)

$$\langle J'(v), \delta v\rangle = \int_\Omega \vec{\nabla}(v - \xi)\cdot\vec{\nabla}\delta v\, d\Omega - \langle T'(v)\cdot\delta v, v - \xi\rangle \; . \qquad (97)$$

We recognize in (97) $J'(v) \in H^{-1}(\Omega)$ linear functional defined on by (98)

$$\phi \to \int_\Omega \vec{\nabla}(v - \xi)\cdot\vec{\nabla}\phi\, d\Omega - \langle T'(v)\cdot\phi, v - \xi\rangle \qquad (98)$$

Then g^n is the solution of the variational problem (99)

$$\begin{cases} g^n \in H_0^1(\Omega) \\ \int_\Omega \vec{\nabla} g^n \cdot \vec{\nabla}\phi\, d\Omega = \int_\Omega \vec{\nabla}(v^n - \xi^n)\vec{\nabla}\phi\, d\Omega - \langle T'(v^n)\phi, v^n - \xi^n\rangle \; , \quad \forall \phi \in H_0^1(\Omega) \end{cases} \qquad (99)$$

with ξ^n solution of

$$(100)\quad \xi^n \in H_0^1(\Omega) \tag{100}$$ /41

The algorithm (86)-(93) shall be used systematically in the applications of T to transonic flows and the the Navier-Stokes equations.

7. - THE LEAST SQUARES METHOD IN H^{-1} APPLIED TO TRANSONIC FLOWS

7.1. Subsonic Non Lifting Case

By retaking the problem with limits (8), the non linear operator T is given in (101)

$$T(\phi) = \vec{\nabla}\cdot\rho(\phi)\vec{\nabla}\phi \tag{101}$$

By retaking (85) with T in the form (101) the least squares formulation in H^{-1} of (8) is given in (102), (103)

$$\underset{\phi\in V_g}{\mathrm{Min}}\ \frac{1}{2}\int_\Omega |\vec{\nabla}\xi|^2 dx \tag{102}$$

$$\text{With } V = \{v\in H^1(\Omega)\,|\,v|_{\Gamma_1} = 0\}$$

$$V_g = \{\phi\in V\,|\,\rho(\phi)\frac{\partial\phi}{\partial n} = g|_{\Gamma_2}\}$$

$$\xi = \xi(\phi) \text{ via } (103)$$

$$\int_\Omega \vec{\nabla}\xi\cdot\vec{\nabla}\omega\,dx = \int_\Omega \rho(\phi)\vec{\nabla}\phi\cdot\vec{\nabla}\omega\,dx - \int_{\Gamma_2} g\,\omega\,d\Gamma \quad,\ \forall\,\omega\in V. \tag{103}$$

The physical interpretation of (103) is given in (104)

$$\Delta\xi = \vec{\nabla}\cdot\rho(\phi)\vec{\nabla}(\phi) \text{ in } \Omega \qquad \xi\in V \tag{104}$$

$$\rho(\phi)\frac{\partial\phi}{\partial n}\Big|_{\Gamma_2} = g \Longrightarrow \frac{\partial\xi}{\partial n}\Big|_{\Gamma_2} = 0\ .$$

7.2. Transonic Non Lifting Case

In the case of a transonic flow (18), in order to prevent non physical decompression shocks, a condition of entropy, which may be treated, must be added to (102) (103)

-either as a linear constraint of inequality (105) /42

$$\Delta\phi < K\ . \tag{105}$$

In this case, a penalty functional of type (106) must be added to (102)

$$\int_\Omega |(\Delta\phi-K)^+|^2\,dx \quad \text{where} \tag{106}$$

$$(\Delta\phi-K)^+ = \sup(0,\Delta\phi-K)$$

leading to the least squares method $(102)_p$ with <u>penalty</u>

$$\underset{\phi\in V}{\text{Min}}\ \frac{1}{2}\int_\Omega |\vec{\nabla}\xi|^2 dx + \mu\int_\Omega |(\Delta\phi - K)^+|^2 dx \qquad (102)_P$$ /42

with $\mu > 0$ and ξ solution of (103)

Two possible alternatives of $(102)_P$ are given in $(102)_{R1}$ and $(102)_{R2}$ with K=0 : this is a least squares method with <u>regularization</u>

$$\underset{\phi\in V}{\text{Min}}\ \frac{1}{2}\left\{\int_\Omega |\vec{\nabla}\xi|^2 dx + \mu\int_\Omega |(\Delta\phi)^+|^2 dx\right. \qquad (102)_{R1}$$

with $\mu > 0$ and ξ solution of (103)

$$\underset{\phi\in V}{\text{Min}}\ \frac{1}{2}\int_\Omega |\vec{\nabla}\xi|^2 dx + \mu_1\int_\Omega |\Delta\phi|^{+2}\, dx + \mu_2\int_\Omega [\vec{u}\cdot\vec{n}]^{+2}\, d\Omega \qquad (102)_{R2}$$

with $(\ )^+_+$ = positive intensity of a discontinuity = sup $(0, (\ ))$

-or by <u>artificial viscosity</u>, in this case the functional (102) remains unchanged, but $\xi = \xi(\phi)$ via $(103)_V$

$$\int_\Omega \vec{\nabla}\xi\cdot\vec{\nabla}\omega\, dx = \int_\Omega \rho(\phi)\vec{\nabla}\phi\cdot\vec{\nabla}\omega\, dx + \nu\int_\Omega \sigma(\phi)\omega\, dx - \int_{\Gamma_2} g\,\omega\, d\Gamma \qquad (103)_V$$

$\forall\omega\in V$; $\xi\in V$ σ defined in (19).

In the applications, $(102)_P$ is preferred to $(102)_R$ due to the sensitivity of μ in $(102)_R$. In both methods, μ is added to obtain a same magnitude for both terms of cost function. Finally, it is also possible to combine the regularization given in $(102)_R$ with the artificial viscosity $(103)_V$ to eliminate the numerical instabilities in the region of shock.

7.3. <u>Transonic Lifting Case</u>

By using the notations of 1.2 and by referring to the lifting flow shown on figure 3, the circulation ℓ of $\vec{u} = \vec{\nabla}\Phi$ around an airfoil is in general $\neq 0$. Thus, Φ is discontinuous and a cut (C) (figure 3) must be made.

Assuming $\mathring{\Omega} = \widehat{\bar{\Omega} - (C)}$ & JK : $\mathbb{R} \to \mathbb{R}$ the function defined by

$$JK(\ell) = |(\vec{\nabla}\Phi_\ell)_{BF^+}|^2 - |(\vec{\nabla}\Phi_\ell)_{BF^-}|^2 \qquad (107)$$

where (ℓ, ϕ_ℓ) is the solution of the physical problem (107), (108)

$$\begin{aligned}
&\vec{\nabla}\cdot\rho\vec{\nabla}\Phi_\ell = 0 \quad \text{in } \Omega \\
&\frac{\partial\Phi_\ell}{\partial n}\Big|_{\Gamma_\infty} = \vec{u}_\infty\cdot\vec{n} \ , \ \frac{\partial\Phi}{\partial n}\Big|_{\Gamma_P} = 0 \\
&\Phi_\ell|_{C^+} - \Phi_\ell|_{C^-} = \ell \ , \ \frac{\partial\Phi}{\partial n^+}\Big|_{C^+} + \frac{\partial\Phi}{\partial n^-}\Big|_{C^-} = 0
\end{aligned} \qquad (108)$$

The method of decomposition described in (49)-(54) is applied to the lifting transonic case.

By selecting the least squares method with regularization $(102)_R$ or artificial viscosity $(103)_V$, the following algorithm ϕ_ℓ is searched for in the form (109) /43

$$\phi_\ell = \phi_{NP} + \ell\phi_R \tag{109}$$

where ϕ_{NP} represents the NON LIFTING compressible part of the potential and $\ell\phi_R$ the LIFTING incompressible part of the potential. ϕ_R discontinuous on (C) is solution of $(49)_{NP}$. ϕ_ℓ is solution of two iterative algorithms (TRANSONIC FLOW CHART 1-2)

1. External fixed point algorithm defines ℓ solution of the non linear monodimensional equation (110)

$$JK(\ell) = 0 \tag{110}$$

2. Internal conjugate gradient algorithm gives ϕ_{NP}, at ℓ fixed, as solution of optimal control problem (111) (112)

INITIALIZATION (ξ^o, ℓ^o) (g^o, h^o)

ELEMENTARY LIFT — PORT?NCE ELEMENTAIRE ϕ_R

$$\Delta\phi_R = 0$$

$$\left.\frac{\partial\phi_R}{\partial n}\right|_{\Gamma_\infty \cup \Gamma_p} = 0$$

$$\phi_R^+ = \phi_R^- + 1 \quad (C)$$

$$\phi_R(BF) = 0$$

INCOMPRESSIBLE NON LIFTING — INCOMPRESSIBLE NON PORTANT ϕ_{NP}^o

$$\Delta\phi_{NP}^o = 0$$

$$\frac{\partial\phi_{NP}^o}{\partial n} = \begin{matrix} 0 & \Gamma_p \\ g & \Gamma_\infty \end{matrix}$$

$$\phi_{NP}^o(BF) = 0$$

INCOMPRESSIBLE LIFTING PREDICTOR — INCOMPRESSIBLE PORTANT (ϕ^o, ℓ^o) PREDICTEUR ξ^o

$$|\vec{\nabla}(\phi_{NP}^o + \ell^o\phi_R)^+|^2 = |\vec{\nabla}(\phi_{NP}^o + \ell^o\phi_R)^-|^2$$

$$\phi^o = \phi_{NP}^o + \ell^o\phi_R$$

$$\xi_{NP}^o = \phi_{NP}^o$$

PREDICTOR g^o, h^o IN H^1 — PREDICTEUR g^o, h^o DANS H^1

$$-\Delta g^o = J'(\xi_{NP}^o)$$

$$h^o = g^o$$

TRANSONIC LIFT FLOW CHART 1

?RGANIGRAMME TRANSSONIQUE PORTANT 1

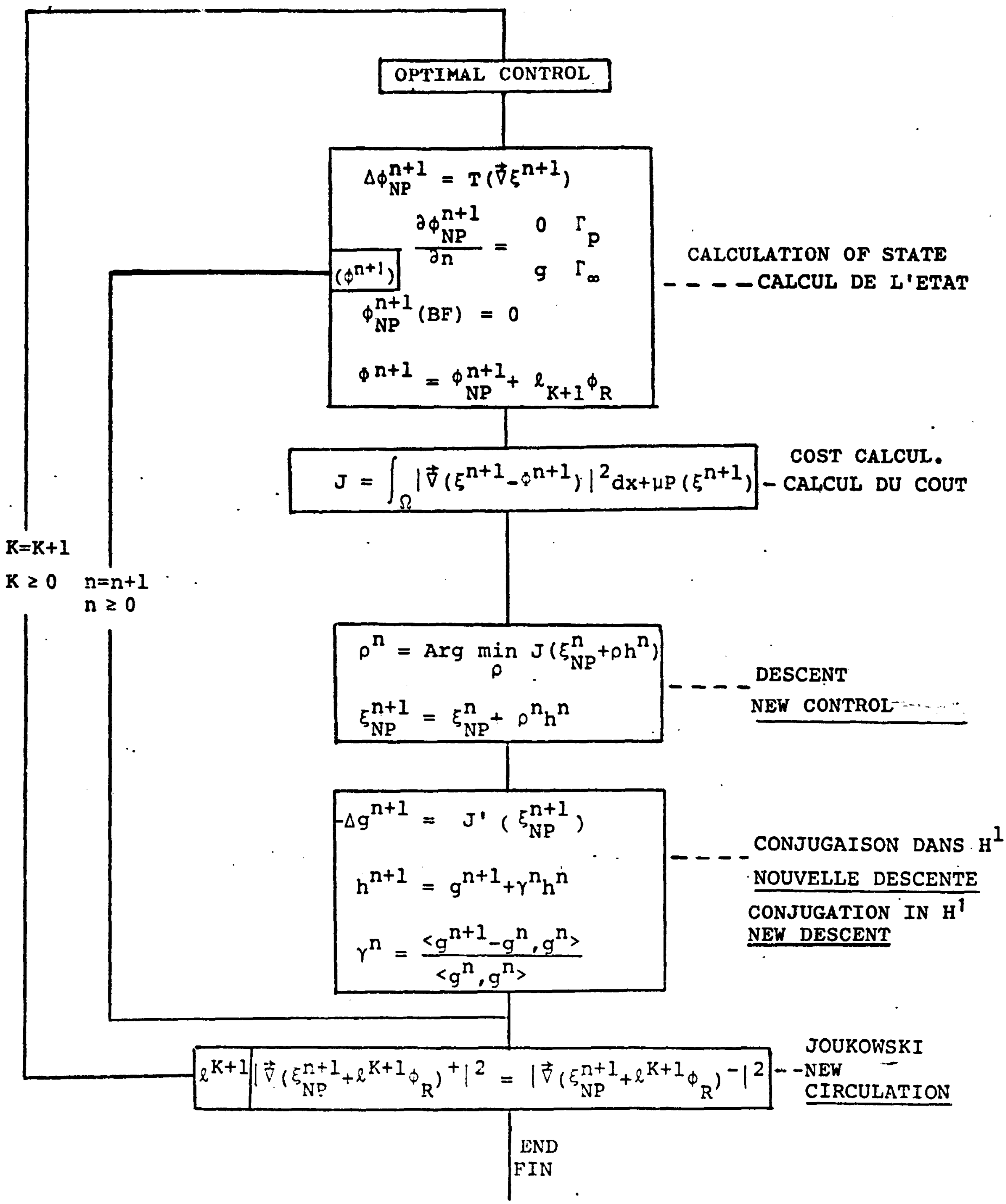

TRANSONIC LIFT FLOW CHART 2
ORGANIGRAMME TRANSSONIQUE PORTANT 2

$$\underset{\phi_{NP}\in V}{\mathrm{Min}} J_\ell^{n+1}(\phi_{NP}) = \frac{1}{2}\int_\Omega |\vec{\nabla}\xi|^2 dx + \mu\int_\Omega |(\Delta\phi_\ell^{n+1})^+|^2 \, dx \tag{111}$$

WITH $\xi = \xi(\phi_{NP})$ via (112), * $\phi^{n+1} = \phi_{NP} + \ell^{n+1}\phi_R$ *where

$$\int_\Omega \vec{\nabla}\xi\cdot\vec{\nabla}\omega \, dx = \int_\Omega \rho(\phi_\ell^{n+1})\vec{\nabla}\phi_\ell^{n+1}\cdot\vec{\nabla}\omega \, dx - \int_{\Gamma_2} g\omega \, d\Gamma \quad \forall\omega\in V \tag{112}$$

7.4. Conjugate Gradient Solution of Non Lifting Transonic Problem

46

For reasons of simplicity, we are limiting the problem to regularization $(102)_R$ i.e.

$$\underset{\phi\in V}{\mathrm{Min}} J(\phi) \tag{113}$$

with

$$J(\phi) = \frac{1}{2}\{\int_\Omega |\vec{\nabla}\xi|^2 dx + \mu\int_\Omega |(\Delta\phi)^+|^2 \, dx \tag{114}$$

where V and ξ defined in (102) (103).

In this case, the conjugate gradient algorithm similar to the one given in (86)-(93) consists of three phases :

1°) Initialization

ϕ^o is selected as solution of the incompressible flow i.e. (115)

$$\phi^o = 0 \text{ in } \Omega$$

$$\phi^o|_{\Gamma_1} = 0 \; , \; \rho\frac{\partial\phi^o}{\partial n}|_{\Gamma_2} = g \tag{116}$$

of which the variational formulation is given in (117)

$$\int_\Omega \vec{\nabla}\phi^o\vec{\nabla}\omega \, dx = \int_{\Gamma_2} \frac{g}{\rho}\omega \, d\Gamma \quad \forall\, \omega\in V \; ; \; \phi^o\in V \tag{117}$$

(if $\vec{u}$ is known on boundary Γ_2 , ρ is also known by $\rho = \rho_o(1-k|\vec{u}|^2)^\alpha$) since $g^o\in V$ is calculated as the solution of the variational equation (118)

$$\int_\Omega \vec{\nabla}g^o\cdot\vec{\nabla}\omega \, dx = \langle J'(\phi^o),\omega\rangle \quad \forall\, \omega\in V \; , \; g^o\in V \tag{118}$$

Accordingly, we set $h^o = g^o$.. Now for $n\geq 0$,, assuming ϕ^n, g^n, h^n as known, we compute $\phi^{n+1}, g^{n+1}, h^{n+1}$ in two phases.

2°) <u>Descent</u> to calculate ϕ^{n+1} by minimizing the functional to one single variable (119)

$$\lambda^n = \operatorname{Arg}\min_{\lambda \geq 0} J(\phi^n - \lambda h^n) \tag{119}$$

we can then set

$$\phi^{n+1} = \phi^n - \lambda^n h^n \tag{120}$$

3° <u>Construction of the New Direction of Descent</u>

Define $g^{n+1} \in V$ as the solution of the variational equation (121)

$$\int_\Omega \vec{\nabla} g^{n+1} \cdot \vec{\nabla}\omega \, dx = \langle J'(\phi^{n+1}), \omega \rangle \quad \forall \omega \in V, \; g^{n+1} \in V \tag{121}$$

calculate the coefficient of conjugation γ^{n+1} in the metric relating to V

$$\gamma^{n+1} = \frac{\int_\Omega \vec{\nabla} g^{n+1} \cdot \vec{\nabla}(g^{n+1} - g^n) dx}{\int_\Omega |\vec{\nabla} g^n|^2 \, dx} \tag{122}$$

set then

$$h^{n+1} = g^{n+1} + \gamma^{n+1} h^n \tag{123}$$

and return to (119)

<u>Note</u> : Each iteration requires on the average 5 solutions of the Dirichlet problems :

- 2 for the calculation of the gradient g^{n+1} in the good metric
- 3 on the average to calculate the optimal step

Let us now expand the calculation of $J'(\phi^{n+1})$

If $\langle \cdot, \cdot \rangle$ represents the duality between V' and V, by using (114)

$$\langle J'(\phi), \delta\phi \rangle = \underbrace{\int_\Omega \vec{\nabla}\xi \cdot \vec{\nabla}\delta\xi \, dx}_{①} + \mu \underbrace{\int_\Omega (\Delta\phi)^+ \Delta\delta\phi \, dx}_{②} \tag{124}$$

where $\delta\xi$ is the solution of the differentiated variational equation

$$\int_\Omega \vec{\nabla}\delta\xi \cdot \vec{\nabla}\omega \, dx = \int_\Omega \rho(\phi) \vec{\nabla}\delta\phi \cdot \vec{\nabla}\omega \, dx + \int_\Omega \delta\rho(\phi) \vec{\nabla}\phi \cdot \vec{\nabla}\omega \, dx \tag{125}$$

$$\forall \omega \in V, \; \delta\xi \in V$$

and $\delta\rho$ is expressed via the relationship $\rho(\phi) = (1-k|\vec{\nabla}\phi|^2)^\alpha$

$$\delta\rho(\phi) = -2k\alpha(1-k|\vec{\nabla}\phi|^2)^{\alpha-1} \vec{\nabla}\phi \cdot \vec{\nabla}\delta\phi \tag{126}$$

in (124) may then be expressed as a function of $\delta\phi$ with (126) and (125) written with $\omega = \xi$

$$\int_\Omega \vec{\nabla}\xi\vec{\nabla}\delta\xi \, dx = \int_\Omega \rho(\phi)\vec{\nabla}\xi\cdot\vec{\nabla}\delta\phi \, dx - 2k_\alpha\int_\Omega (\rho(\phi))^{1-1/\alpha}(\vec{\nabla}\phi\cdot\vec{\nabla}\xi)(\vec{\nabla}\phi\cdot\vec{\nabla}\delta\phi)dx \quad (127)$$

With (127) $\langle J'(\phi),\omega\rangle$ may then be identified with the linear functional

$$\omega \to \int_\Omega \rho(\phi)\vec{\nabla}\xi\cdot\vec{\nabla}\omega \, dx - 2k\alpha\int_\Omega (\rho(\phi))^{1-1/\alpha}(\vec{\nabla}\phi\cdot\vec{\nabla}\xi)(\vec{\nabla}\phi\cdot\vec{\nabla}\omega)dx + \mu\int_\Omega (\Delta\phi)^{+}\Delta\omega \, dx \quad (128)$$

From (121) (128) we obtain g^{n+1} from ϕ^{n+1} by solving

$$\begin{aligned}\int_\Omega \vec{\nabla}g^{n+1}\cdot\vec{\nabla}\omega \, dx = \int_\Omega [\rho(\phi^{n+1})\vec{\nabla}\xi^{n+1}\cdot\vec{\nabla}\omega - 2k\alpha \, (\rho(\phi^{n+1}))^{1-1/\alpha}(\vec{\nabla}\phi^{n+1}\cdot\vec{\nabla}\xi^{n+1})\times \\ (\vec{\nabla}\phi^{n+1}\cdot\vec{\nabla}\omega)] \, dx + \mu\int_\Omega (\Delta\phi^{n+1})^{+}\Delta\omega \, dx \quad , \quad \forall\, \omega\in V, \; g^{n+1}\in V\end{aligned} \quad (129)$$

with ξ^{n+1} solution of (103) corresponding to $\phi = \phi^{n+1}$.

8. - THE LEAST SQUARES METHOD IN H^{-1} APPLIED TO THE NAVIER-STOKES EQUATIONS

8.1. The Steady Case

8.1.1. Functional Least Squares Methcd of Steady Navier-Stokes Equations

In the following, we shall designate by (130) the scalar product $\langle\cdot,\cdot\rangle$ of two functions $\vec{u},\vec{v}\in(H^1(\Omega))^N$ N standing for the dimension of the space

$$\langle\vec{u},\vec{v}\rangle = \int_\Omega \vec{\nabla}\vec{u}\cdot\vec{\nabla}\vec{v} \, dx = \sum_{i=1}^{N}\int_\Omega \vec{\nabla}u_i\cdot\vec{\nabla}v_i \, dx \, , \; \forall\, \vec{u},\vec{v}\in(H^1(\Omega))^N \quad (130)$$

$\vec{u} = \{u_i\}_{i=1}^N$, $\vec{v} = \{v_i\}_{i=1}^N$.

Let us define $W_{\vec{z}}$ in (131)

$$W_{\vec{z}} = \{\vec{v}\in(H^1(\Omega))^N, \; \vec{\nabla}\cdot\vec{v} = 0 \;\text{ in } \Omega \, , \; \vec{v}|_\Gamma = \vec{z}\} \quad (131)$$

Then the variational formulation of the unsteady (132) Navier-Stokes problem

$$\begin{aligned} -\nu\Delta\vec{u} + (\vec{u}\cdot\vec{\nabla})\vec{u} + \vec{\nabla}p &= 0 \qquad (\Omega) \\ \vec{\nabla}\cdot\vec{u} &= 0 \qquad (\Omega) \\ \vec{u}|_\Gamma &= \vec{z} \end{aligned} \quad (132)$$

is given in (133)

$$\nu\int_\Omega \vec{\nabla}\vec{u}\cdot\vec{\nabla}\vec{v}\ dx + \int_\Omega \vec{v}\cdot(\vec{u}\cdot\vec{\nabla})\vec{u}\ dx = 0 \quad \forall\ \vec{v}\in W_{\vec{0}},\ \vec{u}\in W_{\vec{z}}\ . \tag{133}$$

49

A least squares method of (132) (133) is given by the optimal control problem (134)

$$\min_{\vec{v}\in W_{\vec{z}}} \{J(\vec{v}) = \frac{\nu}{2}\int_\Omega |\vec{\nabla}(\vec{\xi}-\vec{v})|^2\ dx\ \} \tag{134}$$

where $\vec{\xi}$ in (134) is a function of $\vec{v}$ via the state equation (135)

$$\begin{aligned} &-\Delta\vec{\xi}+\vec{\nabla}\pi = -(\vec{v}\cdot\vec{\nabla})\vec{v} && (\Omega)\\ &\vec{\nabla}\cdot\vec{\xi} = 0 && (\Omega)\\ &\vec{\xi}|_\Gamma = \vec{z} && \end{aligned} \tag{135}$$

of which the variational formulation is given in (136)

$$\nu\int_\Omega \vec{\nabla}\vec{\xi}\cdot\vec{\nabla}\vec{\eta}\ dx = -\int_\Omega \vec{\eta}\cdot(\vec{v}\cdot\vec{\nabla})\vec{v}\ dx \quad \forall\ \vec{\eta}\in W_0,\ \vec{\xi}\in W_{\vec{z}} \tag{136}$$

It is essential to note that (135) (136) is a Stokes problem, acting as a pressure in (135)

8.1.2. <u>Conjugate Gradient Solution of</u> (134) (136)

The algorithm is composed of 3 phases:

i) **Initialization :**

Take for $\vec{u}^o$ the solution of the Stokes problem (137)

$$\begin{aligned} &-\nu\Delta\vec{u}^o + \vec{\nabla}p^o = 0 && (\Omega)\\ &\vec{\nabla}\cdot\vec{u}^o = 0 && (\Omega)\\ &\vec{u}^o = \vec{z} && \end{aligned} \tag{137}$$

of which the variational formulation is given in (138)

$$\nu\int_\Omega \vec{\nabla}\vec{u}^o\cdot\vec{\nabla}\vec{\eta}\ dx = 0 \quad \forall\ \vec{\eta}\in W_o\ ,\ \vec{u}^o\in W_{\vec{z}} \tag{138}$$

Take for $\vec{g}^{o} \in W_o$ the solution of the variational equation (139)

$$\int_\Omega \vec{\nabla}\vec{g}^{o} \cdot \vec{\nabla}\vec{\eta}\, dx = \langle J'(\vec{u}^{o}), \vec{\eta} \rangle \quad \forall\, \vec{\eta} \in W_o \;,\; \vec{g}^{o} \in W_o \tag{139}$$

and set $\vec{h}^{o} = \vec{g}^{o}$. ∠50

For $n \geq 0$, assuming as known, calculate by

ii) descent phase (140) (144)

$$\lambda^n = \operatorname{Arg}\min_{\lambda > 0} J(\vec{u}^{n} - \lambda \vec{h}^{n}) \tag{140}$$

$$\vec{u}^{n+1} = \vec{u}^{n} - \lambda^n \vec{h}^{n} \tag{141}$$

iii) phase of constructing the new descent direction

Take for $\vec{g}^{n+1} \in W_o$ the solution of the variational equation (142)

$$\int_\Omega \vec{\nabla}\vec{g}^{n+1} \cdot \vec{\nabla}\vec{\eta}\, dx = \langle J'(\vec{u}^{n+1}), \vec{\eta} \rangle \quad \forall\; \vec{\eta} \in W_o ,\; \vec{g}^{n+1} \in W_o \tag{142}$$

Calculate γ^{n+1} in (143)

$$\gamma^{n+1} = \frac{\int_\Omega \vec{\nabla}\vec{g}^{n+1} \cdot \vec{\nabla}(\vec{g}^{n+1} - \vec{g}^{n})\, dx}{\int_\Omega |\vec{\nabla} g^n|^2\, dx} \tag{143}$$

The new direction of descent $\vec{h}^{n+1}$ is given in (144)

$$\vec{h}^{n+1} = \vec{g}^{n+1} + \gamma^{n+1} \vec{h}^{n} \tag{144}$$

do n=n+1 and go in ii).

It may be observed that (139) (140) (141) are Stokes problems.

8.1.3. Calculations of J' and of $\vec{g}^{n+1}$.

By definition, the calculation of J' is given in (145)

$$\delta J = \langle J'(\vec{v}), \delta\vec{v} \rangle = \nu \int_\Omega \vec{\nabla}(\vec{v} - \vec{\xi}) \cdot \vec{\nabla}\delta(\vec{v} - \vec{\xi})\, dx \tag{145}$$

It is possible to express $\delta\vec{\xi}$ as a function of $\delta\vec{v}$ by using the differentiation of (136)

$$\nu \int_\Omega \vec{\nabla} \vec{\delta\xi} \cdot \vec{\nabla} \vec{\eta} \, dx = \int_\Omega \vec{\eta} \cdot [(\vec{\delta v} \cdot \vec{\nabla}) \vec{v} + (\vec{v} \cdot \nabla) \vec{\delta v}] \, dx \quad \forall \vec{\eta} \in W_o \; ; \; \delta\vec{\xi} \in W_o \tag{146}$$

Since $(\vec{v}-\vec{\xi}) \in W_o$, let us select $\vec{\eta} = \vec{v}-\vec{\xi}$ in (146) and $\delta\vec{v} = \vec{\eta}$ in (145) which is expressed :

$$\langle J'(\vec{v}), \vec{\eta} \rangle = \nu \int_\Omega \vec{\nabla}(\vec{v}-\vec{\xi}) \vec{\nabla} \eta \, dx + \int_\Omega [(\vec{v}-\vec{\xi}) \cdot (\vec{v} \cdot \vec{\nabla}) \vec{\eta} + (\vec{v}-\vec{\xi}) \cdot (\vec{\eta} \cdot \vec{\nabla}) \vec{v}] \, dx \tag{147}$$

$$\forall \vec{\eta} \in W_o$$

To calculate $\vec{g}^{n+1}$, we must therefore begin by $\langle J'(\vec{u}^{n+1}), \vec{\eta} \rangle$ which requires the solution of the state equation (145) for $\vec{v} = \vec{u}^{n+1}$ giving $\vec{\xi}^{n+1}$ (147) may then be expressed in (148)

$$\langle J'(\vec{u}^{n+1}), \vec{\eta} \rangle = \nu \int_\Omega \vec{\nabla}(\vec{u}^{n+1} - \vec{\xi}^{n+1}) \cdot \vec{\nabla} \vec{\eta} \, dx + \int_\Omega [(\vec{u}^{n+1} - \vec{\xi}^{n+1}) \cdot (\vec{u}^{n+1} \cdot \vec{\nabla}) \vec{\eta} + \tag{148}$$

$$+ (\vec{u}^{n+1} - \vec{\xi}^{n+1}) \cdot (\vec{\eta} \cdot \vec{\nabla}) \vec{u}^{n+1}] \, dx$$

Finally $\vec{g}^{n+1}$ is given by (142).

In conclusion, each optimal control iteration requires <u>several Stokes</u> problems :

- Stokes problem (136) to calculate the state $\vec{\xi}^{n+1}$ from $\vec{u}^{n+1}$
- Stokes problem (142) to calculate the gradient $\vec{g}^{n+1}$ from $\vec{u}^{n+1}$ and $\vec{\xi}^{n+1}$
- Stokes problem (140) to calculate λ.

Furthermore, an <u>efficient</u> Stokes algorithm shall prove to be a particularly important tool in the solution of the Navier-Stokes equations via the least squares method (134)-(136). Its implementation shall be described later on in paragraph 8.3.

8.2. The Unsteady Case

8.2.1. Formulation of the Unsteady Navier-Stokes Problem

As was presented in paragraph 4, the unsteady Navier-Stokes problem consists of (149) (150) (151)

$$\begin{cases} \dfrac{\partial \vec{u}}{\partial t} - \nu\Delta\vec{u} + (\vec{u}\cdot\vec{\nabla})\vec{u} + \vec{\nabla}p = 0 & (\Omega) \\ \vec{\nabla}\cdot\vec{u} = 0 & (\Omega) \end{cases} \tag{149}$$

$$\vec{u}|_{\Gamma} = \vec{z} \ ; \ \int_{\Gamma} \vec{z}\cdot\vec{n}\, d\Gamma = 0 \qquad (\Gamma) \tag{150}$$

$$\vec{u}(x,0) = \vec{u}_o(x) \tag{151}$$

where the function $\vec{z}$, given, may eventually depend on t.

8.2.2. Quantification in Time of the Problem (149) (150) (151)

Several schemes may be used to solve (149) (150) (151). For reasons of simplification, we are presenting two very simple ones with a constant quantification time step. 52

8.2.2.1. Semi-implicit Scheme

Assuming $k = \Delta t$ the quantification time step. A semi-implicit scheme in time, which is very simple, is given by

$$\text{i)} \quad \vec{u}^o = \vec{u}_o \text{ given} \tag{152}$$

then for $n \geq 0$, $\vec{u}^{n+1}$ is obtained from $\vec{u}^n$ by solving (153)

$$\text{ii)} \begin{cases} \dfrac{\vec{u}^{n+1} - \vec{u}^n}{k} - \nu\Delta\vec{u}^{n+1} + \vec{\nabla}p^{n+1} = \boxed{-(\vec{u}^n\cdot\vec{\nabla})\vec{u}^n} & (\Omega) \\ \vec{\nabla}\cdot\vec{u}^{n+1} = 0 \quad (\Omega) \\ \vec{u}^{n+1}|_{\Gamma} = \vec{z}^{n+1} = \vec{z}((n+1)k) \end{cases} \tag{153}$$

with $\vec{u}^n$ in (153) an approximation of $\vec{u}(nk)$ where $\vec{u}$ is the solution of (149) (151). It may be noted that in (153) $\vec{u}^{n+1}$ is obtained from $\vec{u}^n$ by solving a linear problem, variant of the steady Navier-Stokes problem 8.1 (here also the operator $S = -\nu\Delta$ is substituted by $S_k = \dfrac{Id}{k} - \nu\Delta$). Accordingly, it is necessary to develop an efficient Stokes algorithm relating to S_k in order to solve (149) (150) (151).

8.2.2.2. Implicit Scheme

The simplest implicit scheme for solving (149) (151) consists of /52

$$\text{i)} \quad \vec{u}^{\,o} = \vec{u}_o \ \text{ given} \tag{154}$$

Then for $n \geq 0$, $\vec{u}^{\,n+1}$ is obtained from $\vec{u}^{\,n}$ by solving (155)

$$\text{ii)} \begin{cases} \dfrac{\vec{u}^{\,n+1} - \vec{u}^{\,n}}{k} - \nu\Delta\vec{u}^{\,n+1} + \boxed{(\vec{u}^{\,n+1}\cdot\vec{\nabla})\vec{u}^{\,n+1}} + \vec{\nabla}p^{n+1} = 0 & (\Omega) \\ \vec{\nabla}\cdot\vec{u}^{\,n+1} = 0 & (\Omega) \\ \vec{u}^{\,n+1}\big|_\Gamma = \vec{z}^{\,n+1} \end{cases} \tag{155}$$

It may be observed that in (155) $\vec{u}^{\,n+1}$ is obtained from $\vec{u}^{\,n}$ by solving a NON LINEAR problme, variant of the steady Navier-Stokes problem 8.1 (here also, the operator $S = -\nu\Delta$ is substituted by $S_k = \frac{Id}{k} - \nu\Delta$) . It is from (155) that we shall present a least squares method similar to that given in 8.1 for the steady problem.

4

8.2.3. Abstract Least Squares Method from (155)

In fact (155) is a special case of a family of non linear problems S_α $(\alpha > 0)$ (156) /52

$$\begin{aligned}
&\alpha\vec{u} - \nu\Delta\vec{u} + (\vec{u}\cdot\vec{\nabla})\vec{u} + \vec{\nabla}p = \vec{f} && (\Omega)\\
&\vec{\nabla}\cdot\vec{u} = 0 && (\Omega)\\
&\vec{u}|_\Gamma = \vec{z} \text{ avec } \int_\Gamma \vec{z}\cdot\vec{n}\, d\Gamma = 0 && (\Gamma)
\end{aligned} \tag{156}$$

of which the variational formulation is given in (157)

$$\alpha\int_\Omega \vec{u}\cdot\vec{v}\, dx + \nu\int_\Omega \vec{\nabla}\vec{u}\cdot\vec{\nabla}\vec{v}\, dx + \int_\Omega \vec{v}\cdot(\vec{u}\cdot\vec{\nabla})\vec{u}\, dx = \int_\Omega \vec{f}\cdot\vec{v}\, dx,\ \forall\vec{v}\in W_0\ ;\ \vec{u}\in W_{\vec{z}} \tag{157}$$

By following 8.1 an optimal control least squares method of (156) (157) is given in (158)

$$\operatorname*{Min}_{\vec{v}\in W_{\vec{z}}} J(\vec{v}) = \frac{\alpha}{2}\int_\Omega |\vec{v}-\vec{\xi}|\, dx + \frac{\nu}{2}\int_\Omega |\vec{\nabla}(\vec{v}-\vec{\xi})|^2\, dx$$

where $\vec{\xi}$ is a function of $\vec{v}$ via the state equation (159)

$$\begin{aligned}
&\alpha\vec{\xi} - \nu\Delta\vec{\xi} + \vec{\nabla}\pi = \vec{f} - (\vec{v}\cdot\vec{\nabla})\vec{v} && (\Omega)\\
&\vec{\nabla}\cdot\vec{\xi} = 0 && (\Omega)\\
&\vec{\xi}|_\Gamma = \vec{z}
\end{aligned} \tag{159}$$

π, acting as a pressure.

8.2.4. Conjugate Gradient Solution of (158) (159)

Tracing paragraph 8.1.2., the conjugate gradient algorithm for solving the least squares problem (158) (159) is given by

i) $\vec{u}^0 \in W_{\vec{z}}$, given (160)

calculate g^0 solution of the variational equation

$$\alpha\int_\Omega \vec{g}^o\cdot\vec{\eta}\,dx + \nu\int_\Omega \vec{\nabla} g^o\cdot\vec{\nabla}\vec{\eta}\,dx = \langle J'(\vec{u}^o),\vec{\eta}\rangle \;,\; \forall\,\vec{\eta}\in W_o \;;\; g^o\in W_o \tag{161}$$ ∠53

and set $\vec{h}^o = \vec{g}^o$.

Then, for $m\geq 0$, assuming $\vec{u}^m,\vec{g}^m,\vec{h}^m$ as known, calculate $\vec{u}^{m+1},\vec{g}^{m+1},\vec{h}^{m+1}$ by

ii) Descent Phase

$$\lambda^m = \operatorname*{Arg\,min}_{\lambda>0} J(\vec{u}^m - \lambda\vec{h}^m) \tag{162}$$

$$\vec{u}^{m+1} = \vec{u}^m - \lambda^m\vec{h}^m \tag{163}$$ ∠54

iii) Phase of constructing the new direction of descent

Define g^{m+1} solution of the variational equation (164)

$$\alpha\int_\Omega \vec{g}^{m+1}\cdot\vec{\eta}\,dx + \nu\int_\Omega \vec{\nabla}\vec{g}^{m+1}\cdot\vec{\nabla}\vec{\eta}\,dx = \langle J'(\vec{u}^{n+1}),\vec{\eta}\rangle \;,\; \forall\,\vec{\eta}\in W_o,\; \vec{g}^{n+1}\in W_o \tag{164}$$

then
$${}^{m+1} = \frac{\alpha\int_\Omega \vec{g}^{m+1}\cdot(\vec{g}^{m+1}-\vec{g}^m)\,dx + \nu\int_\Omega \vec{\nabla}\vec{g}^{m+1}\cdot\vec{\nabla}(\vec{g}^{m+1}-\vec{g}^m)\,dx}{\alpha\int_\Omega |\vec{g}^m|^2\,dx + \nu\int_\Omega |\vec{\nabla}\vec{g}^m|^2\,dx}$$

the new direction of descent $\vec{h}^{m+1}$ is then

$$\vec{h}^{m+1} = \vec{g}^{m+1} + \gamma^{m+1}\vec{h}^m \tag{165}$$

do m=m+1 and go in ii).

The calculation of $J'(\vec{u}^{m+1})$ is not detailed, as it is a trivial variant of 8.1.3.

In a similar manner as the algorithm (137)- 144), each iteration of (160) (165) requires the solution of several Stokes problems S_k of type (149) without non linear term.

- the Stokes problem S_k to obtain $\vec{\xi}^{m+1}$ from $\vec{u}^{m+1}$
- the Stokes problem S_k to obtain $\vec{g}^{m+1}$ from $\vec{u}^{m+1}$, $\vec{\xi}^{m+1}$
- the Stokes problems S_k to calculate λ^n.

Note : The algorithm -m (160)-(165) permits the calculation $\vec{u}^{n+1}$ from $\vec{u}^n$ as a result $(\vec{u}^{n+1,m})$ is initialized in (160) by $\vec{u}^{n+1,o} =$

8.3. A Rapid Stokes Algorithm (The Continuous Case).

8.3.1. Summary

Paragraphs 8.1 and 8.2 have demonstrated the necessity of developing an efficient Stokes algorithm S_α defined in (166)

$$\begin{aligned} &\alpha\vec{u} - \Delta\vec{u} + \vec{\nabla}p = \vec{f} \qquad (\Omega) \\ &\vec{\nabla}\cdot\vec{u} = 0 \qquad (\Omega) \\ &\vec{u}|_\Gamma = \vec{z} \end{aligned} \tag{166}$$

55

for solving the steady and unsteady Navier Stokes equations. In (166) $\alpha=0$ corresponds to the steady case, whereas $\alpha > 0$ corresponds to the unsteady case.

We shall show that the solution of (166) by following GLOWINSKI-PIRONNEAU (18)(19)(49) is reduced to the decomposition of the solution into a finite number of Dirichlet problems coupled with an integral equation.

8.3.2. Principles of the Method

Let us note that by taking the divergence $\vec{\nabla}$ of the first equation of (166), we obtain an equation on pressure of type (167)

$$\Delta p = \vec{\nabla}\cdot\vec{f} \tag{167}$$

If we know $p|_\Gamma = \lambda$ then the solution $(\vec{u},p)$ of (166) should be obtained by solving the N+1 Dirichlet problems (168) (169)

$$\begin{aligned} &\Delta p = \vec{\nabla}\cdot\vec{f} \qquad (\Omega) \\ &p|_\Gamma = \lambda \end{aligned} \tag{168}$$

$$\begin{aligned} &\alpha u_i - \Delta u_i = -\frac{\partial p}{\partial x_i} + f_i \quad (\Omega) \quad i=1,\dots,N \quad N = \text{dimension of the space} \\ &u_i|_\Gamma = z_i \end{aligned} \tag{169}$$

But we don't know λ !

The introduction of ϕ solution of (170) will make it possible to SET λ, i.e. the pressure trace on the edge, so that the constraint distributed $\vec{\nabla}\cdot\vec{u} = 0$ is satisfied.

$$-\Delta\phi = \vec{\nabla}\cdot\vec{u} \qquad (\Omega) \tag{170}$$
$$\phi|_\Gamma = 0$$

In fact, by applying the laplacien Δ at (170), we obtain (171) via (166)

$$-\Delta(\Delta\phi) = \Delta(\vec{\nabla}\cdot\vec{u}) = \vec{\nabla}\cdot(\Delta\vec{u}) = \quad \Delta p - \vec{\nabla}\cdot\vec{f} + \alpha\vec{\nabla}\cdot\vec{u} \tag{171}$$

$$\begin{cases} \Delta^2\phi + \alpha\Delta\phi = 0 & (\Omega) \\ \phi|_\Gamma = 0 \end{cases} \tag{172}$$

If we now select λ so that $\frac{\partial\phi}{\partial n} = 0$, then after (172) $\phi \equiv 0$ and therefore $\vec{\nabla}\cdot\vec{u} = 0$. The application $\lambda \to \frac{\partial\phi_\lambda}{\partial n}|_\Gamma$ via (168) (169) (170) being affine, there is (A,b) (A linear operator, b constant) so that (173) occurs /56

$$\frac{\partial\phi}{\partial n}|_\Gamma = A\lambda + b \tag{173}$$

Also, the (N+1 Dirichlet problems (168) (169) coupled with the integral equation (174)

$$A\lambda + b = \dot{0} \tag{174}$$

give the solution $(\vec{u},p)$ of the problem (166). Let us point out that the good conditioning of the operator A is necessary to solve (174) easily.

8.3.3. Functional Support of the Method

To define (A,b) in (173), it is necessary to introduce

$$\mathcal{H}^{1/2}(\Gamma) = \{\mu \in H^{1/2}(\Gamma), \int_\Gamma \mu d\Gamma = 0\} \tag{175}$$

The method of decomposing the Stokes algorithm is then based on the following result :

<u>Theorem 8.3.3.1.</u> : Assuming $\lambda \in H^{-1/2}(\Gamma)$; assuming $H^{-1/2}(\Gamma) \to H^{1/2}(\Gamma)$ the linear operator defined by

$$\Delta p_\lambda = 0 \quad (\Omega) \;;\; p_\lambda \in H^1(\Omega) \quad p_\lambda - \lambda \in H^1_o(\Omega) \tag{176}$$

$$\alpha\vec{u}_\lambda - \Delta\vec{u}_\lambda = -\vec{\nabla}p_\lambda \quad (\Omega) \quad ; \vec{u}_\lambda \in (H^1_o(\Omega))^N \tag{177}$$

$$\begin{cases} -\Delta\phi_\lambda = \vec{\nabla}\cdot\vec{u}_\lambda & (\Omega) \quad \phi_\lambda \in H^1_o(\Omega) \\ A_\lambda = -\frac{\partial\phi_\lambda}{\partial n}|_\Gamma \end{cases} \tag{178}$$

Therefore A is an isomorphism of $H^{-1/2}(\Gamma)/\mathbb{R}$ on $H^{1/2}(\Gamma)$ and also the bilinear form $a(\cdot,\cdot)$ defined by (179)

$$a(\lambda,\mu) = \langle A\lambda,\mu\rangle \tag{179}$$

where $\langle\cdot,\cdot\rangle$ designates the duality product between $H^{1/2}(\Gamma)$ and $H^{-1/2}(\Gamma)$ is continuous, symmetrical and highly elliptical in $H^{-1/2}(\Gamma)/\mathbb{R}$.

The application of theorem 8.3.3.1. to the solution of the Stokes problem will now be possible thanks to theorem 8.3.3.2.

Let $\vec{f} \in (L^2(\Omega))^N$; & $p_o, \vec{u}_o, \phi_o$ defined by

$$\Delta p_o = \vec{\nabla}\cdot\vec{f} \quad (\Omega) \quad ; \; p_o \in H_o^1(\Omega) \tag{180}$$

$$\alpha\vec{u}_o - \Delta\vec{u}_o = \vec{f} - \vec{\nabla} p_o \quad (\Omega) \quad ; \; \vec{u}_o - \vec{z} \in (H_o^1(\Omega))^N \tag{181}$$

$$-\Delta\phi_o = \vec{\nabla}\cdot\vec{u}_o \quad (\Omega) \quad ; \; \phi_o \in H_o^1(\Omega) \tag{182}$$

<u>Theorem 8.3.3.2.</u> : If $(\vec{u},p)$ is the solution of the Stokes problem (166), then the trace λ of p_Γ is the solution of the <u>linear</u> variational equation (E)

$$(E) \begin{cases} \lambda \in H^{-1/2}(\Gamma)/\mathbb{R} \\ \langle A\lambda,\mu\rangle = \langle \dfrac{\partial\phi_o}{\partial n},\mu\rangle \quad \forall\, \mu \in H^{-1/2}(\Gamma)/\mathbb{R} \end{cases} \tag{183}$$

The demonstration of these theorems is given in R. GLOWINSKI-O. PIRONNEAU (18).

<u>Notes</u> :

1) Theorems 8.3.3.1. - 8.3.3.2. show that the Stokes problem (166) may be decomposed into a <u>finite</u> number of Dirichlet problems $(-\Delta)$ (resp. $\alpha Id-\Delta$) ($N+2$ to obtain ϕ_o, $N+1$ to obtain $\{\vec{u},p\}$ when λ is <u>known</u> plus the problem (E) ;

2) In the approximation (E_h) of (E) $\frac{\partial\phi_o}{\partial n}$ shall not occur explicitely due to the Green formula applied in (184) if μ is sufficiently steady.

$$\left\langle \frac{\partial \phi_o}{\partial n}, \mu \right\rangle = \int_\Omega \vec{\nabla}\phi_o \cdot \vec{\nabla}\tilde{\mu}\, dx - \int_\Omega \vec{\nabla}\cdot\vec{u}_o\, \tilde{\mu}\, dx$$

$$= \int_\Omega (\vec{\nabla}\phi_o + \vec{u}_o)\cdot\vec{\nabla}\tilde{\mu}\, dx \qquad (184)$$ /58

where $\tilde{\mu}$ designates a steady rise of μ in Ω.

3) The main difficulty lies in the fact that the operator A is not explicitely known.

To overcome this difficulty, a new variational formulation of the Stokes problem shall be used in the approximation of (E), requiring a quantification into mixed finite elements.

8.3.4. Mixed Variational Formulation of the Stokes Algorithm

Let us introduce

$$W_{\vec{z}} = \{\{v,\phi\} \in (H^1(\Omega))^N \times H^1_o(\Omega),\ \vec{v}|_\Gamma = \vec{z},\ \int_\Omega \vec{\nabla}\phi\vec{\nabla}\omega\, dx = \int_\Omega \vec{\nabla}\cdot\vec{v}\ \omega\, dx,\ \forall\omega \in H^1(\Omega)$$

$$W_o = \{\{\vec{v},\phi\} \in (H^1_o(\Omega))^{N+1},\ \int_\Omega \vec{\nabla}\phi\cdot\vec{\nabla}\omega\, dx = \int_\Omega \vec{\nabla}\cdot\vec{v}\ \omega\, dx \quad \forall\omega \in H^1(\Omega)\} \qquad (185)$$

It is easy to demonstrate proposition 8.3.4.1. :

If $\{\vec{v},\phi\} \in W_{\vec{z}}$, then $\{\vec{v},\phi\}$ solution of (186)

$$-\Delta\phi = \vec{\nabla}\cdot\vec{v} \quad (\Omega) \quad ;\ \phi = \frac{\partial\phi}{\partial n} = 0 \quad (\Gamma) \qquad (186)$$

We have only to use the definition of W_z and the Green formula in (185). Let us consider the variational problem (P) (187)

Find $\{\vec{u},\psi\} \in W_z$ so that

$$\alpha\int_\Omega \vec{u}\cdot\vec{v}\, dx + \int_\Omega \vec{\nabla}\vec{u}\cdot\vec{\nabla}\vec{v}\, dx = \int_\Omega \vec{f}\cdot(\vec{v}+\vec{\nabla}\phi)\, dx,\ \forall\{\vec{v},\phi\} \in W_o \qquad (187)\ (P)$$

Theorem 8.3.4.2. : (P) has only one solution $\{\vec{u},\psi\}$ where $\psi = 0$ and $\vec{u}$ is the solution of the Stokes problem (166). The demonstration of this theorem is given in R. GLOWINSKI-O. PIRONNEAU (19) shows that (P) is a mixed formulation which is interpreted below :

If $\vec{v} \in (H^1(\Omega))^N$ and Γ is sufficiently steady $\exists\phi \in H^2(\Omega) \cap H^1_o(\Omega)$ and $\vec{\omega} = \vec{\nabla}\wedge\vec{\chi} \in (H^1(\Omega))^N$ so that the decompostion (188) is the only one.

$$\vec{v} = -\vec{\nabla}\phi \oplus \vec{\omega} \tag{188}$$

In the formulation (P), insteady of setting directly $\vec{\nabla}\cdot\vec{v} = 0$ we try to set $\phi \equiv 0$, which is equivalent in the continuous case, but not in the discrete case. The approximation of $(P)_h$ from (P) via the mixed finite elements shall be presented in paragraph 10.

9. - APPROXIMATION BY THE FINITE ELEMENTS METHOD OF THE TRANSONIC FLOWS

9.1. Summary

In this paragraph the approximations by the Lagrange finite elements of the transonic flows considered in paragraph 7 are briefly reviewed. Refer to the works of M.O. BRISTEAU (6), (20) (38) and R. GLOWINSKI and O. PIRONNEAU (21) for more details.

For reasons of simplicity, only external flows around airfoils shall be considered.

9.2. 2-D Flows

9.2.1. Case of Non Lifting Airfoils (profiles)

The situation is summarized on figure 15.

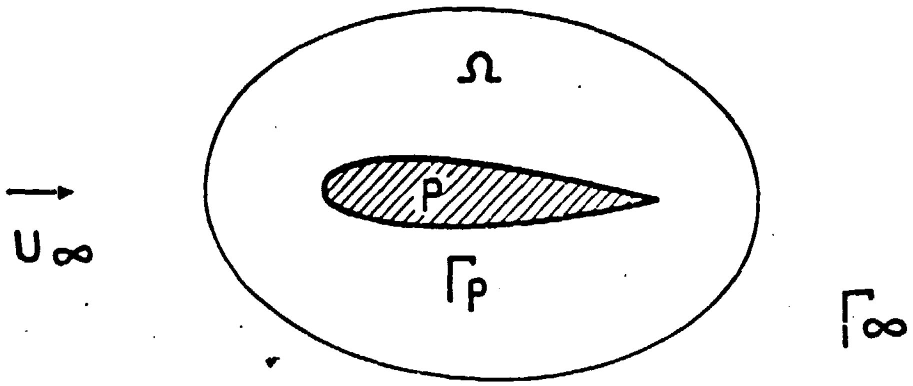

Figure 15

The transonic flow around a symmetrical airfoil P is without incidence ($\vec{u}_\infty$ parallel to the chord of the airfoil) and is modeled by the relationships of paragraphs 7.1, 7.2. The flow symmetry results in automatic satisfaction of the Joukowski condition (107).

9.2.1.1. Approximation of the Space V

By retaking the definition (189) of the space V in 7.1, 7.2

$$V = \{\phi \in H^1(\Omega) \cap C^0(\bar{\Omega}),\ \phi = 0 \text{ at trailing edge} \tag{189}$$

If Ω_h d signates a polygonal approximation of the domain Ω occupied by the fluid and if $\mathcal{T}_h$ is the set of triangles (T_k) or TRIANGULATION such that, in a standard way /60

$$\bar{\Omega}_h = \bigcup_k T_k \ ;\ T_i \cap T_j = \phi \ \text{if } i \neq j \tag{190}$$

then V is approximated by the space of the finite dimension V_h

$$V_h = \{\phi_h \in C^0(\bar{\Omega}_h),\ \phi_h|T \in P_k \quad \forall\, T \in \mathcal{T}_h,\ \phi_h = 0 \text{ at trailing edge} \tag{191}$$

Similarly, if we define V_{hg} by $(191)_g$

$$V_{hg} = \{\phi_h \in V_h \mid \rho(\phi_h)\ \frac{\partial \phi_n}{\partial n} = g\ \} \tag*{$(191)_g$}$$

In (191) P_k designates the space of polynomials with two variables with degree $\leq k$. In practice, the numerical tests require k=1 or 2.

9.2.1.2. Approximation of the State Equation

The state equation expressed in (103) is approached in (192)

$$\int_{\Omega_h} \vec{\nabla}\xi_h \cdot \vec{\nabla}\omega_h \, dx = \int_{\Omega_h} \rho(\phi_h)\ \vec{\nabla}\phi_h \cdot \vec{\nabla}\omega_h \, dx - \int_{\Gamma_h} g_h\, \omega_h \, d\Gamma_h \tag{192}$$

$$\phi_h \in V_{hg}\ ,\ \forall\, \omega_h \in V_h$$

where g_h is a suitable approximation of g on the edge Γ_h.

If <u>k=1</u> $\vec{\nabla}\phi_h$, $\vec{\nabla}\omega_h$ are piece-wise constant over each $T \in \Omega_h$, conquently, $\rho(\phi_h)$ is also constant and (192) may be calculated accurately.

If <u>k=2</u>, $\vec{\nabla}\phi_h$, $\vec{\nabla}\omega_h$ are piece-wise linear and a numerical integration of $\rho(\phi_h)$ is necessary. We may proceed as follows : each is divided into 4 sub-triangles (Figure 16)

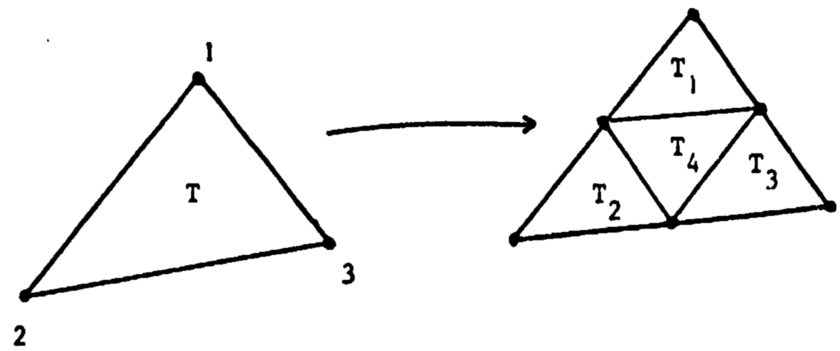

Figure 16

On each T_j $(j=1,2,3,4)$ $\rho(\phi_h)$ is substituted by a linear interpolation P_1. This approximation permits again an accurate integration of (192) via the FORMAC system, A. LAPLACE (22). /61

9.2.1.3. Approximation of the Cost Function and of the Penalty Functional

We approach the cost function by (193)

$$J_h(\phi_h) = \frac{1}{2}\int_{\Omega_h} |\vec{\nabla}\xi_h|^2 dx \tag{193}$$

For the penalty functional, two approximations shall be considered : k=1 ; k=2.

The linear constraint of inequality (105) is expressed in a weak form (194)

$$-\int_{\Omega_h} \vec{\nabla}\phi_h \cdot \vec{\nabla}\omega_h \, dx + \int_{\Gamma_{2h}} g\omega_h \, d\Gamma \le K \int_{\Omega_h} \omega_h \, dx \quad \forall\, \omega_h \in V_h^+ \tag{194}$$

where V_h^+ is the sub-unit of V_h according to

$$V_h^+ = \{\omega_h \in V_h \,|\, \omega_h \ge 0\} \tag{195}$$

If the bounded K is also defined with the weak meaning by the variational formulation (197) from (196)

$$\begin{cases} \Delta\phi_{oh} = K & (\Omega_h) \\ \phi_{oh} = 0 & (\Gamma_{1h}) \\ \dfrac{\partial\phi_{oh}}{\partial n} = g_{h|\rho} & (\Gamma_{2h}) \end{cases} \tag{196}$$

$$\int_{\Omega_h} \vec{\nabla}\phi_{oh} \cdot \vec{\nabla}\omega_h \, dx = -K\int_{\Omega_h} \omega_h \, dx + \int_{\Gamma_h} g_h \, \omega_h \, d\Gamma_h \tag{197}$$

The constraint (194) is substituted by the discrete condition (198)

$$-\int_{\Omega_h} \vec{\nabla}(\phi_h - \phi_{oh}) \cdot \vec{\nabla}\omega_h \, dx \le 0 \quad \forall\, \omega_h \in V_h^+ \tag{198}$$

Let $\mathcal{B}_h$ be a base of V_h produced by the functions of form N_i

$$\mathcal{B}_h = \{N_i\}_{i=1}^{N_h} \text{ with } N_h = \dim(V_h) \tag{199}$$

$N_i \in V_h$

$N_i(M_j) = \delta_{ij}$, $\forall M_j \in \{\text{nodes of } \mathcal{T}_h\}$ (Trailing edge node)

$$(200)$$

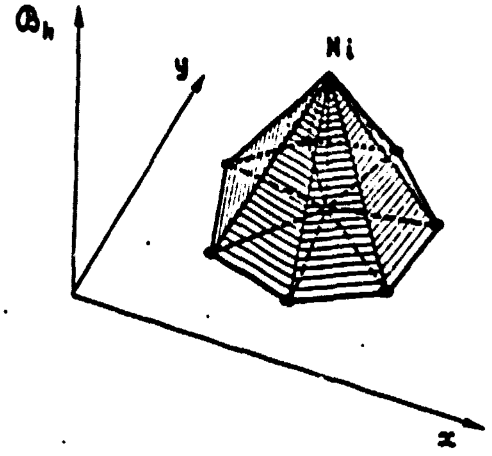

If $\underline{k=1}$
It is obvious that $N_i \geq 0 \ \forall i$ on figure 16.

Figure 16

We may then substitute for (198) the N_h constraints of inequality (201)

$$Q_i = -\int_{\Omega_h} \vec{\nabla}(\phi_h - \phi_{oh}) \cdot \vec{\nabla} N_i \, dx \quad 0 \quad \forall i = 1, \ldots, N_h \tag{201}$$

One way of satisfying them is to add to criterion (193) the <u>discrete</u> penalty functional (202)

$$P_{123} = \sum_{i \in N_h} |Q_i^+|^2 \tag{202}$$

If $\underline{k=2}$, the base functions N_i are not all positive. In this case may be decomposed as follows in (303)

$$\mathcal{B}_h = \mathcal{B}_h^{1,2,3} \oplus \mathcal{B}_h^{4,5,6} \quad ; \quad N_h = N_h^{123} + N_h^{456} \tag{203}$$

$$\mathcal{B}_h^{1,2,3} = \{N_i \ , \ i \in \text{tops } 1,2,3 \text{ of triangle } T \in \mathcal{T}_h\}$$

$$\mathcal{B}_h^{4,5,6} = \{N_i, \ i \in \text{middles } 4,5,6 \text{ of triangle } T \in \mathcal{T}_h\}$$

A function of form N_i of the sub-families (203) are shown on figure (17)

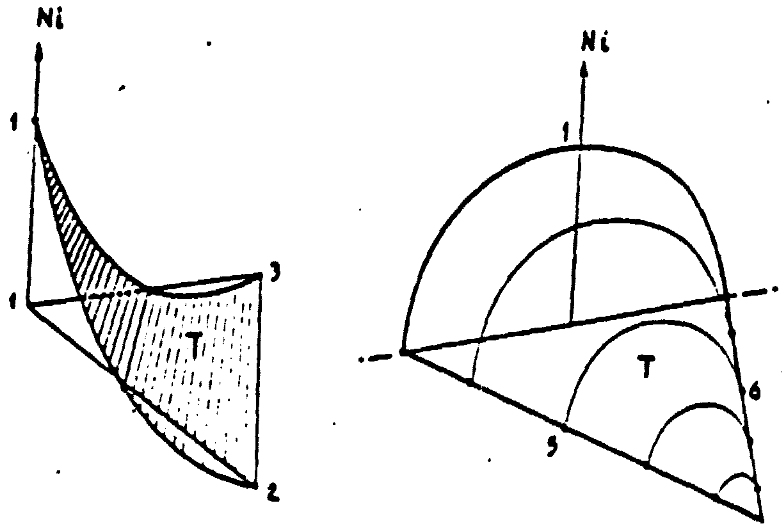

17.1 17.2

Figure 17

It is obvious that $N_i \geq 0$ if $N_i \in \mathcal{E}_h^{456}$ (figure 17.2), but it may be observed that on figure 17.1 that $N_i \in \mathcal{E}_h^{123}$ may take on negative values.

In this case, we shall substitute for (198) the $N_h^{123} + N_h^{456}$ constraints of inequality (204)

$$\begin{aligned} Q_i &= -\int_{\Omega_h} \vec{\nabla}(\phi_h - \phi_{oh}) \cdot \vec{\nabla} N_i^+ \, dx \leq 0 \quad \forall N_i \in \mathcal{E}_h^{123} \quad N_i^+ = \mathrm{Max}\,(0, N_i) \\ Q_i &= -\int_{\Omega_h} \vec{\nabla}(\phi_h - \phi_{oh}) \cdot \vec{\nabla} N_i \, dx \leq 0 \quad \forall N_i \in \mathcal{E}_h^{456} \end{aligned} \tag{204}$$

One way of satisfying them is to add to the criterion (193) the penalty functional (205)

$$P_h = \sum_{i \in N_h^{123}} |Q_i^+|^2 + \sum_{i \in N_h^{456}} |Q_i^+|^2 \tag{205}$$

In the numerical tests, the second term of (205) shall practically be sufficient. In the case of approximation $(162)_{R2}$, the discrete penalty term of (206)

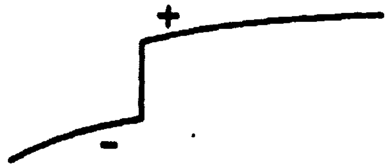

Figure 18

$$S = \int_{\Omega} [\vec{u}\cdot\vec{n}]^{+2}\, dx \tag{206}$$

/64

A contribution of S due to a discontinuity of speed of positive intensity is shown on figure 18.

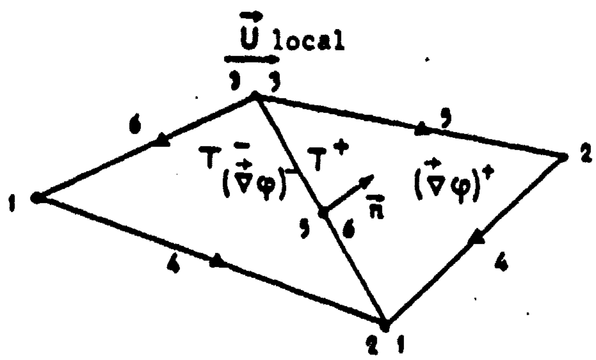

Figure 19

In the case k=2 the discrete discontinuity of figure 18 is calculated at intersection 4, 5 or 6 in the direction of the bars of two triangles T^- and $T^+ \in \mathcal{T}_h$. The illumination + and - occurs by using the local speed on figure 19.

$\vec{u}_{56} = \frac{1}{2}(\vec{u}_5 + \vec{u}_6)$ calculated in the middle of bar (23) view of T_1 and in the middle of bar (13) view of T_2 makes it possible to illuminate T_1, T_2 in T^- and T^+ in the following direction

- $\vec{u}_{56}$ is exiting T_1 at node 5 $\Longrightarrow T_1 \rightarrow T^-$
- $\vec{u}_{56}$ is entering T_2 at node 6 $\Longrightarrow T_2 \rightarrow T^+$

In this semi-node, the discrete constraint to be satisfied is expressed by (207)

$$S_i = [\vec{u}\cdot\vec{n}]_i = (\vec{\nabla}\phi_i^+ - \vec{\nabla}\phi_i^-)\cdot\vec{n} \le 0 \tag{207}$$

discrete analogue of (206) may then be expressed in (208)

$$S_h = \sum_{i \in N_h^{456}} |S_i^+|^2\, \ell(B_i)\ ;\ \ell(B_i) = \text{length of bar} - B_i \tag{208}$$

which permits the final approximation of 102 in (209) to be given /65

$$\min_{\phi_h} (J_h(\phi_h) + \mu_1 P_h + \mu_2 S_h) \tag{209}$$

Note : it is possible to form a model when k=1, the condition of entropy by adding a penalty to a functional S^{α} odd power of a positive step of speed, which is impossible according to fluid dynamics (decompression shocks) given in (210)

$$S_{\alpha} = \int_{\Omega} |[\vec{u}\cdot\vec{n}]^{+\alpha}|^2 \, dx \quad \text{with} \alpha=3 \tag{210}$$

The discrete analogue S_{3h} is expressed then

$$S_{3h} = \sum_{i\in N_h} {}^{456} R_i^{+2} \, \ell(B_i) \text{ with this time}$$
$$R_i^{+} = (((\vec{\nabla}\phi_i^{+} - \vec{\nabla}\phi_i^{-})\cdot\vec{n})^{+})^3 \tag{211}$$

Numerical results using (211) with k=1 shall be presented later on.

M.O. BRISTEAU (20) may be consulted for the numerical approximation of the constraint of entropy by the artificial viscosity.

9.2.1.4. Approximation of the Cost Function Gradient and of the Penalty Functional Gradient

The cost function gradient $\langle J'(\phi), N_i\rangle = J_i'$ is approached by (212)

$$\langle J_h'(\phi_n), N_i\rangle = \int_{\Omega_h} \rho(\phi_h)\vec{\nabla}\xi_h\cdot\vec{\nabla}N_i \, dx - 2k\alpha\int_{\Omega_h} \rho(\phi_h)^{1-1/\alpha}(\vec{\nabla}\phi_h\cdot\vec{\nabla}\xi_h)(\vec{\nabla}\phi_h\cdot\vec{\nabla}N_i)\, dx \tag{212}$$

$\forall N_i \in V_h$; $\xi_h \in V_h$, $\phi_h \in V_{hg}$

The discrete analogue of the menalty functional gradient (202) is expressed by (213) (214) (215)

$$<P'_{123}, N_i> = 2 \sum_{i\in N_h^{123}} Q_j^+ \ \delta Q_j^+(i) \text{ with } Q_j^+,\ Q_j^+(i), \text{ given in (214)(215)} \tag{213}$$

$$Q_j^+ = \left(-\int_\Omega (\vec{\nabla}\phi_h - \vec{\nabla}\phi_{oh})\cdot\vec{\nabla}N_j\,dx\right)^+ \tag{214}$$

$$\delta Q_j^+(i) = \int_\Omega \vec{\nabla}Q_j^+\cdot\vec{\nabla}N_i\ dx \tag{215}$$

If the entropy constraint modelling (211) is used, we obtain the differentiation formulas (216) (217) /66

$$<S'_{3h}, N_i> = 2 \sum_{j\in N_h^{456}} R_j^+ \ \delta R_j^+(i)\ell(B_j) \tag{216}$$

with δR_j^+ given in (217)

$$\delta R_j^+(i) = 3\{(\vec{\nabla}\phi_j^+ - \vec{\nabla}\phi_j^-)\cdot\vec{n}\}^2\cdot\{(\vec{\nabla}N_i^+ - \vec{\nabla}N_i^-)\cdot\vec{n}\} \tag{217}$$

9.2.2. Case of Lifting Profiles (Airfoil Sections)

9.2.2.1. Approximation of Spaces V, V_g and V_C^ℓ

If V_h and V_{gh} designate the approximations in finite dimensions of spaces V and V_g ; if V_C is the sub-space of $H^1(\Omega)$ defined in 7.3 so that

$$V_C = \{\phi \in H^1(\dot{\Omega}),\ \phi=0 \text{ trailing edge} ;\ \phi|_{C^+} - \phi|_{C^-} = \ell\ ,\ \ell \text{ any value}$$

where C designates a cut in the domain occupied by the fluid exiting the trailing edge and joining a point of Γ_∞ (Figure 20) and that V_{Ch}^1 designates the approximation in finite dimension of space V_C^1

$$V_{Ch}^1 = \{\phi_h | \phi_h \in C^0(\bar{\dot{\Omega}}),\ \phi_h|_T \in P_k \quad \forall T \in \mathcal{T}_h,\ \phi_h|_{BP}=0 ;\ \phi_h|_{C^+} - \phi_h|_{C^-} = 1\}$$

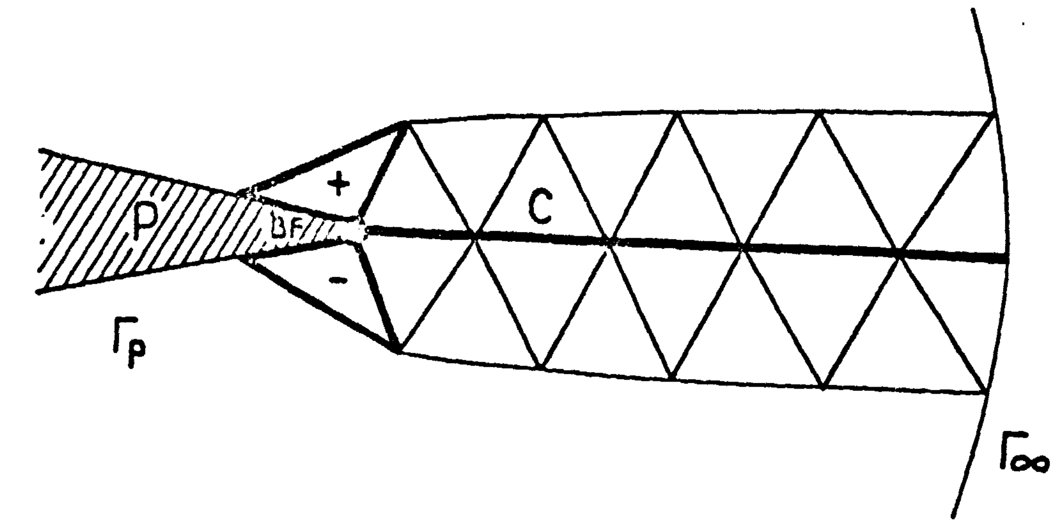

Figure 20

then the discrete analogue of (109) is given by (218) /67

$$\phi_{\ell h} = \phi_{NPh} + \ell\phi_{Rh} \in V_h \oplus V^{\ell}_{Ch} \tag{218}$$

9.2.2.2. Approximation of the State Equation (112)

In (218) ϕ_{Rh} and ϕ_{NPh} are the approached solutions (219) (220) of the variational equations (52) (112)

$$\int_{\dot{\Omega}} \vec{\nabla}\phi_{Rh} \cdot \vec{\nabla}\omega_h \, dx = 0 \quad \forall\, \omega_h \in V^{\ell}_{Ch} \ ; \ \phi_{Rh} \in V^{1}_{Ch} \tag{219}$$

The step condition on C is treated as a condition of pseudo-periodicity. We define ξ_h which approaches ξ as solution of the discrete equation (220)

$$\int_{\Omega} \vec{\nabla}\xi_h \cdot \vec{\nabla}\omega_h \, dx = \int_{\Omega} \rho_h(\phi_{\ell h}) \vec{\nabla}\phi_{\ell h} \cdot \vec{\nabla}\omega_h \, dx + \int_{\Gamma_{2h}} g_h \omega_h \, d\Gamma \tag{220}$$

$$\forall\, \omega_h \in V_h$$

$$\xi_h \in V_h \ , \ \phi_{\ell h} = \phi_{NPh} + \ell\phi_{Rh} \ \text{with}\ \phi_{NPh} \in V_h$$

9.2.2.3. Approximation of the Joukowski Condition

If T_{BF}^{+} and T_{BF}^{-} designate respectively the last element at the extrados (resp. at the intrados) attached to the airfoil following a side of a triangle, and to the trailing edge shown on figure 21.

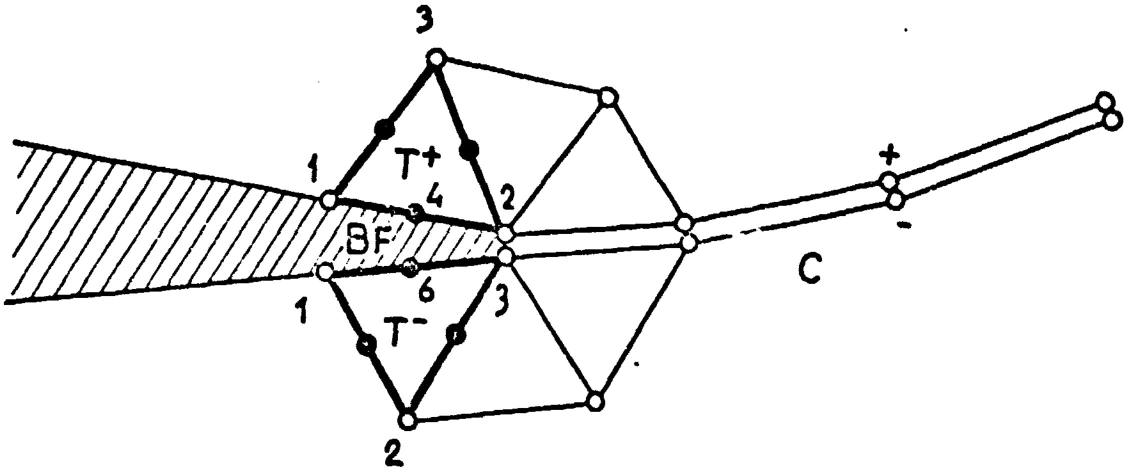

Figure 21

we approach JK(ℓ) by $JK_h(\ell)$ defined in (221) /68

$$JK_h(\ell) = |\vec{\nabla}\Phi_{\ell h}|^2_{T^+} - |\vec{\nabla}\Phi_{\ell h}|^2_{T^-} \tag{221}$$

If k=1, $\vec{\nabla}\Phi_{\ell h}$ is constant on each trangle and the Joukowski condition cannot be applied punctially on the airfoil, but only as an average on the two triangles $T^+ - T^-$.

If k=2, $\vec{\nabla}\Phi_{\ell h}$ is linear on each triangle, we may selecte one of the nodes (1-4-2) or (1-6-3) on the body or an interpolation of these points (refer to MARTIN (23)).

9.3. 3-D Flows

The numerical implementation of the tridimensional flows is developed in detail in J. PERIAUX (9). In the case of lifting flows (for example, around a wing), a sheet of discontinuity (ND) must be introduced, originating at the line of the trailing edge (LBF) and joining Γ_∞ as on figure 22.

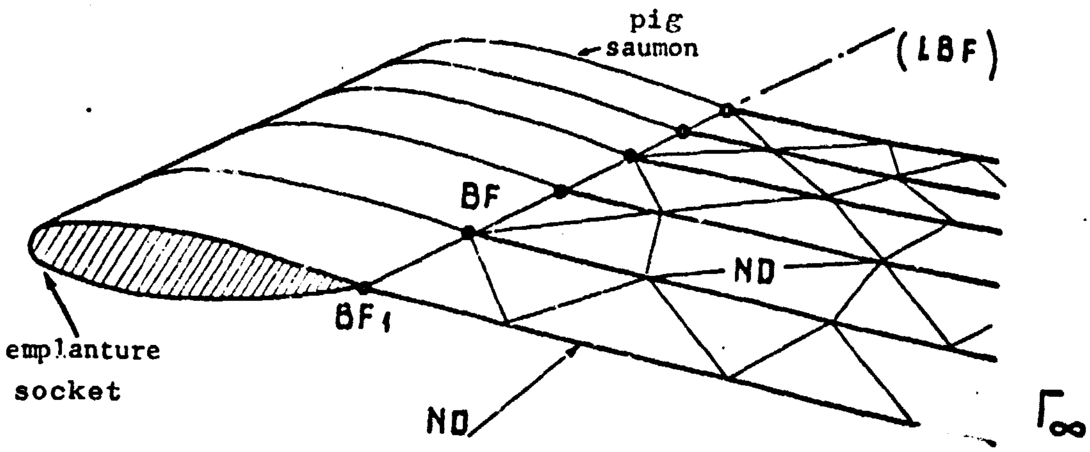

Figure 22

The discrete Joukowski condition is applied on (LBF), trailing edge line of the wing. If $\ell(y)$ designates the circulation spread, starting from the socket of the wing up to the "pig" the discretization of (LBF) into NBF points on which the sheet of discontinuity is applied, provides NBF Joukowski conditions (non linear) (222)

$$JK_h(\ell_K) = |\vec{\nabla}\phi_h|^2_{BF_K^+} - |\vec{\nabla}\phi_h|^2_{BH_K^-} \quad ; \; K=1,NBF \qquad (222)$$

with ϕ_h decomposed as follows in (223)

/69

$$\begin{cases} \phi_h = \phi_{NPh} + \sum\limits_{K=1}^{NBF} \ell_K \, \phi_{Rh,K} \\ \phi_h \in V_h \oplus \Big(\sum\limits_{K=1}^{NBF} V^{\ell_K}_{(ND)_K, h} \Big) \end{cases} \qquad (223)$$

with $V^{\ell_K}_{(ND)_K}$ defined in (224)

$$\begin{cases} V^{\ell_K}_{(ND)_{K,h}} = \{ \phi_{Rh} \,|\, \phi_{Rh} \in \mathcal{C}^0(\bar{\Omega}) \; , \; \phi_{Rh}|_T \in P_k \quad \forall\, T \in \mathcal{T}_h \, , \\ \phi_{Rh}|_{BF_{K_o}} = 0 \; ; \; \phi_{Rh}|_{(ND)_K^+} - \phi_{Rh}|_{(ND)_K^-} = \ell_K \} \end{cases} \qquad (224)$$

If $\mathcal{C}_h$ is a tetrahedron of Ω then ND shall be the trace of tetrahedrons having at least one node belonging to the sheet of discontinuity /69

$(ND)^+$ shall be the trace of the sheet, view from above
$(ND)^-$ shall be the trace of the sheet, view from below

The definition + and - are defined from the line of the trailing edge by designating by + the extrados of the wing and by - the intrados of the wing. I shall be observed, then, that the discretization of $(ND)_h$ is composed of a set of triangles (see figure 22).

O.C. ZIENIEWICS (24) may be consulted for the approximation P_k k=1, 2 and the coordinates of surface area (L_i) used in (225) as well as the derivatives

$$\hat{\phi}|_T = \sum_{i=1}^{4} \phi_i L_i \; ; \; \hat{\phi}|_T = \sum_{i=1}^{10} \phi_i N_i(L_j) \; ; \; \hat{\phi}|_T \in P_k \tag{225}$$

of the functions of forms appearing in the exact integrations.

10. - MIXED APPROXIMATION BY THE METHOD OF CONFORM FINITE ELEMENTS OF THE NAVIER-STOKES EQUATIONS

10.1. Summary

This chapter presents the mixed approximation of the Stokes equations and the Navier-Stokes equations by the method of conform finite elements taken into consideration in chapter 8. For simplicity Ω shall be assumed to be a bound polygonal of R^2, but the numerical implementation extends to the domains of R^3, the applications of which shall be presented during the presentation of numerical results in chapter 12.

10.2. Approximation of the Functional Spaces

If $\mathcal{C}_h$ designates a standard triangulation of the domain Ω, the following spaces of finite dimension (226) (227) (228) (229) (230) (231) shall be used subsequently /70

$$H_h^1 = \{\phi_h \in \mathcal{C}^o(\bar{\Omega}) \;,\; \phi_h|_T \in P_1 \quad \forall\, T \in \mathcal{C}_h\} \tag{226}$$

$$H_{oh}^1 = H_o^1(\Omega) \cap H_h^1 = \{\phi_h \in H_h^1 \;,\; \phi_h|_T = 0\} \tag{227}$$

$$V_h = \{\vec{v}_h \in (\mathcal{C}^o(\bar{\Omega}))^2 \;,\; \vec{v}_h|_T \in (P_2)^2,\; \forall\, T \in \mathcal{C}_h\} \tag{228}$$

$$V_{zh} = \{\vec{v}_h \in V_h \;,\; \vec{v}_h|_\Gamma = \vec{z}_h\} \tag{229}$$

with $\vec{z}_h$, an appropriate approximation of $\vec{z}$.

$$W_{zh} = \{(\vec{v}_h,\phi_h)\in V_{zh}\times H^1_{oh}\ ,\ \int_\Omega \vec{\nabla}\phi_h\cdot\vec{\nabla}\omega_h\,dx = \int_\Omega \vec{\nabla}\cdot\vec{v}_h\omega_h dx \quad \forall\, \omega_h\in H^1_h\} \tag{230}$$

A widely used variant in numerical tests consists of defined in (231)

$$\tilde{V}_{h/2} = \{\vec{v}_{h/2}\in (\mathcal{C}^0(\bar{\Omega}))^2,\ \vec{v}_{h/2}|_T\in (P_1)^2,\ \forall\, T\in \tilde{\mathcal{T}}_{h/2}\} \tag{231}$$

where $\tilde{\mathcal{T}}_{h/2}$ is the triangulation obtained from $\mathcal{T}_h$ bysubdivision of each triangle $T\in\mathcal{T}_h$ into 4 sub-triangles obtained on figure 23 by joining the middles of the sides.

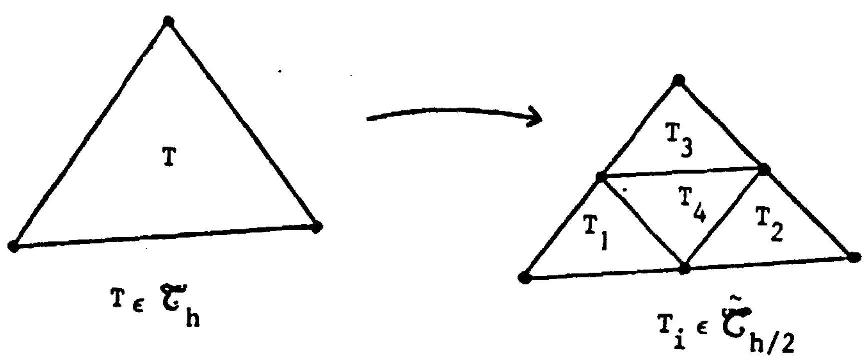

Figure 23

10.3. Approximation of the Steady Navier-Stokes Equations /71

The approximation of equations (132) by the mixed method (187) is given in (232)

$$(P_h)\begin{cases}\text{Find } \{\vec{u}_h,\psi_h\}\in W_{zh} \text{ so that}\\ \nu\int_\Omega \vec{\nabla}\vec{u}_h\cdot\vec{\nabla}\vec{v}_h\,dx + \int(\vec{u}_h\cdot\vec{\nabla})\vec{u}_h\cdot(\vec{v}_h+\vec{\nabla}\phi_h)dx = 0\ ,\ \forall\,\{\vec{v}_h,\phi_h\}\in W_{oh}\end{cases} \tag{232}$$

We shall find in P. LE TALLEC (26) reasonable assumptions on $\mathcal{T}_h$ and $\nu\geq\nu_o$ so that (P_h) permits one solution. Moreover, passing to the boundary is the solution of problem (132)

$$\lim_{h\to 0}\{\vec{u}_h,\psi_h\} = \{\vec{u},0\} \tag{233}$$

It may be observed that if $\psi_h = \phi_h = 0$ is set in W_{zh} and in (P_h), the Taylor-Hood (25) scheme is recovered

10.4. Mixed Approximation of the Unsteady Navier-Stokes Equations

Subsequently, $k = \Delta t$ shall stand for the discretization time step. Presented now are two possible discretization schemes of which one is semi-implicit and the other one is entirely implicit.

10.4.1. Semi-implicit Scheme

This is the discrete version of scheme (152) (153). It is composed of (234) (235)

$$\vec{u}_h^{\,o} \in V_h \text{ , is an approximation of } \vec{u}^{\,o}\text{, given} \tag{234}$$

Then, for $n \geq 0$, by using (232), we obtain $\{\vec{u}_h^{\,n+1}, \psi_h^{n+1}\}$ from $\vec{u}_h^{\,n}$ by solving (236) (235)

$$\int_\Omega \frac{\vec{u}_h^{\,n+1} - \vec{u}_h^{\,n}}{k} \cdot \vec{v}_h \, dx + \nu \int_\Omega \vec{\nabla} \vec{u}_h^{\,n+1} \cdot \vec{\nabla} \vec{v}_h \, dx = -\int_\Omega (\vec{u}_h^{\,n} \cdot \vec{\nabla}) \vec{u}_h^{\,n} \cdot (\vec{v}_h + \vec{\nabla}\phi_h) \, dx \tag{236}$$

$$\forall \{\vec{v}_h, \phi_h\} \in W_{oh} \text{ , } \{\vec{u}_h^{\,n+1}, \psi_h^{n+1}\} \in W_{zh}.$$

It may be noted that (236) is a sequence of discrete Stokes pseudo-problems and that the scheme (235) (236) is a truncation error $0(\Delta t)$ and is only conditionally stable.

10.4.2. Implicit Scheme

The scheme taken into consideration above in (237) (238) is an entirely implicit two step Crank-Nicholson scheme /72

$$\vec{u}^{\,o}, \vec{u}_h^{\,1} \text{ given} \tag{237}$$

Then for $n \geq 1$, we obtain by using (232) $\vec{u}_h^{\,n+1}$ from $\vec{u}_h^{\,n}, \vec{u}_h^{\,n-1}$ the solution of (238)

$$\int_\Omega \frac{\frac{3}{2} \vec{u}_h^{\,n+1} - 2\vec{u}_h^{\,n} + \frac{1}{2} \vec{u}_h^{\,n-1}}{k} \cdot \vec{v}_h dx + \nu \int_\Omega \vec{\nabla} \vec{u}^{\,n+1} \cdot \vec{\nabla} \vec{v}_h dx + \int_\Omega (\vec{u}_h^{\,n+1} \cdot \vec{\nabla}) \vec{u}_h^{\,n+1} \cdot \tag{238}$$

$$(\vec{v}_h + \vec{\nabla}\phi_h) dx = 0 \quad \forall \{\vec{v}_h, \phi_h\} \in W_{oh} \text{ , } \{\vec{u}_h^{\,n+1}, \psi_h^{n+1}\} \in W_{zh}$$

It may be noted that (238) is a sequence of discrete non-linear problems analogous to (232) and that the scheme (237) (238) has a truncation error $0(\Delta t^2)$ and is unconditionally stable.

10.5. Least Squares Solution of Discrete Unsteady Navier-Stokes Equations

10.5.1. Discrete Mixed Formulation of the Problem P_h^I

We are taking into consideration in this paragraph the discrete analogue of chapter 8.2.3., the mixed formulation of which is a generalization (239) of (232)

Find $(\vec{u}_h,\psi_h) \in W_{zh}$ so that

$$\alpha\int_\Omega \vec{u}_h\cdot\vec{v}_h dx + \nu\int_\Omega \vec{\nabla}\vec{u}_h\cdot\vec{\nabla}\vec{v}_h dx + \int_\Omega (\vec{u}_h\cdot\vec{\nabla})\vec{u}_h\cdot(\vec{v}_h+\vec{\nabla}\phi_h)dx = \tag{239}(P_h^I)$$

$$= \int_\Omega \vec{f}_{oh}\cdot\vec{v}_h dx + \int_\Omega \vec{f}_{1h}\cdot(\vec{v}_h+\vec{\nabla}\phi_h)dx \quad \forall(\vec{v}_h,\phi_h) \in W_{oh}$$

Two terms may be observed in (239)

- $\vec{f}_{oh}$ corresponding to the choices of the quantification time scheme

$\frac{1}{k}\int_\Omega (2\vec{u}_h^n - \frac{1}{2}\vec{u}_h^{n-1})dx$ (in (238))

- $\vec{f}_{1h}$ density of external forces

P_h^I is a nonlinear problem.

10.5.2. Least Squares Method of P_h^I. /73

By analogy with (158) of chapter 8.2.3., the least squares method of P_h^I given in (240) (241) (242) is taken into consideration

$$\underset{\{\vec{v}_h,\phi_h\}\in W_{zh}}{\mathrm{Min}} J_h(\vec{v}_h,\phi_h) \quad \text{with} \tag{240}$$

$$J_h(\vec{v}_h,\phi_h) = \frac{\alpha}{2}\int_\Omega |\vec{v}_h-\vec{\xi}_h|^2 dx + \frac{\nu}{2}\int_\Omega |\vec{\nabla}(\vec{v}_h-\vec{\xi}_h)|^2 dx \tag{241}$$

where $\vec{\xi}_h$ is a function of $\{\vec{v}_h,\phi_h\}$ via the discrete state equation (242)

$$\alpha\int_\Omega \vec{\xi}_h\cdot\vec{\eta}_h dx + \nu\int_\Omega \vec{\nabla}\vec{\xi}_h\cdot\vec{\nabla}\eta_h dx = \int_\Omega \vec{f}_{oh}\cdot\vec{\eta}_h dx + \int_\Omega \vec{f}_{1h}\cdot(\vec{\eta}_h+\vec{\nabla}\omega_h)dx$$

$$- \int_\Omega (\vec{v}_h\cdot\vec{\nabla})\vec{v}_h\cdot(\vec{\eta}_h+\vec{\nabla}\omega_h)dx \;,\; \forall \{\vec{\eta}_h,\omega_h\} \in W_{oh} \;;\; (\vec{\xi}_h,\chi_h) \in W_{zh} \tag{242}$$

10.5.3. Calculation of Gradient J'_h

The differentiation of criterion (241) is given in (243)

$$\delta J_h = \alpha\int_\Omega (\vec{v}_h-\vec{\xi}_h)\cdot\delta(\vec{v}_h-\vec{\xi}_h)dx + \nu\int_\Omega \vec{\nabla}(\vec{v}_h-\vec{\xi}_h)\cdot\vec{\nabla}\delta(\vec{v}_h-\vec{\xi}_h)dx \qquad (243)$$

$$\forall\ (\delta\vec{v}_h,\delta\phi_h)\in W_{oh}$$

whereas the one of the state equation is given in (244)

$$\begin{cases} \alpha\int_\Omega \delta\vec{\xi}_h\cdot\vec{\eta}_h dx + \nu\int_\Omega \vec{\nabla}\delta\xi_h\cdot\vec{\nabla}\eta_h dx = -\int_\Omega (\delta\vec{v}_h\cdot\vec{\nabla})\vec{v}_h\cdot(\vec{\eta}_h+\vec{\nabla}\omega_h)dx \\ -\int_\Omega (\vec{v}_h\cdot\vec{\nabla})\delta\vec{v}_h\cdot(\vec{\eta}_h+\vec{\nabla}\omega_h)dx \end{cases} \qquad (244)$$

with $(\delta\vec{\xi}_h,\delta\chi_h)\in W_{oh}$; $\forall\ (\vec{\eta}_h,\omega_h)\in W_{oh}$.
Since $\{\vec{v}_h-\vec{\xi}_h,\phi_h-\chi_h\}\in W_{oh}$, it is possible to express the variation of criterion δJ_h uniquely as a function of $\delta\vec{v}_h$ by using (244).

We obtain (245) by selecting $\{\vec{\eta}_h = \vec{v}_h-\vec{\xi}_h \ ;\ \omega_h = \phi_h-\chi_h\}$

$$\alpha\int_\Omega \delta\vec{\xi}_h\cdot(\vec{v}_h-\vec{\xi}_h)dx + \nu\int_\Omega \vec{\nabla}\delta\vec{\xi}_h\cdot\vec{\nabla}(\vec{v}_h-\vec{\xi}_h)dx = -\int_\Omega (\delta\vec{v}_h\cdot\vec{\nabla})\vec{v}_h\cdot((\vec{v}_h-\vec{\xi}_h) + \vec{\nabla}(\phi_h-\chi_h))dx - \int_\Omega (\vec{v}_h\cdot\vec{\nabla})\delta\vec{v}_h\cdot((\vec{v}_h-\vec{\xi}_h)+\vec{\nabla}(\phi_h-\chi_h))dx \qquad (245)$$

By putting (243) (245) together, δJ_h is finally given by (246) /74

$$\delta J_h = \alpha\int_\Omega (\vec{v}_h-\vec{\xi}_h)\cdot\delta\vec{v}_h\ dx + \nu\int_\Omega \vec{\nabla}(\vec{v}_h-\vec{\xi}_h)\cdot\vec{\nabla}\delta v_h\ dx + \int_\Omega((\delta\vec{v}_h\cdot\vec{\nabla})\vec{v}_h + (\vec{v}_h\cdot\vec{\nabla})\delta\vec{v}_h)\cdot((\vec{v}_h-\vec{\xi}_h)+\vec{\nabla}(\phi_h-\chi_h))dx \qquad (246)$$

By expressing that $\delta J_h = \langle J'_h(\vec{v}_h,\phi_h), \{\vec{\eta}_h,\omega_h\}\rangle$, J'_h may be identified with the linear form $J_h : W_{oh} \to \mathbb{R}$ defined by (247)

$$\langle J'_h(\vec{v}_h,\phi_h), \{\vec{\eta}_h,\omega_h\}\rangle = \alpha\int_\Omega (\vec{v}_h-\vec{\xi}_h)\cdot\vec{\eta}_h\ dx + \nu\int_\Omega \vec{\nabla}(\vec{v}_h-\vec{\xi}_h)\cdot\vec{\nabla}\vec{\eta}_h\ dx + \int_\Omega ((\vec{\eta}_h\cdot\vec{\nabla})\vec{v}_h + (\vec{v}_h\cdot\vec{\nabla})\vec{\eta}_h)\cdot((\vec{v}_h-\vec{\xi}_h)+\vec{\nabla}(\phi_h-\chi_h))dx \qquad (247)$$

10.5.4. Conjugate Gradient Solution of (240) (241) (242)

The algorithm given above is the discrete analogue of the one described in (160)...(165) in chapter 8.2.4. It consits of 3 phases.

Phase 0 : Initialization (248) (249) (250)

$$\{\vec{u}_h^o, \phi_h^o\} \in W_{oh} \text{ given} \tag{248}$$

Calculate $\{\vec{g}_h^o, \theta_h^o\}$ solution of the discrete variational equation (249)

$$\alpha\int_\Omega \vec{g}_h^o \cdot \vec{\eta}_h dx + \nu\int_\Omega \vec{\nabla} g_h^o \cdot \vec{\nabla}\vec{\eta}_h dx = \langle J_h'(u_h^o, \psi_h^o), \{\eta_h, \omega_h\}\rangle$$
$$\forall \{\vec{\eta}_h, \omega_h\} \in W_{oh}, \quad \{\vec{g}_h^o, \theta_h^o\} \in W_{oh} \tag{249}$$

with J_h' defined in (247)

$$\text{set} \quad \{\vec{h}_h^o, \tau_h^o\} = \{\vec{g}_h^o, \theta_h^o\} \tag{250}$$

Then for $m \geq 0$, assuming $\{\vec{u}_h^m, \psi_h^m\} \in W_{zh}$, $\{\vec{h}_h^m, \tau_h^m\} \in W_{oh}$ known, calculate $\{\vec{u}_h^{m+1}, \psi_h^{m+1}\}$; $\{\vec{g}_h^{m+1}, \theta_h^{m+1}\}\{\vec{h}_H^{m+1}, \tau_h^{m+1}\}$

Phase 1 : Descent (251) (252) (253)

$$\lambda^m = \arg\min_{\lambda>0} J_h(\vec{u}_h^m - \lambda h_h^m, \psi_h - \lambda\tau_h^m) \tag{251}$$

$$\vec{u}_h^{m+1} = \vec{u}_h^m - \lambda^m \vec{h}_h^m \tag{252}$$

$$\psi_h^{m+1} = \psi_h^m - \lambda^m \tau_h^m \tag{253}$$

Phase_2 : Construction of the New Direction of Descent

Compute $\{\vec{g}_h^{m+1},\theta_h^{m+1}\}$ solution of the discrete variational equation (254)

$$\alpha\int_\Omega \vec{g}_h^{m+1}\cdot\vec{\eta}_h dx + \nu\int_\Omega \vec{\nabla} g_h^{m+1}\cdot\vec{\nabla}\vec{\eta}_h\, dx = \langle J_h'(\vec{u}_h^{m+1},\psi_h^{m+1}),\ \{\vec{\eta}_h,\omega_h\}\rangle$$

$$\forall\ \{\vec{\eta}_h,\omega_h\}\in W_{oh}\ ,\ \{\vec{g}_h^{m+1},\theta_h^{m+1}\}\in W_{oh} \tag{254}$$

Then calculate the coefficient of conjugation γ^{m+1} in (255)

$$\gamma^{m+1} = \frac{\alpha\int_\Omega \vec{g}_h^{m+1}\cdot(\vec{g}_h^{m+1}-\vec{g}_h^{m})dx + \nu\int_\Omega \vec{\nabla} g_h^{m+1}\cdot\vec{\nabla}(\vec{g}_h^{m+1}-\vec{g}_h^{m})\, dx}{\alpha\int_\Omega |\vec{g}_h^{m}|^2\, dx + \nu\int_\Omega |\vec{\nabla} g_h^{m}|^2\, dx} \tag{255}$$

The new direction of descent is given, then, in (256) (257)

$$\vec{h}_h^{m+1} = \vec{g}_h^{m} + \gamma^{m+1}\vec{h}_h^{m} \tag{256}$$

$$\tau_h^{m+1} = \theta_h^{m} + \gamma^{m+1}\tau_h^{m} \tag{257}$$

Do m=m+1 and go in (251)

It may be observed that each iteration of the algorithm (248)-(257) requires the solution of several discrete Stokes problems $S_{\alpha h}$

- one Stokes problem to solve the state (242) $\{\xi_h^{m+1},\chi_h^{m+1}\}$ with $\{\vec{v}_h,\phi_h\} = \{\vec{u}_h^{m+1},\psi_h^{m+1}\}$
- one Stokes problem to calculate $\{\vec{g}_h^{m+1},\theta_h^{m+1}\}$ from $\{\vec{u}_h^{m+1},\psi_h^{m+1}\}$ and $\{\xi_h^{m+1},\chi_h^{m+1}\}$ via (254)
- several Stokes problems ($\simeq$ 3) to calculate λ^m.

Flow chart 1 of the unsteady Navier-Stokes algorithm is presented below. The discrete solution of problems $S_{\alpha h}$ is presented in the follow. : chapter. 10.6.

10.6. The Stokes Algorithm (Discrete Case)

10.6.1. Introduction

The presentation of the Navier-Stokes equations (discrete in the steady case (10.3) and unsteady case (10.4) in the form of a repetitive sequence of discrete Stokes problems, implies a highly efficient numerical algorithm of problem $(S_{\alpha h})$ (258).

SOLUTION 2-D BY THE CONJUGATE GRADIENT OF THE LEAST SQUARES METHOD

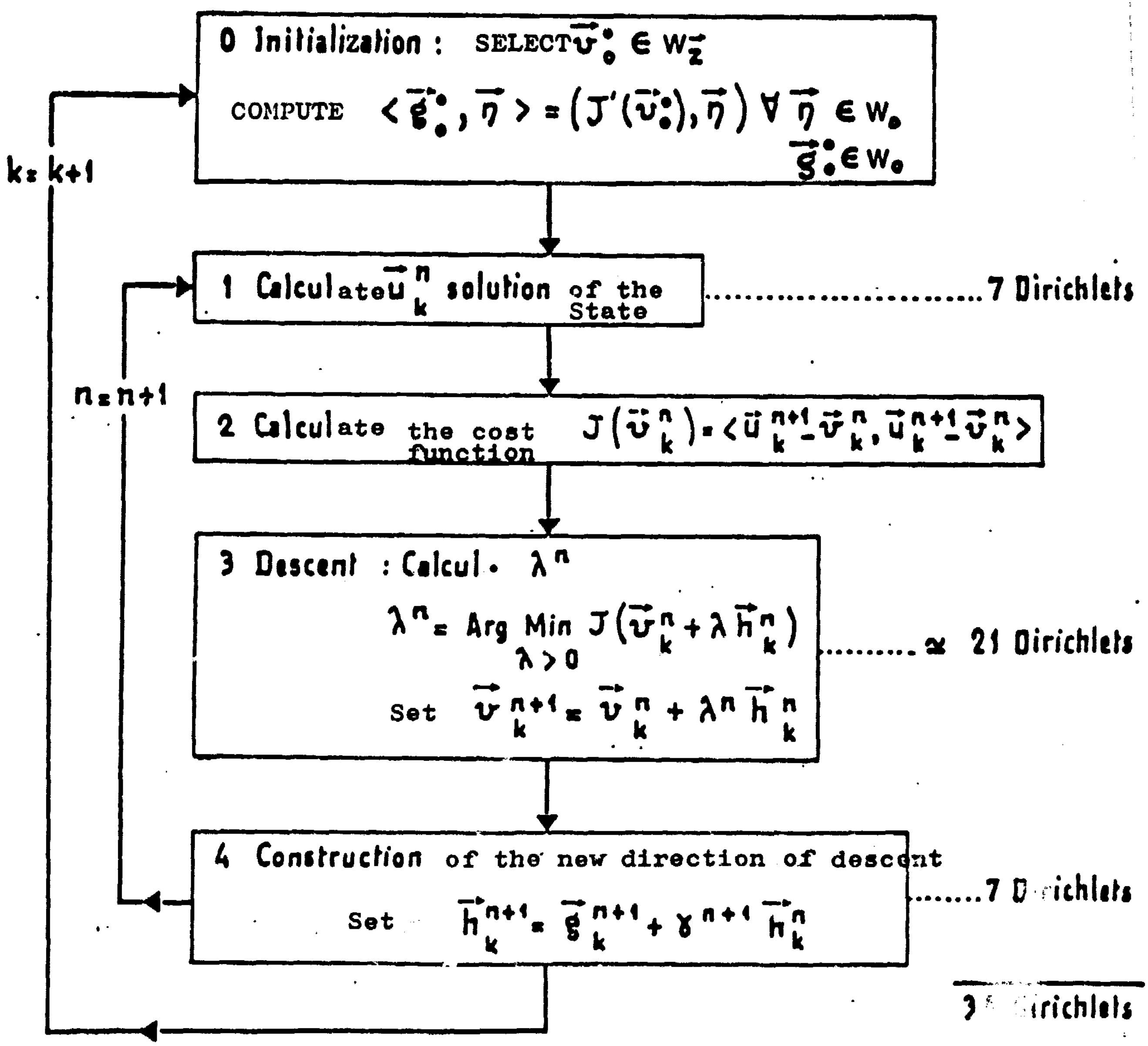

k : index (time loop)

n index (control loop)

NAVIER - STOKES FLOW CHART 1

Find $\{\vec{u}_h, \psi_h\} \in W_{zh}$ so that (258) $(S_{\alpha h})$

$$\alpha\int_\Omega \vec{u}_h\cdot\vec{v}_h dx+\nu\int_\Omega \vec{\nabla} u_h\cdot\vec{\nabla} v_h\,dx = \int_\Omega \vec{f}_{oh}\vec{v}_h dx + \int_\Omega \vec{f}_{1h}\cdot(\vec{v}_h+\vec{\nabla}\phi_h)dx \quad \forall \{\vec{v}_h,\phi_h\} \in W_{oh}$$

In the following presentation, we shall find again the discrete analogue of 8.3 in the solution of $(S_{\alpha h})$

(27) (28) may be referred to for demonstrations of the theorems used.

10.6.2. Characterization of the Solution $(\vec{u}_h, \psi_h, p_h)$

We may easily prove that (258) has a unique solution which is the one of the problem of minimization (259) with distributed linear constraints

$$\underset{\{(\vec{v}_h,\phi_h)\}\in W_{zh}}{\mathrm{Min}} \left\{\frac{\alpha}{2}\int_\Omega |\vec{v}_h|^2 dx + \frac{\nu}{2}\int_\Omega |\vec{\nabla} v_h|^2\,dx - \int_\Omega \vec{f}_{oh}\cdot\vec{v}_h dx - \int_\Omega \vec{f}_{1h}\cdot(\vec{v}_h+\vec{\nabla}\phi_h)dx\right. \quad (259)$$

where it is recalled that

$$W_{zh} = \{(\vec{v}_h,\phi_h)\in V_{zh}\times H^1_{oh},\ \int_\Omega \vec{\nabla}\phi_h\cdot\vec{\nabla} q_h dx = \int_\Omega \vec{\nabla}\cdot v_h\, q_h dx \ \forall\, q_h\in H^1_h\}$$

The number of constraints of (259) is $\dim(H^1_h)$. We may combine with (259) the Lagrangien $\mathcal{L}_h : V_h\times H^1_{ho}\times H^1_h \to \mathbb{R}$ defined by (260)

$$\mathcal{L}_h(\vec{v}_h,\phi_h,q_h) = j_h(\vec{v}_h,\phi_h) + \int_\Omega \vec{\nabla}\phi_h\cdot\vec{\nabla} q_h dx - \int_\Omega \vec{\nabla}\cdot\vec{v}_h q_h dx \quad (260)$$

where $j_h(\vec{v}_h,\phi_h)$ equals (261)

$$j_h(\vec{v}_h,\phi_h) = \frac{\alpha}{2}\int_\Omega |\vec{v}_h|^2 dx + \frac{\nu}{2}\int_\Omega |\vec{\nabla} v_h|^2 dx - \int_\Omega \vec{f}_{oh}\cdot\vec{v}_h dx - \int_\Omega \vec{f}_{1h}\cdot(\vec{v}_h+\vec{\nabla}\phi_h)dx \quad (261)$$

(259) being a problem of minimization with linear constraints of finite dimension for which there is a solution and a distributed Lagrange multiplier $p_h \in H^1_h$ so that $\{\vec{u}_h,\psi_h,p_h\}$ is a saddle point of $\mathcal{L}_h$ on $V_{2h}\times H^1_{oh}\times H^1_h$ with $\{\vec{u}_h,\psi_h\}$ solution of (258) (259).

The extreme conditions of $\mathcal{L}_h$ at point $\{\vec{u}_h,\psi_h,p_h\}$ (262) (263) (264) characterize the solution of (258)

$$\int_\Omega \vec{\nabla} p_h \cdot \vec{\nabla} \phi_h \, dx = \int_\Omega \vec{f}_{1h} \cdot \vec{\nabla} \phi_h \, dx \;\forall\, \phi_h \in H^1_{oh} \;,\; p_h \in H^1_h \tag{262}$$

$$\begin{cases} \alpha \int_\Omega \vec{u}_h \cdot \vec{v}_h dx + \nu \int_\Omega \vec{\vec{\nabla}} u_h \; \vec{\vec{\nabla}} v_h dx + \int_\Omega \vec{\nabla} p_h \cdot \vec{v}_h dx = \int_\Omega (\vec{f}_{oh} + \vec{f}_{1h}) \cdot \vec{v}_h \, dx \\ \forall\, \vec{v}_h \in V_{oh} \;;\; \vec{u}_h \in V_{zh} \end{cases} \tag{263}$$

$$\int_\Omega \vec{\nabla} \psi_h \cdot \vec{\nabla} q_h \, dx = \int_\Omega \vec{\nabla} \cdot u_h \, q_h \, dx \quad \forall\, q_h \in H^1_h \tag{264}$$

/78

From (262), it may be deduced that the Lagrange P_h multiplier is the discrete pressure.

10.6.3. <u>The Space</u> $\mathcal{M}_h$

By using the observations made in 10.2., $\mathcal{M}_h$ is introduced as a supplement to H^1_{oh} in H^1_h , i.e.

$$H^1_h = H^1_{oh} \oplus \mathcal{M}_h$$

with $N_h = \dim(\mathcal{M}_h)$.

In practice, by using the Lagrange finite elements, $\mathcal{M}_h$ shall be defined as follows (265)

$$\mu_h \in \mathcal{M}_h \Longrightarrow \mu_h|_T = 0 \;\; \forall\, T \in \mathcal{C}_h \text{ so that } \partial T \cap \partial\Omega = \phi \qquad (2..$$

$\mathcal{M}_h$ has a finite dimension N_h. It is the number of nodes of $\mathcal{C}_h$ belonging to $\partial\Omega$. Moreover, (265) implies that with

$$\operatorname{supp}(\mu_h) \;\; \bar{\Omega}_{\Gamma_h} = \bigcup_{T \cap \partial\Omega \neq \phi} T \text{ with } \lim_{h \to 0} \operatorname{mes}(\bar{\Omega}_{\Gamma_h}) = 0.$$

$\bar{\Omega}_{\Gamma_h}$ is shown on figure 24.

10.6.4. <u>Converting Problem</u> $\mathcal{S}_{\alpha h}$ <u>into a Variational Problem</u> (E_h) <u>in</u> $\mathcal{M}_h$

10.6.4.1. Approximation of $a(\cdot,\cdot)$

In reference to the observations made in paragraph 8.3.3., that if μ is sufficiently steady, the Green formula leads to (266)

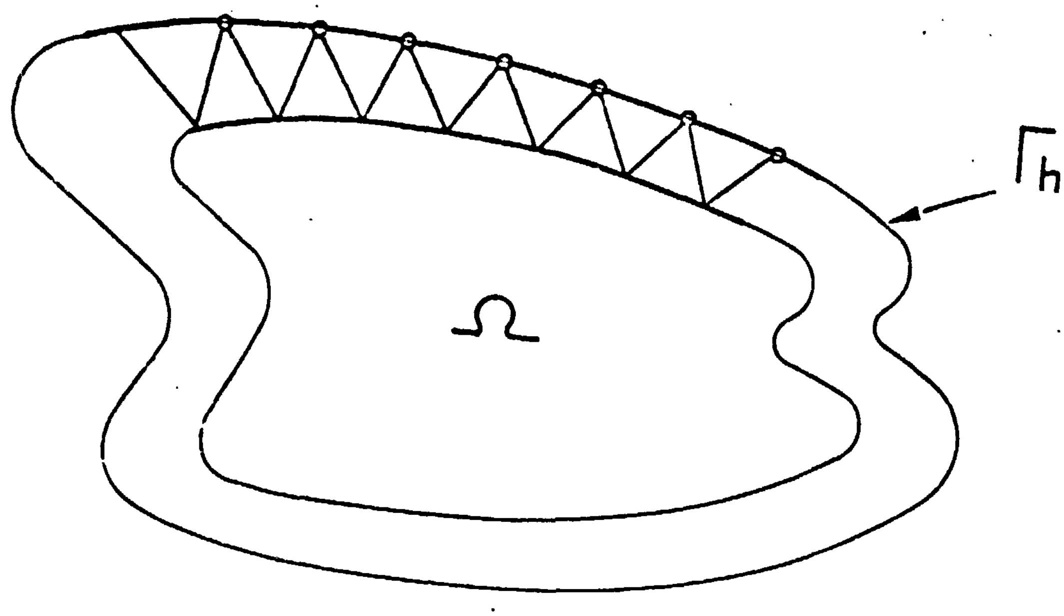

Figure 24

$$a(\lambda,\mu) = -\int_\Gamma \frac{\partial\psi_\lambda}{\partial n}\mu\, d\Gamma = -\int_\Omega \vec{\nabla}\psi_\lambda\cdot\vec{\nabla}\tilde{\mu}\, dx - \int_\Omega \Delta\psi_\lambda\, \tilde{\mu}\, dx$$

$$= -\int_\Omega \vec{\nabla}\psi_\lambda\cdot\vec{\nabla}\tilde{\mu}\, dx + \int_\Omega \vec{\nabla}\cdot u_\lambda\, \tilde{\mu}\, dx = -\int_\Omega (\vec{\nabla}\psi_\lambda+\vec{u}_\lambda)\vec{\nabla}\tilde{\mu}\, dx \qquad (266)$$

/79

where $\tilde{\mu}$ is a measurement of μ in Ω.

Now let $\lambda_h, \mu_h \in \mathcal{M}_h$. If we define $a_h(\cdot,\cdot) : \mathcal{M}_h \times \mathcal{M}_h \to \mathbb{R}$ by the sequence of problems (267) (268) (269) (270)

$$\int_\Omega \vec{\nabla}p_{\lambda h}\cdot\vec{\nabla}q_h\, dx = 0 \quad \forall\, q_h \in H^1_{oh}\ ,\ p_{\lambda h}-\lambda_h \in H^1_{oh} \qquad (267)$$

$$\alpha\int_\Omega \vec{u}_{\lambda h}\cdot\vec{v}_h\, dx + \int_\Omega \vec{\vec{\nabla}}u_{\lambda h}\cdot\vec{\vec{\nabla}}v_h\, dx = -\int_\Omega \vec{\nabla}p_{\lambda h}\, \vec{v}_h\, dx \quad \forall\, \vec{v}_h \in V_{oh},\ \vec{u}_{\lambda h} \in V_{oh} \qquad (268)$$

$$\int_\Omega \vec{\nabla}\psi_{\lambda h}\cdot\vec{\nabla}\phi_h \, dx = \int_\Omega \vec{\nabla}\cdot\vec{u}_{\lambda h}\phi_h dx, \ \forall\phi_h \in H_h^1 \ , \psi_h \in H_{oh}^1 \tag{269}$$

$$a_h(\lambda_h,\mu_h) = -\int_\Omega (\vec{\nabla}\psi_{\lambda h}+\vec{u}_{\lambda h})\cdot\vec{\nabla}\tilde{\mu}_h \, dx \tag{270}$$

Then, the theorem (10.6.4.1.) demonstrated in (31), discrete analogue of the theorem 8.3.3.1., characterizes the properties of the bilinear form $a_h(.,.)$.

Theorem 10.6.4.1. : Let us assume that $\forall T \in \mathcal{C}_h$, T has at the most one side $\in \partial\Omega$, therefore $a_h(.,.)$ is a bilinear, symmetrical form and is defined positive on

$(\mathcal{M}_h/R_h) \times (\mathcal{M}_h/R_h)$ where

$$R_h = \{\mu_h \in \mathcal{M}_h \mid \mu_h = \text{cste on } \partial\Omega\}$$

Based on theorem 10.6.4.1., we can now convert the problem $S_{\alpha h}$ into a variational problem in $\mathcal{M}_h$ thanks to theorem 10.6.4.2., discrete analogue of theorem 8.3.3.2.

10.6.4.2. Approximation of (E)

Theorem 10.6.4.2. : Let P_h be the discrete pressure and λ_h the trace of p_h on $\mathcal{M}_h$. Therefore if theorem 10.6.4.1. is verified, then λ_h is the unique solution in $\mathcal{M}_h/R_h$ of the variational linear problem (E_h) (271)

$$\lambda_h \in \mathcal{M}_h/R_h$$

/80

$$a_h(\lambda_h,\mu_h) = \int_\Omega (\vec{\nabla}\psi_{oh}+\vec{u}_{oh})\cdot\vec{\nabla}\tilde{\mu}_h \, dx \quad \forall \mu_h \in \mathcal{M}_h/R_h \tag{271)(E_h}$$

where p_{oh}, $\vec{u}_{oh}$, ψ_{oh} are defined by the sequence of problems (272) (273) (274)

$$\int_\Omega \vec{\nabla}p_{oh}\cdot\vec{\nabla}q_h \, dx = \int_\Omega \vec{f}_{1h}\cdot\vec{\nabla}q_h \, dx \ \forall \ q_h \in H_{oh}^1, \ p_{oh} \in H_{oh}^1 \tag{272}$$

$$\begin{cases} \alpha\int_\Omega \vec{u}_{oh}\cdot\vec{v}_h dx + \nu\int_\Omega \vec{\nabla}\vec{u}_{oh} \cdot \vec{\nabla}\vec{v}_h \, dx = \int_\Omega (\vec{f}_{oh}+\vec{f}_{1h}-\vec{\nabla}p_{oh})\cdot\vec{v}_h \, dx \\ \forall\, \vec{v}_h \in V_{oh}\,,\ \vec{u}_{oh}\in V_{zh} \end{cases} \tag{273}$$

$$\int_\Omega \vec{\nabla}\psi_{oh}\cdot\vec{\nabla}\phi_h \, dx = \int_\Omega \vec{\nabla}\cdot\vec{u}_{oh}\phi_h dx \ \forall\, \phi_h \in H^1_{oh}\,,\ \psi_{oh}\in H^1_{oh}\,. \tag{274}$$

10.6.5. The Solution of Problem (E_h)

10.6.5.1. Summary

The choice of the method used for solving the problem depends uniquely on industrial applications. For 2-D fluid flows, the number of boundary points N_h ($\simeq 100$) with $\dim N_h \ll \dim H^1_h$, the solution of (E_h) by a direct method is preferred, for the core space and manufacturing time required for matrice A_h is relatively compatible with the current size of large computers (370/168). On the other hand, for three dimensional applications (separated flows around a wing with high incidence), the number of boundary points N_h ($\simeq 1000$) results in an unallowable core use and computation time and in this case, a conjugate gradient type iterative method is preferred for the solution of (E_h), which does not require information about A_h.

Both methods are expanded in the following text.

10.6.5.2. Solution of (E_h) by a Direct Method

10.6.5.2.1. Construction of a Linear System Equivalent to (E_h)

General :

The space $\mathcal{M}_h$ defined in (263) being of finite dimension, let $\mathcal{B}_h = \{\omega_i\}_{i=1}^{N_h}$, a base of $\mathcal{M}_h$. That means that $\forall\, \mu_h \in \mathcal{M}_h$

$$\mu_h = \sum_{i=1}^{N_h} \mu_i w_i \ ; \ r_h\mu_h = \{\mu_1,\ldots\mu_{N_h} \in \mathbb{R}^{N_h}\} \tag{275}$$

The functions w_i are defined as follows :

$\forall\, i=1,\ldots,N_h$ /81

$$w_i \in V_h \quad w_i(P_i) = 1 \tag{276}$$

$$w_i(Q) = 0 \quad \forall\, Q \text{ node of } \mathcal{T}_h\,,\ Q \neq P_i$$

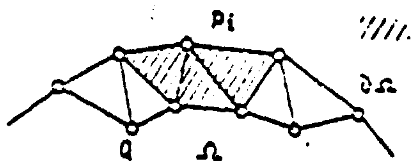

Figure 25

The hachure zone of figure 25 represents the support of w_i. /81

With the definition (276) of the w_i, that means that in (275) $\mu_i = \mu_h\,(P_i)$. The problem (E_h) is therefore equivalent to the linear system (277)

$$\sum_{j=1}^{N_h} a_h(w_j,w_i)\lambda_i = \int_\Omega (\vec{\nabla}\psi_{oh}+\vec{u}_{oh})\cdot\vec{\nabla}w_i\,dx\ ,\ 1 \le i \le N_h .$$

Set $a_{ij} = a_h(w_j,w_i)$; $A_h = (a_{ij})_{1<i,j<N_h}$; $b_i = \int_\Omega (\vec{\nabla}\psi_{oh}+\vec{u}_{oh})\vec{\nabla}w_i\,dx$ (277)

$b_h = \{b_i\}_{i=1}^{N_h}$

According to theorem 10.6.4.1., the matrice A_h is complete, symmetrical and semi-defined positive

Construction of A_h : A_h is constructed column by column according to the relationship $a_{ij} = a_h(w_j,w_i)$. To compute the j^{th} column of A_h, the sequence of problems (267)...(269) is solved for $\lambda_h = w_j$ and $(a_{ij})_{i=1,\dots N_h}$ is deduced by using (270). Each column of A_h requires, then, the solution of 4 discrete Dirichlet problems (5 in the case of $\Omega \subset \mathbb{R}^3$). As the matrice A_h is symmetrical, the problem may be limited to indices $i \ge j$.

Taking into account the choice of $\mathcal{T}_h$, the integrals defining (270) involve only the functions having a support of about $\partial\Omega$ (Figure 25).

Flow Chart 2 of the construction of operator A is presented below.

Construction of b_h : to construct the second member of (277), the sequence of problems (272) (273) (274) is solved, which requires 4 discrete Dirichlet problems (5 if $\Omega \subset \mathbb{R}^3$). /83

Considering the choice of $\mathcal{T}_h$, the integrals defining the second member of (277) involve only the functions having a support in the proximity of (Figure 25).

10.6.5.2.2. Solution of System $A_h\lambda_h = b_h$ by the Chloski Method

A) CONSTRUCTION DE L'OPÉRATEUR SYMÉTRIQUE DÉFINI POSITIF A (i,j) COLONNE PAR COLONNE

KEY A) CONSTRUCTION OF THE SYMMETRICAL OPERATOR DEFINED POSITIVE AT (i,j) COLUMN BY COLUMN
B) For all nodes...

B) → Pour tous les nœuds $I \in \Gamma$ /82

$$\int_\Omega \vec{\nabla} P_k \cdot \vec{\nabla} M \, d\Omega = 0$$

$$P_k|_\Gamma = \delta_{Ik}$$

↓

$$\int_\Omega \alpha \vec{u}_k \cdot \vec{N} + \nu \vec{\nabla} \vec{u}_k \cdot \vec{\nabla} N \, d\Omega = \int_\Omega \vec{\nabla} P_k \cdot \vec{N} \, d\Omega$$

$$\vec{u}_k|_\Gamma = 0$$

↓

$$\int_\Omega \vec{\nabla} \phi_k \cdot \vec{\nabla} M \, d\Omega = \int_\Omega \vec{\nabla} \cdot \vec{u}_k M \, d\Omega$$

$$\phi_k|_\Gamma = 0$$

↓

$$A(I,J) = \int \vec{\nabla} \cdot \vec{u}_k M_j + \vec{\nabla} \phi_k \cdot \vec{\nabla} M_J \, d\Omega$$

support J, $J \in \Gamma$

NAVIER STOKES FLOW CHART 2

ORGANIGRAMME NAVIER-STOKES 2

Account taken of theorem 10.6.4.1. and of the definition of $\mathcal{B}_h$

$$\mathrm{Ker}(A_h) = \{\vec{v} \in \mathbf{R}^{N_h} | \nu_1 = \nu_2 = \nu_{N_h}\}$$

and since the matrix A_h is singular, it is necessary to fix a component of λ_h ($\lambda_{N_h} = 0$, for example) in order for the sub matrix

$A_h = (a_{ij})_{1<i,j\leq N_h-1}$ to be symmetrical, defined positive.

The sub-system to be solved is therefore expressed (278)

$$\tilde{A}_h \tilde{r}_h \lambda_h = \tilde{b}_h \quad \text{where} \tag{278}$$

$$\tilde{r}_h \lambda_h = \{\lambda_1, \ldots, \lambda_{N_h-1}\} \ , \quad \tilde{b}_h = \{b_1, b_2, \ldots, b_{N_h-1}\}$$

(278) is solved by the Choleski method via the standard factorization (279)

$$\tilde{A}_h = \tilde{L}_h \tilde{L}_h^{\,t} \quad \text{where } \tilde{L}_h \text{ is a non singular lower triangular matrix} \tag{279}$$

In summary, the solutions to be computed to obtain the solution $(\vec{u}_h, p_h)$ derived from (E_h) by the Choleski method are the following

- 4 discrete Dirichlet problems to calculate $p_{oh}, \vec{u}_{oh}, \psi_{oh}$ $\tilde{b}_h$ (5 if $\Omega \subset \mathbf{R}^3$)
- $4(N_h-1)$ discrete Dirichlet problems to construct $\tilde{A}_h$ ($5(N_h-1)$ if $\Omega \subset \mathbf{R}^3$)
- 2 triangular or descent-climb systems to calculate λ_h $\tilde{L}_h \tilde{y}_h = \tilde{b}_h$; $\tilde{L}^t \tilde{r}_h \lambda_h = \tilde{y}_h$
- 3 discrete Dirichlet problems to obtain p_h and $\vec{u}_h$ from λ_h (4 if $\Omega \subset \mathbf{R}^3$).

Flow Chart 3 of the rapid Stokes algorithm is presented below.

In practice, the matrices of the Dirichlet problems are factorized once and for all outside of the control loop. They are two symmetrical matrices defined positive, one approaching $-\Delta$ by elements P_1, the other $\alpha \mathrm{Id}-\Delta$ by elements P_2 (or P_1 on a triangulation $\mathcal{T}_{h/2}$ defined in (213). /85

10.6.5.3. Solution of (E_h) by a Conjugate Gradient Method

General : It is interesting to solve (E_h) by an iterative method

SOLVEUR RAPIDE DE STOKES

RAPID STOKES ALGORITHM

/84

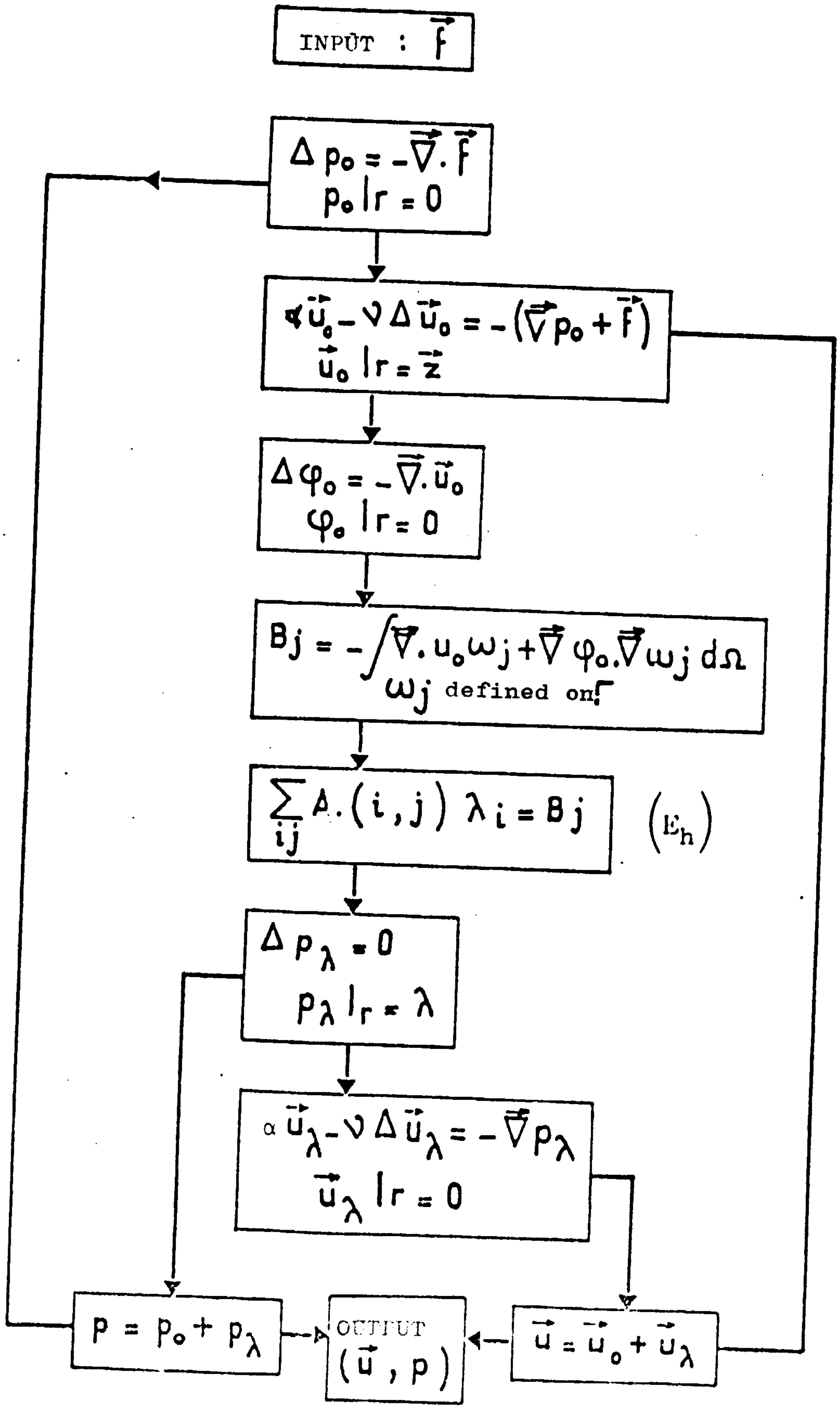

NAVIER STOKES FLOW CHART 3

ORGANIGRAMME NAVIER-STOKES 3

which does not require the EXPLICIT computation of A_h, but only, at each iteration, the solution of 4 discrete Dirichlet problems (5 if $\Omega \subset \mathbb{R}^3$). It is subsequently interesting to introduce the isomorphism

$$r_h : \mathcal{M}_h \to \mathbb{R}^{N_h} \text{ defined by}$$

$$r_h \mu_h = \{\mu_1, \mu_2, \ldots, \mu_{N_h}\} \quad \forall \mu_h \in \mathcal{M}_h$$

$$\text{with } \mu_h = \sum_1^{N_h} \mu_i w_i \; ; \; w_i \in \mathcal{B}_h \text{ base of } \mathcal{M}_h \text{ introduced in (273)}$$

$(\cdot,\cdot)_h$ shall designate the standard euclidian scalar product in $\mathbb{R}^{N_h}$ & $\|\cdot\|_h$ the corresponding standard.

By using the observations above, the two members of problem (E_h) (271) are expressed

$$\begin{cases} a_h(\lambda_h,\mu_h) = (A_h r_h \lambda_h, r_h \mu_h)_h & \forall \lambda_h, \mu_h \in \mathcal{M}_h \\ \int_\Omega (\vec{\nabla}\psi_{oh} + \vec{u}_{oh}) \vec{\nabla}\mu_h \, dx = (b_h, r_h \mu_h)_h & \forall \mu_h \in \mathcal{M}_h \end{cases} \tag{280}$$

Description of the Algorithm in (281) (282) (283) (284)

Phase 0 : Initialization

$$\begin{cases} r_h \lambda_h^o \in \mathbb{R}^{N_h} \text{ is given arbitrarily} \\ g_h^o = A_h r_h \lambda_h^o - b_h \\ h_h^o = g_h^o \end{cases} \tag{281}$$

Then, for $n \geq 0$, $\lambda_n^n, g_h^n, h_h^n$ being known, compute $\lambda_h^{n+1}, g_h^{n+1}, h_h^{n+1}$ by

Phase 1 : Descent /86

$$\rho_n = \frac{(h^n, g^n)_h}{(A_h h_n^n, h_n^n)_h} \tag{282}$$

$$\begin{cases} r_h \lambda_h^{n+1} = r_h \lambda_n^n - \rho_h h_h^n \\ g_h^{n+1} = g_h^n - \rho_n A_h h_n^n \end{cases} \tag{283}$$

Phase 2 : Construction of the New Direction of Descent

$$\gamma_n = \frac{\| g_h^{n+1} \|_h^2}{\| g_h^n \|_h^2} \tag{284}$$

$$h_h^{n+1} = g_h^{n+1} + \gamma_h h_n^n$$

$n = n+1$, go in 282.

Notes :

As the matrix A_h is symmetrical, semi-defined positve, it may be shown that the sequence $\{\lambda_h^n\}$ converges toward λ_h solution of (E_h). The component of λ_h defining the pressure level is the same one as the initial pressure λ_h^0. The implementation of (281)... (284) requires the solution of 4 Discrete Dirichlet problems to obtain p_{h,h^n}, u_{n,h^n}, ψ_{n,h^n} at each iteration (5 if $\Omega \subset \mathbf{R}^3$) in order to compute

$A_h h_n^n$ via (285)

$$\begin{cases} a_h(h_n^n, \mu_h) = (A_h h_n^n, r_h \mu_h)_h \\ \quad = \int_\Omega (\vec{\nabla}\psi_{h,h^n} + \vec{u}_{h,h^n}) \cdot \vec{\nabla}\mu_h \, dx \end{cases} \tag{285}$$

The prefactorization phase of the discrete Dirichlet matrices, recommended in the direct method, is also obvious, upstream of algorithm (281)...(284) and leading to considerable gain in calculation time.

10.6.5.4. Acceleration of Algorithm (281)...(284) by Preconditioning

Let $s_h : \mathcal{M}_h \times \mathcal{M}_h \to R$ be a symmetrical bilinear form defined positive to which the symmetrical matrix defined positive S_h is related via (286)

$$a_h(\lambda_h, \mu_h) = (S_h r_h \lambda_h, r_h \mu_h)_h \tag{286}$$

S_h is an auxiliary preconditioning operator in the sense of O. AXELSSON (32). The conjugate gradient variant using a scalar product $((\lambda_h, \mu_h))_{h,S_h} = (\lambda_h, S_h^{-1} \mu_h)$ relating to S_h is defined by (287) (288) (289) (290). /87

Phase 0 : Initialization

$$\begin{cases} r_h\lambda_h^o \in \mathbb{R}^{N_h} \text{ selected arbitrarily} \\ g_h^o = A_h r_h \lambda_h^o - b_h \\ h_h^o = S_h^{-1}\ g_h^o \end{cases} \tag{287}$$

For $n \geq 0$ λ_h^n, g_h^n, h_h^n known, compute λ_h^{n+1}, g_h^{n+1}, h_h^{n+1} by

Phase 1 : Descent

$$\begin{cases} \rho^n = \dfrac{(h_h^n, g^n)_h}{(A_h h_h^n, h_h^n)} \\ r_h\lambda_h^{n+1} = r_h\lambda_h^n - \rho^n h_h^n \\ g_h^{n+1} = g_h^n - \rho^n A_h h_h^n \end{cases} \tag{288}$$

Phase 2 : Construction of the New Direction of Descent (289)

$$\begin{cases} \gamma_n = \dfrac{(g_h^{n+1}, S_h^{-1} g_h^{n+1})_h}{(g_h^n, S_h^{-1} g_h^n)_h} \\ h_h^{n+1} = S_h^{-1} g_h^{n+1} + \gamma_n h_h^n \end{cases} \tag{289}$$

$n=n+1$, go to (288)

Notes : If S_h = Id (identity matrix) is selected, algorithm (281... (284) is found again.

Different choices of S_h are proposed by GLOWINSKI-PIRONNEAU (29 (29) guided by two different types of contradictory arguments (informatics and theoretical).

1. Select $S_h(.,.)$ leading to a hollow or even diagonal matrix S_h. In this case, S_h may be factorizd once and for all by the Choleski method $S_h = T_h T_h^t$ upstream of the algorithm (informatics argument).

2. Since $a_h(.,.)$ is an approximation of $a(.,.)$ defined on $H^{-1/2}(\Gamma)$ and elliptical $H^{-1/2}(\Gamma)$, select $S_h(.,.)$ approximation of a bilinear form $S(.,.)$ also elliptical $H^{-1/2}(\Gamma)$ This alternative, however, leads to a complete matrix S_h (theoretical argument)

We give to (290) (291) (29) three possible $S_h(.,.)$ leading to sparse S_h matrices, provided that the boundary nodes Γ have been numbered properly (minimum band width). /88

$$S_h(\lambda_h,\mu_h) = \int_\Gamma \lambda_h \mu_h \, d\Gamma \qquad (290)$$

$$S_h(\lambda_h,\mu_h) = \int_\Omega \lambda_h \mu_h \, d\Omega \qquad (291)$$

$$S_h(\lambda_h,\mu_h) = \int_\Omega \vec{\nabla}\lambda_h \cdot \vec{\nabla}\mu_h \, d\Omega \,. \qquad (292)$$

Assuming $_h$ defined in (275) (276) and that the Lagrange finite elements are used for the problem (271), it is then possible through numerical integration to combine with (290) (291) bilinear forms for which S_h is diagonal. This is the approximation (293) for (290)

$$S_h(\lambda_h,\mu_h) = \sum_1^{N_h} \frac{|M_{i-1}M_i| + |M_iM_{i+1}|}{2} \lambda_i \mu_i \qquad (293)$$

$(M_i)_{i=1,N_h}$ described on figure 26

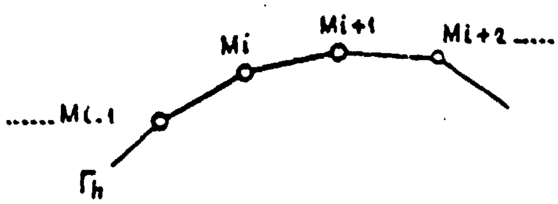

Figure 26

Whereas approximation (294
(294) is related to (291);
(M_i) describes figure 27

$$S_h(\lambda_h,\mu_h) = \sum_1^{N_h} \frac{1}{3} \text{ mes } (\text{supp } (M_i))\lambda_i\mu_i \qquad (294)$$

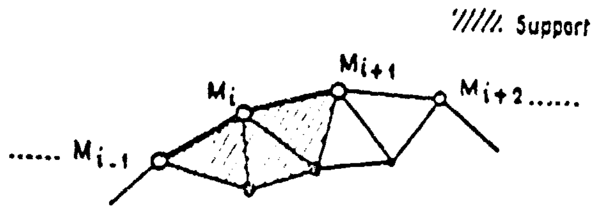

Figure 27

In (294) we recognize the scalar product L^2 approached $(\cdot,\cdot)_h$ defined on V_h by (295) /89

$$(f_h,g_h)_h = \frac{1}{(N+1)} \sum_{T \in \mathcal{T}_h} \text{mes}(T) \sum_{i=1}^{N+1} f_h(M_i) g_h(M_i) \text{ if } \Omega \subset \mathbb{R}^N, \ N=2 \text{ or } 3 \tag{295}$$

with mes (T) : area or volume of T
M_i : nodes of triangle or tetrahedron T.

We shall check whether the matrix S_h is diagonal by using the definition of $\mathcal{B}_h$ given in (275) (276) and (294). In fact, in this case

$$(\mathcal{B}_h\lambda_h, w_i)_h = \frac{1}{3}\text{mes}(\text{supp } M_i)\lambda_i.$$

Finally, it seems interesting to select S_h the inverse of the matrix (292) in an approached space of $H^{-1/2}(\Gamma)$, i.e. (296)

$$s_h^{-1}(\lambda_h,\mu_h) = \int_\Omega \vec{\nabla}\lambda_h \cdot \vec{\nabla}\mu_h \, dx \tag{296}$$

Various numerical tests of possible conditioning of (290) (291) (292) have been applied to the solution of the discrete Stokes problem via (287) (288) (289). The rapidity of convergence (number of iterations) and the calculation time are presented in chapter 12.

11. - ON THE METHODS OF INCOMPLETE FACTORIZATION

11.1. Summary

This chapter deals with the difficulties of informatics implementation of least squares algorithms on two and three dimensional configurations of large dimension.

We show how to use the methods of incomplete factorization as auxiliary operators of preconditioning or as auxiliary metrics in order to overcome excessive transfers of data on auxiliary memories (disk and or bands) outside of the main computer center.

11.2. Auxiliary Operator of a Problem of Model Evolution

We shall now consider the parabolic linear problem of standard evolution defined in (297) (298) (299)

$$\frac{\partial\phi}{\partial t} - \Delta\phi = f(x,t) \text{ in } \Omega \times]0,T[\tag{297}$$

$$\phi|_\Gamma = 0 \quad \text{on } \Gamma \times]0,T[\tag{298}$$

$$\phi(\vec{x},0) = \phi_o(\vec{x}) \quad \text{when} \quad t=0 \tag{299}$$

/90

where $\mho$ designates a bound domain of R^n of boundary Γ with f and ϕ_o sufficiently stable.

Any quantification in implicit time of (297) such that

$$\frac{1}{\Delta t}\phi^{k+1} - \Delta\phi^{k+1} = \frac{1}{\Delta t}\phi^k + f(\vec{x},k\Delta t) \tag{300}$$

with $\phi^k = \phi(\vec{x},k\Delta t)$, Δt time step leading to the solution of a linear system (301) after quantification of space (of finite differences or finite elements type)

$$A\phi^{k+1} = F^k \tag{301}$$

where $A = (a_{ij})\ 1 \le i,j \le N$ is usally a positive defined symmetrical matrix (N X N) with half band width m (N representing the number of nodes strictly included in the quantified domain Ω_h).

Since (301) must be solved numerous times and that A is independent from k, it is better to use a Choleski type direct method. Since A is symmetrical, defined positive, there is an inversible and unique lower triangular matrix L, having the same band width as m, so that

$$A = LL^t \tag{302}$$

with $\ell_{ii} > 0\ ;\ 1 \le i \le N$

where ℓ_{ii}, $1 \le i \le N$ are elements of the diagonal of L.
if ℓ_{ij} are elements of L so that

$$\ell_{ij} = 0 \quad \text{if } 1 \le i < j \le N$$

We bring back the algorithm of factorization of A (303) (304)

$$\begin{cases} \text{for } j=1 \\ \ell_{11} = \sqrt{a_{11}} \\ \ell_{i1} = \dfrac{a_{i1}}{\ell_{11}}, \ \forall\ 2 \le i \le N \end{cases} \tag{303}$$

$$\begin{cases} \text{For } 2 \le j < N \\ \ell_{jj} = (a_{jj} - \sum_{k=1}^{j-1} \ell_{jk}^2)^{1/2} \end{cases} \tag{304.1}$$

$$\ell_{ij} = \frac{1}{\ell_{ii}} (a_{ij} - \sum_{k=1}^{j-1} \ell_{ik}\ell_{jk}) \quad \forall\ j+1 \le i \le N \tag{304.2}$$

Once L is calculated, the determination of ϕ^{k+1} is immediate via a "descent-climb" (305) /91

$$\begin{cases} L\,\psi = F^k \\ L^t\,\phi^{k+1} = \psi \end{cases} \tag{305}$$

In industrial applications N may be very large ! ($\approx$ 10000), making the storage of A and L in the main core of the computer even impossible. Moreover, even though the non zero elements of A are not numerous (A is a sparse matrix); as for the matrix L, it is unfortunately always full.

Consequently, auxiliary core stations (disks or bands) must therefore be used, and this requires costly data transfers, which becomes excessive in an industrial context (problems of input-output, process time, etc...).

In order to preserve the advantages of direct methods such as the Choleski factorization, it is desireable to find a sparse lower triangular matrix $\tilde{L}$ close to L regarding their spectrum, and kept COMPLETELY in the main memory.

With $\tilde{L}$ it is possible to construct $\tilde{A}$ for (306)

$$\tilde{A} = \tilde{L}\tilde{L}^t \tag{306}$$

We substitute, then, for (301) the iterative process (307)

$$\tilde{A}\,\phi^{k+1} = (\tilde{A}-A)\,\phi^k + F^k \tag{307}$$

In (307) $\tilde{A}$ plays the role of auxiliary operator of A. It may be pointed out that the strategy to be adopted is different in selecting $\tilde{A}$ depending on whether (307) must be solved once or several times.

In the first case, we shall look for incomplete, fast and efficient factorizations in storage usage $\tilde{L}$ (see MEIJERINK and VAN DER VORST (30)) or similar iterative techniques (see VARGA (31)), AXELSSON (32), MANTEUFEL (33)), whereas in the second case, it is worthwhile to perform a significant computation upstream of (307) (proces time, memory) to benefit from extremely fast solutions at each Δt.

According to AXELSSON (32), $\tilde{A}$ may be used in another way, by having it play the role of a preconditioning matrix for a conjugate gradient solution of (301). If $\tilde{A}$ is used to define the scalar product (308) in R^N instead of the usual scalar product (309)

$$\langle\phi,\psi\rangle = \phi^t \tilde{A} \psi \qquad (308)$$

$$(\phi,\psi) = \phi^t \psi \qquad (309)$$

Therefore, the conjugate gradient solution for solving (301) corresponding to the minimization (310)

$$J(\phi) = \frac{1}{2} \phi^t A \phi - F\phi \qquad (310)$$

is given in (311) (312) (313)

Phase 0 : Let ϕ^o be selected arbitrarily

$$\text{Calculate} \quad G^o = A\phi^o - F$$
$$\text{Set} \quad \begin{cases} R^o = \tilde{A}^{-1} G^o \\ H^o = R^o \end{cases} \qquad (311)$$

then, for $n \geq 0$, assuming ϕ^n, G^n, H^n as known, calculate ϕ^{n+1}, G^{n+1}, H^{n+1} by

Phase 1 : descent

$$\begin{cases} \lambda^n = \underset{\lambda\geq 0}{\text{Arg min}}\; J(\phi^n - \lambda H^n) = \dfrac{H^{n^t} G^n}{H^{n^t} A H^n} \\ \phi^{n+1} = \phi^n - \lambda^n H^n. \end{cases} \qquad (312)$$

Phase 2 : Construction of the New Direction of Descent

C-2

$$
\begin{cases}
G^{n+1} = G^n - \lambda^n AH^n \\
R^{n+1} = \tilde{A}^{-1} G^{n+1} \\
\gamma^{n+1} = \dfrac{G^{n+1\,t} R^{n+1}}{G^{n\,t} R^n} \\
H^{n+1} = R^{n+1} + \gamma^{n+1} H^n
\end{cases}
\tag{313}
$$

do n=n+1 and go to (312)

/93

Note : The closer $\tilde{A}$ is to A, fewer the iterations are required : to obtain the convergence of (311) (312) (313). At the extreme, if = A, the algorithm converges easily in on iteration. The number of iterations required for convergence is a verification, a posteriori, of the efficiency of $\tilde{A}$.

11.3. Auxiliary Metric Related to a Functional Least Squares Method

A situation similar to 11.2 exists for another class of equations with nonlinear partial derivatives : this is for solving transonic and Navier-Stokes equations expanded below by the functional least s uares method.

We combine with (314) (315)

$$
\mathcal{C}(\phi) = \vec{\nabla}\cdot\rho(|\vec{\nabla}\phi|^2)\vec{\nabla}\phi = f \qquad (\Omega) \tag{314}
$$

$$
\phi|_\Gamma = 0 \qquad (\Gamma) \tag{315}
$$

where ρ is a nonlinear, positive, bound, given value of $|\vec{\nabla}\phi|^2$ The minimization (316) in H^{-1} of (314)

$$
\min_{\phi\in H_0^1(\Omega)} J(\phi) = \|\mathcal{C}(\phi)-f\|^2_{H^{-1}(\Omega)} \tag{316}
$$

is equivalent to the optimal control problem (317)

$$
\min_{\phi\in H_0^1(\Omega)} \left\{ \int_\Omega |\vec{\nabla}\varepsilon|^2 dx \;|\Delta\varepsilon = \mathcal{C}(\phi)-f \;,\; \varepsilon|_\Gamma = 0 \right\} \tag{317}
$$

The qua fication of (317) leads to the problem of minimization in R^N wi constraints (318)

$$\min_{\Phi \in \mathbb{R}^N} \{E^t BE \mid BE = T(\Phi) - F\} \qquad (318)$$

where B designates the matrix corresponding to the discrete Dirichlet operator and T the transonic operator obtained by quantification of (314).

Now, let us assume we know how to construct $\tilde{B}$ close to B as in 11.2, then in place of (318) we propose to solve (319)

$$\min_{\Phi \in \mathbb{R}^N} \{\tilde{E}^t \tilde{B} \tilde{E} \mid \tilde{B} \tilde{E} = T(\Phi) - F\} \qquad (319)$$

If $\tilde{B}$ is defined positive (318) and (319) are strictly equivalent.. However, if $\tilde{B}$ is not selected well (319) may be not as well conditioned as (318) and consequently, a conjugate gradient solution of (319) shall require considerably more iterations than of (318).

In this case, $\tilde{B}$ defined in (320) is the auxiliary metric of the nonlinear operator T

$$\langle \Phi_1, \Phi_2 \rangle = \Phi_1^t \tilde{B} \Phi_2 \qquad (320)$$

11.4. <u>Construction of the Auxiliary Operator</u> $\tilde{A}$ (resp. metric $\tilde{B}$)

We shall expand, in this paragraph, a methodology giving access to a class of sparse matrices $\tilde{A}$ or $\tilde{B}$ close to A or B.

Let $A = (a_{ij})_{1 \le i,j \le N}$ a positive defined symmetrical matrix with half band width <u>m</u> so that (Figure 28)

$$a_{ij} = 0 \text{ if } |i-j| > m \qquad (321)$$

Since A is factorized by the Choleski method (304) (305)

$$A = LL^t \qquad (322)$$

L is a lower triangular matrix, also of band width m. Furthermore, it may be observed that even if A has MANY zero elements INSIDE the band (Figure 28), it is not the case of L, which has NONE (Figure 29).

<u>Definition</u> : Let us define in (323) the set of indices K of zero elements of A inside band m

$$K = \{(i,j) \mid a_{ij} = 0\} \qquad (323)$$

CHOLESKY FACTORIZATION

$A = LL^t$

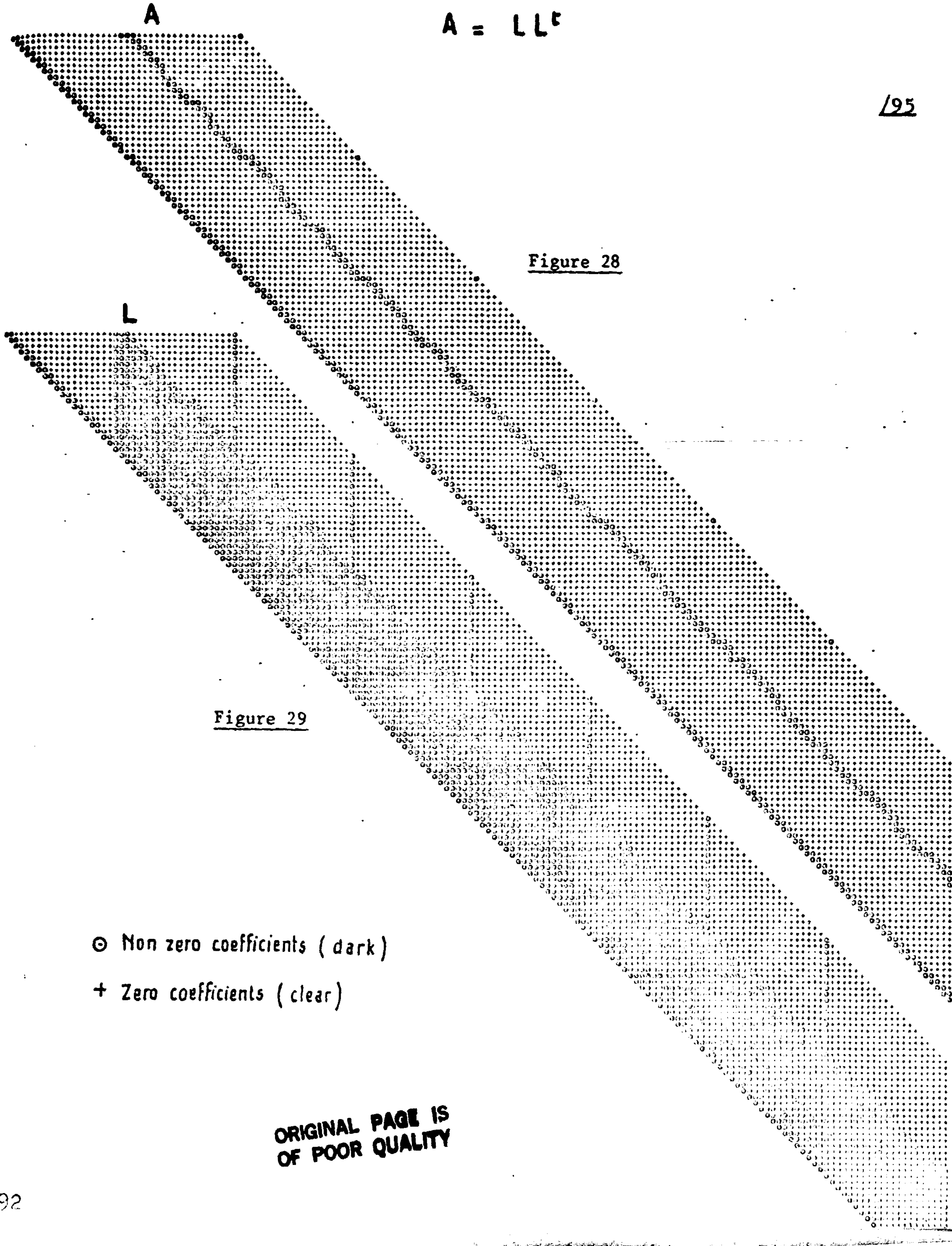

Figure 28

Figure 29

⊙ Non zero coefficients (dark)

\+ Zero coefficients (clear)

and let us designate by $n(K)$ the number of elements K. Since a positive constant C is now given, it is possible to define 2 auxiliary operators $\tilde{L}_C$ and $\tilde{L}'_C$ as follows

$\tilde{L}_C$ is defined by (324)

$$\begin{cases} \tilde{\ell}_{ij} = 0 \text{ if } (i,j) \in K \;\&\; |\ell_{ij}| \le C \\ \tilde{\ell}_{ij} = \ell_{ij} \text{ otherwise} \end{cases} \tag{324}$$

$\tilde{L}'_C$ is defined by (325)

$$\begin{cases} \tilde{\ell}'_{ij} = 0 \text{ if } (i,j) \in K \;\&\; |\ell_{ij}| \le C \min\limits_{i,j} (\ell_{ii},\ell_{jj}) \\ \tilde{\ell}'_{ij} = \ell_{ij} \text{ otherwise} \end{cases} \tag{325}$$

The constructions of $\tilde{L}_C$ and $\tilde{L}'_C$ bring to light the following observations :

1. If $C \le \min\limits_{i,j} |\ell_{ij}|$ then $\tilde{L}_C = L$
2. If $C \le \min\limits_{i,} \{\frac{|\ell_{ij}|}{\min\limits_{i,j}(\ell_{ii},\ell_{jj})}\}$ then $\tilde{L}'_C = L$
3. If $C \le \max\limits_{i,j} |\ell_{ij}|$ then $\{(i,j) | \tilde{\ell}_{ij} = 0\} = K$
4. If $C \le \max\limits_{i;} \{\frac{|\ell_{ij}|}{\min\limits_{i;}(\ell_{ii},\ell_{jj})}\}$ then $\{(i,j) | \tilde{\ell}'_{ij} = 0\} = K$.

In cases 3 and 4, 4, $\tilde{L}_C$ and $\tilde{L}'_C$ have their non zero elements located in the same position as those belonging to A and are very close to the incomplete Choleski operators proposed by MEIJERINK-VAN DER VORST (30) and D. KERSHAW (34). Nevertheless, they construct $\tilde{L}$ DURING the factorization of A (which means that L is NEVER constructed !) and economize store usage with the possible disadvantage of obtaining a singular $\tilde{L}$ matrix (to be pointed out that (304.1) requires the root of a positive number !). In the construction selected, L_C and L'_C are always non singular ; furthermore, if A is the dominant diagonal, $\tilde{L}_C$ and $\tilde{L}'_C$ are equivalent.

Finally, it may be observed that if the construction of $\tilde{L}_C$ or $\tilde{L}'_C$ leads to an allowable dimension in the main core of the computer, it is impossible to construct L for very large systems without auxilieary disks. Nevertheless, these external transfers to the main center are required ONLY ONCE during the phase of factorization.

For practical applications, having a size of a main core which is not to be exceeded, it is worthwhile to choose the constant C so a given percentage d/100 of non zero elements of $\tilde{L}_C$ or of $\tilde{L}'_C$ are mem-/97 orized. Therefore, since $d \leq 100$, we may define $L_{d/100}$ and $\tilde{L}'_{d/100}$ as follows :

For a given constant C, let us define $\tilde{K}_C$ and $\tilde{K}'_C$ in (326) (327)

$$\tilde{K}_C = \{(i,j) \mid \tilde{\ell}_{ij} \neq 0\} \tag{326}$$

$$\tilde{K}'_C = \{(i,j) \mid \tilde{\ell}'_{ij} \neq 0\} \tag{327}$$

if $n(\tilde{K}_C)$ and $n(\tilde{K}'_C)$ designate respectively the number of elements of $\tilde{K}_C$ (resp. $\tilde{K}'_C$), then the relationships between the sets $(\tilde{L}_{d/100}, \tilde{L}'_{d/100})$ $(\tilde{L}_C, \tilde{L}'_C)$

$$\tilde{L}_{d/100} = \tilde{L}_C \text{ with } C \text{ so that } n(\tilde{K}_C) = n(K)d/100 \tag{328}$$

$$\tilde{L}'_{d/100} = \tilde{L}'_C \text{ with } C \text{ so that } n(\tilde{K}'_C) = n(K)d/100. \tag{329}$$

By analogy to remarks 3.4

If $d=100$, $\tilde{L}_{100/100}$ & $\tilde{L}'_{100/100}$ are identical to L

If $d=0$, ; $\tilde{L}_o$ & $\tilde{L}'_o$ correspond to the Meijerink-Van der Vorst type Choleski incomplete factorizations.

It should be pointed out that there is another $\tilde{L}_{VV}$ construction, which is interesting theoretically, even though in 3-D applications it leads to excessive d/100 percentages. This construction is valid only for matrices using the finite elements method.

If $\mathcal{T}$ designates a standard triangulation of domain Ω, $\mathcal{T}$ is a set of adjacent polyhedrals T, composed of $(M_i)^N$ nodes.

The complementary K_V of K may be expressed then (330)

$$K_V = \{(i,j) \mid M_i, M_j \in T \text{ for at least one } T \text{ of } \mathcal{T}\}. \tag{330}$$

From K_V it is possible to define in (331) K_{VV} serving in the construction of $\tilde{L}_{VV}$ (332)

$$K_{VV} = \{(i,j) \mid \exists\, M_K \text{ so that } \begin{matrix} M_i, M_k \in T_1 \\ M_i, M_j \in T_2 \end{matrix} \tag{331}$$

for at least one couple T_1, T_2 of $\mathcal{T}_h\}$

$$\tilde{L}_{VV} = \{\tilde{\ell}_{ij} \mid \tilde{\ell}_{ij} = \ell_{ij} \text{ if } (i,j) \in K_{VV}\} \tag{332}$$

$$\tilde{\ell}_{ij} = 0 \text{ otherwise}$$

/98

With such a construction, $\tilde{L}_{VV}$ is independent from the numbering of . Unfortunately, the case is that $\tilde{L}_{VV}$ has few zero elements within its band (20% in 2-D, 50% in 3-D).

Remarks : The introduction of $\tilde{L}'_C$ is also motivated by the finite elements method. In fact, it is easy to verify that if $\Omega \subset \mathbb{R}^3$, then $\ell_{ij} = O(h)$ where h is the average length of the sides of $T \in \mathcal{T}$, whereas if $\Omega \subset \mathbb{R}^2$, then $\ell_{ij} = O(1)$. It is also necessary to eliminate the small elements by a test along their width relating to the diagonal elements and not along their absolute width.

11.5 Applications of Incomplete Factorizations to Transonic Flows and to the Navier-Stokes Equations.

The matrices $\tilde{L}_{d/100}$, $\tilde{L}'_{d/100}$, $\tilde{L}_{VV}$ have been introduced in the lifting least squares methods on industrial applications of large dimension in order to treat the algorithm ENTIRELY within the main core of the computer.

Two strategies are presented and compared with respect to informatics (computation time, memory space).

$\boxed{S_1}$ $\tilde{L}_{d/100}$, $\tilde{L}'_{d/100}$, $\tilde{L}_{VV}$ are used uniquely as preconditioning operators in the solution of discrete Dirichlet problems within the algorithm, thus keeping the metric H^1. We have only to substitute for the direct descent-climb LL^t, a preconditioned conjugate gradient algorithm $\tilde{\tilde{L}}$ d/100 of which the convergence speed depends essentially on the percentage d/100. Two iterative algorithms on the pressure of the Stokes algorithm are presented on Flow Charts 4 and 5.

$\boxed{S_2}$ $\tilde{L}_{d/100}$, $\tilde{L}'_{d/100}$, $\tilde{L}_{VV}$ are used as auxiliary metrics modifying this time the convergence speed of the least squares algorithm. The direct descent-climbs LL^t are substituted by the direct descent-climbs $\tilde{L}\tilde{L}^t$. In this case a minimum percentage d/100 is required to keep the convergence velocities at an acceptable rate.

ITERATIVE SOLUTION ON THE PRESSURE IN $L^2(\Omega)$

OF THE STOKES ALGORITHM P1/P2 (TAYLOR-HOOD ELEMENT)

WITH (*) SOLVED BY PRECONDITIONED CONJUGATE GRADIENT $\tilde{L}\tilde{L}^t$

$$(S_{TH}) \quad \min_{p \in L^2(\Omega)} \{J(p) = \frac{1}{2} \int_\Omega p\, \vec{\nabla}\cdot\vec{u}_p \, dx \mid -\Delta\vec{u}_p = -\vec{\nabla}p + \vec{f}\ ,\ \vec{u}_p - \vec{z} \in (H_o^1(\Omega))^N\} \quad (*)$$

In (S_{TH}) $p \rightsquigarrow Ap = \vec{\nabla}\cdot\vec{u}_p$ is coercive in $L^2(\Omega)$

$$\exists \alpha > 0 \quad (Aq,q)_{L^2} \geq \alpha \|q\|^2_{L^2} \quad \forall\, q \in L^2(\Omega)$$

<u>FLOW CHART 4</u>

Preconditioned Stokes Algorithm (T-H)

FLOW CHART 4 (cont) /10

<u>ALGORITHME</u> (S_{TH}) - <u>Initiali ation</u>

$$p^o \in L^2$$

(*) $$-\Delta\vec{u}^o = \vec{f} - \vec{\nabla}p^o \;,\; \vec{u}^o - \vec{z} \in (H_o^1(\Omega))^N$$

$$g^o = \vec{\nabla}\cdot\vec{u}^o$$

$$h^o = g^o \;;\; \vec{\chi}^o = \vec{u}^o$$

<u>Descent</u>

$$\rho_n = \frac{\|g^n\|^2_{L^2}}{(\vec{\nabla}\cdot\vec{\chi}^n, h^n)_{L^2}}$$

$$p^{n+1} = p^n - \rho_n h^n$$

<u>New direction</u>

$$g^{n+1} = g^n - \rho_n \vec{\nabla}\cdot\vec{\chi}^n$$

$$\gamma^n = \frac{\|g^{n+1}\|_{L^2}}{\|g^n\|_{L^2}}$$

$$h^{n+1} = g^{n+1} + \gamma^n h^n$$

(*) $$\Delta\vec{\chi}^{n+1} = \vec{\nabla}h^{n+1} \;;\; \vec{\chi}^{n+1} \in (H_o^1(\Omega))^N$$

$n = n+1$

(*) N Dirichlet problems decoupled by iteration, solved by preconditioned gradient $\tilde{\Delta} = \tilde{L}\tilde{L}^t$

N = dimension of the space

ITERATIVE SOLUTION OF THE PRESSURE TRACE IN $H^{-1/2}(\Gamma)$ OF THE STOKES ALGORITHM P1/P2 (GLOWINSKI-PIRONNEAU ELMENT) WITH (*) (**) SOLVED BY THE PRECONDITIONED CONJUGATE GRADIENT ALGORITHM $\begin{cases}\tilde{L}\tilde{L}^t\\ \tilde{S}\tilde{S}^t\end{cases}$ $\tilde{\Delta} = \tilde{L}\tilde{L}^t$; $\tilde{A} = \tilde{S}\tilde{S}^t$ /101

$$(E_h) \qquad \min_{\lambda \in H^{-1/2}(\Gamma)/\mathbb{R}} \underbrace{\left\{ \frac{1}{2}\int_\Gamma A\lambda\ \lambda\ d\Gamma \right.}_{(**)} \underbrace{\left| \begin{array}{l} \Delta p_\lambda = \vec{\nabla}\cdot\vec{f}\ ,\ p-\lambda \in H^1_o(\Omega) \\ -\Delta\vec{u}_\lambda = \vec{f}-\vec{\nabla}p_\lambda,\ \vec{u}-\vec{z} \in (H^1_o(\Omega))^N \\ -\Delta\phi_\lambda = \vec{\nabla}\cdot\vec{u}_\lambda\ ,\ \phi \in H^1_o(\Omega) \end{array} \right\}}_{(*)}$$

In (E_h) $\lambda \to A\lambda = -\dfrac{\partial\phi_\lambda}{\partial n}$ is coercive in $H^{-1/2}(\Gamma)$

$$\exists\, \alpha > 0 \qquad \langle A\lambda,\lambda\rangle \geq \alpha\|\lambda\|^2_{H^{-1/2}} \qquad \forall\, \lambda \in H^{-1/2}(\Gamma)$$

where $\langle\cdot,\cdot\rangle$ designates the duality product $H^{1/2}(\Gamma)$ in $H^{-1/2}(\Gamma)$

N = dimension of the space

* N+2 Dirichlet problems in Ω, solved by preconditioned conjugate gradient $\tilde{L}\tilde{L}^t$

** descent-climb on Γ with $\tilde{A} = \tilde{S}\tilde{S}^t$

ALGORITHM (E_h)

Initialization

$$\lambda^0 \in \mathcal{M}_h$$

(*) $$\Delta p^0 = \vec{\nabla}\cdot\vec{f} \quad , \quad p^0 - \lambda^0 \in H^1_0(\Omega)$$

(*) $$\Delta \vec{u}^0 = \vec{\nabla} p^0 - \vec{f} \quad , \quad \vec{u}^0 - \vec{z} \in (H^1_0(\Omega))^N$$

(*) $$\Delta \phi^0 = \vec{\nabla}\cdot\vec{u}^0 \quad , \quad \phi^0 \in H^1_0(\Omega)$$

$$g^0 = A\lambda^0 = \frac{\partial \phi^0}{\partial n}\Big|_\Gamma$$

(**) $$r^0 = \tilde{A}^{-1} g^0$$

$$h^0 = r^0 \ ; \ \vec{\chi}^0 = \vec{u}^0$$

Descent

$$\rho_n = \frac{(h^n, g^n)}{(Ah^n, h^n)}$$

$$\lambda^{n+1} = \lambda^n - \rho_n h^n$$

New direction

$$g^{n+1} = g^n - \rho_n A h^n$$

(**) $$r^{n+1} = \tilde{A}^{-1} \ g^{n+1}$$

$$\gamma^n = \frac{(g^{n+1}, r^{n+1})}{(g^n, r^n)}$$

$$h^{n+1} = r^{n+1} + \gamma_n h^n$$

(*) $$\Delta p^{n+1} = 0 \ , \ p^{n+1} - h^{n+1} \in H^1_0(\Omega)$$

(*) $$\Delta \vec{\chi}^{n+1} = \vec{\nabla} p^{n+1}, \ \vec{\chi}_n^{n+1} \in (H^1_0(\Omega))^N$$

(*) $$\Delta \phi^{n+1} = \vec{\nabla}\cdot\vec{\chi}^{n+1} \quad , \quad \phi^{n+1} \in H^1_0(\Omega)$$

$$Ah^{n+1} = \frac{\partial \phi^{n+1}}{\partial n}\Big|_\Gamma$$

$n=n+1$

Numerical experiences of these two strategies applied to 2-D, 3-D transonic flo s, on the one hand, and to the Stokes algorithm (E_h) 2-D, 3-D, expanded in chapter 10, from the Navier-Stokes equations, on the other hand, are presented in chapter 12.

12. - NUMERICAL EXPERIENCES

12.1. Data Processing Aspects

The numerical simulations presented below have been applied on the IBM 370-168 computer.

In the case of the approximations P_k, k=2, the various integrals involved in the derivation of nonlinear systems with finite dimension discrete transonic equation (T) - discrete Navier-Stokes equations (NS) are computed EXACTLY with FORMAC (A. LAPLACE (22)).

For example; (T) requires the implementation of a polygonal with degree 3 (333), whereas the (NS) convection terms require the integration of polynomials with degree 5 (334)

$$\int_\Omega \rho\, \vec{\nabla}\phi \cdot \vec{\nabla} N_k dx \; ; \; N_k = \begin{cases} L_k(2L_k-1) & k=1,2,3 \\ 4L_iL_j & k=4,5,6 \quad i\neq j \quad i,j=1,2,3 \end{cases} \qquad (333)(T)$$

$$\int_\Omega (\vec{u}\cdot\vec{\nabla})\vec{u}\cdot\vec{N}_k \, dx \qquad (334)(NS)$$

The expression of (333) (334) as a function of area coordinates (L_i) together with their derivatives (refer to O.C. ZIENKIEWICZ (24)) the standard relationships (335) (336) following dimension 2 or 3 of the space.

$$\int_{T\in \mathcal{T}_h} L_1^\alpha L_2^\beta L_3^\gamma \, d\Gamma = \frac{\alpha!\beta!\gamma!\;2}{(\alpha+\beta+\gamma+2)!} \qquad (T) \; ; \; \sum_{i=1}^{3} L_i = 1 \, , \qquad (335)$$

$$\alpha+\beta+\gamma \leq 5 \; , \; \alpha,\beta,\gamma \geq 0$$

$$\int_{T\in \mathcal{T}_h} L_1^\alpha L_2^\beta L_3^\gamma L_4^\delta \, d\Gamma = \frac{\alpha!\beta!\delta!\gamma!\;6}{(\alpha+\beta+\gamma+\delta+3)} \, \mathrm{Vol}(T) \; ; \; \sum_{i=1}^{4} L_i = 1 \qquad (336)$$

$$\alpha+\beta+\gamma+\delta \leq 5 \; , \; \alpha,\beta,\gamma,\delta \geq 0$$

The various triangulations $\mathcal{T}_h$ used are generated (case 2-D) automatically by the MODULEF techniques (35). The large number of solutions of the discrete Dirichlet problems justifies the choice of a Choleski band or Choleski-profile type direct method (35).

It is obvious that the factorization phase of the Dirichlet matrices shall always be performed ONCE AND FOR ALL prior to the iterative process. The matrices are solved entirely in the main core in the case of simple 2-D tests, whereas in most applications in industry 2-D/3-D, their memorization requires ONCE AND FOR ALLdata transfers with the use of auxiliary disks. For more details, MODULEF (35) may be consulted. /104

Finally, mention should be made of the preliminary phase of renumbering the triangulation nodes $\mathcal{T}_h$ for reducing the band widths of the Dirichlet matrices, by the CUTHILL-MCKEE algorithms (36).

12.2. Calculations of Transonic Flows

12.2.0. Characteristics of a Transonic Calculation

12.2.0.1. The Outputs

For each case of calculation (difference of potential) α_∞ incidence), we have acces, in the form of plottings, to the flow analysis

-either in the fluid by the Machs distribution (337) on elements or the iso-Machs

$$M^2 = \frac{2}{(\gamma+1)}\left[\frac{|\vec{\nabla}\phi|^2}{1-\frac{\gamma-1}{\gamma+1}|\vec{\nabla}\phi|^2}\right];\ \phi = \frac{\phi}{C^*} \tag{337}$$

-or on the bodies by the suface distribution of pressures Kp (intrados-extrados in the case of an airfoil profile)

$$Kp = \frac{p-p_\infty}{\frac{1}{2}\rho_\infty|\vec{v}_\infty|^2} = \frac{1}{\frac{\gamma}{2}M_\infty^2}\left[\left(\frac{1-\frac{\gamma-1}{\gamma+1}|\vec{\nabla}\phi|^2}{1-\frac{\gamma-1}{\gamma+1}|\vec{\nabla}\phi_\infty|^2}\right)^{\gamma/\gamma-1}-1\right] \tag{338}$$

Remarks :

1) The pressure and the Mach depend on the gradient of the potential. In the case of the approximation P1, the velocity $(\vec{\nabla}\phi)$ is constant on each triangle. The Mach and the pressure on the profile are from two ADJACENT triangles. In the case of the approximation P2, the speed $(\vec{\nabla}\phi)$ is linear. We may therefore represent the Mach and the pressure on the profile by a linear variation on the bar of the DJACENT triangles, but a discontinuity at the inter-bars may be observed. (Figure 30).

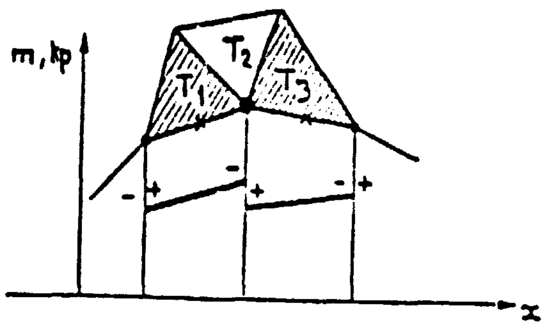

.discontinuity of the pressure and of the Mach depending on (T_1, T_2, T_3)

/105

xcontinuity of the pressure and of the Mach depending only on T_1 or T_3

2) The location of the shock (numerical) <u>depends on the approximation</u>.

In P1, a shock is located necessaritly at the inter-elements (Figure 31), whereas in P2 it may be taken into account inside an element (Figure 32)

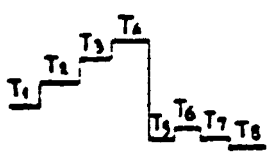

Figure 31

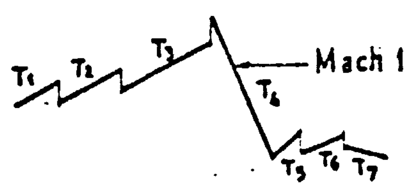

Figure 32

12.2.0.2. Finite Elements P1/Finite Elements P2 Comparisons

For a <u>same</u> domain and a same case of computation (M_∞ = .45 for example for a flow around a circle), we have tested the effect of the triangulations of Figure 33 (P1) and 34 (P2) on the convergence of th the schemes.

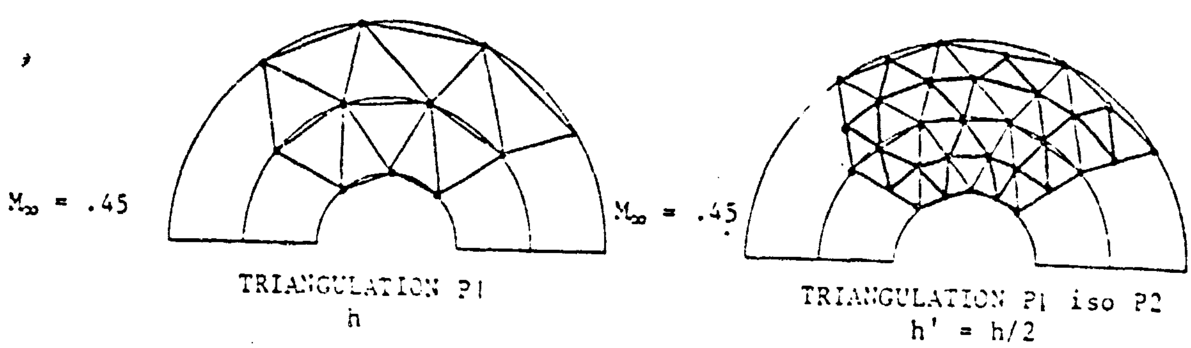

Figure 33

$M_\infty = .45$

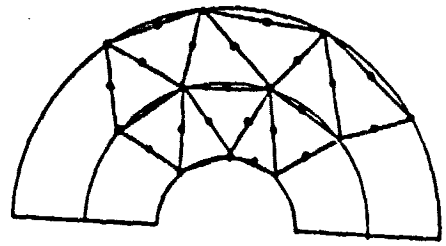

Figure 34 - Triangulation P2

Bringing to mind the terminology "P1 iso P2" : it is an approximation composed of the same degrees of freedon as the triangulation P2, each triangle P2 gives 4 sub-triangles P1 by joining the middles of the sides.

The convergence of the schemes of optimal control formulations with regulation, penalty or artificial viscosity is verified during N iterations of control in the form of plottings on which are shown

- the evolution of the cost function $(C^0, C^1, \ldots, C^N)$
- the evolution of the gradient $(G^0, G^1, \ldots G^N)$; $G^N = (g^N, g^N)^{1/2}$
- the determination of the circulation (Joukowski condition)
- the determination of the physical shock (supersonic-subsonic domain)
- the local . action of the penalty terms to prevent the development of shock decompression.

12.2.0.3. FINITE ELEMENTS/ FINITE DIFFERENCES Comparisons

The unconservative and conservative codes of A. JAMESON have served as reference for numerical tests on the NACA 0012 airfoil and the KORN airfoil.

It has proven to be instructive to compare locally the shock INTENSITY and LOCATION in lifting and non lifting cases between the two conservative codes (Finite Elements + Penalty) and (Finite Elements+ Artificial Viscosity) of the optimal control and of the two JAMESON codes (Conservatife Finite Differences) and (conservative Finite Differences) at 150 degrees of freedom (on the airfoil profile) and iso case of computation (and identical incidence).

Moreover, the difficulty of treating the Joukowski condition in finite elements ($p^+=p^-$ measured in AVERAGE at trailing edge in P1, exactly on airfoil profile in P2) was able to be disconnnected from comparisons (Finite Elements P1 - Finite Differences) by calculating with iso CZ (CZ : aerodynamic reaction of airfoil). Most of the results which follow have already been presented either in GP4B (37), or in contrac: LABORIA/IRIA/DRET (38).

12.2.1. The Converging-Diverging Pipe /107

The potential Φ is given at the pipe inlet and outlet, whereas the condition of tangency $\frac{\partial \Phi}{\partial n} = 0$ is applied on the sides.

The domain of the flow is quantified in 384 TRIANGLES on figure 35 for an approximation P1 - rough card-index or P2 (resp 1536 in the case P1 ISO P2).

The number of corresponding nodes was 221 (resp 825) for a linear approximation (quadratic resp. or P1 ISO P2°.

Figures 36 and 37 give a comparison without condition of entropy and with condition of entropy treated by REGULATION with $\mu = .1$ (resp $\mu_1 = .2$, $\mu_2 = .1$) of local Machs on axis (3) and the side (4) of the pipe.

4o iterations (resp 60) were required to obtain the convergence of the conjugate gradient algorithm thereby requiring 1.30 mn of process (resp 7mn).

Figures 38 and 39 show a plotting of the iso-machs resulting from P2 measurement in the regions (subsonic -supersonic) and (supersonic - subsonic) of the flow with shocks.

The agreement of the two approximations may be verified.

12.2.2. The circle /113

The NON LIFTING flow around a disk has a double numerical value: the equal distribution of the points of quantification on the circle due to a constant curve and of the compression and decompression shocks with equal intensity located symmetricallly. We have selected a case of transonic calculation $M_\infty = .45$.

For this problem the boundary conditions are the NEUMANN type

$$\frac{\partial \Phi}{\partial n} = \vec{U}_\infty . \vec{n} \text{ at infinity, } \frac{\partial \Phi}{\partial n} = 0 \quad \text{on obstacle).}$$

Numerical considerations require the substitution of a bound domain for the infinite domain with Γ_∞ sufficiently far from the obstacle in the following sense : if ℓ is the chord of the obstacle, the distance of ℓ from the obstacle is equalt to about 4 or 5 times

The domain is divided into 3456 TRIANGLES (resp 834) corresponding to 1813 NODES for one linear approximation (resp. quadratic).

The condition of entropy was treated by PENALTY and the convergence of the algorithm is obtained in 50 iterations (resp. 60) corresponding to 4 mn of process (resp. 8 mn).

TRIANGULATION OF A PIPE (IN P1)

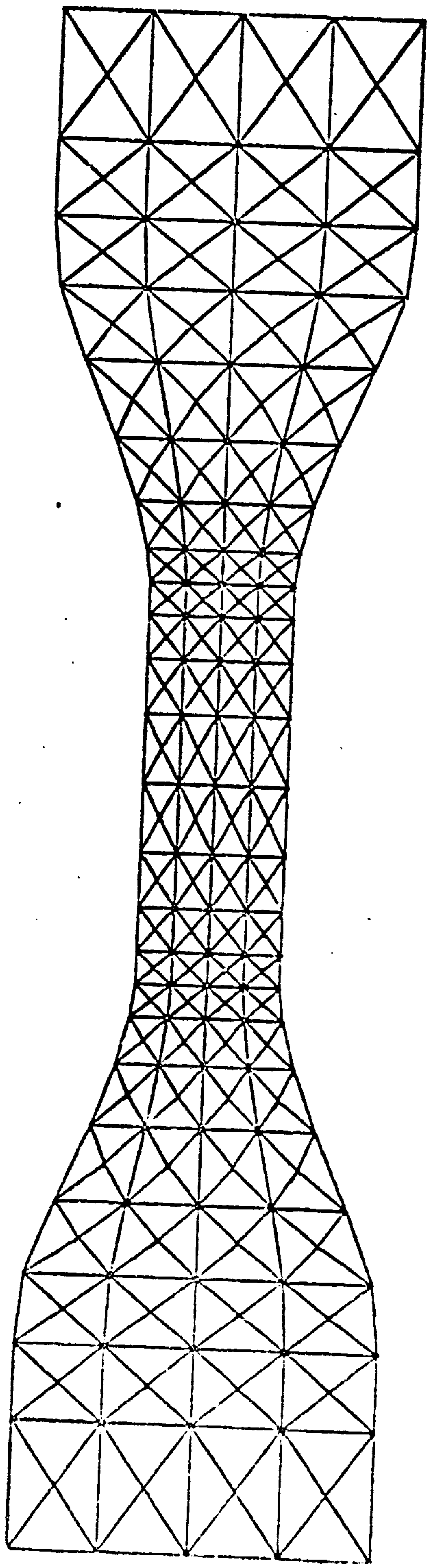

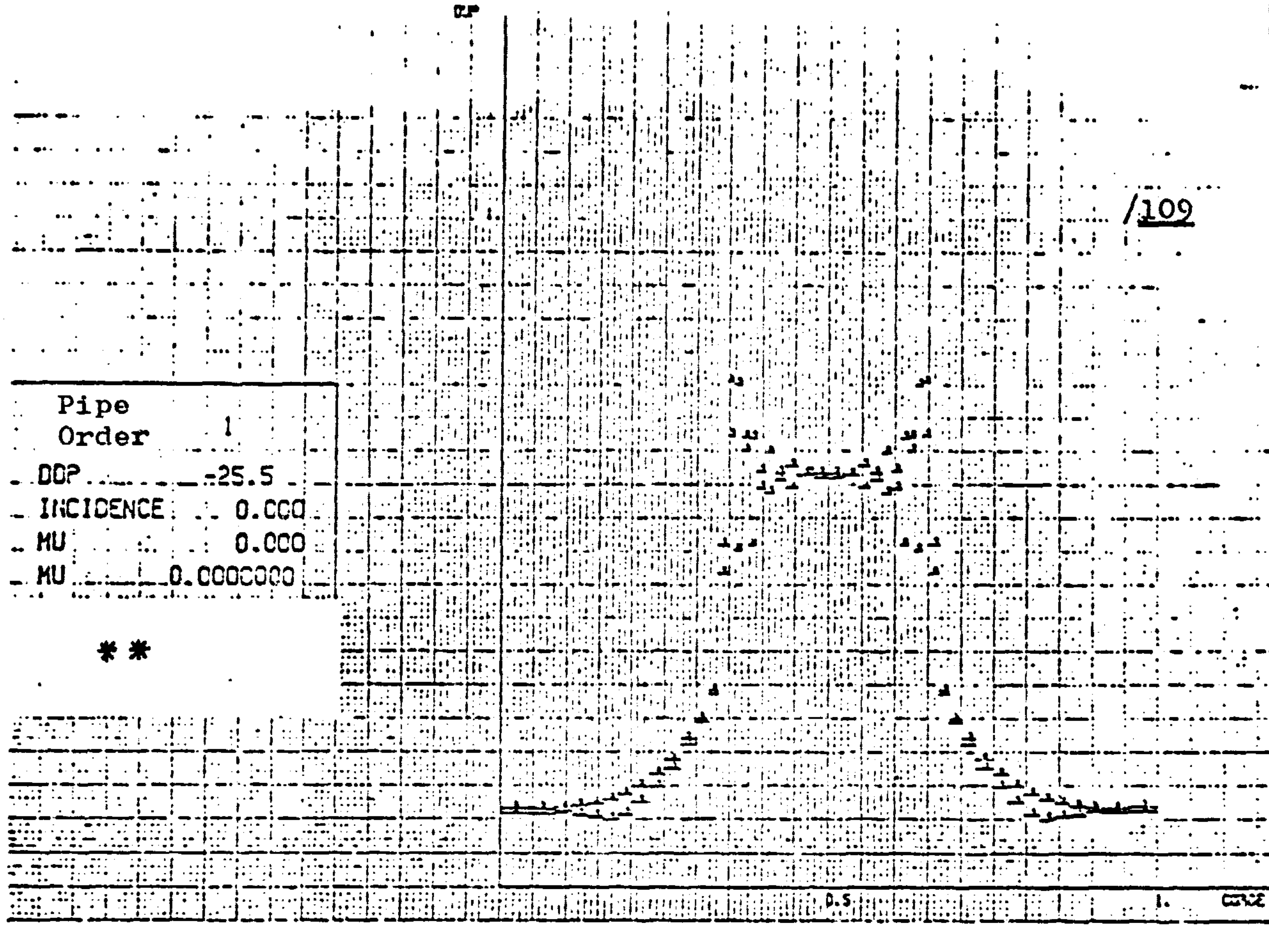

3. PIPE WALL 4. PIPE AXIS

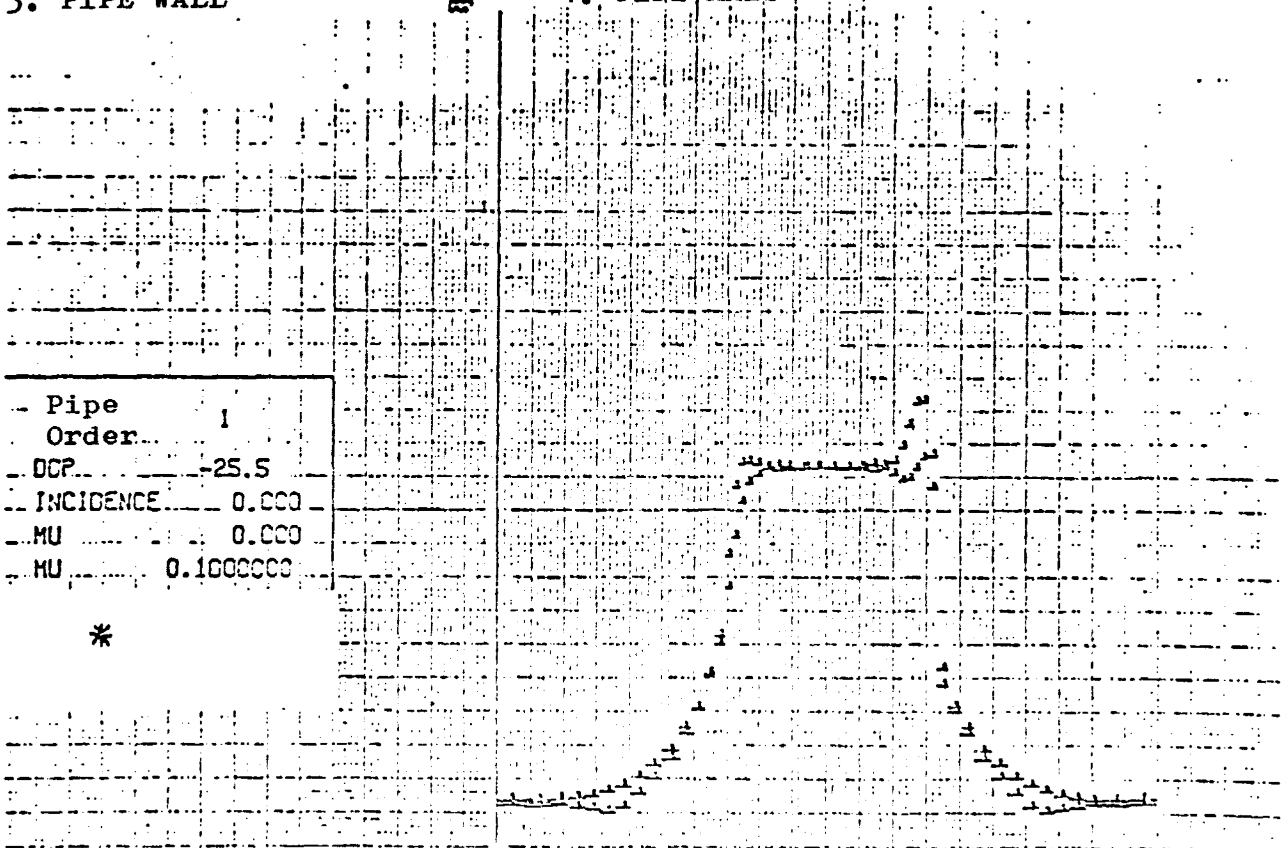

~~E.F. P1 WITH (*) And without (**)~~ CONDITION OF ENTROPY

(*) (**)

/110

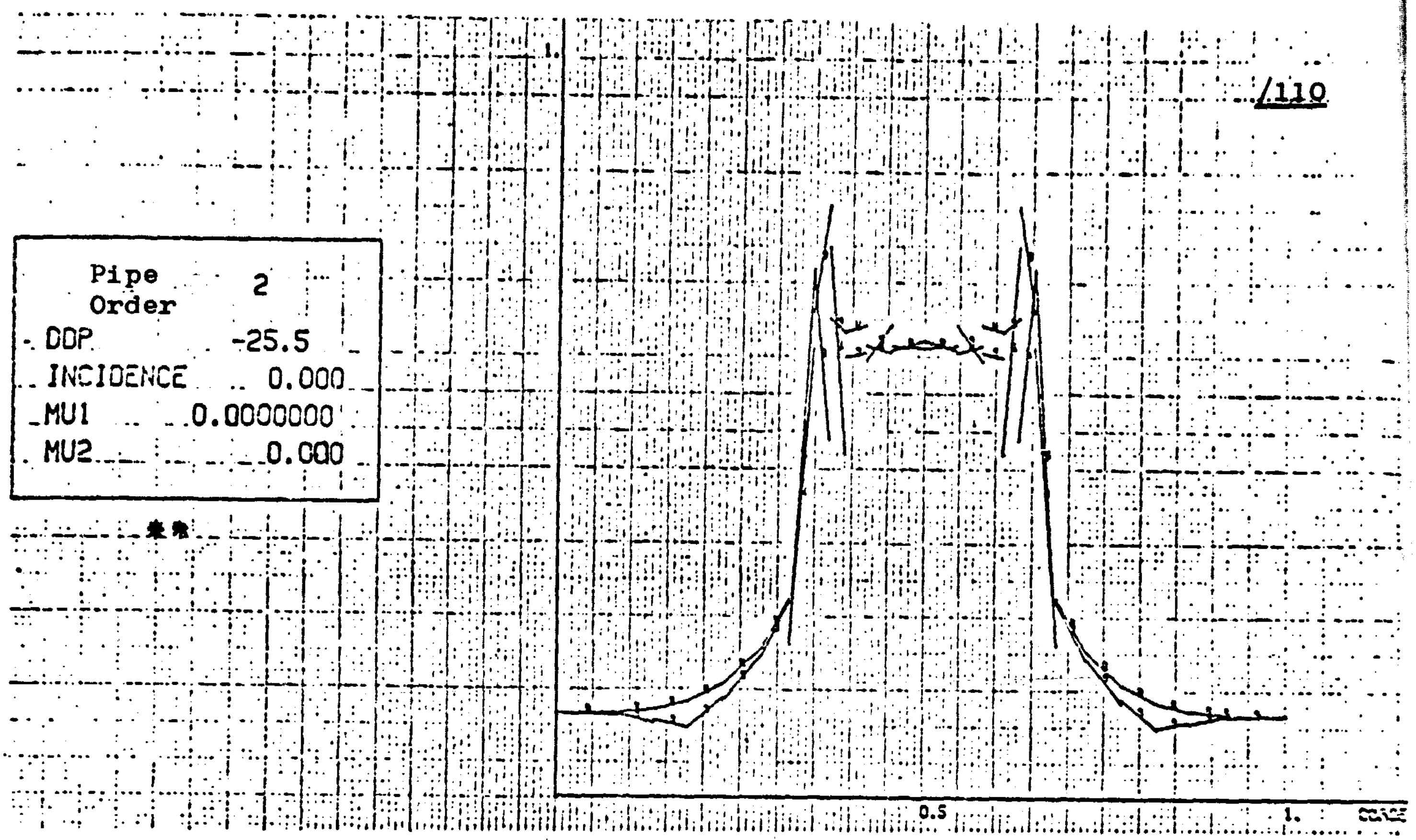

3 _ PIPE WALL

4 _ PIPE AXIS

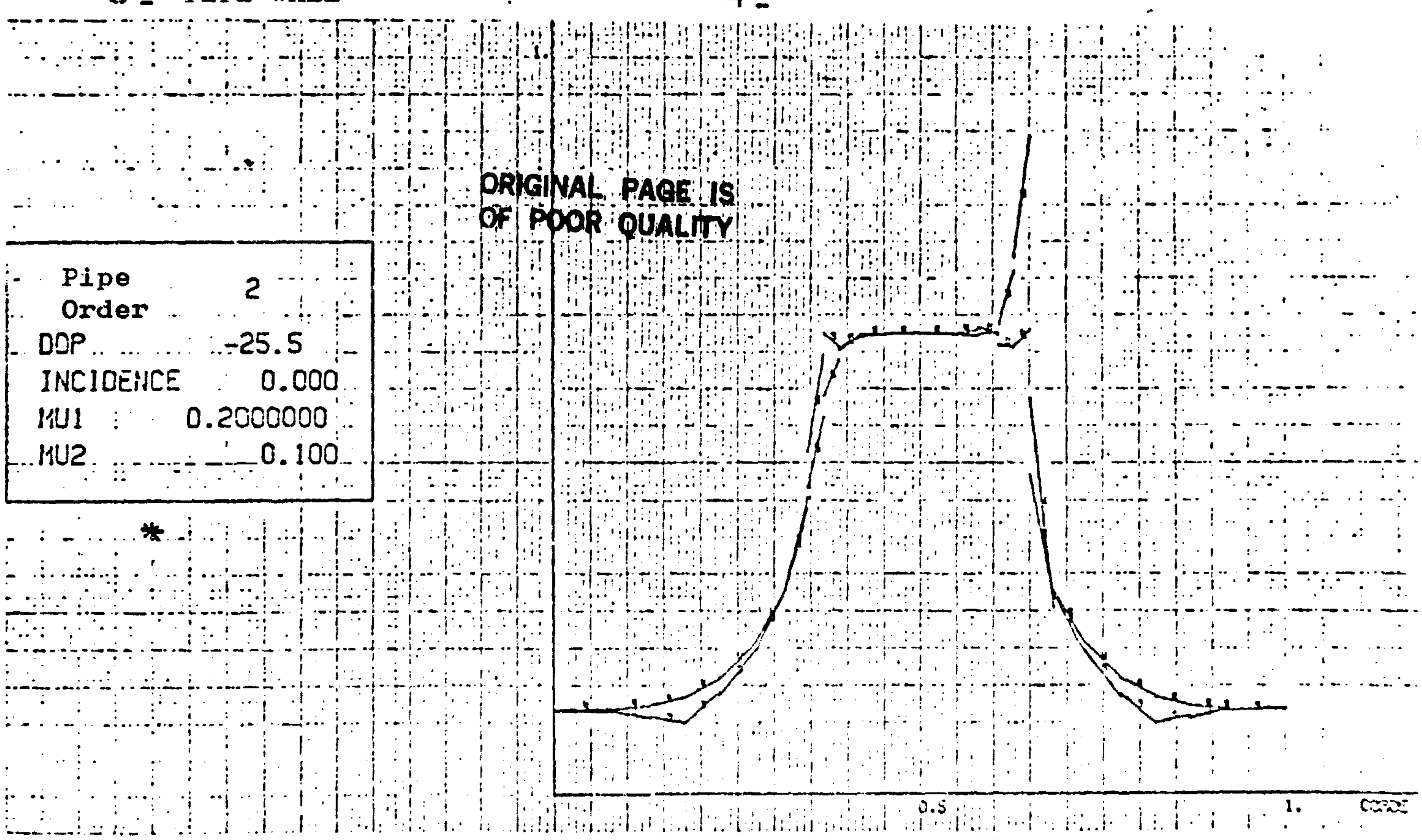

E.F. P2 WITH* AND WITHOUT** CONDITION OF ENTROPY

ISOMACHS P2

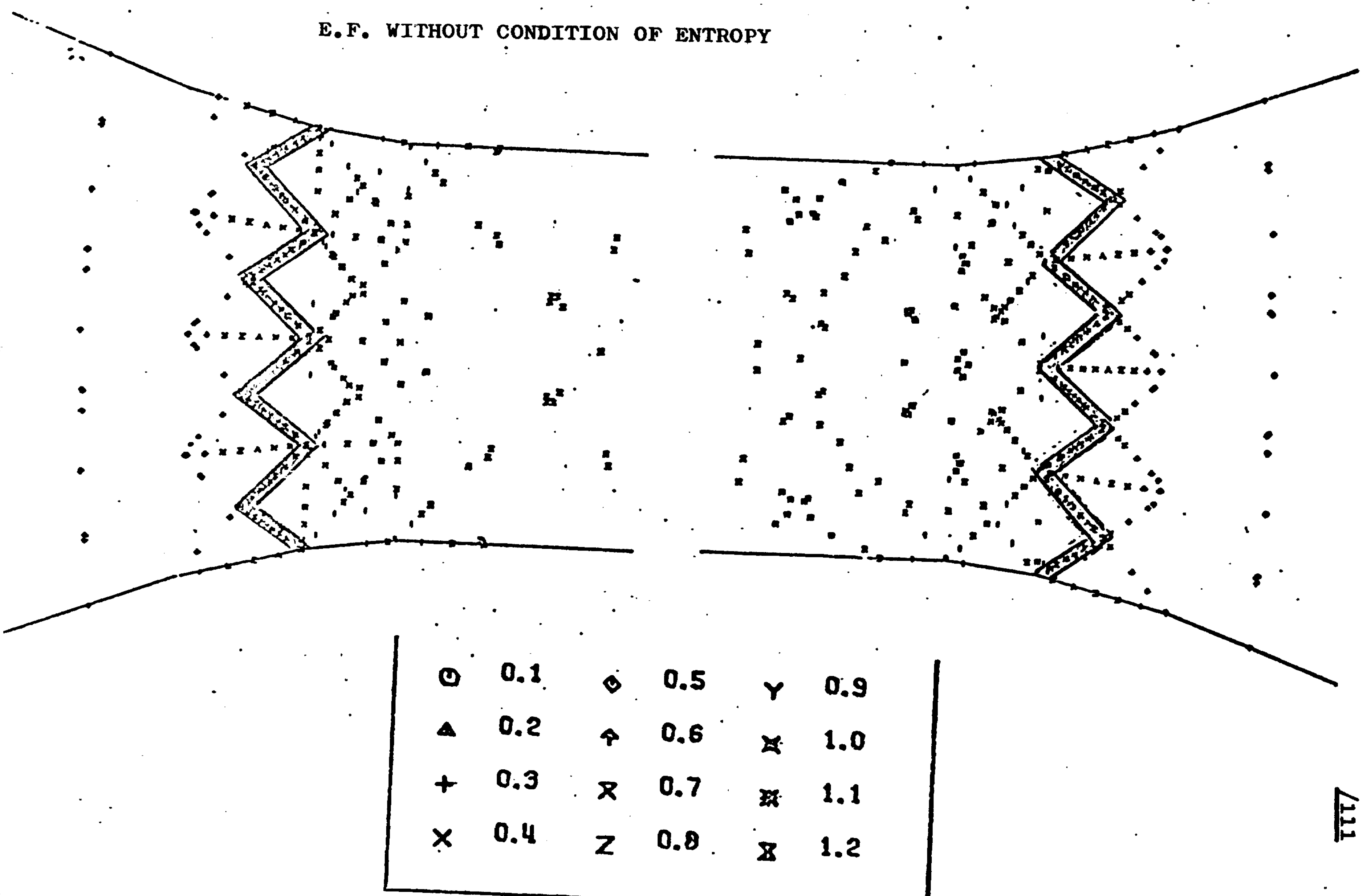
E.F. WITHOUT CONDITION OF ENTROPY
P2
0.1
0.2
0.3
0.4
0.5
0.6
0.7
0.8
Y 0.9
1.0
1.1
1.2

ISOMACHS P2

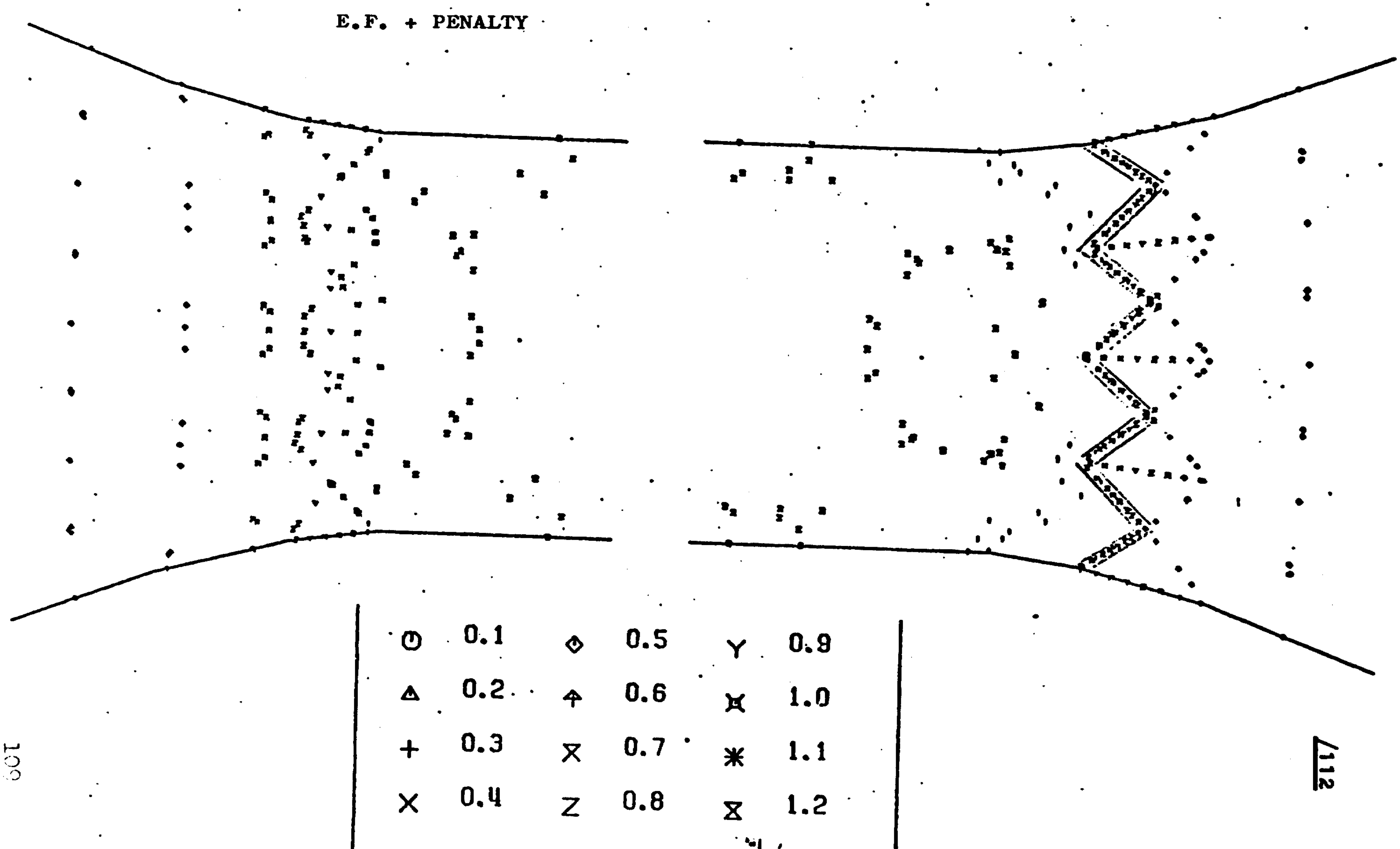

/112

Figure 40 shows a comparison P1 ISO P2/P2 of pressures (Kp) calculated on the ADJANCENT triangles to the circle.

Figure 41 shows in an iso-mach form the case in P2 of the shock /113
on a single element ADJACENT to the circle.

It may be observed that there is a strong shock intensity for the computation case M_∞ obtained by the two codes.

12.2.3. The NACA 0012 Airfoil Section (Profile)

A rough triangulation brought about by a WINSLOW algorithm (39) (resp. fine) (60 points on the airfoil) with enlargement near the obstacle, is given on figure 43. It is composed of 1080 triangles /117
(resp. 4380) and 600 nodes (resp. 2280).

12.2.3.1. The symmetrical non lifting case (without JOUKOVSKI condition

Two test cases have been calculated :

(1) - (M_∞ = .8 ; INC = 0°) "non stiff" case

(2) - (M_∞ = .85; INC = 0°) "stiff". case

Figures 44 through 48 relate to (1)

On figures 44, 46, 47 we have plotted the distribution of pressures on the airfoil profile.

The results of figure 44 (resp.45) correspond to a treatment of the condition of entropy with PENALTY (resp ARTIFICIAL Viscosity + REGULATION) ($\mu = .0015$; $K = .4$)(resp $\nu = .05$; $\mu = .000005$)

In the two cases, the convergence of the conjugate gradient algorithm was obtained in 40 iterations corresponding to 3.5 mn of process. One may notice the clearness of the shock obtained with Penalty.

Figure 46 compares the solution obtained by PENALTY in P1 on the fine triangulation with the ones derived from the conservative and non conservative codes of JAMESON in finite differences .

A comparison in the sense of approximation P1 ISO P2/P2 is made on figure 47 with the PENALTY (P1 ISO P2 : $\mu = .5$; $K = .0$; P2 : $\mu_1 = .1$; $K = .4$; $\mu_2 = .01$).

One may take note of the shock case in P2 on a single element ADJACENT to the airfoil profile together with the recompression after the shock, which marks the conservative form of the equations. The iso Machs near the airfoil profile derived from computations P1 and P2 with the entropy-penalty condition have been plotted on figure 48 and give an idea of the location of the shock and of its intensity in the fluid.

COMPARISONS P1-P2 FINITE ELEMENTS + PENALTY

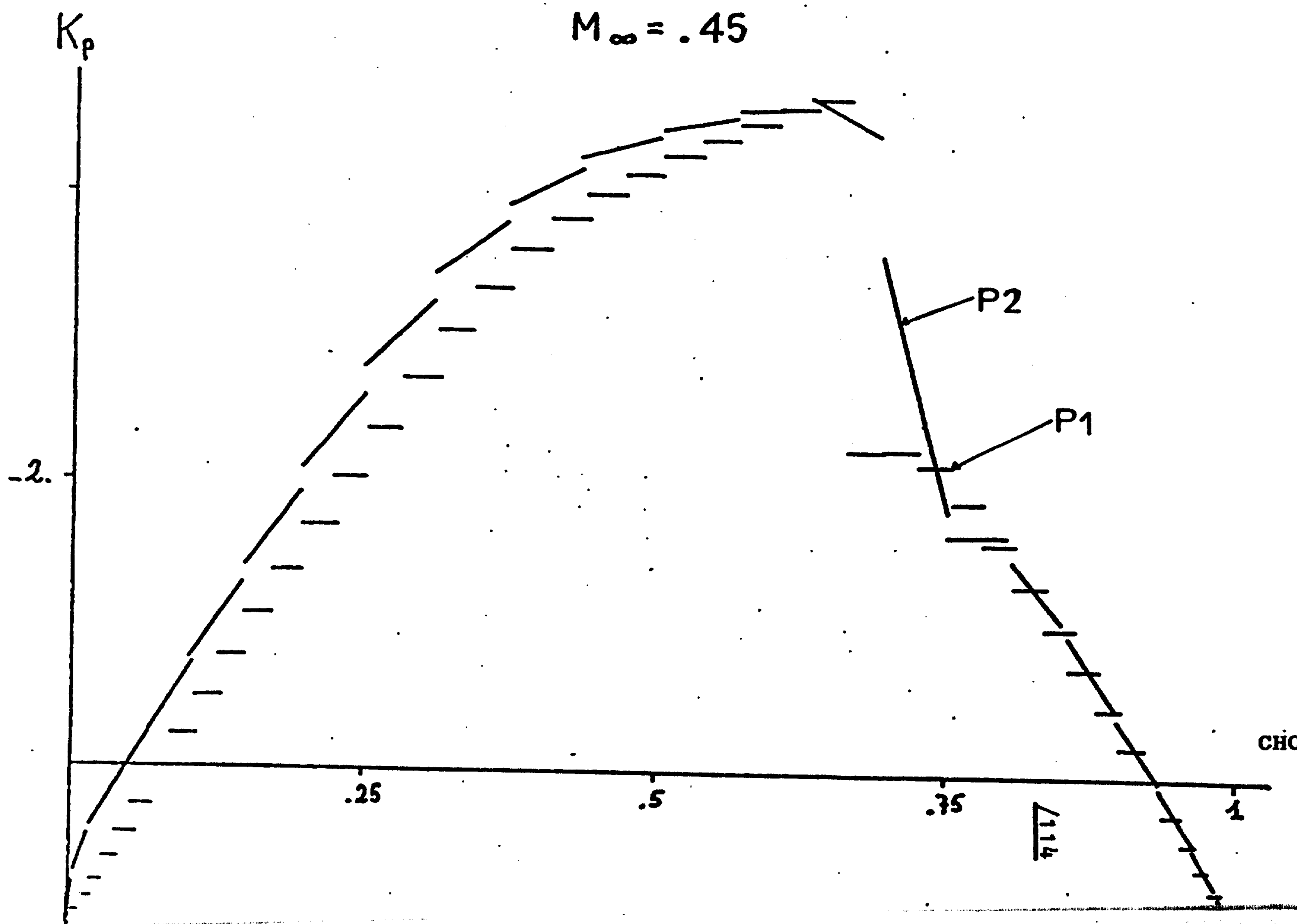

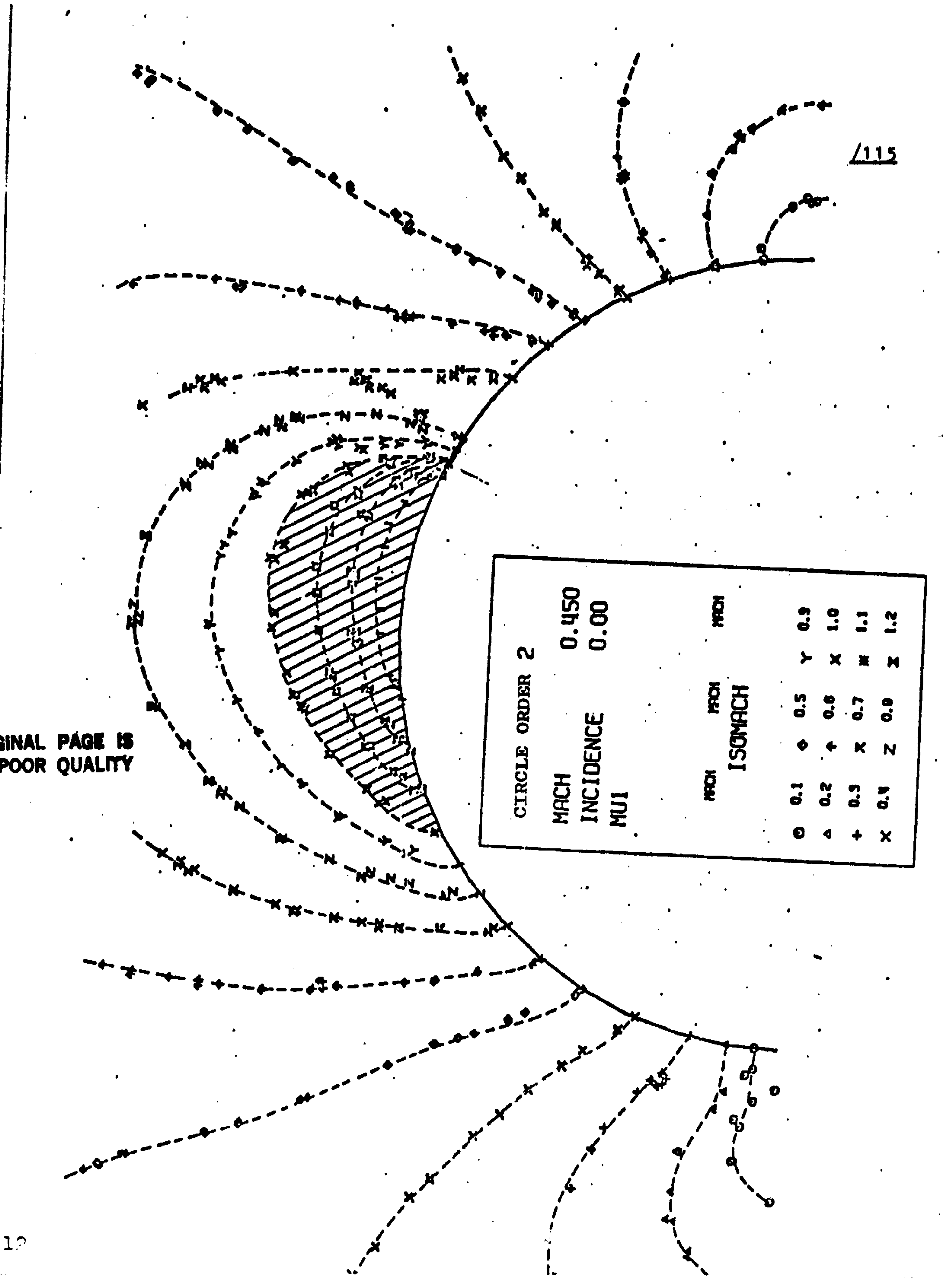
CIRCLE ORDER 2
MACH 0.450
INCIDENCE 0.00
MUI
MACH MACH MACH
ISOMACH
0.1 0.5 Y 0.9
0.2 0.6 X 1.0
0.3 X 0.7 1.1
X 0.4 Z 0.8 1.2

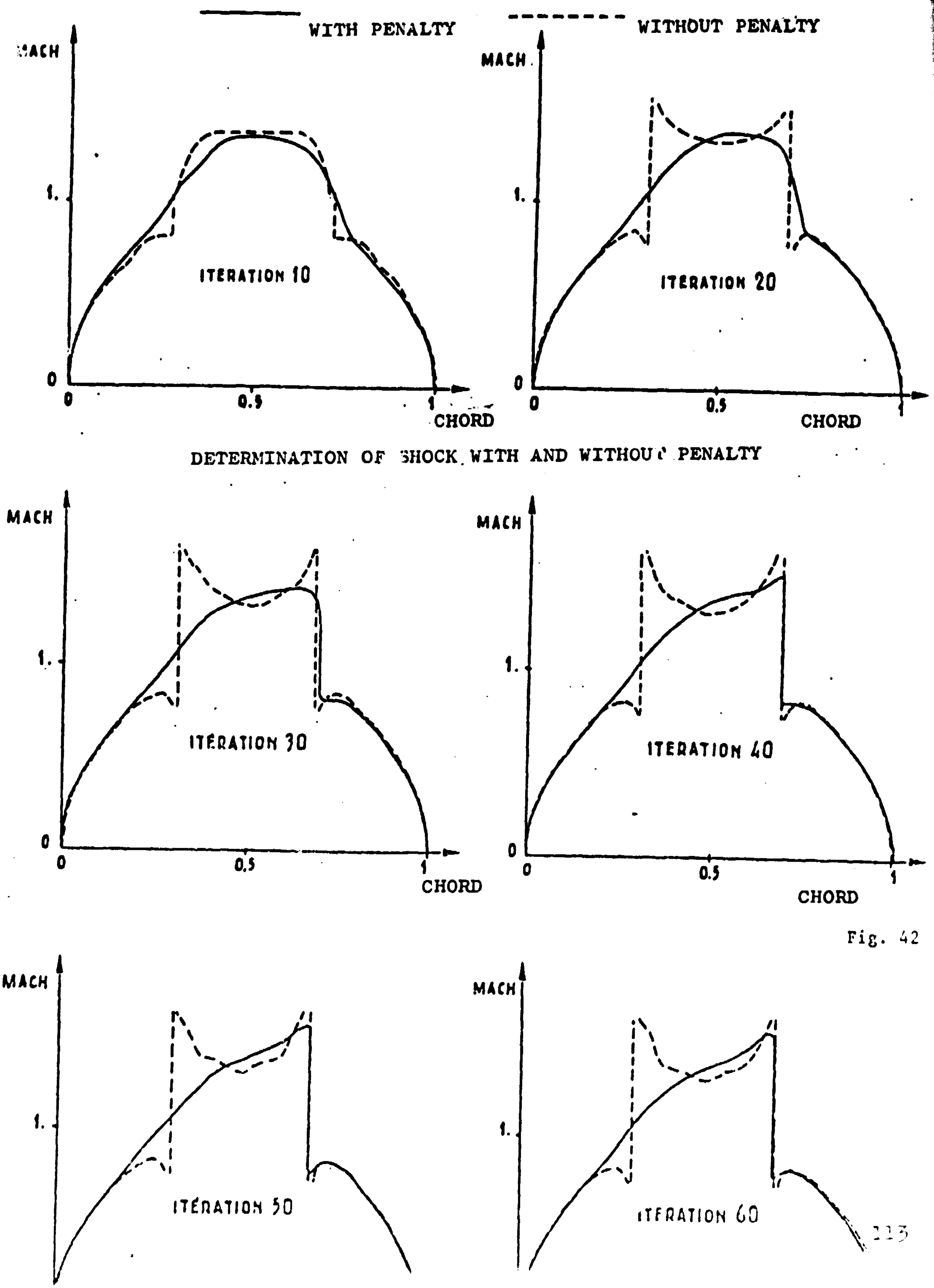
WITH PENALTY
WITHOUT PENALTY
MACH
1.
0
0
0.5
1
CHORD
ITERATION 10
ITERATION 20
DETERMINATION OF SHOCK WITH AND WITHOUT PENALTY
ITERATION 30
ITERATION 40
ITERATION 50
ITERATION 60

Fig. 42

LE NACA 0012

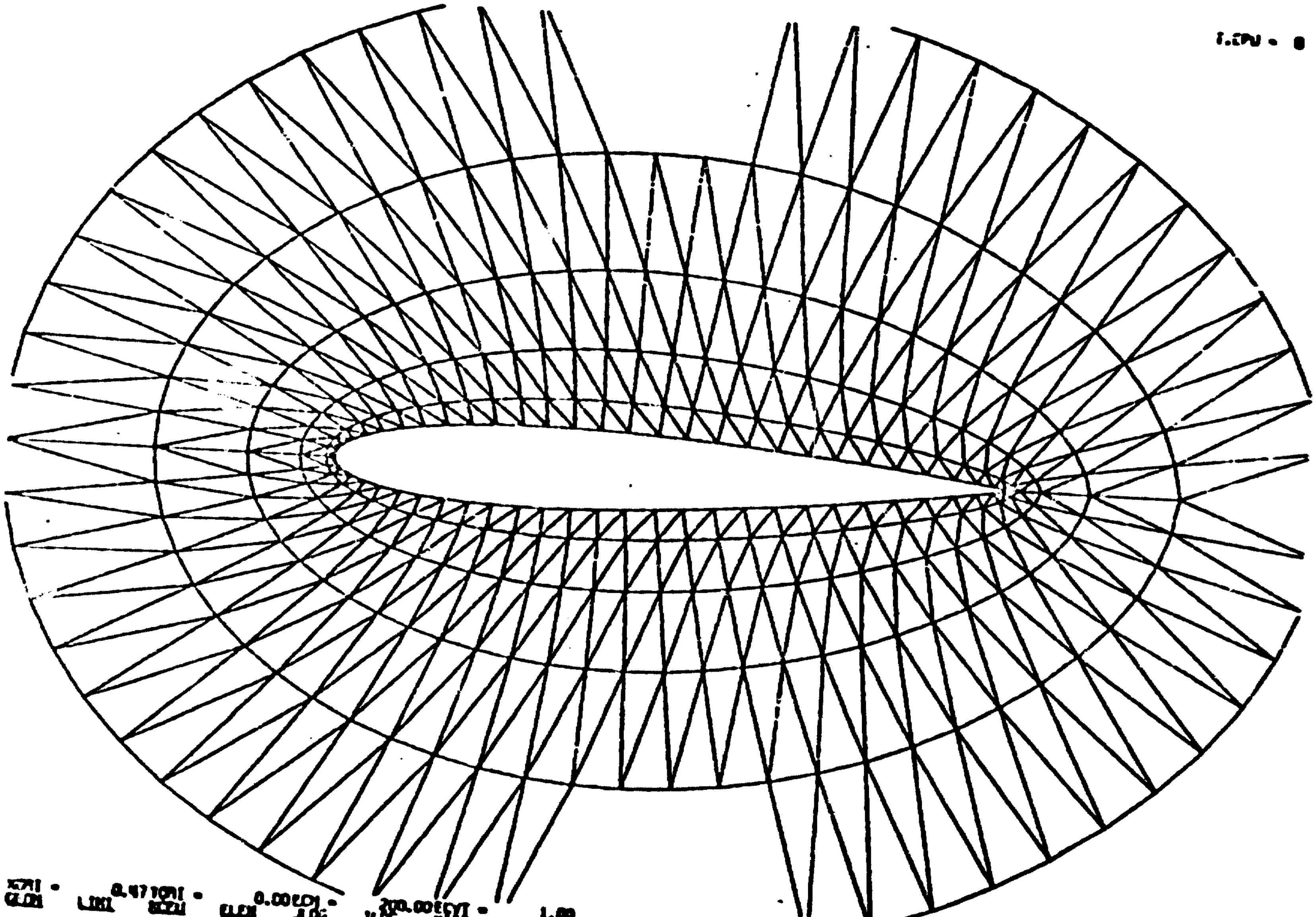

/118

NACA 0012 AIRFOIL

CALCULATION WITH PENALTY

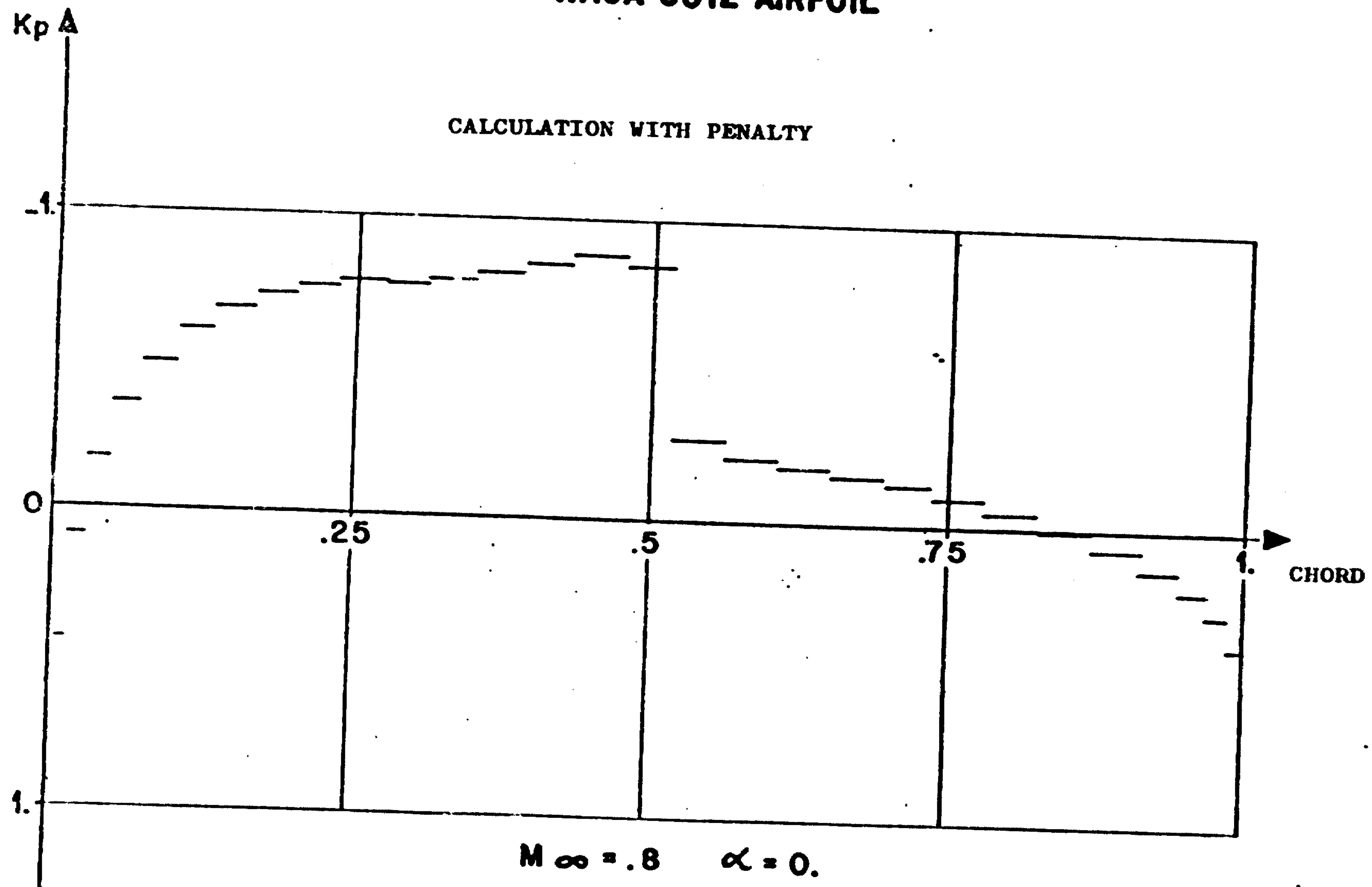

$M_\infty = .8 \quad \alpha = 0.$

$CZ = 0.000$

$CX = 0.019$

NACA 0012 AIRFOIL

CALCULATION WITH ARTIFICIAL VISCOSITY + REGULATION

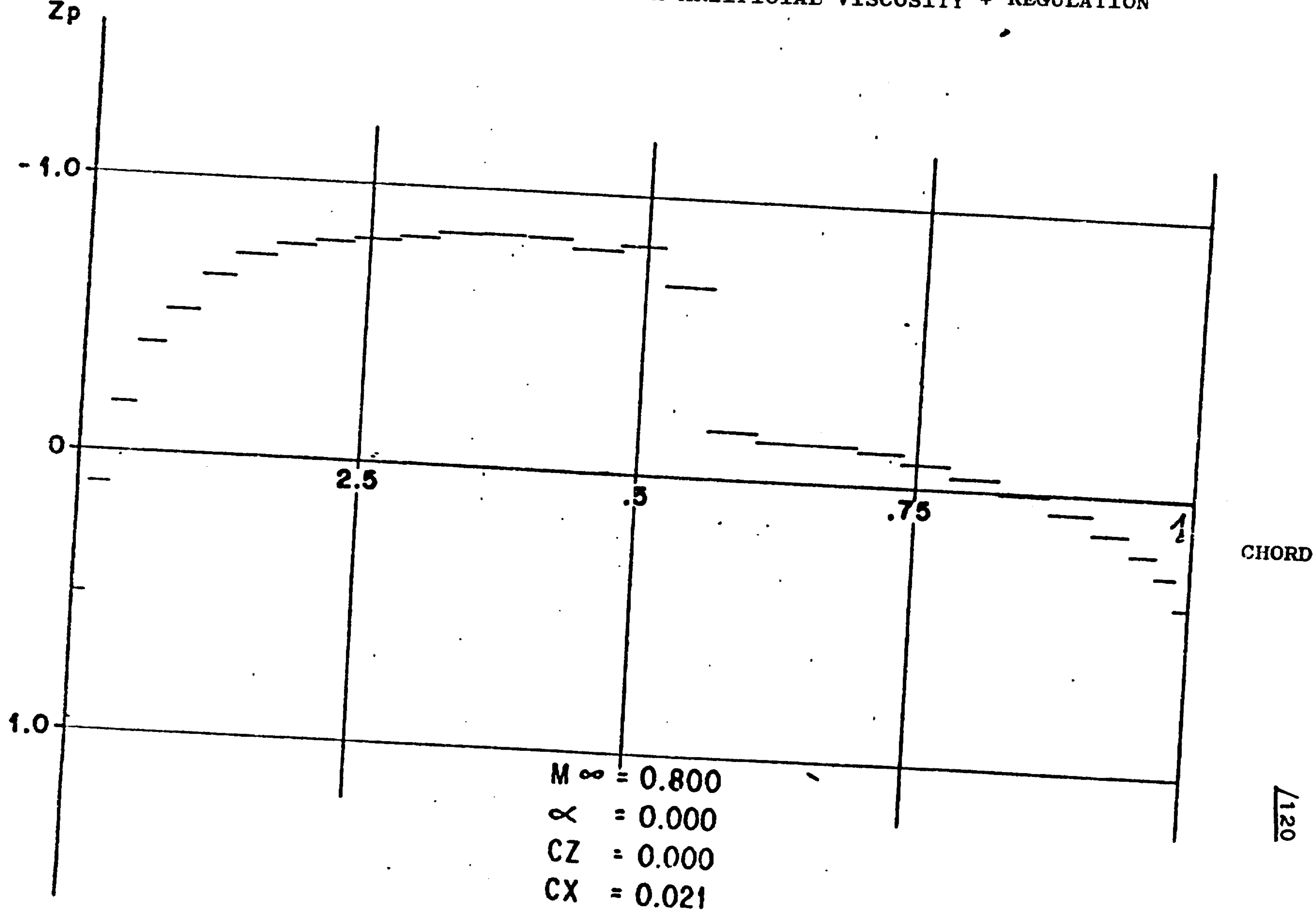

/120

COMPARISONS FINITE ELEMENTS-FINITE DIFFERENCES

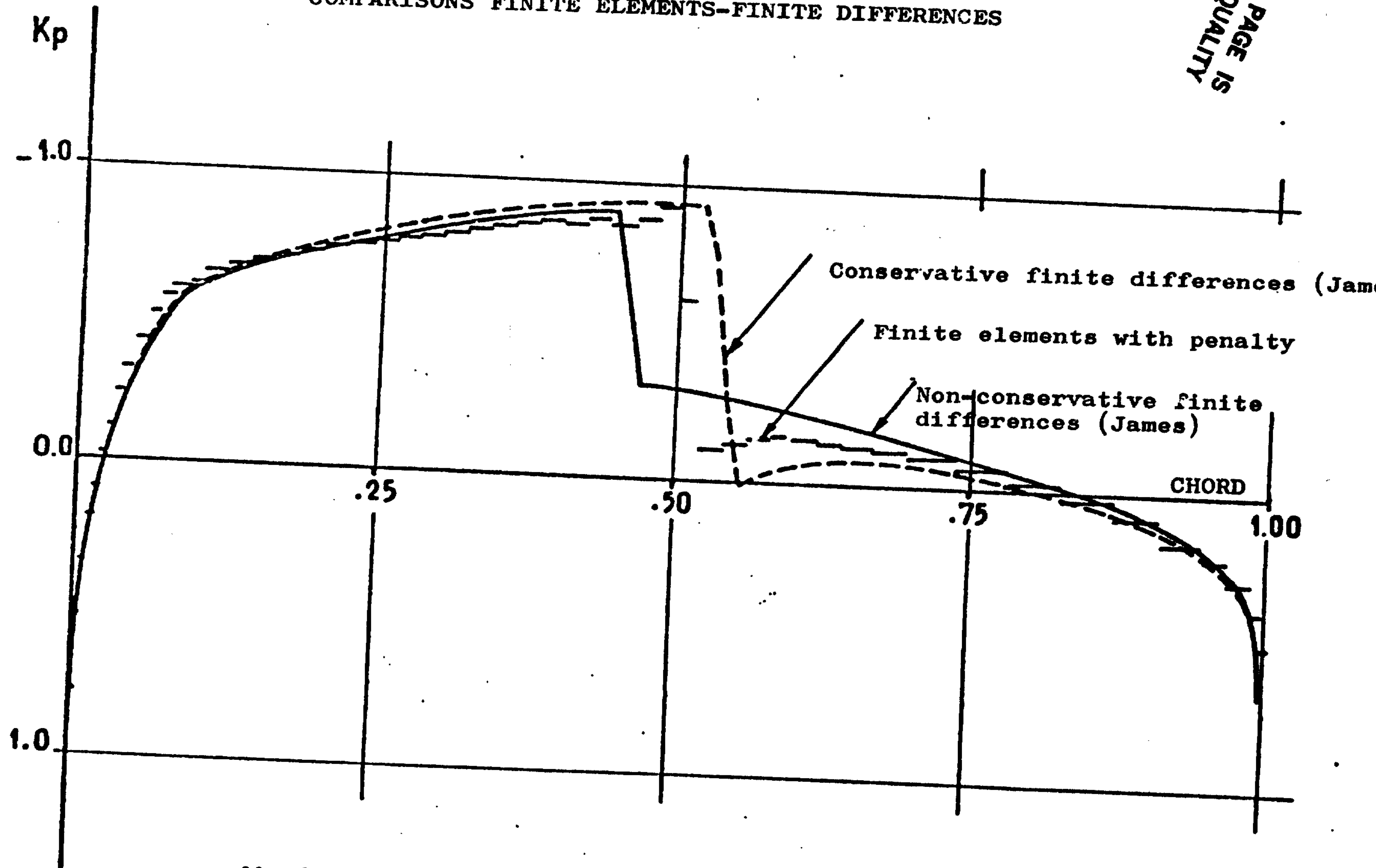

NACA 0012 AIRFOIL $M_{\infty} = .8$ $\alpha = 0.$

/121

Fig. 46

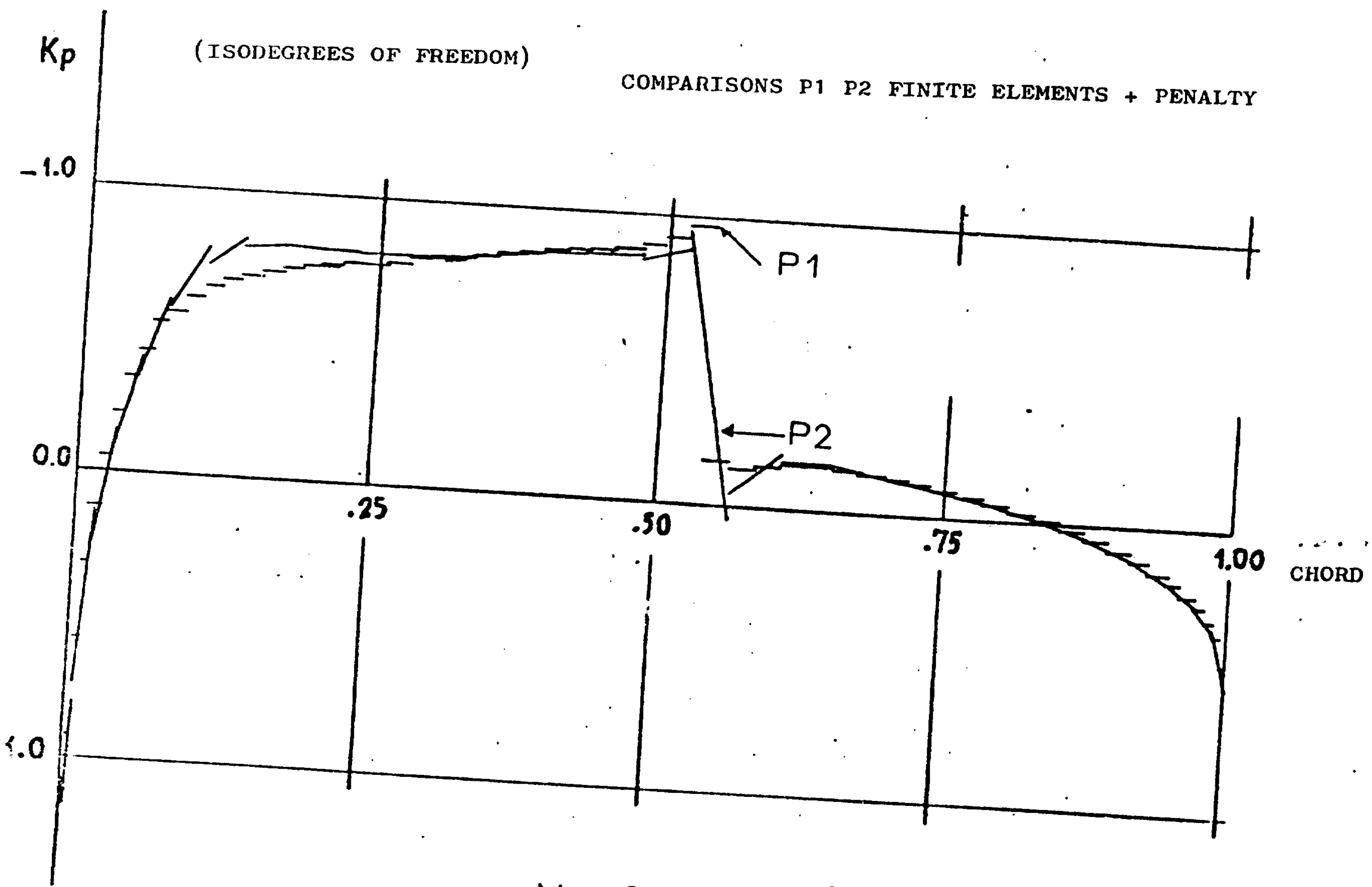

$M_\infty = .8 \qquad \alpha = 0°$

ORIGINAL PAGE IS
OF POOR QUALITY

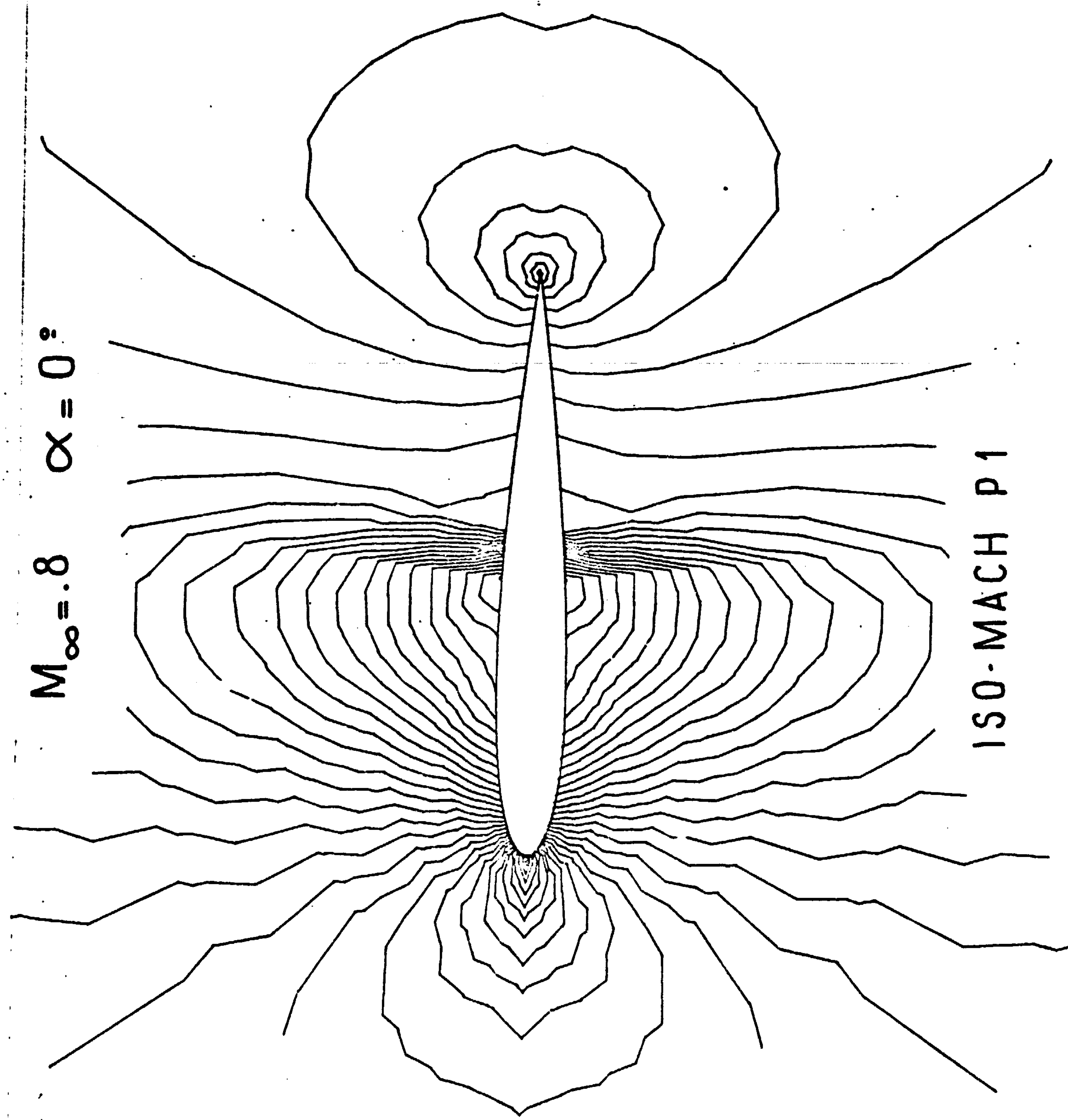

The effect of the artificial viscosity is represented on figures 58 - 59 with the local Machs near the trailing edge (58) and in the shock region (59).

A Fintes Elements comparison is given (on a rough and fine triangulation) on figure 60.

It may be observed that the quality of the compression shock is restored by the PENALTY at the supersonic - subsonic passage.

Finally, a result (P2 - PENALTY) with predictor P1 ISO P2 of artificial viscosity type gives a good result on figure 61. The supersonic zone of the two calculations P1 and P2 in the fluid, in the vicinity of the profile defining the position and the intensity of the shock is represented on figure 62 ; it may be observed that the shock is taken into account in P2 on a single element adjacent to the profile.

The interpolation problem P1/P2 makes it possible to give to code P2 a good predictor P1 and is presented in (40).

Figures 49 through 52 relate to (2). /124

The PENALTY has been used on figure 49 with $\mu = 1$. The convergence is obtained after 60 iterations corresponding to a process time of 4 mn.

The local effect of these terms of PENALTY during the iterations is shown at the bottom of the decompression shock on figure 50.

It may be pointed out that at the end of the computation, the constraints remain active and this brings to light the unstable nature of the solution.

A comparison in the sense of the approximation P1 ISO P2/P2 ($\mu = 1./\mu_1 = 1$ and $\mu_2 = .01$) plotted on figure 51. The location and intensity of the shock on the airfoil are shown by the iso-Machs of computations P1 and P2 on figure 52.

12.2.3.2. - The Lifting Case (With JOUKOVSKI Condition)

Two test cases have been calculated :

(3) ($M_\infty = .6$; INC = 6°) - Small supersonic zone, but strong intensity decompression shock very near the compression shock.

(4) ($M_\infty = .78$; INC = 1°) - Large Supersonic Zone.

Figures 53 through 56 relate to (3).

Figure 53 compares the pressions on the airfoil with the JAMESON finite differences non conservative and conservative method with the pressures obtained in P1 with ARTIFICIAL Viscosity + REGULATION ($\nu = .005$, $\mu = .00001$) on a rough triangulation. The local Machs in the shock region at the extrados of the airfoil are shown on figure 54. A comparison of the supersonic zones in the form of iso machs P1/P2 shows a good agreement between the two approximations on figure 55.

A P1 Finite Elements comparison (PENALTY-VISCOSITY (ARTIFICIAL) on figure 56 brings to light the good behavior of the code with PENALTY which at the same time in a very narrow zone, restores the physical shock and resists the high intensity decompression shock.

Figures 57 through 61 relate to (4).

Figure 57 compares the JAMESON finite differences conservative and non conservative solution with the solution obtained in P1 with ARTIFICIAL VISCOSITY + REGULATION ($\nu = .005$, $\mu = 5.10^{-6}$) on a fine triangulation. 20 iterations on the JOUKOWSKI condition have been performed, representing 80 optimal control iterations for a process time of 15 mn.

NACA 0012 AIRFOIL

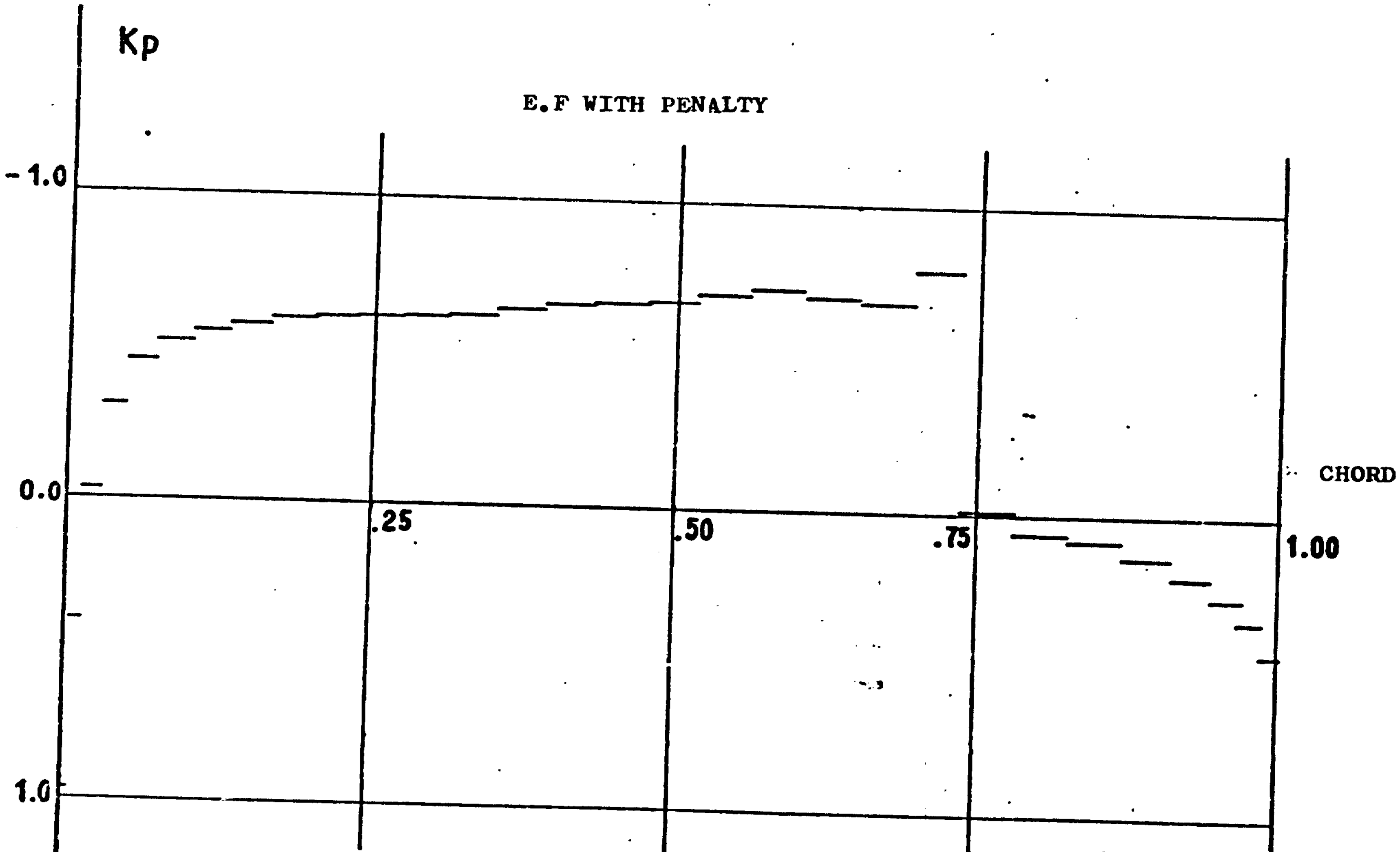

$M_\infty = 0.850$

$\alpha = 0.000$

$CZ = 0.000$

$CX = 0.027$

LOCAL EFFECT OF THE PENALTY AT THE BOTTOM OF THE DECOMPRESSION SHOCK

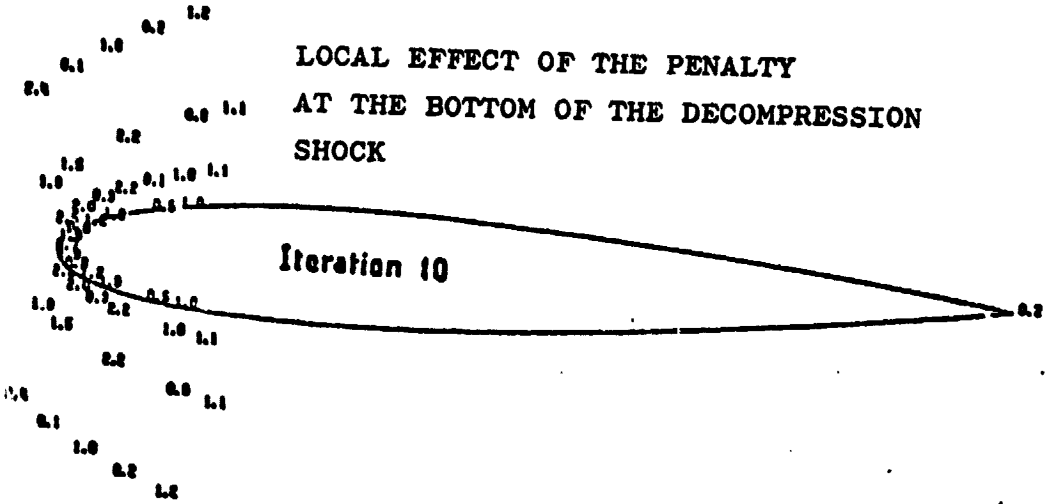

/127

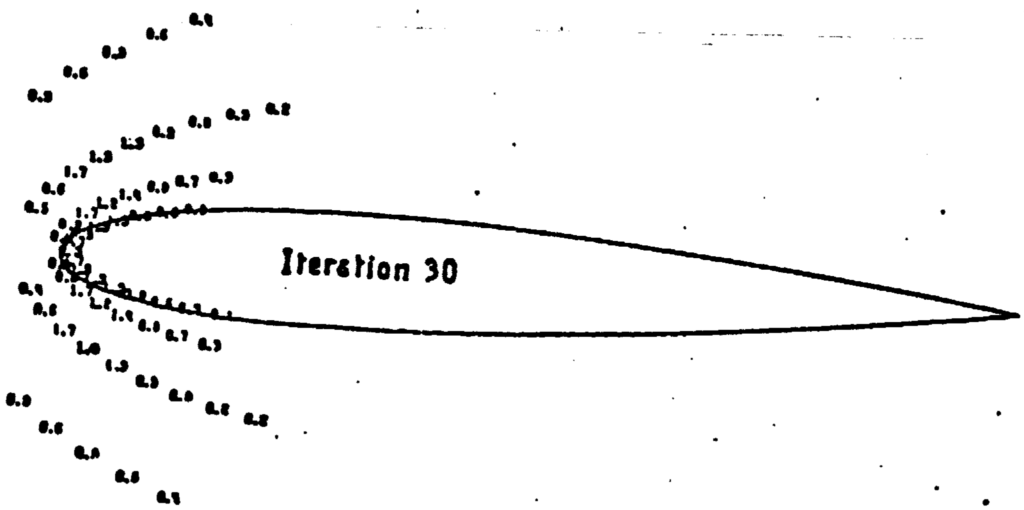

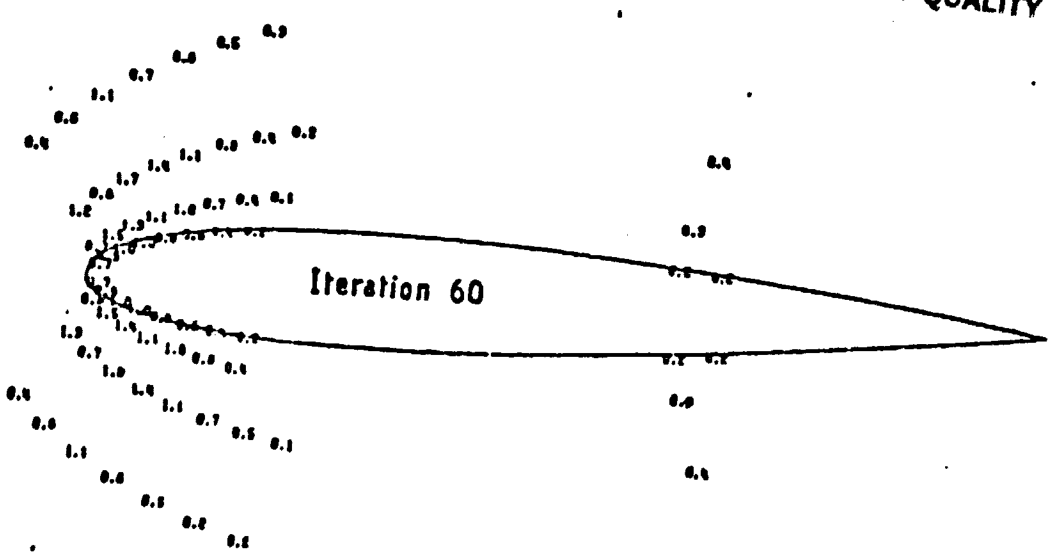

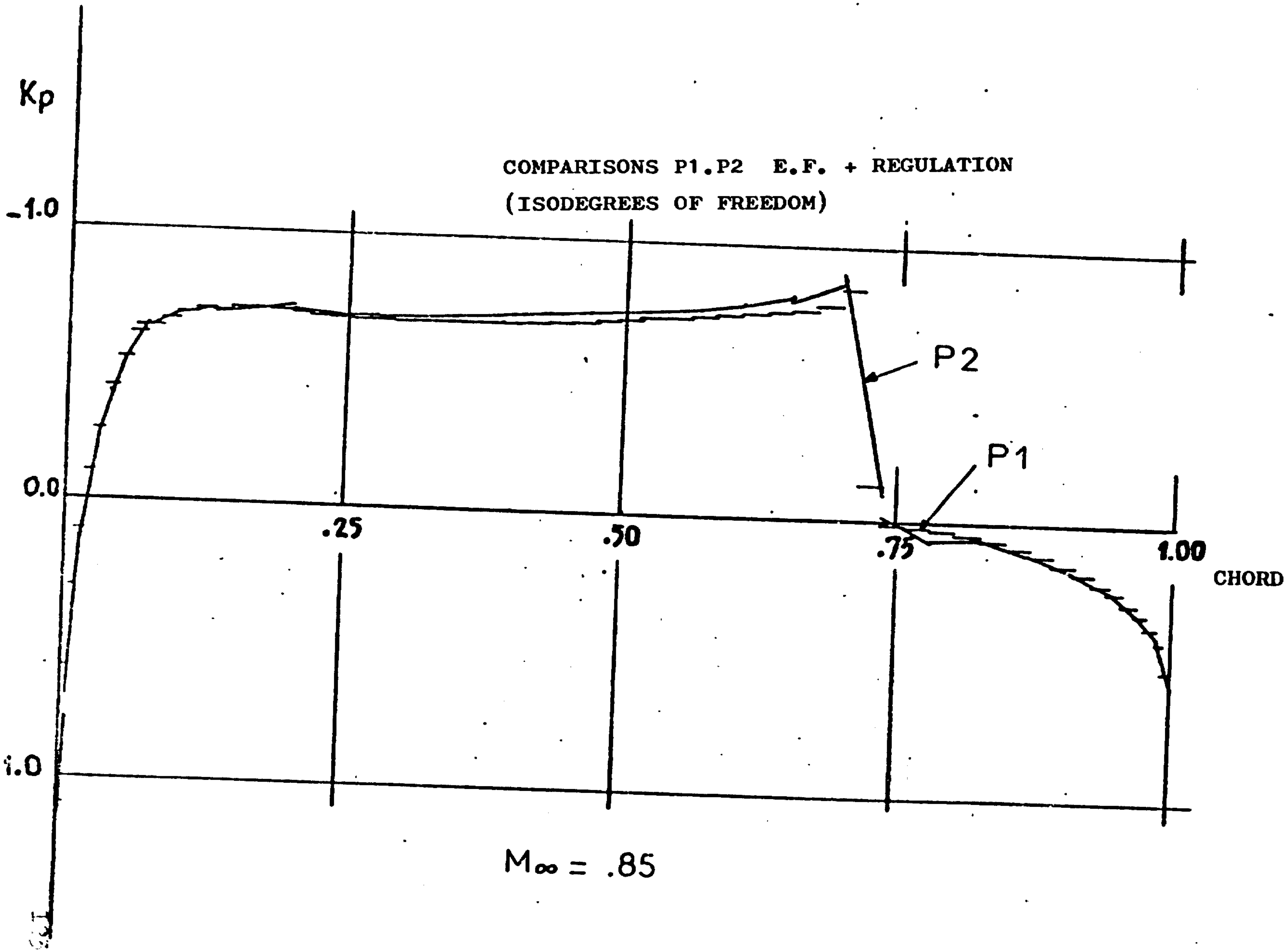
COMPARISONS P1.P2 E.F. + REGULATION
(ISODEGREES OF FREEDOM)
Kp
-1.0
0.0
1.0
.25
.50
.75
1.00
CHORD
P2
P1
M∞ = .85

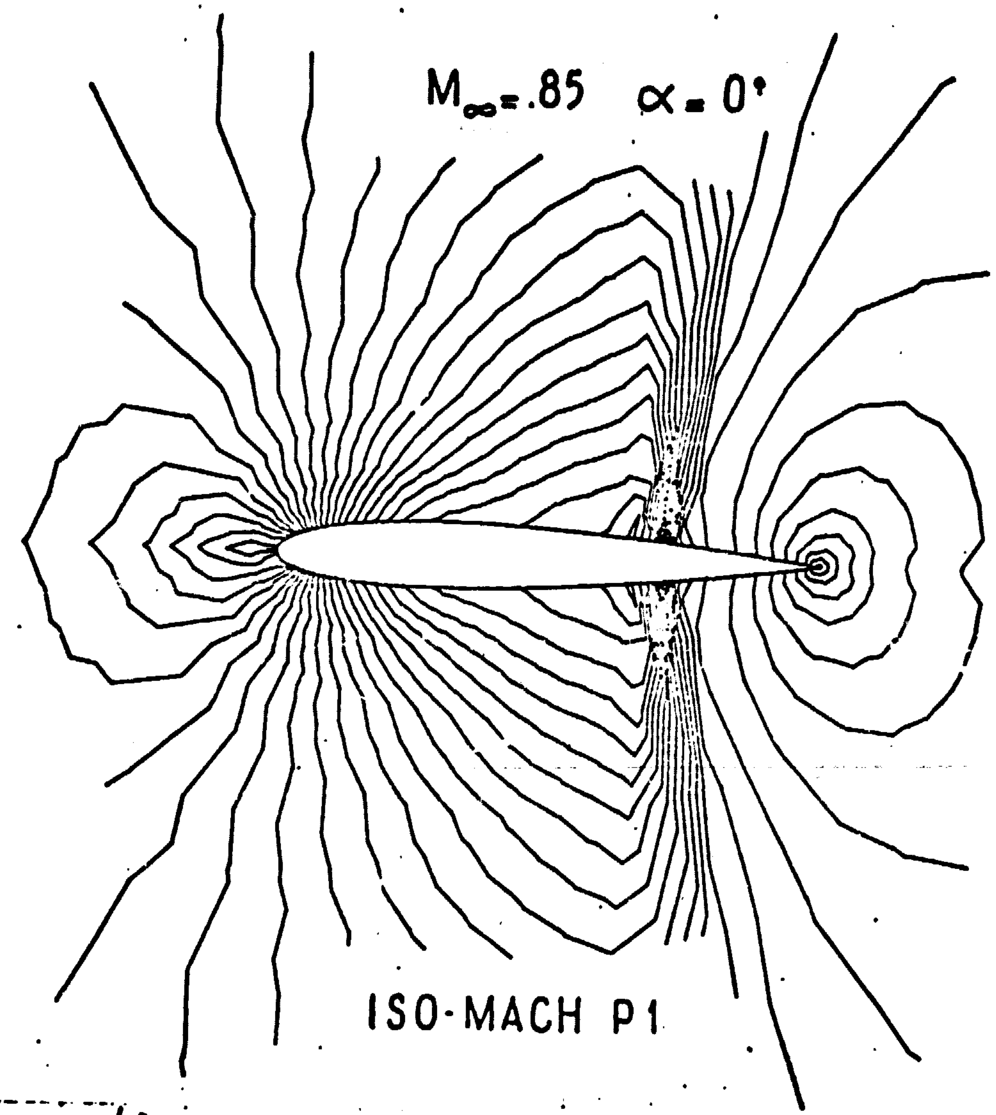

ISO-MACH P1

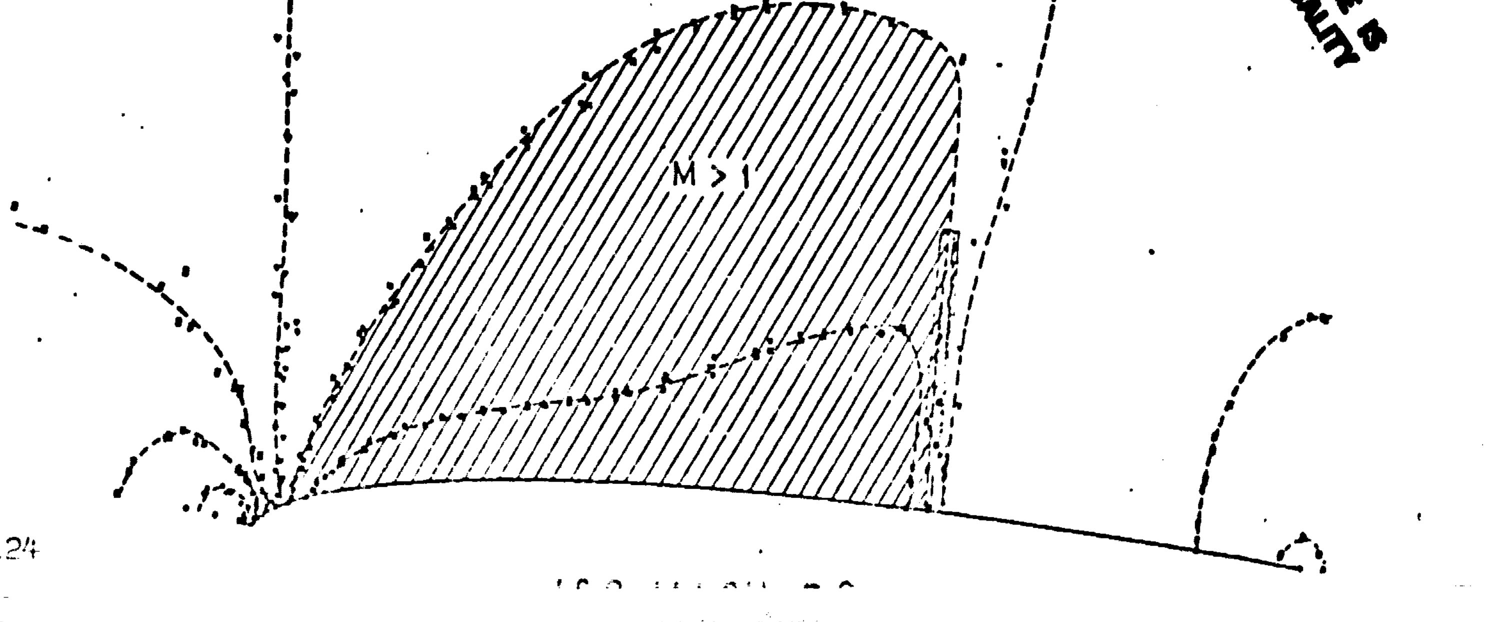

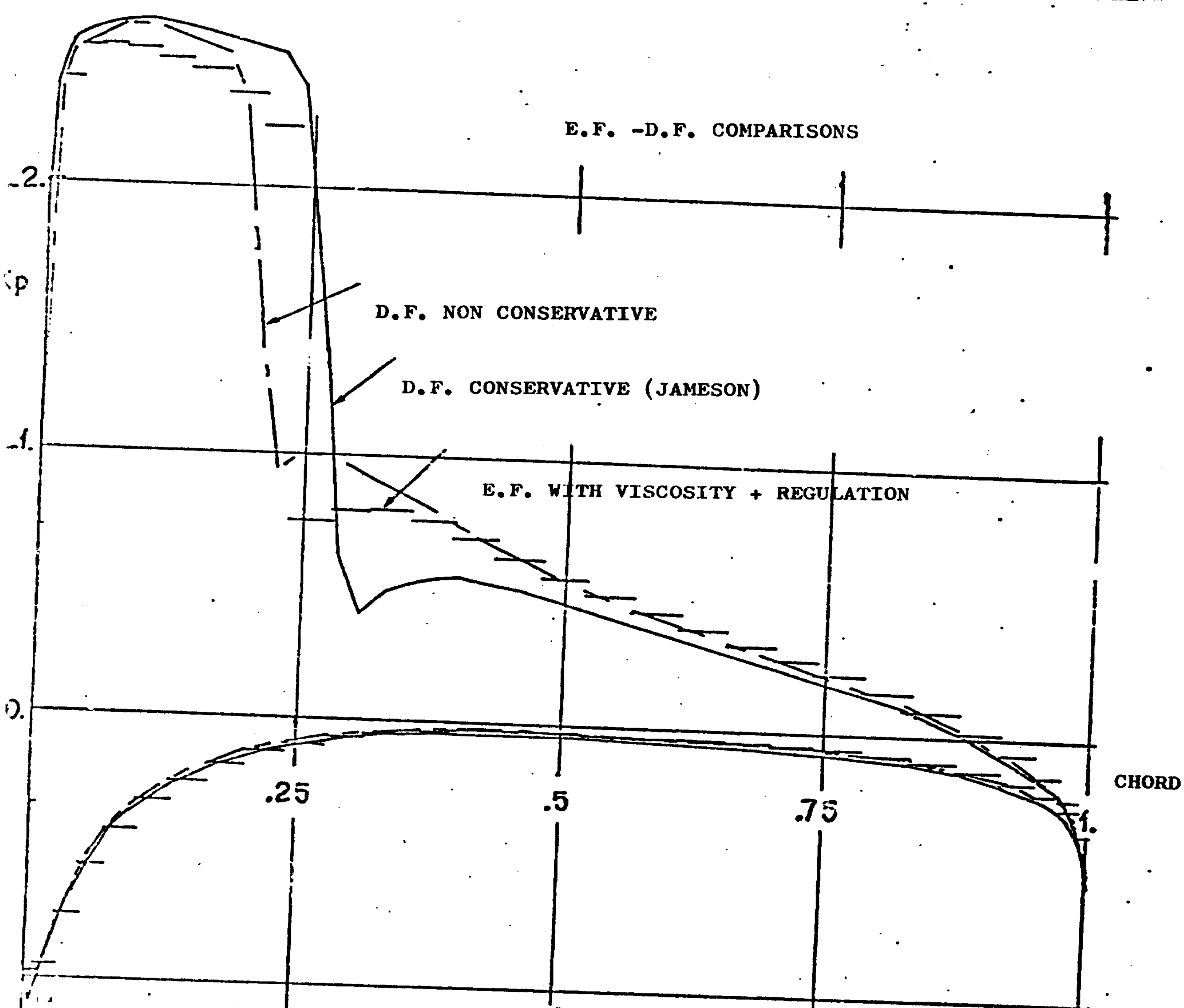

NACA 0012 $M_\infty = .5$ $\alpha = 6^\circ$

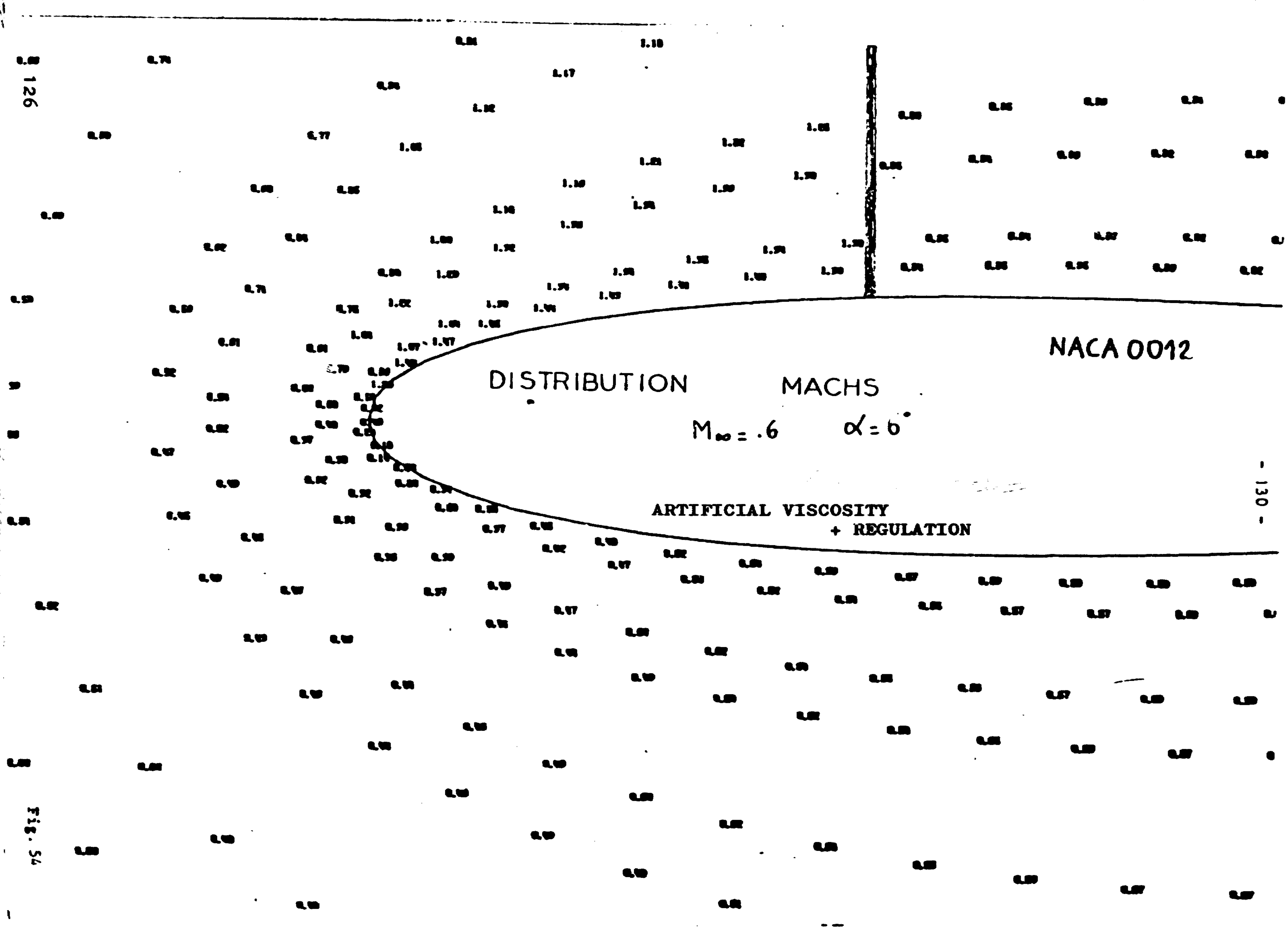
NACA 0012
DISTRIBUTION MACHS
$M_\infty = .6$ $\alpha = 6^\circ$
ARTIFICIAL VISCOSITY
+ REGULATION
126

Fig. 54

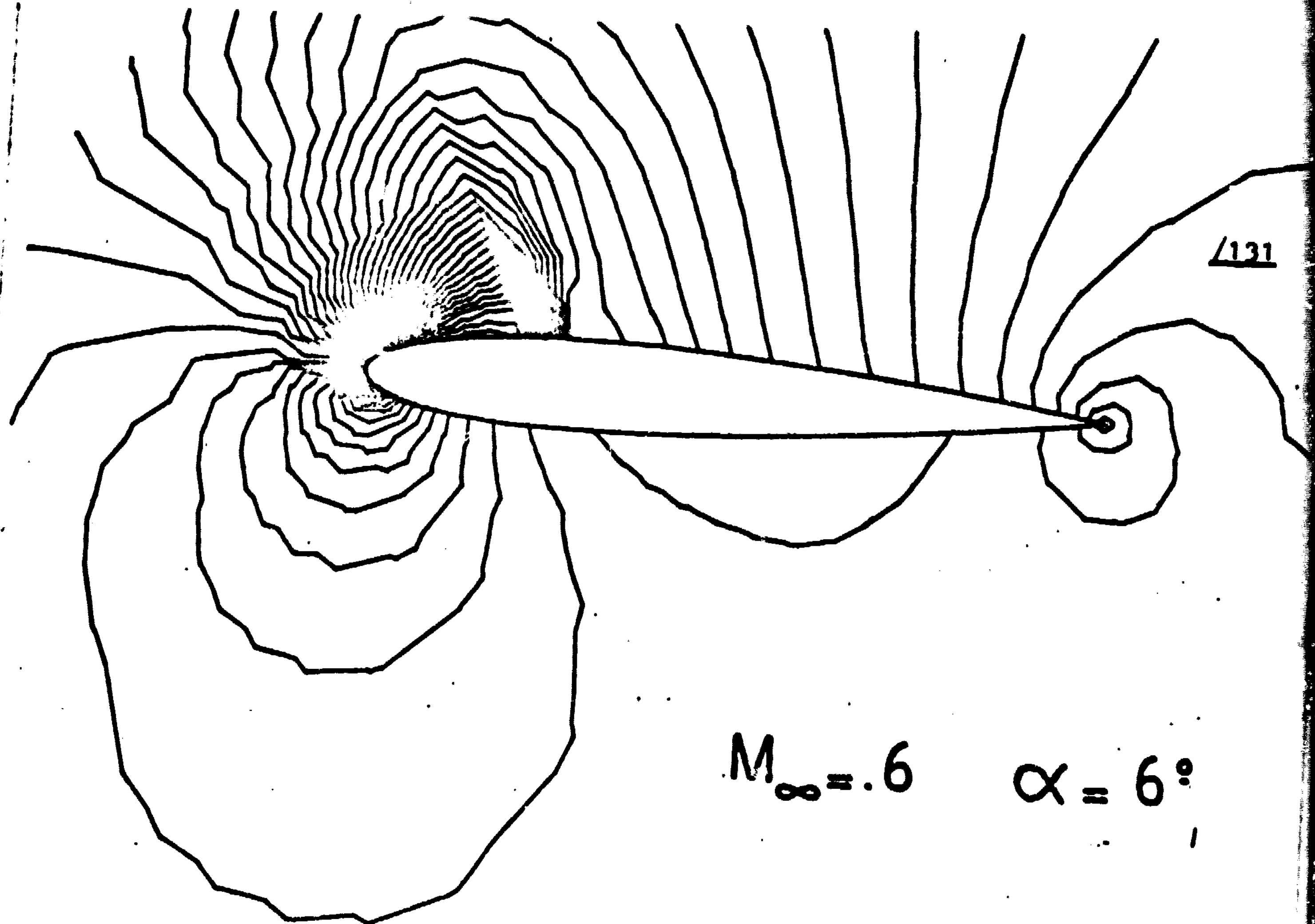

$M_\infty = .6 \quad \alpha = 6°$

ISO·MACH P1

/131

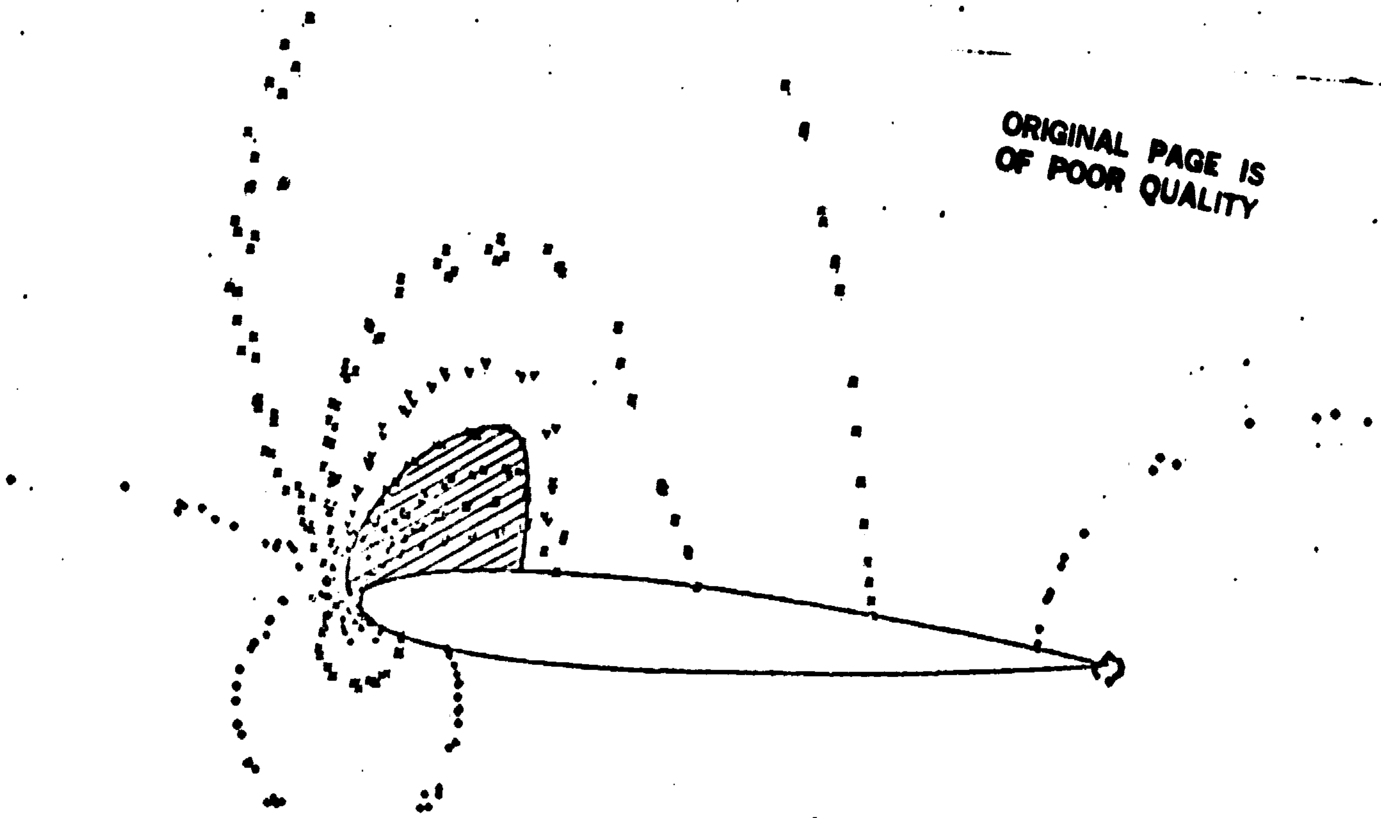

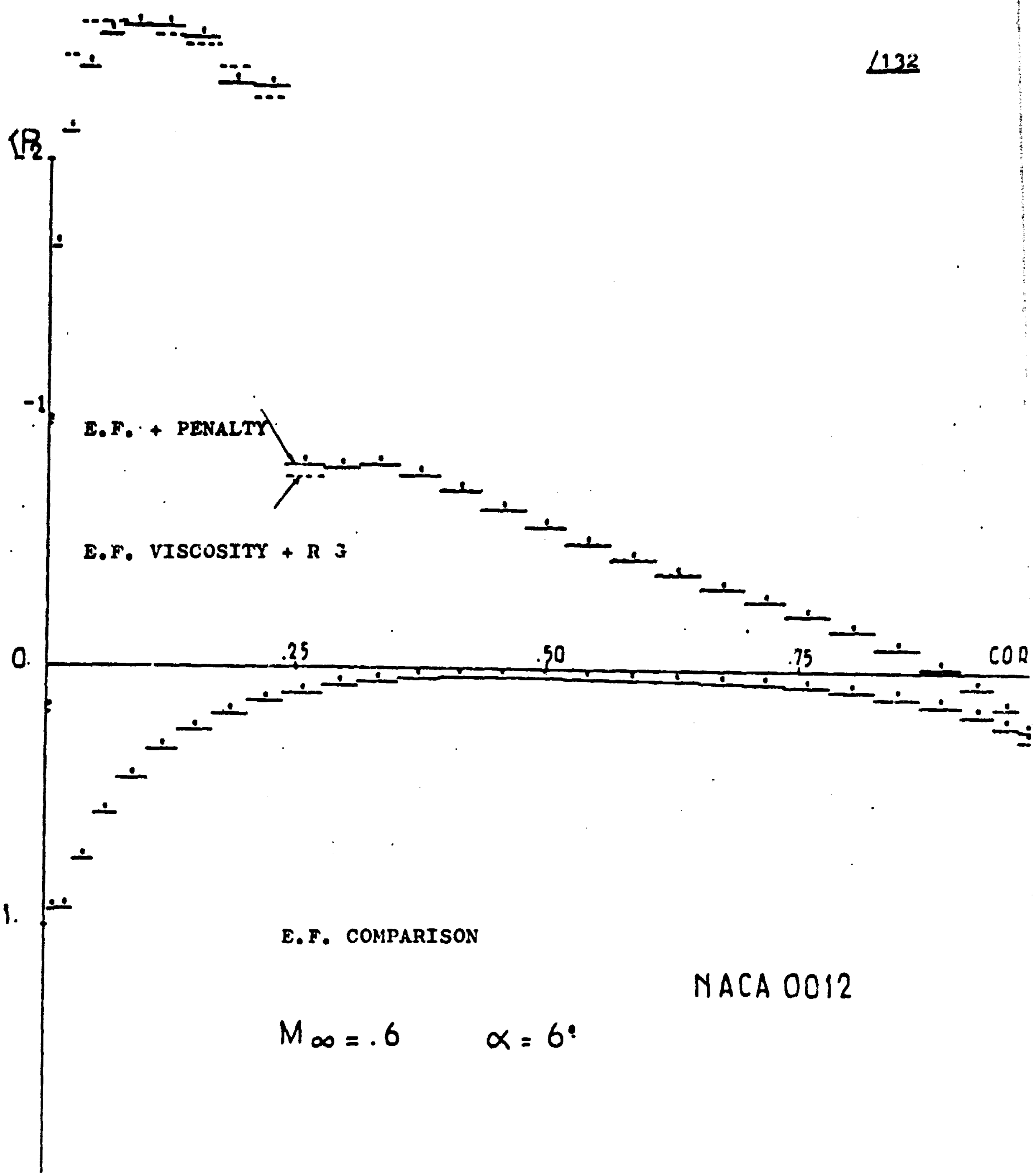
Cp
-1
E.F. + PENALTY
E.F. VISCOSITY + R 3
0.
.25
.50
.75
COR
1.
E.F. COMPARISON
NACA 0012
$M_\infty = .6$ $\alpha = 6°$

Fig. 56

E.F.-D.F. COMPARISONS

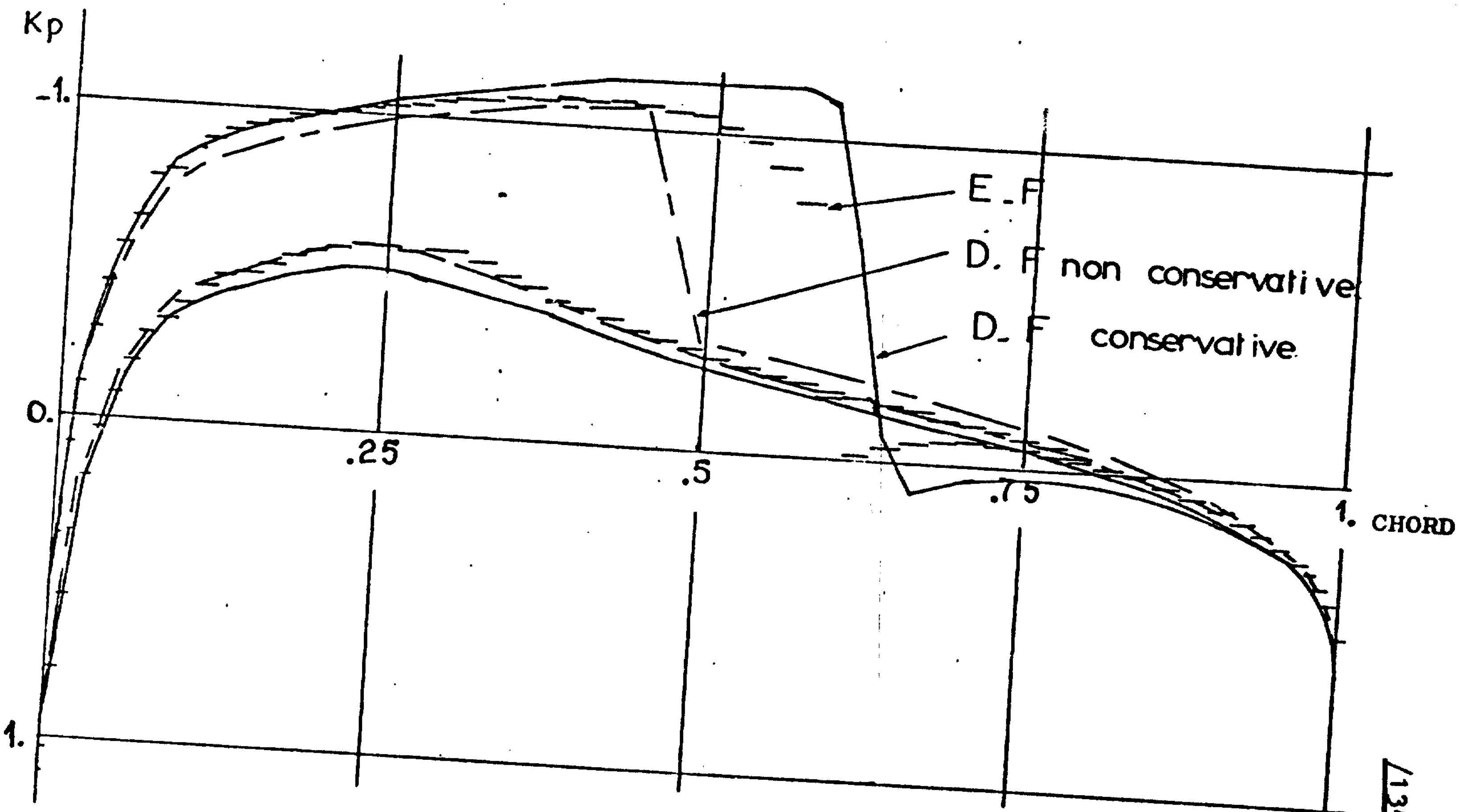

$M_\infty = .78 \quad \alpha = 1^\circ$

/134

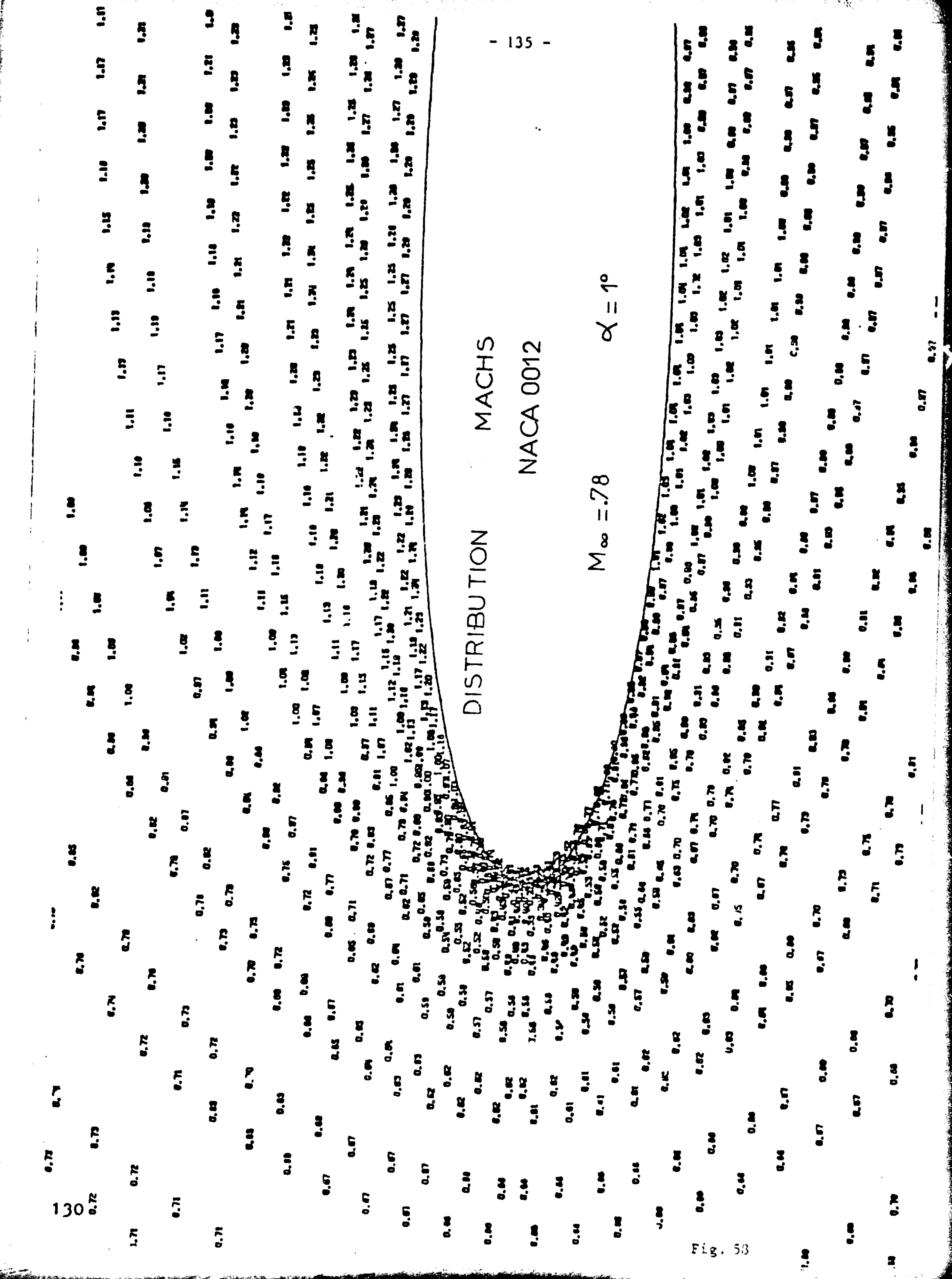

Fig. 53

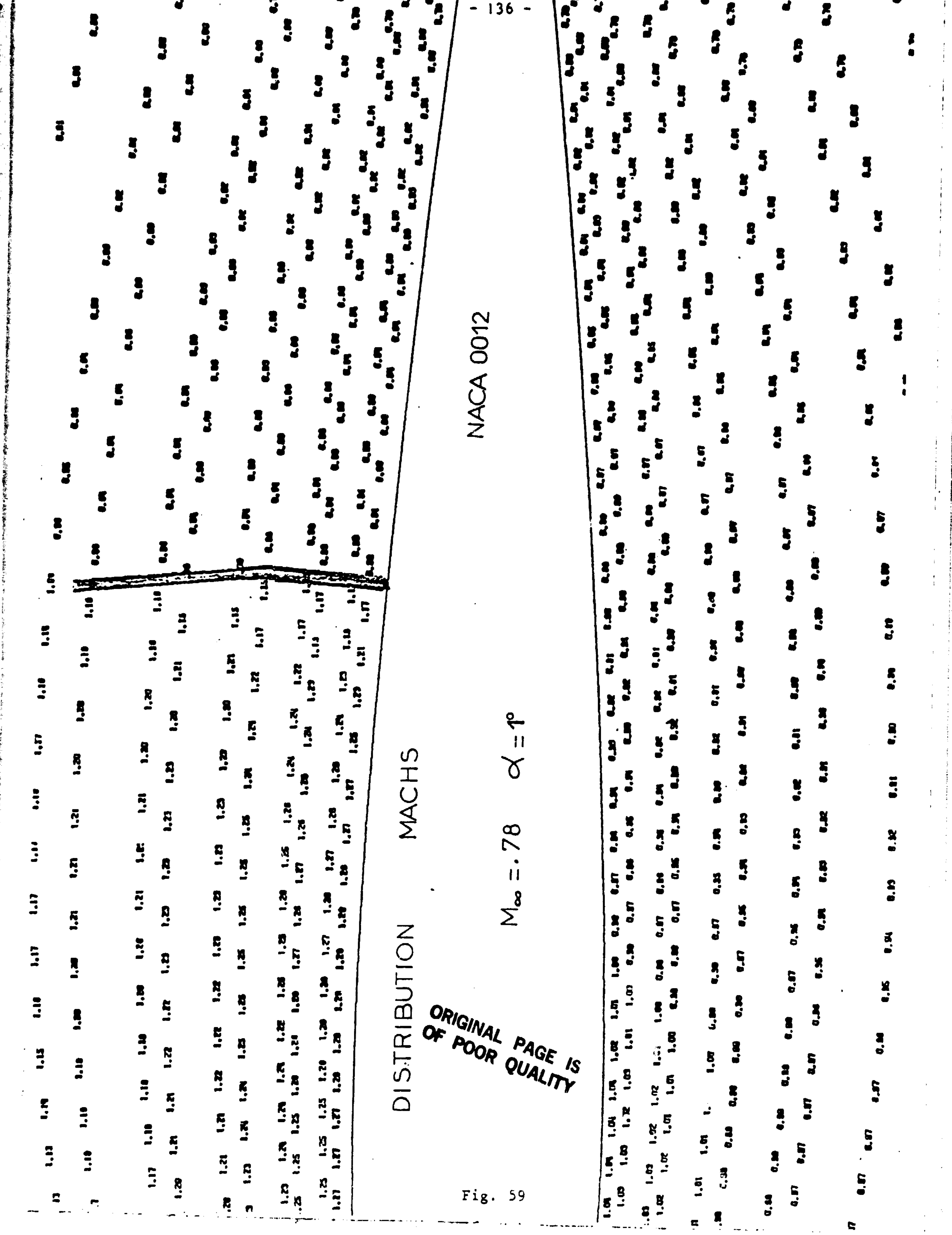
NACA 0012
DISTRIBUTION MACHS
$M_\infty = .78 \quad \alpha = 1°$
ORIGINAL PAGE IS OF POOR QUALITY

Fig. 59

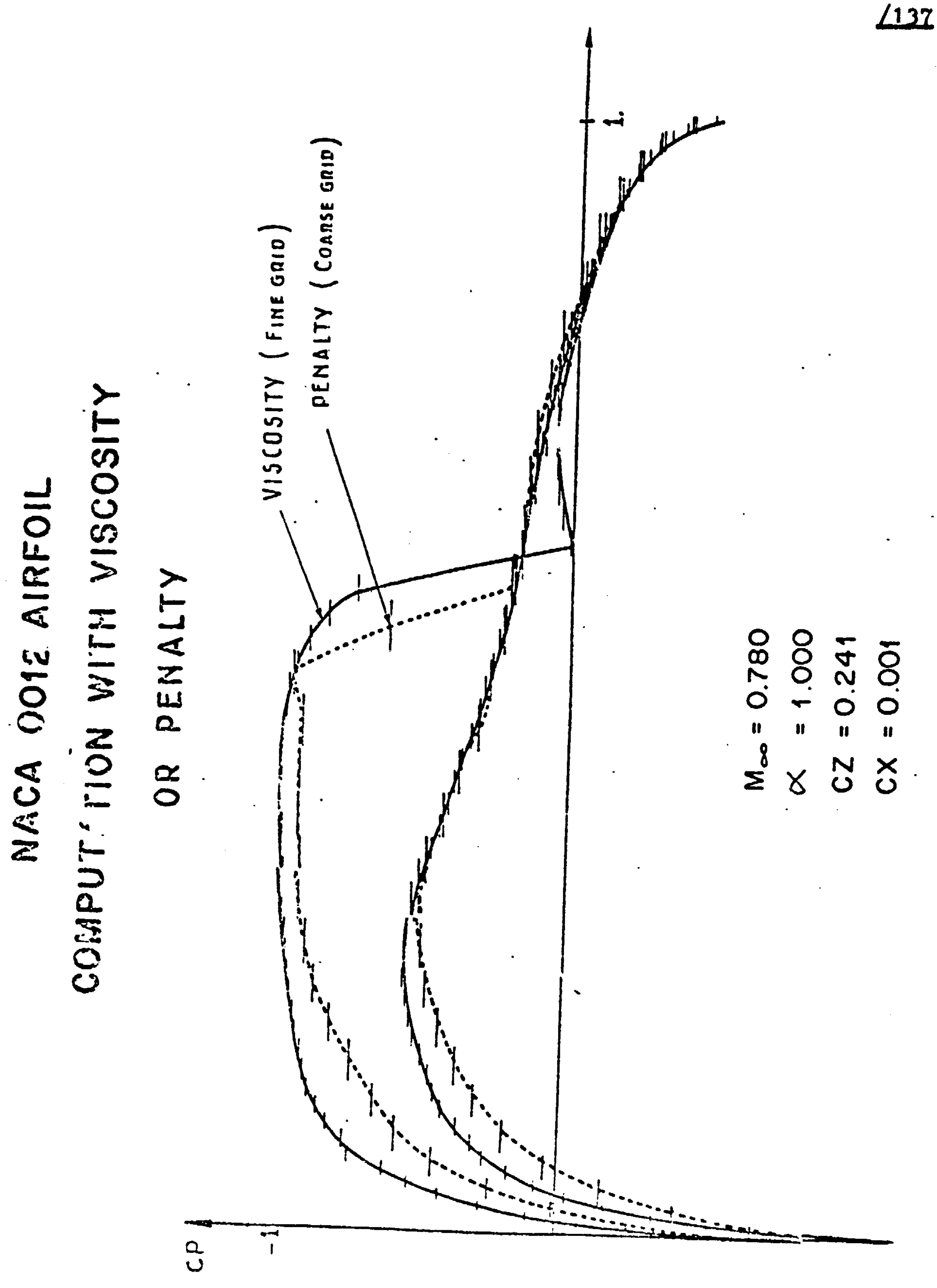
NACA 0012 AIRFOIL
COMPUT'TION WITH VISCOSITY
OR PENALTY
VISCOSITY (FINE GRID)
PENALTY (COARSE GRID)
CP
-1
1.
M_∞ = 0.780
α = 1.000
CZ = 0.241
CX = 0.001

Figure 60

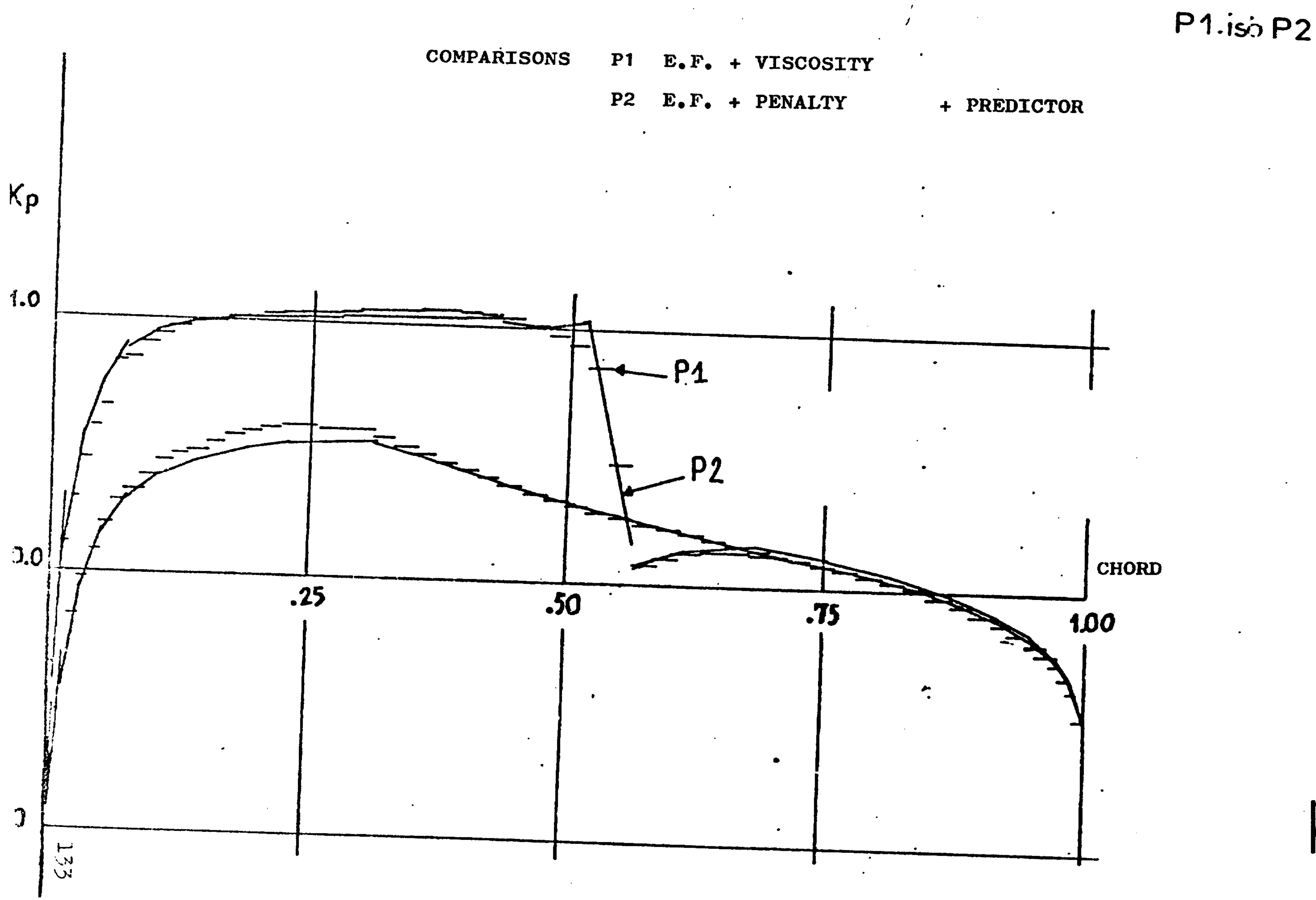
P1.isō P2
COMPARISONS P1 E.F. + VISCOSITY
P2 E.F. + PENALTY + PREDICTOR
Kp
1.0
0.0
0
P1
P2
CHORD
.25
.50
.75
1.00
133

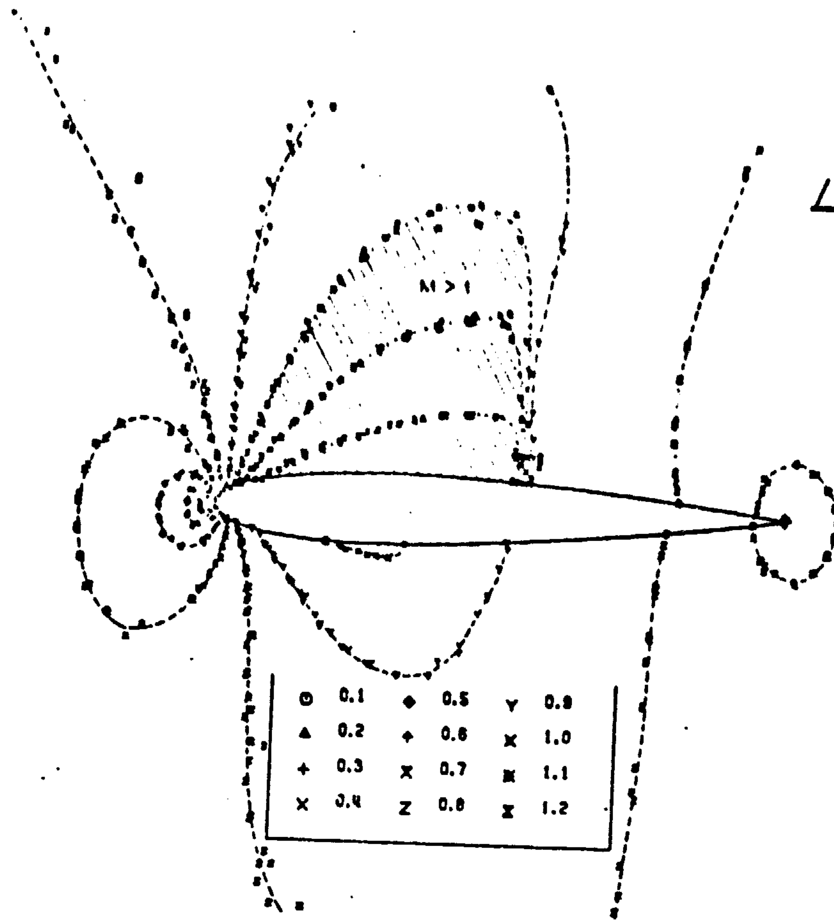

COMPAR ISON ISO-MACH P1, P2

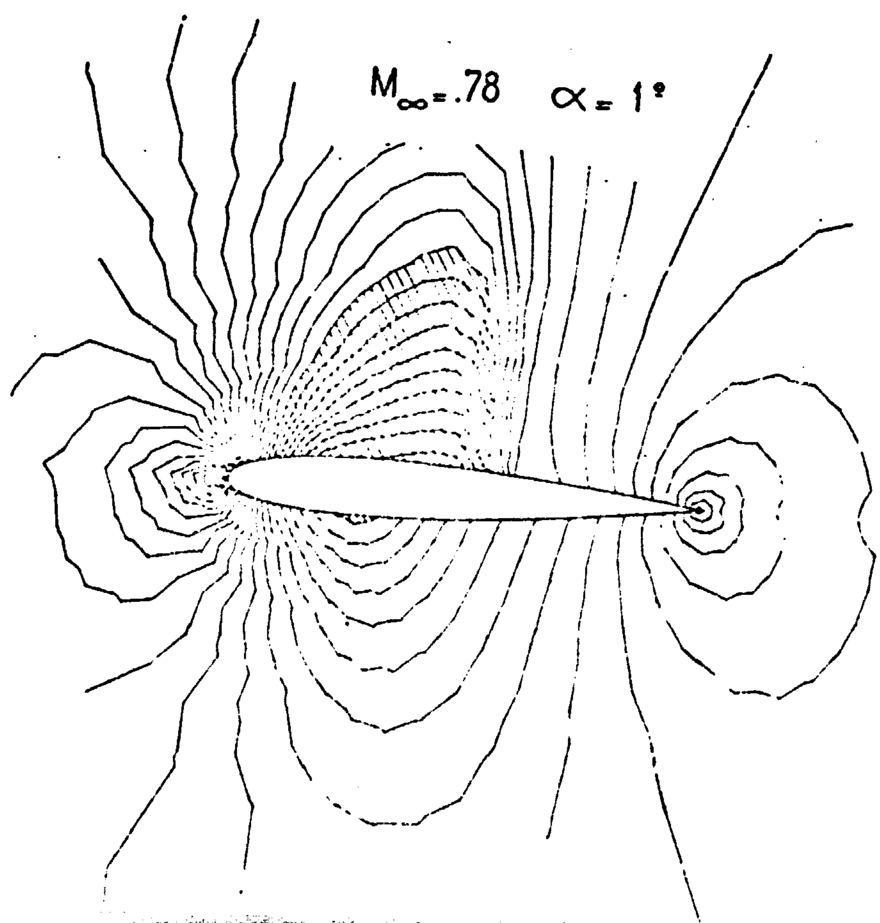

12.2.4. The KORN Airfoil Section (Profile) /140

The Korn airfoil section is a non symmetrical section designed to produce a transonic flow without shock if $M_\infty = .75$ and INC = 0°. Since the flow is not symmetrical, the JOUKOVS condition is applied at the trailing edge.

The domain of calculation surrounding the section has been divided into 2880 triangles (resp 1362) for a piece-wise linear approximation (resp. quadratic) with 1560 NODES of which 120 on the section.

The triangulation with detail near the section is provided on figure 63.

Figure 64 shows an effect of the triangulation (rough and fine on the location and intensity of the shock for the test case $M_\infty = .75$ INC = 0° with artificial viscosity + Regulation $\nu = .005$; $\mu = .00005$).

It may be observed that the shock intensity decreases with h, quantification step.

Comparisons (Finite differences, JAMESON conservative scheme) - (P1 finite elements (rough triangulation))- (P2 finite elements) - are presented on figure 65. The condition of entropy was treated by PENALTY. 60 iterations for a process time of 30 mn are required to obtain the convergence in case P2.

Another case of computation with iso CZ (M_∞ = .75 ; INC = 0.1) disconnecting in order to treat the JOUKOVSKI condition demonstrates the agreement of finite elements + artificial viscosity with conservative JAMESON finite differences on figure 66.

A second test case has been performed $M_\infty = .75$ and INC = .5 /141

A comparison Finite differences - Finite elements with PENALTY ($\mu = .1$) at 150 degrees of freedom is presented on figure 67. Attention shall be brought to the compression shock clearness of the solution with penalty.

Finally, the conservative case $M_\infty = .75$ and INC = .5, calculated either by the JAMESON Finite differences, or by the P1 Finite elements with artificial viscosity ($\nu = .008$, $\mu = .00005$) duct of very similar solutions on figure 68.

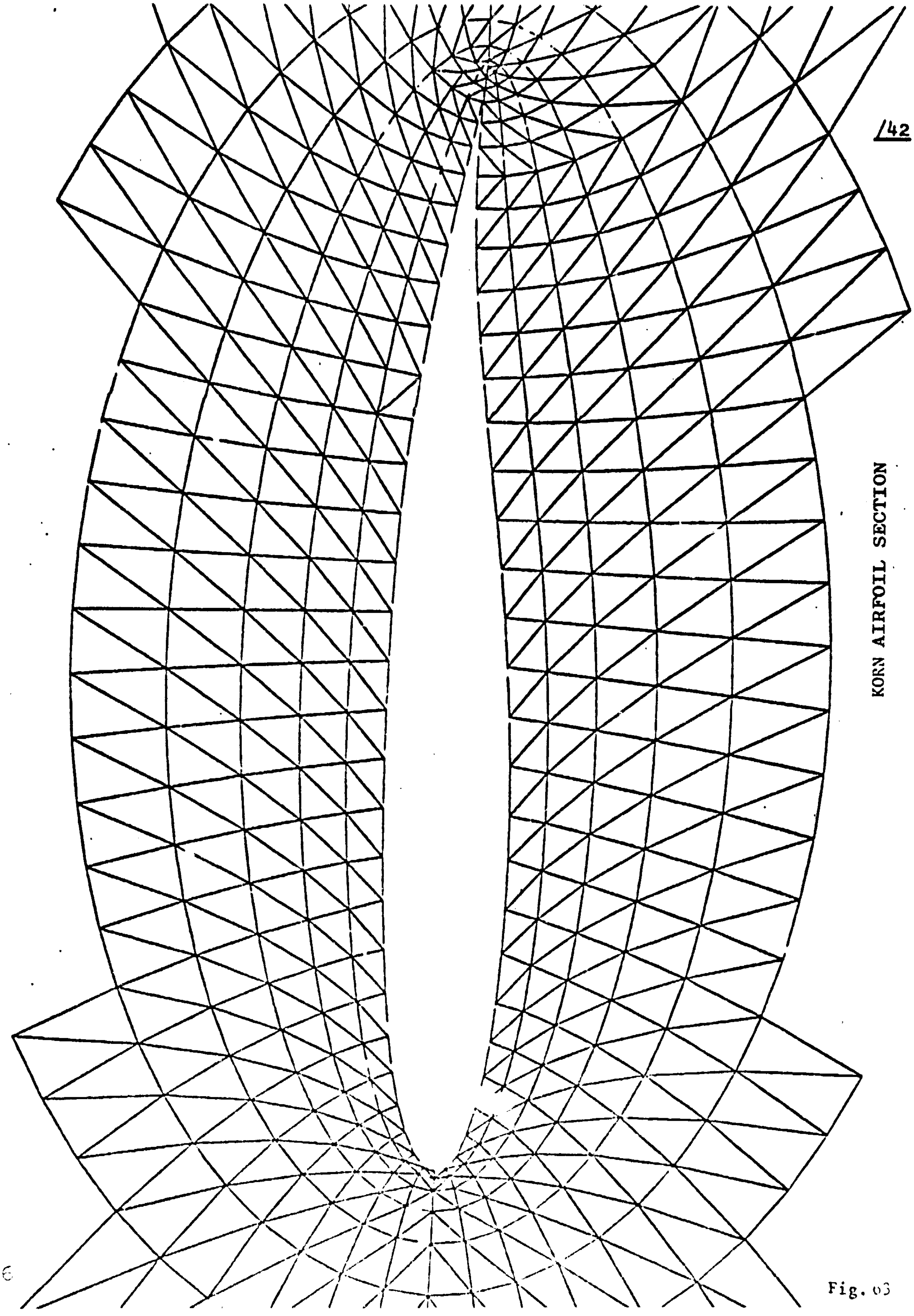

KORN AIRFOIL SECTION

Fig. 63

KORN AIRFOIL

$M_\infty = .75 \quad \alpha = 0$

780 NODES 1440 elements
60 Iterations TCPU = 5'
CL = .554

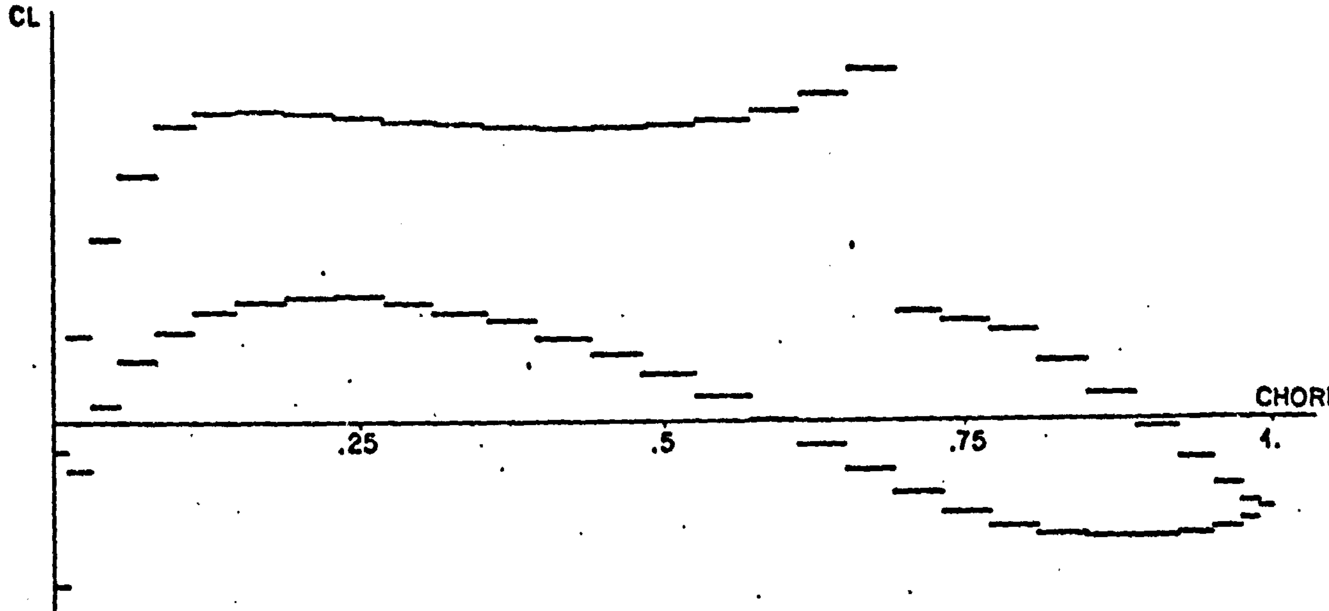

1560 NODES 2880 elements
60 Iterations TCPU = 10'
CL = .585

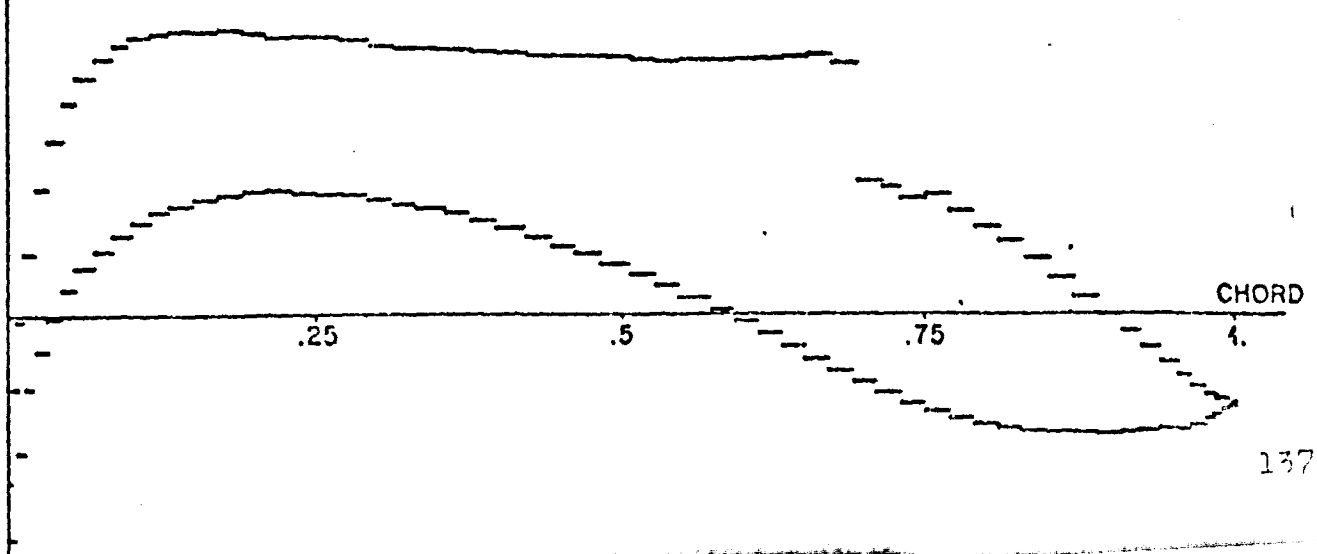

COMPAR ISONS E·F - D·F

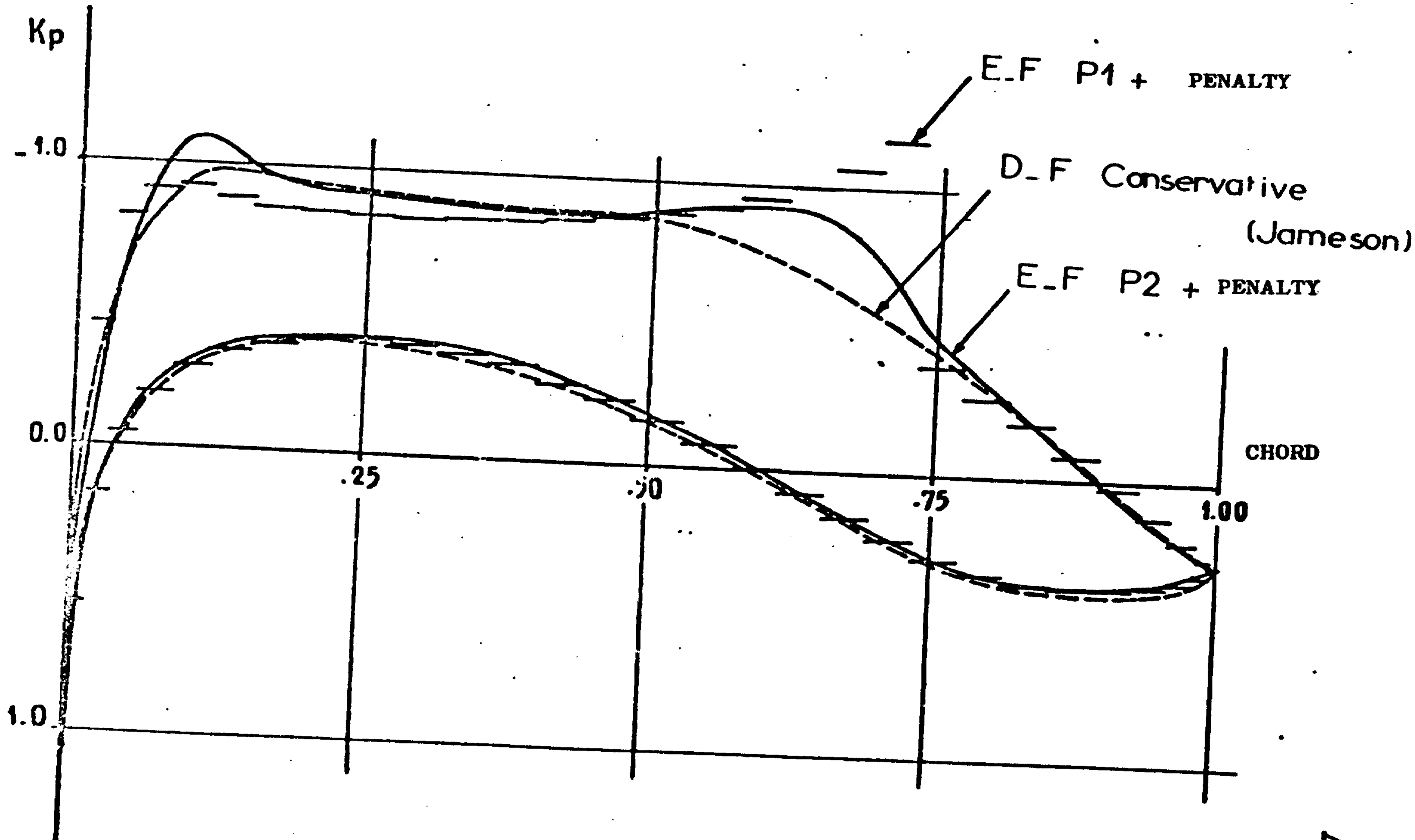

KORN AIRFOIL $M_\infty = .75$ $\alpha = 0.$

/143

KORN AIRFOIL

$M_\infty = .75 \quad \alpha = 0.1$

COMPAR ISONS E·F – D·F

iso-CL

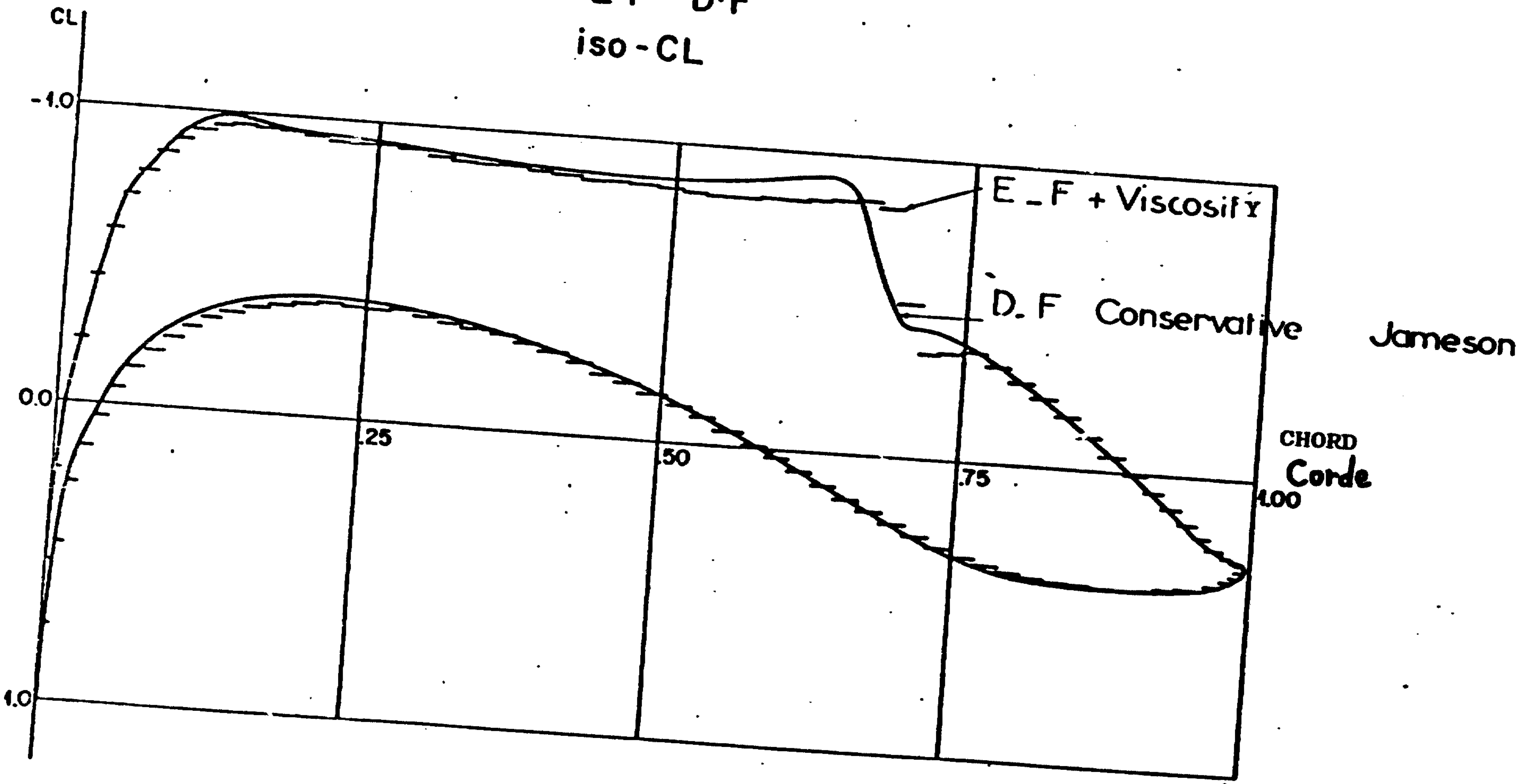

COMPAR ISONS E·F–D·F

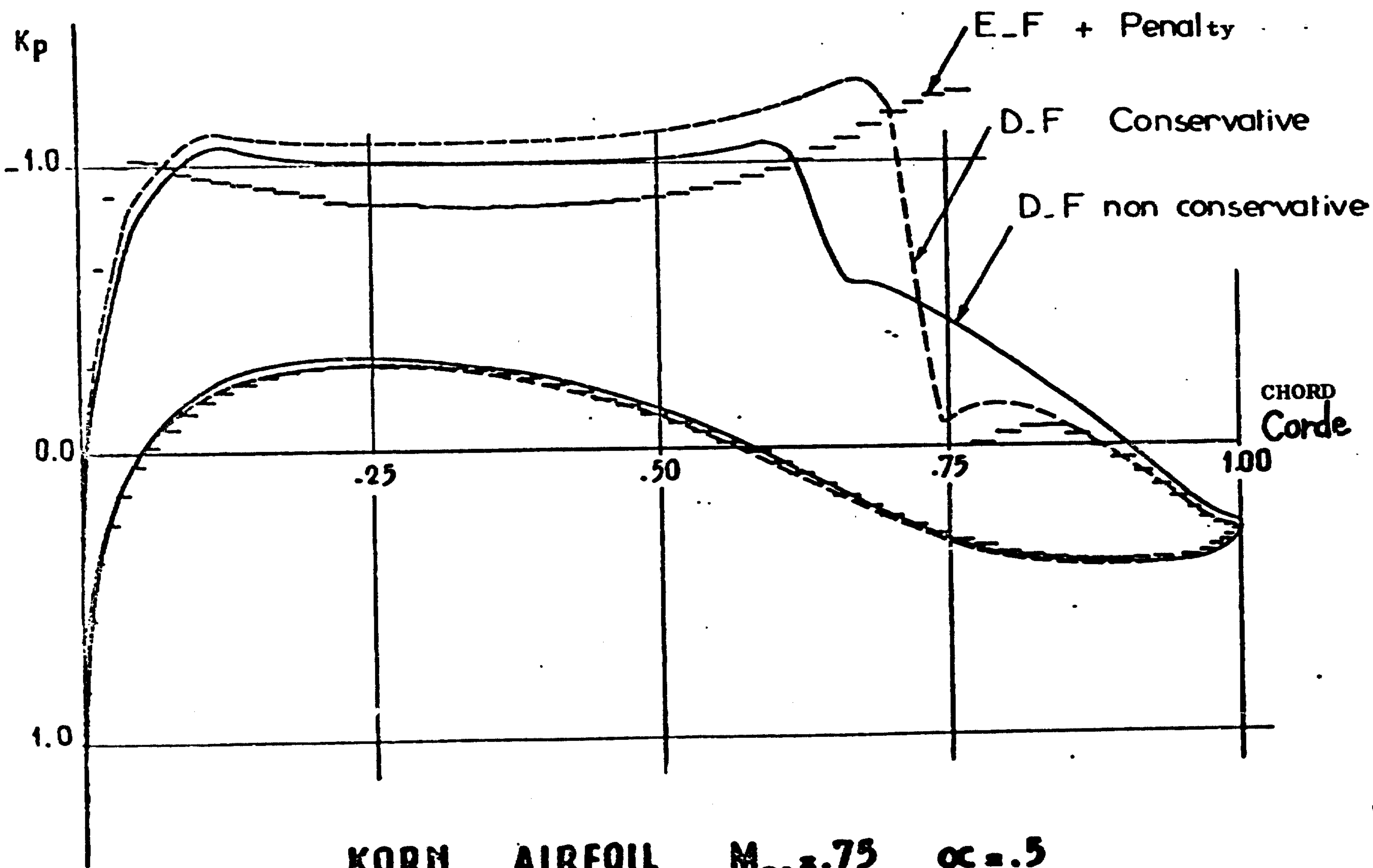

KORN AIRFOIL $M_\infty = .75$ $\alpha = .5$

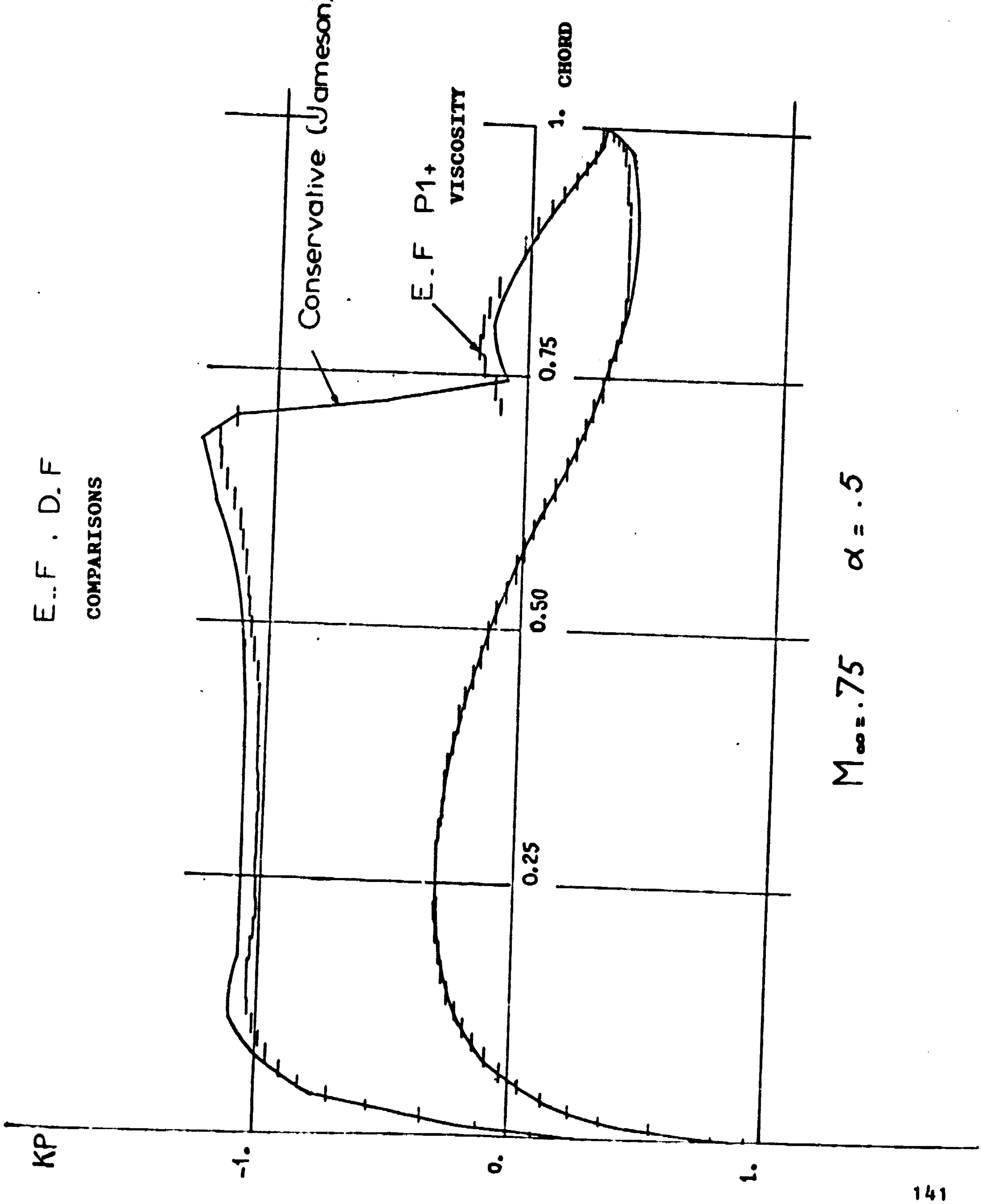
E..F . D.F
COMPARISONS
Conservative (Jameson)
E.F P1+
VISCOSITY
KP
-1.
0.
1.
0.25
0.50
0.75
1. CHORD
$M_\infty = .75$ $\alpha = .5$

Fig. 68

12.2.5. <u>The Multibody (NOZZLE + AIRFOIL SECTION)</u> /148

The lifting transonic flow around an industrial configuration of multibodies has been calculated and compared for approximations P1, P1 iso P2 and P2.

The triangulation around the MUL 2 for a linear approximation (resp. quadratic) consists of 2936 elements (resp. 734) corresponding to 1553 Nodes. The matrix factorized by Cholevski is composed of 200 610 coefficients (resp. 256 276) whereas the number of non zero coefficients of the DIRICHLET matrix is 10533 (resp 17725). Details of the rough triangulation of the nozzle and of the slot is given on figure 69. The Joukovski condition is applied to the trailing edges of the nozzle and of the airfoil section.

The condition of entropy is treated by REGULATION.

The test case M_∞ =.5; TNC=10° calculated on MUL 2 by FINITE ELEMENTS P1 + REGULATION (μ = .2) (resp. P2 μ_1= .5 & μ_2= .05) required 80 control iterations corresponding to a process time of 15 mn (resp. 23 mn). /149

Figures 70, 71, 72 show the surface Mach distribution on the nozzle (1) and the airfoil section (2) for rough triangulations P1, fine P1 iso P2, and P2. One may see the presence of a shock at the extrados of the airfoil section (2).

Details near the mulibodies of the local Machs in the fluid in the form of the Mach number (P1) or iso-Mach (P2) shows the good oper operation of the nozzle, the passage at M=1 at the neck on figures 73 74, 75 (downstream from the slot) and the satisfactory Joukowski condition on the nozzle (1) at the subsonic limit ! (M_{BF} = .95).

The determination of the circulations during the iterations depending on the approximation selected is shown on figure 76, whereas the evolution of the cost function and of the gradient of the criterion depending on the approximation selected are compared on figures 77 and 78.

It may be pointed out on figure 78 the "periodic" discontinuity of the gradient corresponding to the calculation of a new circulation (Joukowski condition) and requires a restoration of the conjugate gradient algorithm in the sense of POWELL (41).

12.2.6. <u>The BI-NACA Multibody AIRFOIL SECTION + AIRFOIL SECTION</u>

The interest of a transonic calculation around a (BI-NAC) configuration lies in the mixed nature of the simultaneously internal-external flow. In fact, the internal domain (Ω_1) made up by the extrados of the lower airfoil section (2) and intrados of the upper airfoil section (1) is the converging-diverging pipe type, whereas the one (Ω_2) formed by the intrados of (2) and by the extrados (1) (Figure 79.1) represents an external flow around a body.

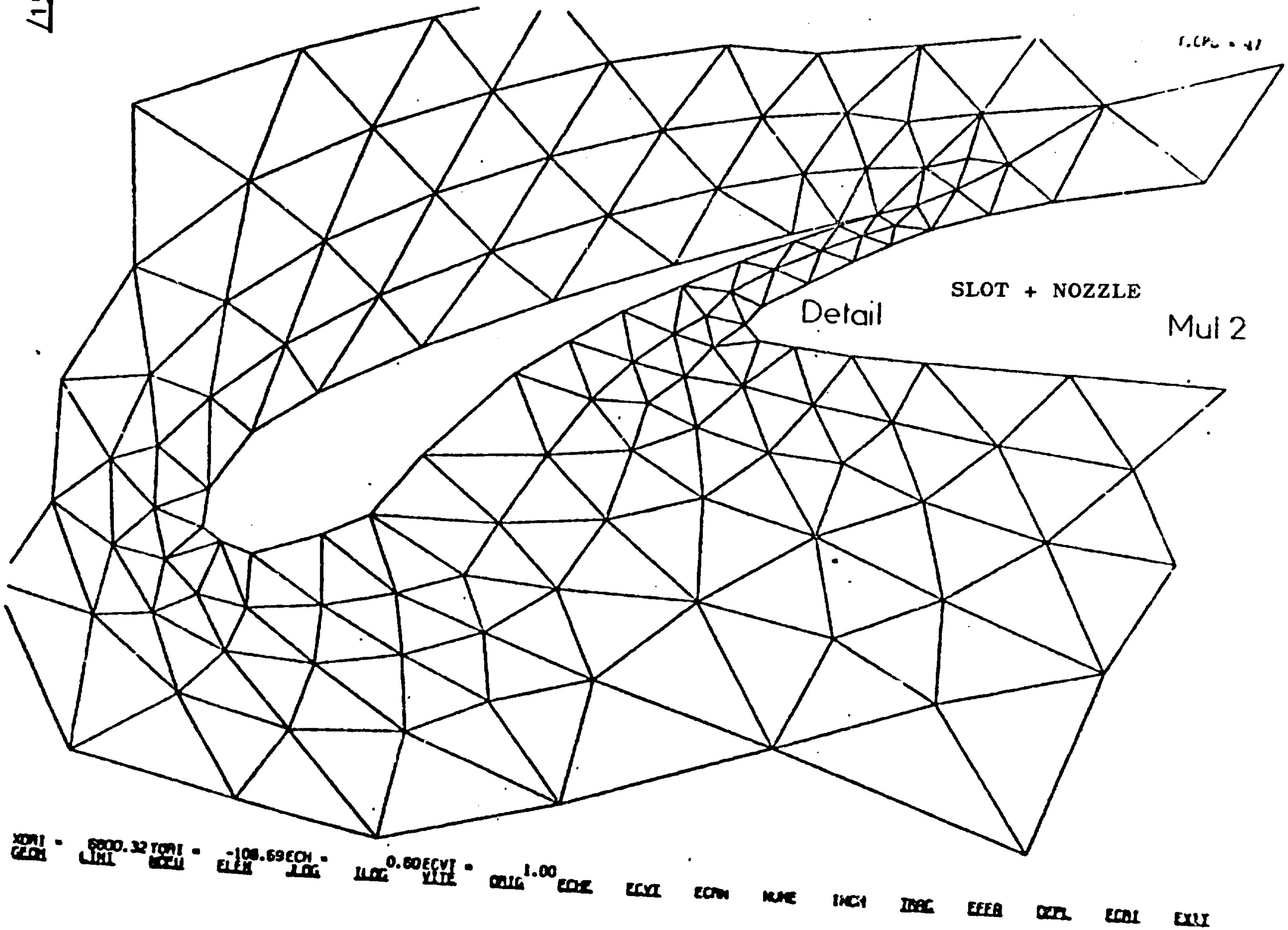
SLOT + NOZZLE
Detail
Mul 2
XORI = 6800.32 YORI = -108.69 ECH = 0.80 ECVI = 1.00
GEOM LIMI MOFU ELEM LOG ILOG VITE ORIG ECHE ECVI ECRN NUME INCH TRAC EFFA DEPL ECRI EXIT

E_F P1

\+ ME PENALTY

MULTIBODY COARSE GRID

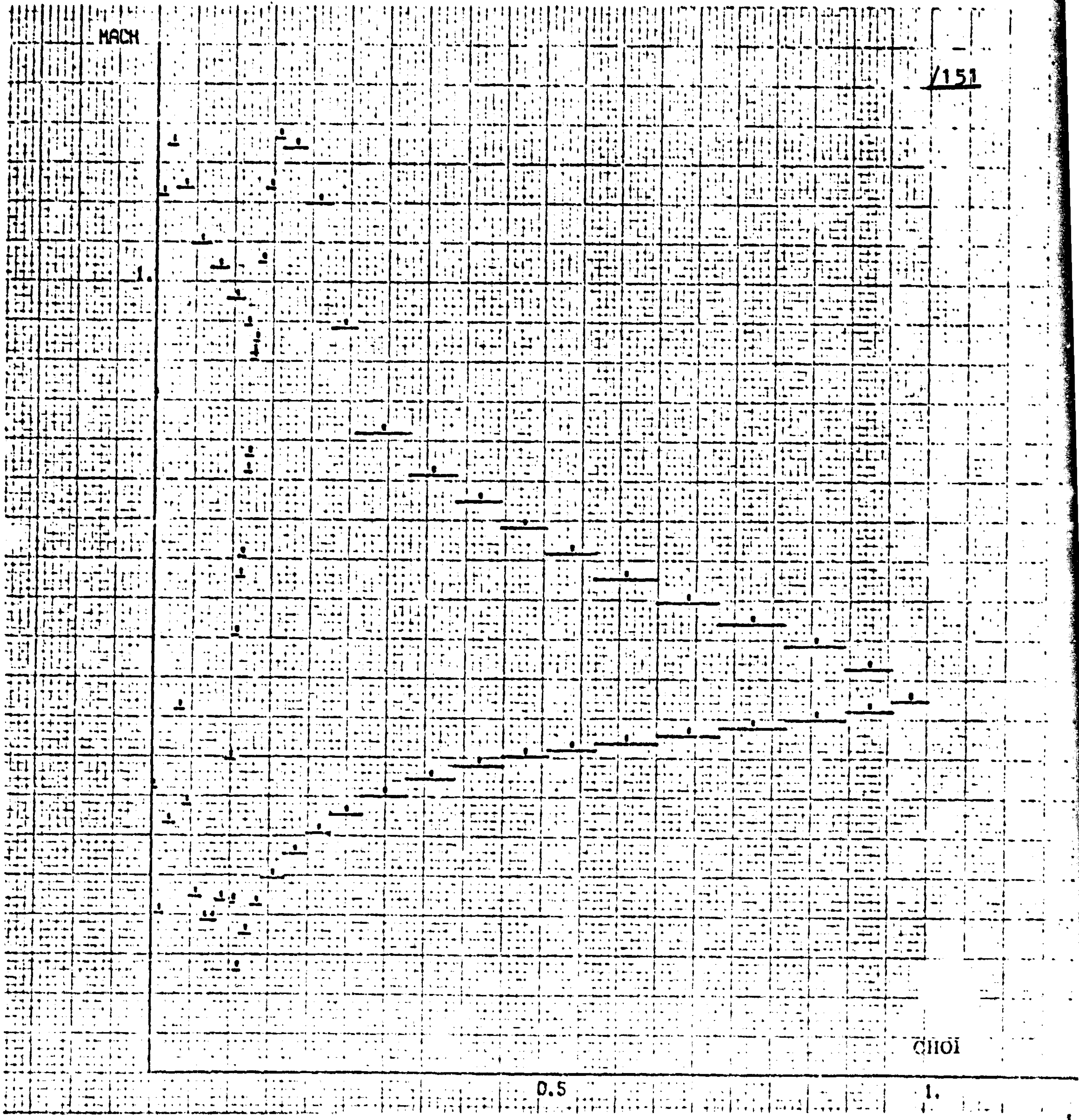

$M_\infty = .5 \qquad \alpha = 10^\circ$

E.F. P1 + PENALTY

MULTIBODY FINE GRID

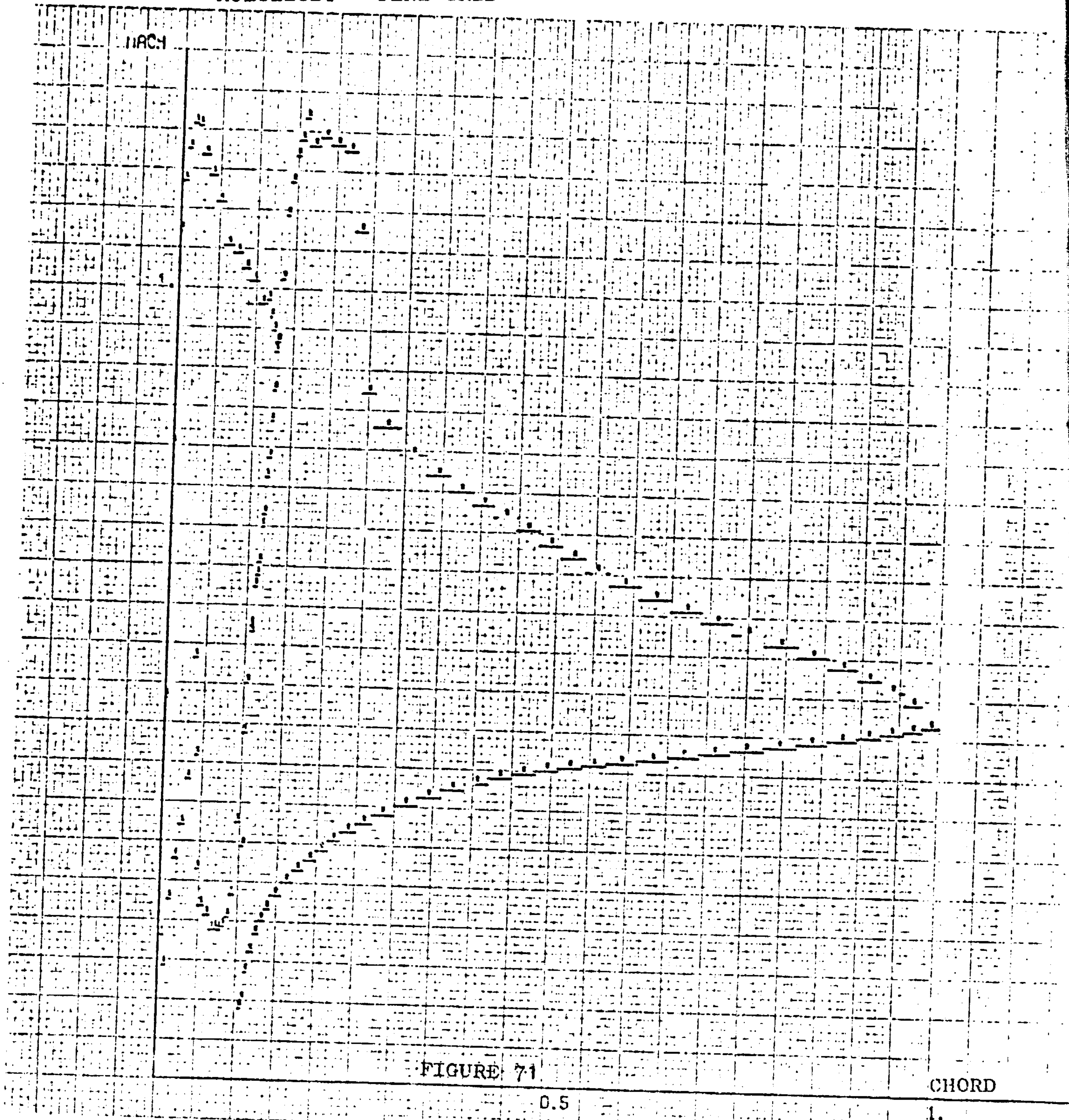

FIGURE 71

$M_\infty = .5 \qquad \alpha = 10°$

E.F . P2

MULTIBODY

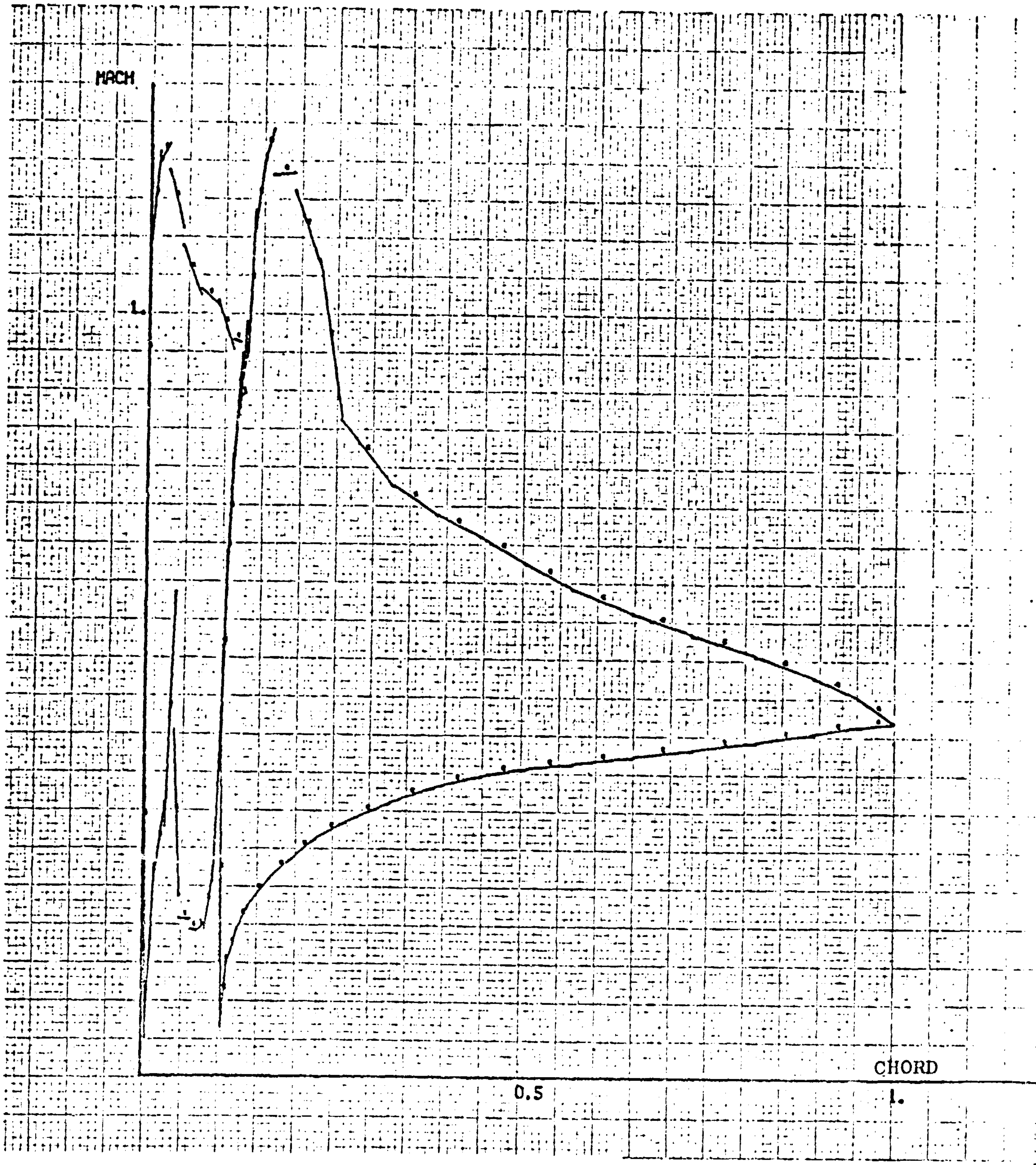

$M_\infty = .5 \quad \alpha = 10°$

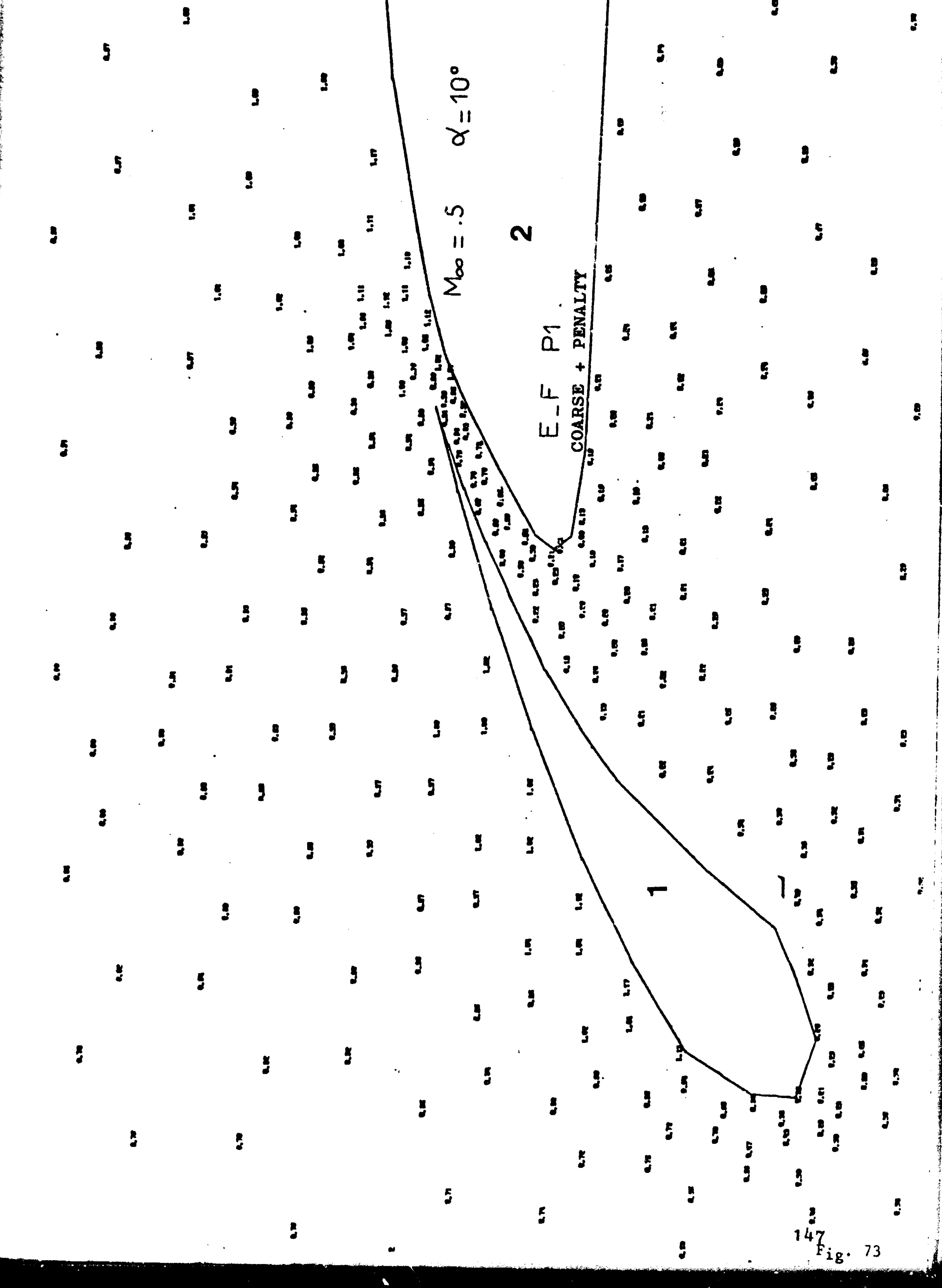

147

Fig. 73

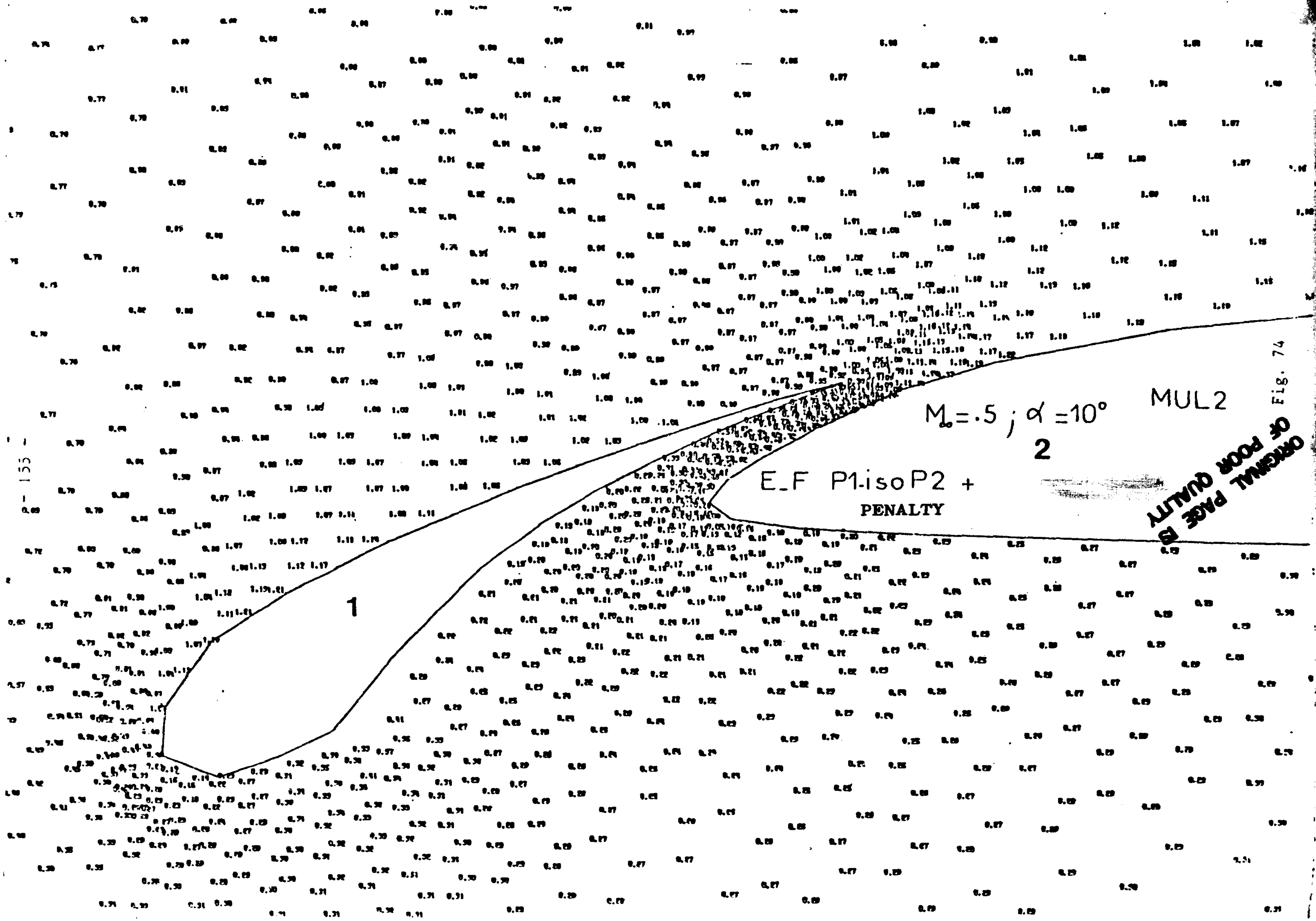

Fig. 74

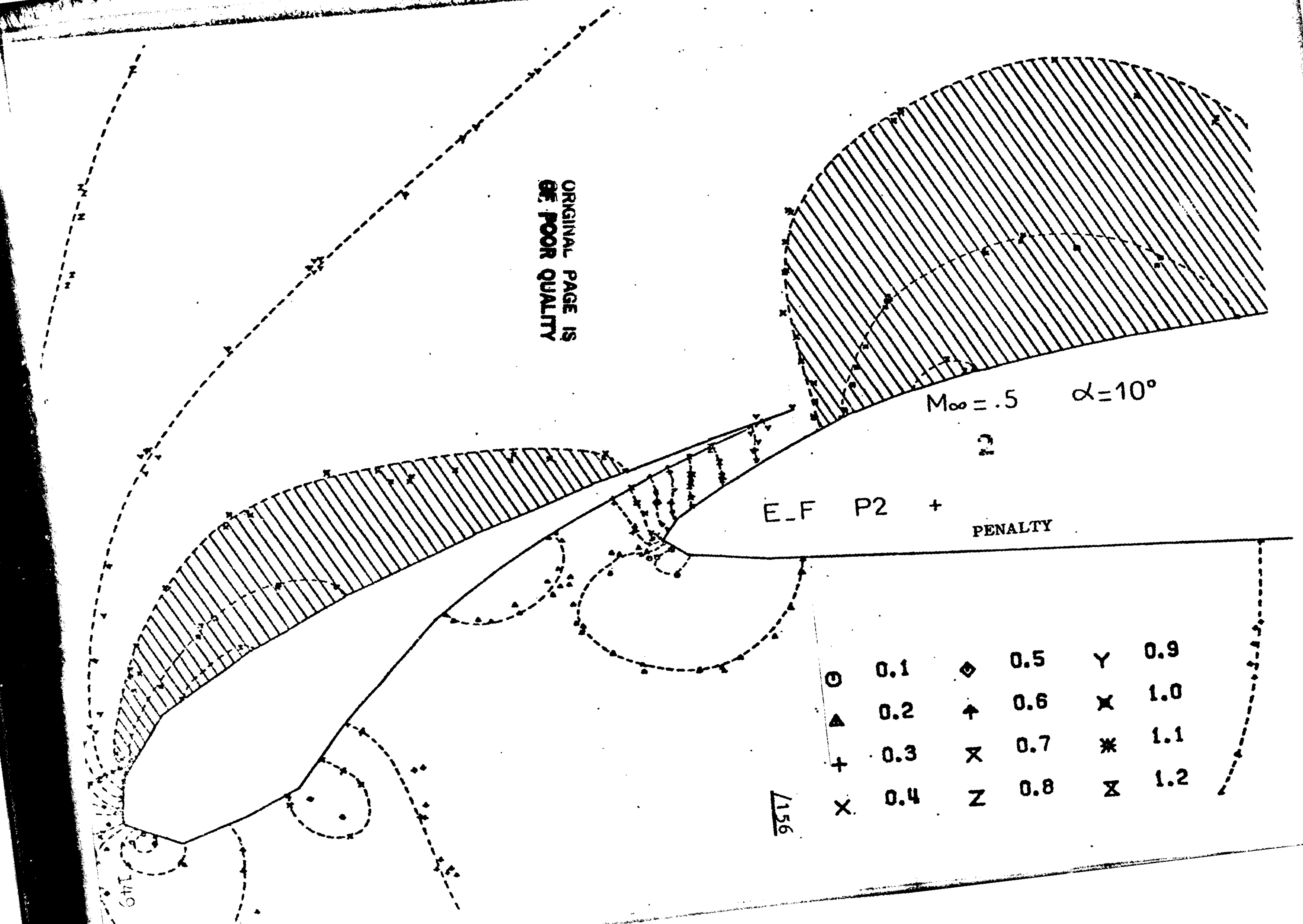

/156

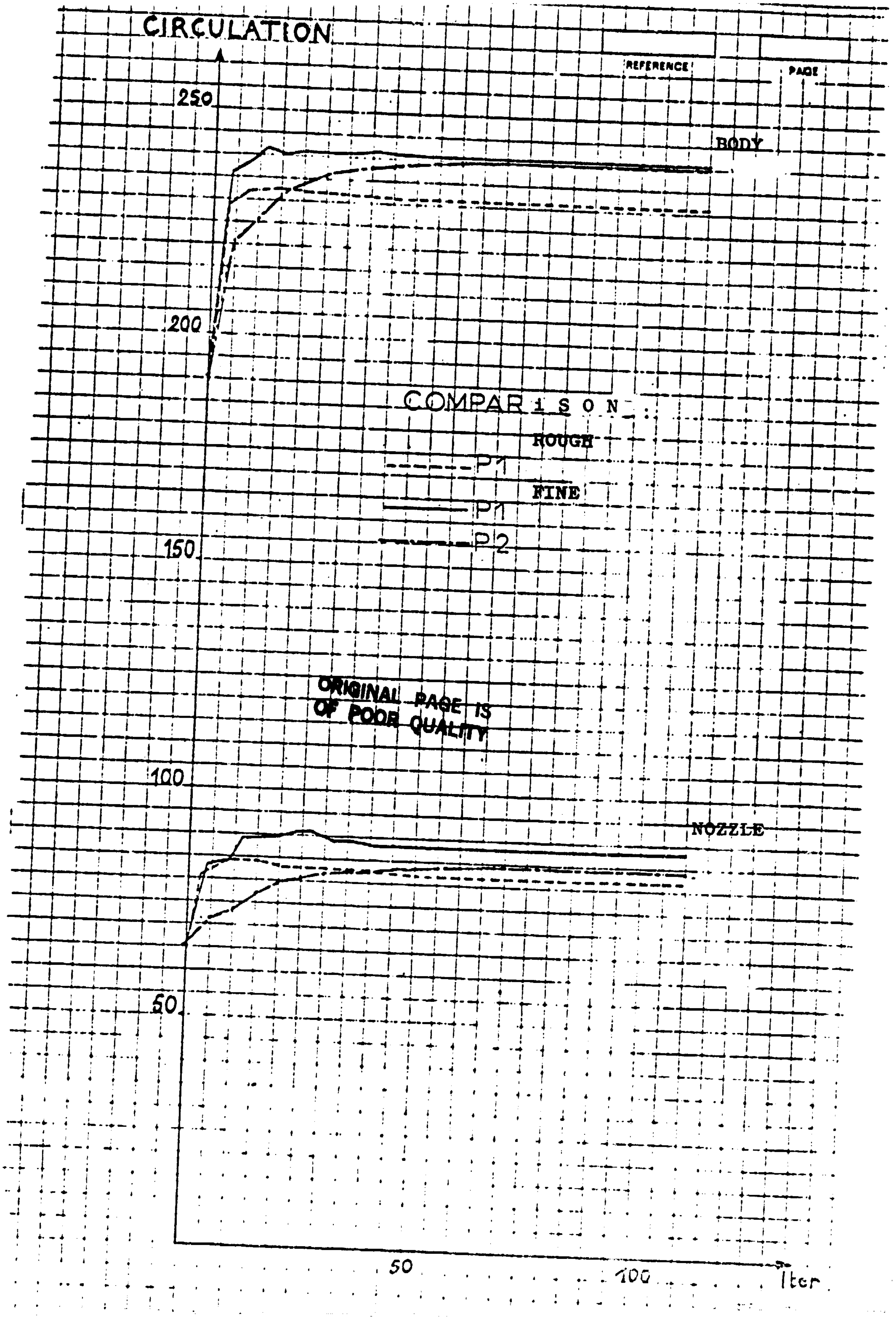

ORIGINAL PAGE IS OF POOR QUALITY

151

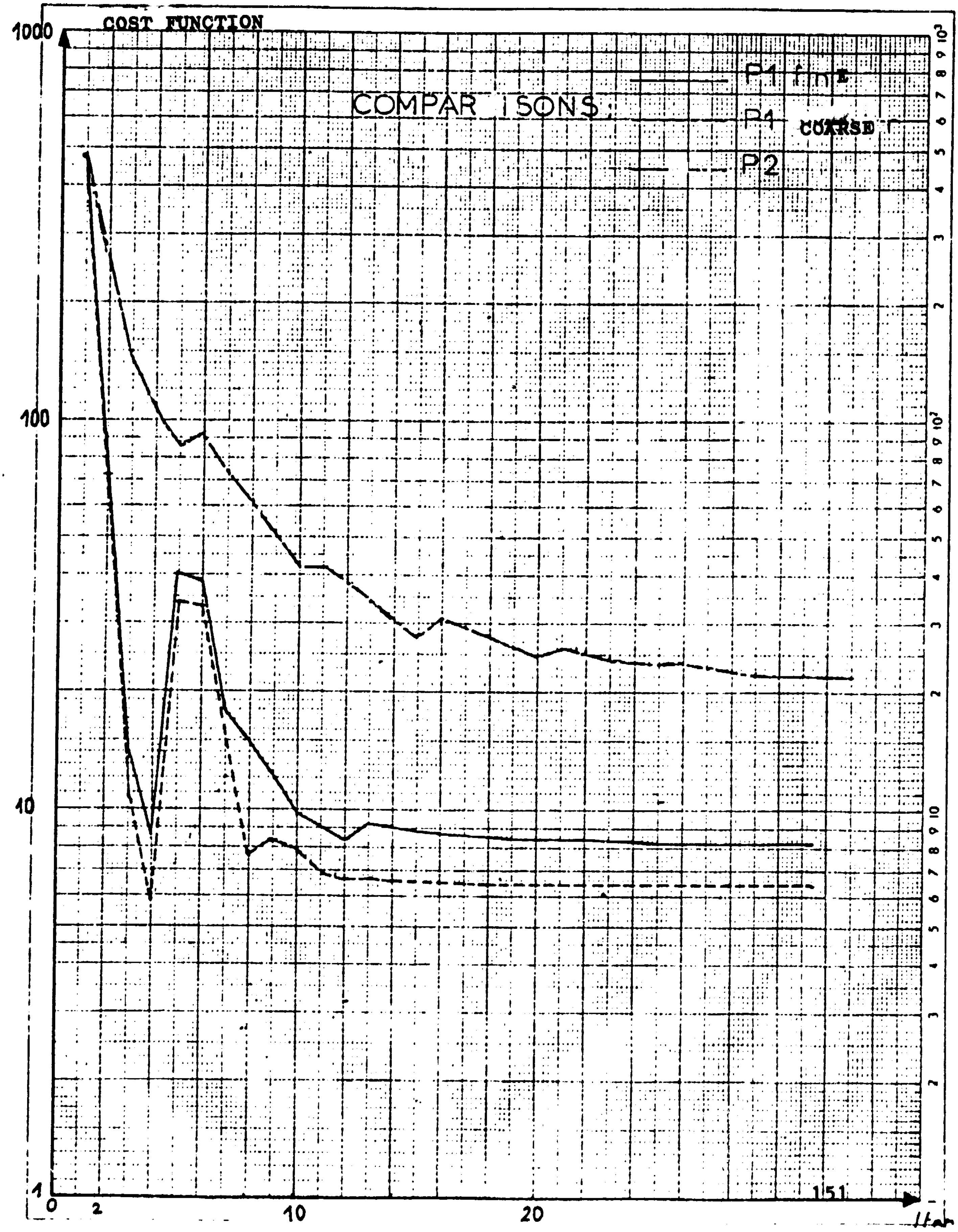

COST FUNCTION
COMPARISONS:
P1 fine
P1 COARSE
P2
1000
100
10
1
0
2
10
20
Iter

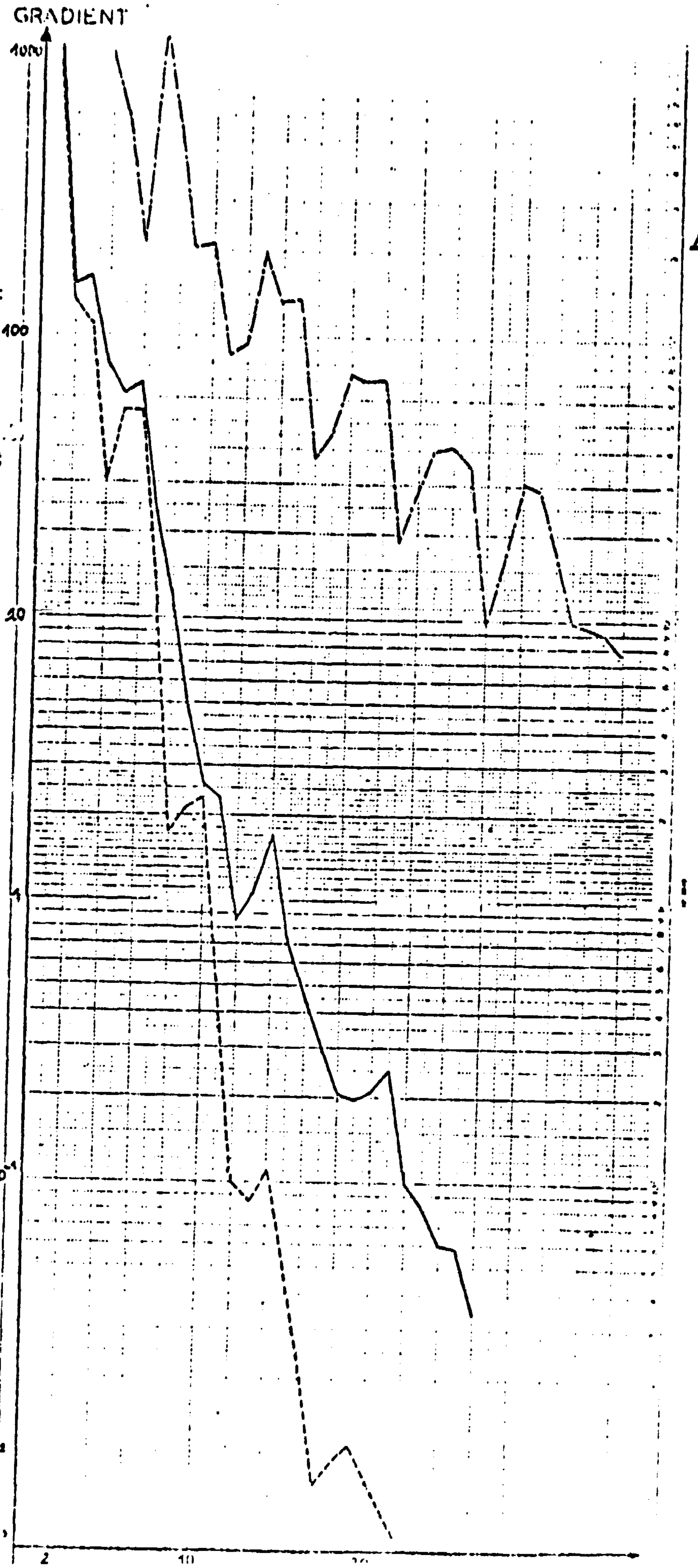

COMPARISONS

P 1 COARSE

P 1 FINE

P 2

ORIGINAL PAGE IS OF POOR QUALITY

/159

The possiblity of several shocks appearing simultaneously and having different intensities is therefore a fundamental numerical test for industrial applications 2-D 3-D composed of several shocks. /160

The triangulation around the BINAC is made by the MODULEF technique and consists of 3298 elements corresponding to 1739 nodes. The number of non zero coefficients of the Dirichlet matrix is 11.800, the one factorized by Choleski has 147.117 coefficients. Details of the triangulation near the 2 airfoil sections showing the internal domain is given on figure 79.2. The Joukowski condition is applied to the trailing edges BF1 and BF2 of the 2 airfoil sections 1-2.

Two cases of computation taking up 2500K of double precision memory 1) (M_∞ = .6, INC = 0°) (non lifting)

2) (M_∞ = .6, INC = 6°) (lifting)

in finite elements P1 with PENALTY are presented and have required 80 iterations corresponding to a process time of 20 mn.

Figures 80-81 show the surface distribution of the pressures on airfoil section 1 and airfoil section 2. It may be observed that there is a perfect symmetry of results o) the pressure intrados of (1 (1) is mixed with the pressure extrados of (2) and vice versa. Case 1 has only one shock inside the domain Ω,, pipe type, whereas in case 2) a second shock is placed extrados of (2), in the external domain Ω_1.

Details near the two airfoil sections of the local Machs on figures 82-83 in the fluid, in the iso-Mach form show a good operation of the internal domain Ω and the satisfaction of the Joukowski condition. The penalty prevents simultaneously the formation of two decompression shocks.

12.2.7. The Converging-Diverging 3-D Pipe /167

This is an ajustment test case of code 3-D. The appearance of compression shocks is verified in the diverging part of the pipe, as the formation of decompression shock was prohibited by the penalty of the condition of entropy.

As in case 2-D, a difference of potential is applied at the inlet and outlet of the pipe which is sufficiently high to obtain a case of transonic operation. On the sides, the tangency conditions ($\frac{\partial \phi}{\partial n}$ = 0) of homogenous Neumann standard type are implicity applied. The domain of the flow is quantified into 1920 tetrahedrons on figure 84.and is composed of 24 sections. 40 iterations lead to convergence of the algorithm in 3 mn of process time.

On figures 85 through 90 may be seen the evolution of the Mach numbers, constant on each tetrahedron, on several fronts adjcent to the sections located in the converging zones (without shock) and diverging zones (with shock) of the pipe. One may note the satisfaction of the entropy condition in a region near the pipe axis.

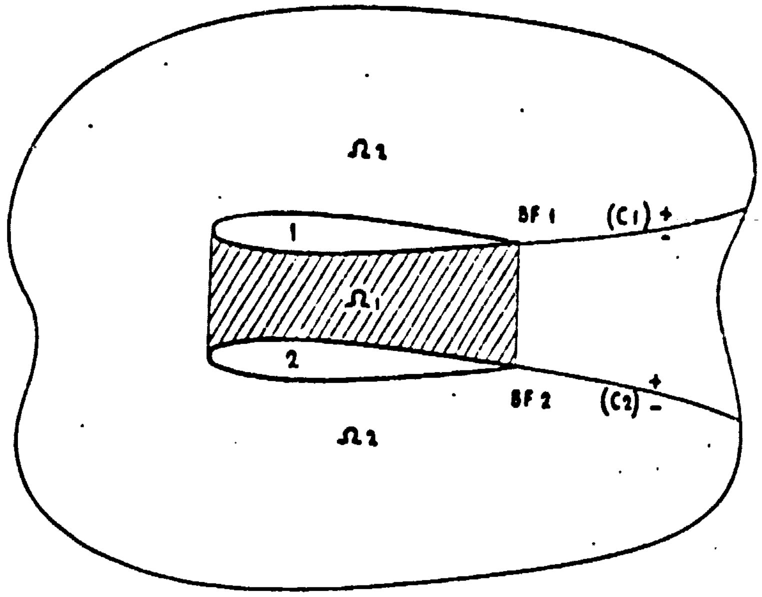

Fig. 79.1

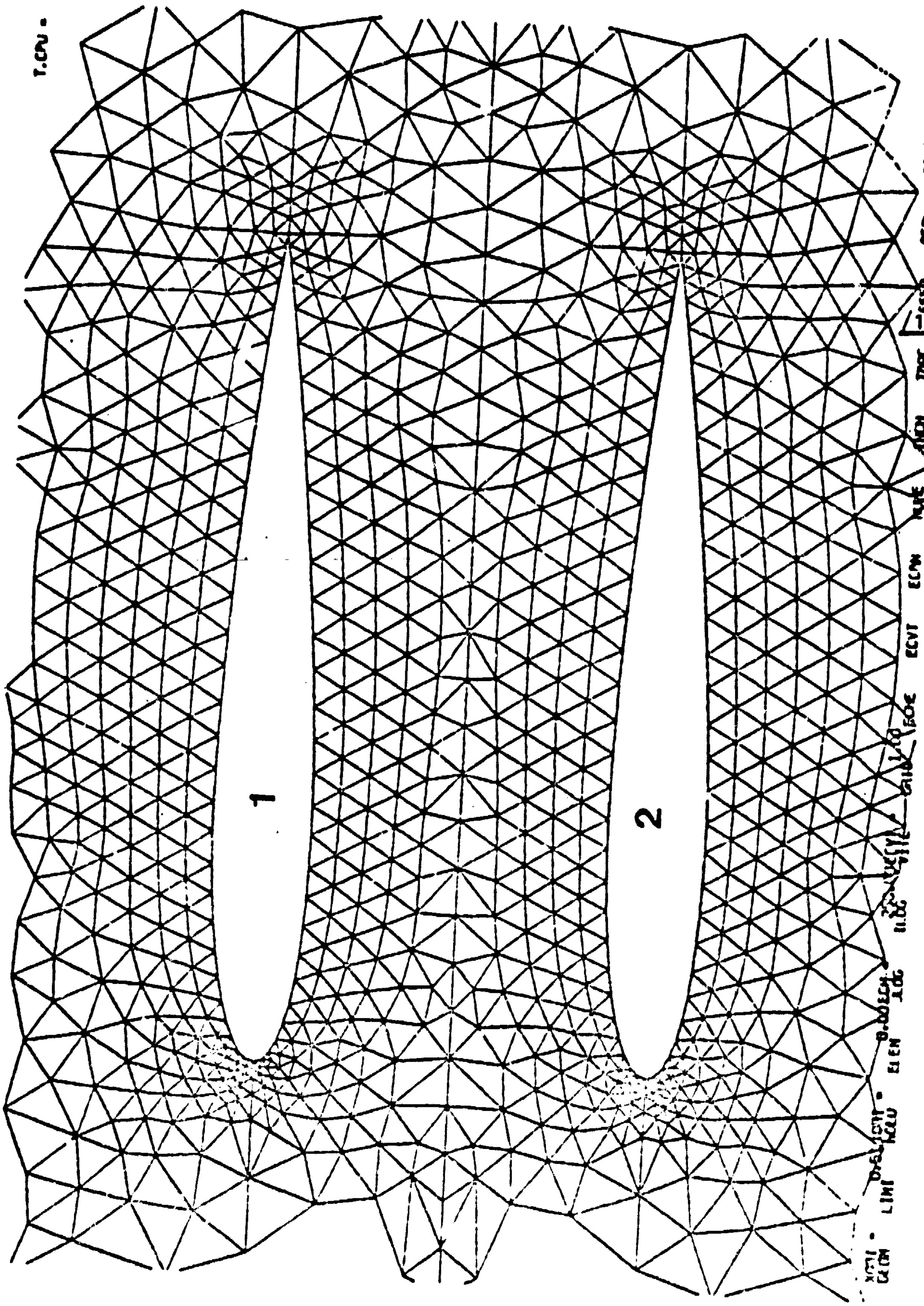

/162

Fig. 79.2

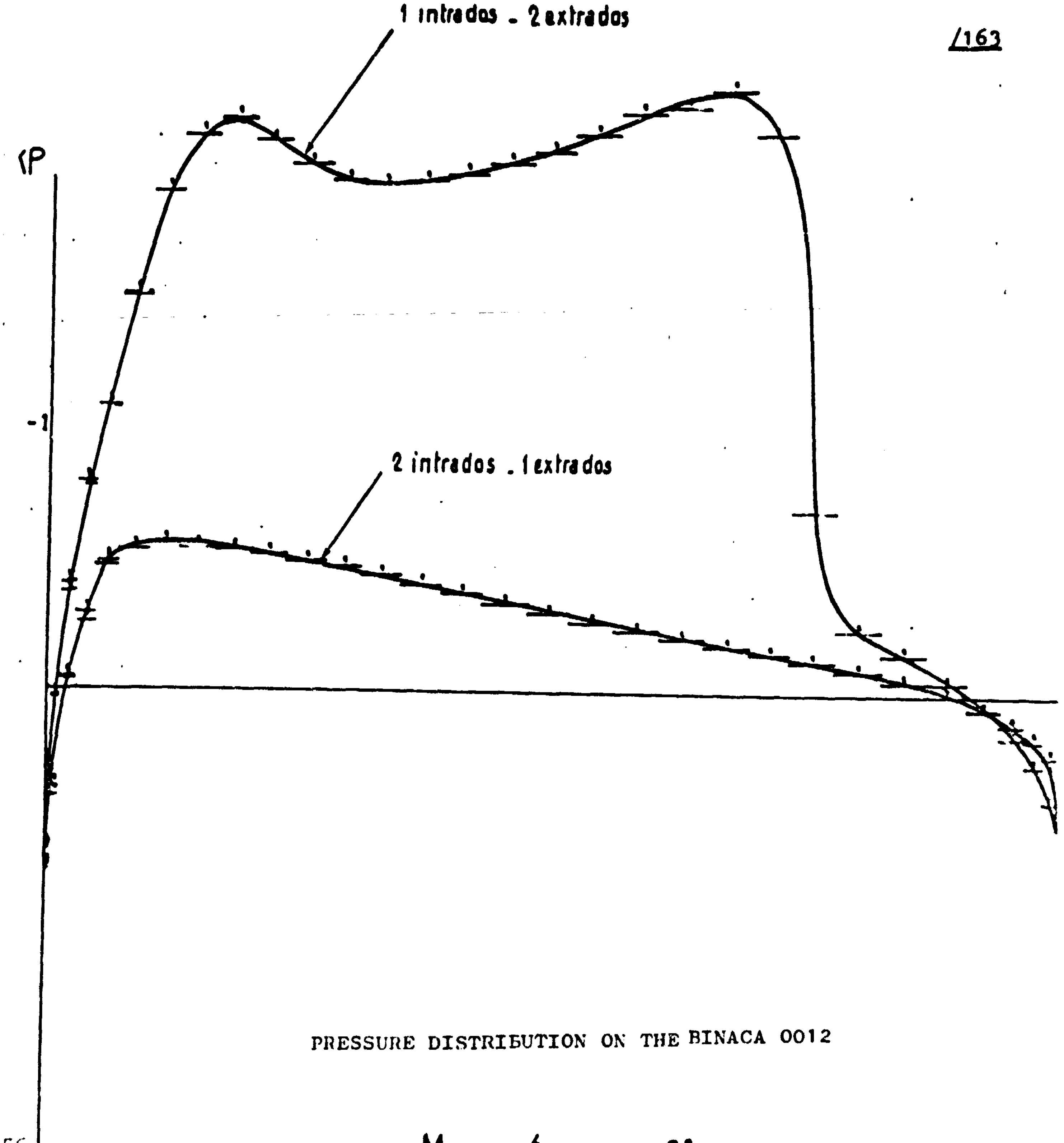

PRESSURE DISTRIBUTION ON THE BINACA 0012

$M_\infty = .6 \quad \alpha = 0°$

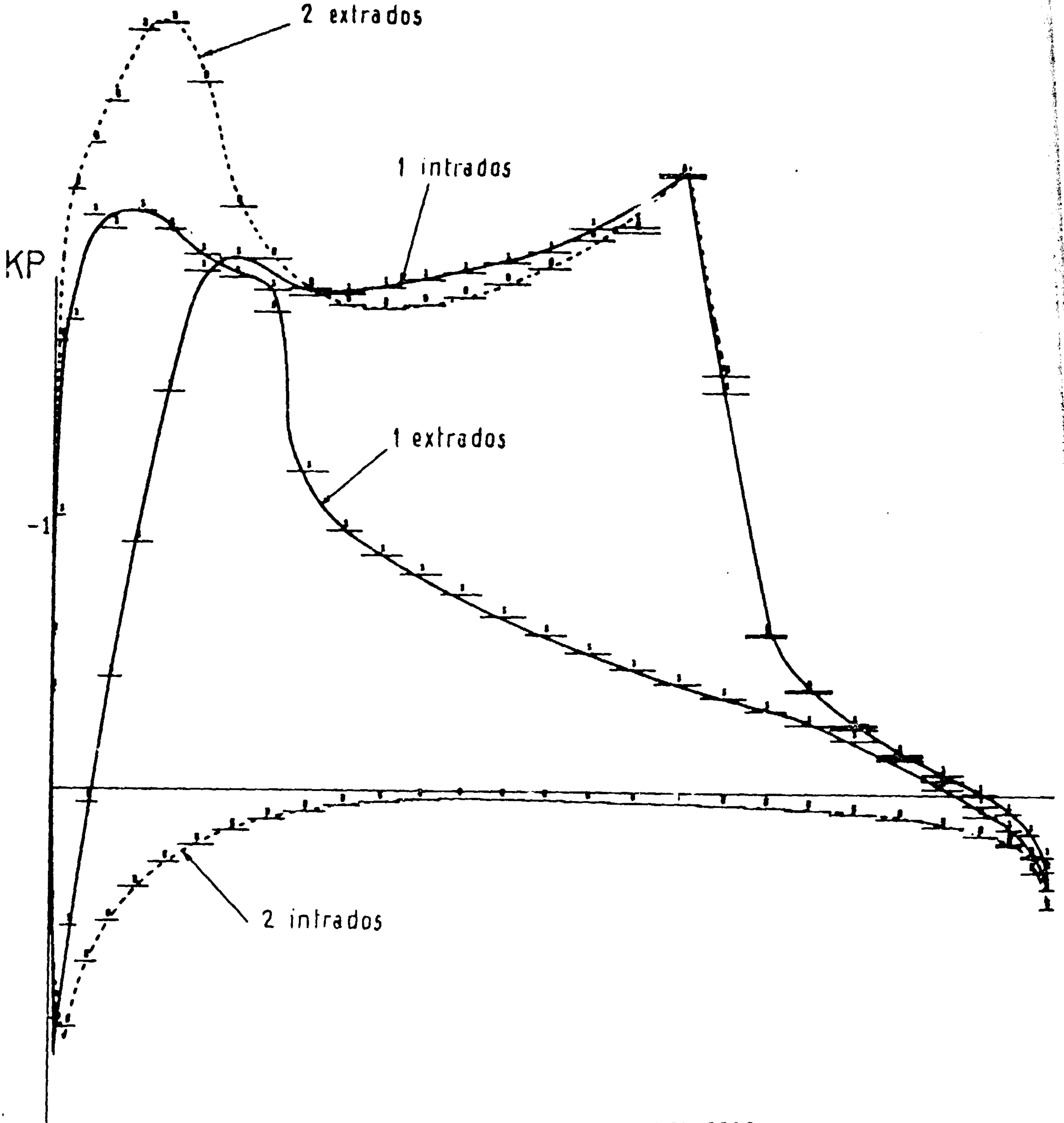

PRESSURE DISTRIBUTION ON THE BINACA 0012

$M_{\infty} = .6 \quad \alpha = 6°$

Fig. 81

/165

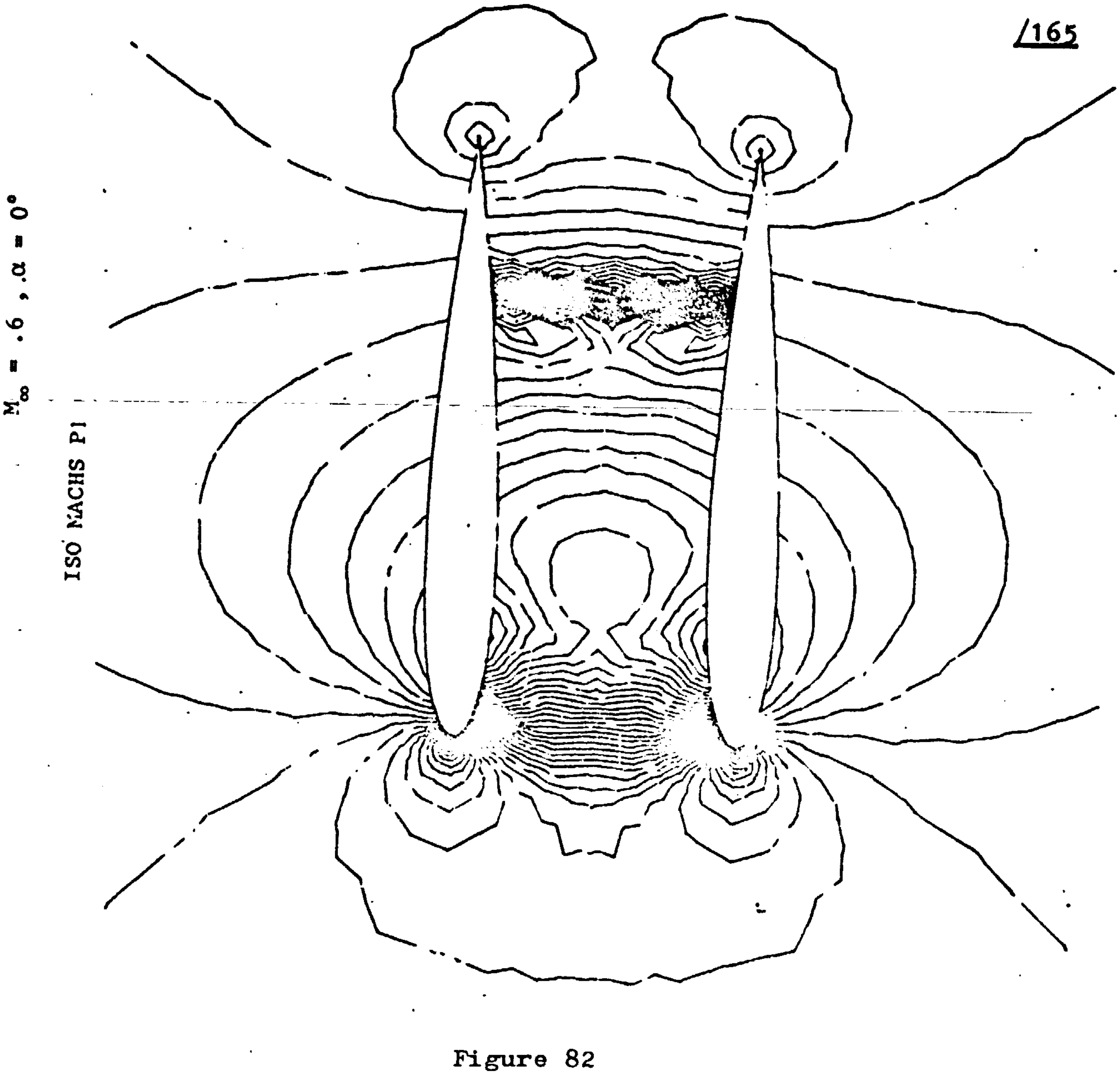

Figure 82

Fig. 82

/166

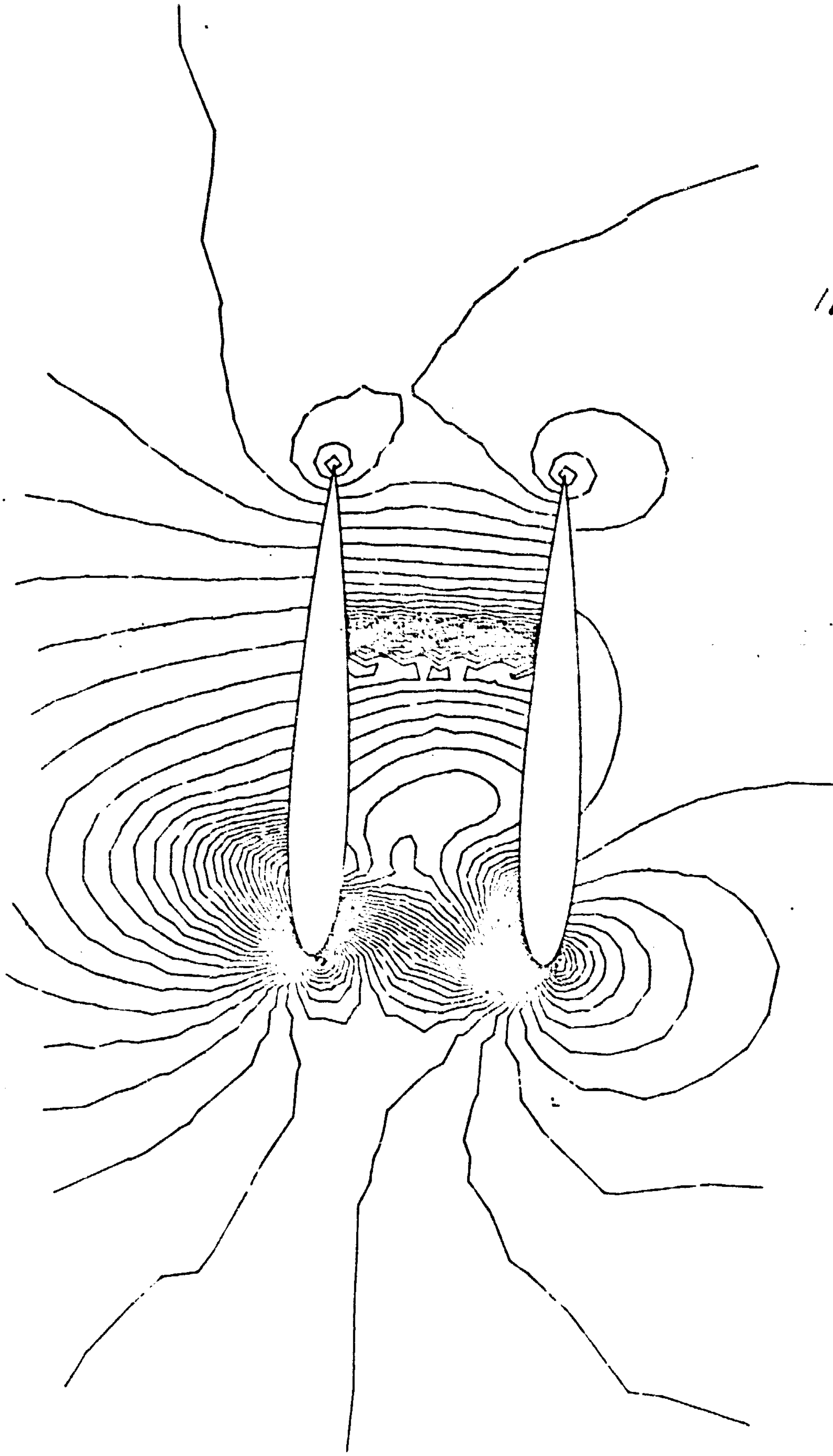

ISO MACHS P1 (M_∞ = .6, α = 6°)

Fig. 83

3-D NOZZLE TRIANGULATION

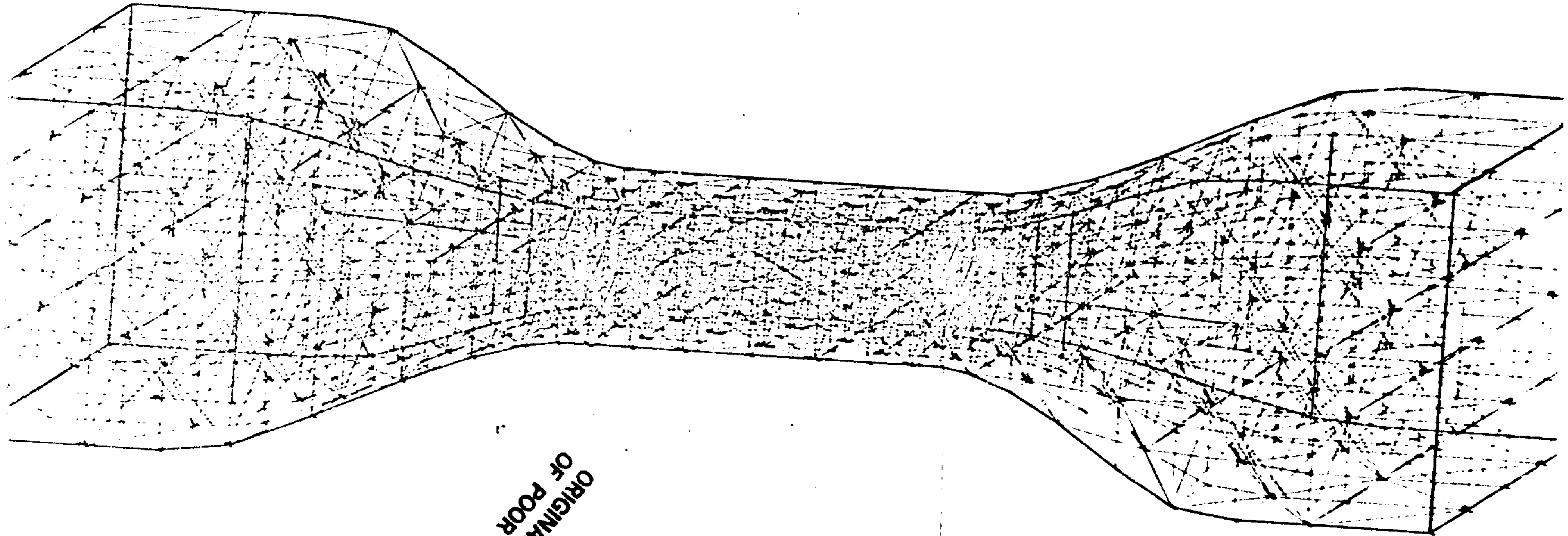

SECTION N= 6 -

/169

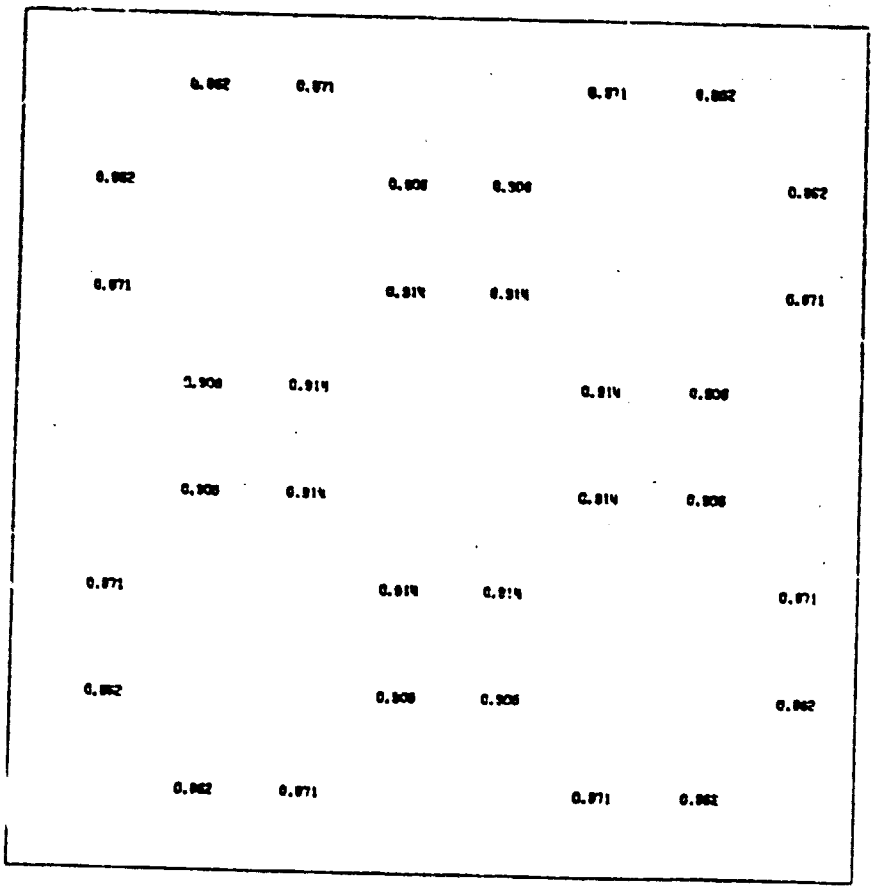

Fig. 85

SECTION N= 6 +

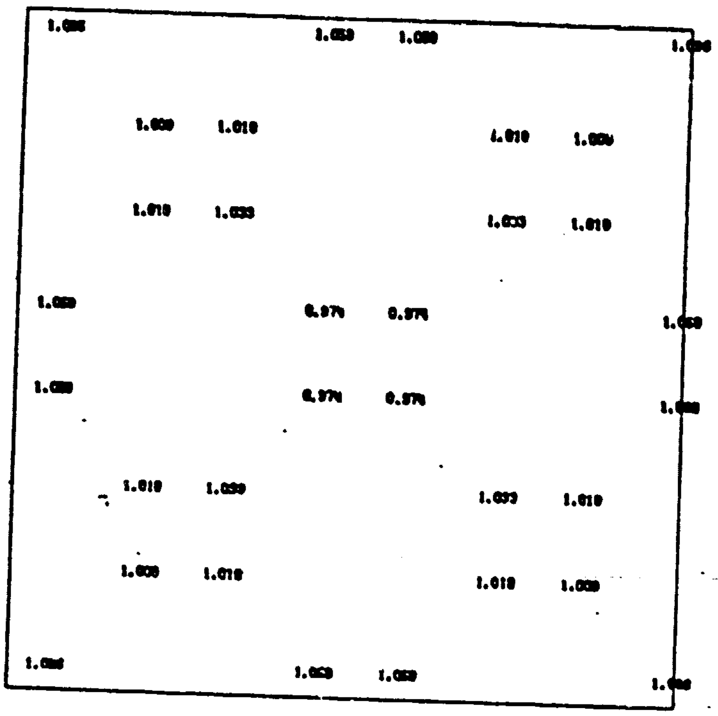

SECTION N= 7 -

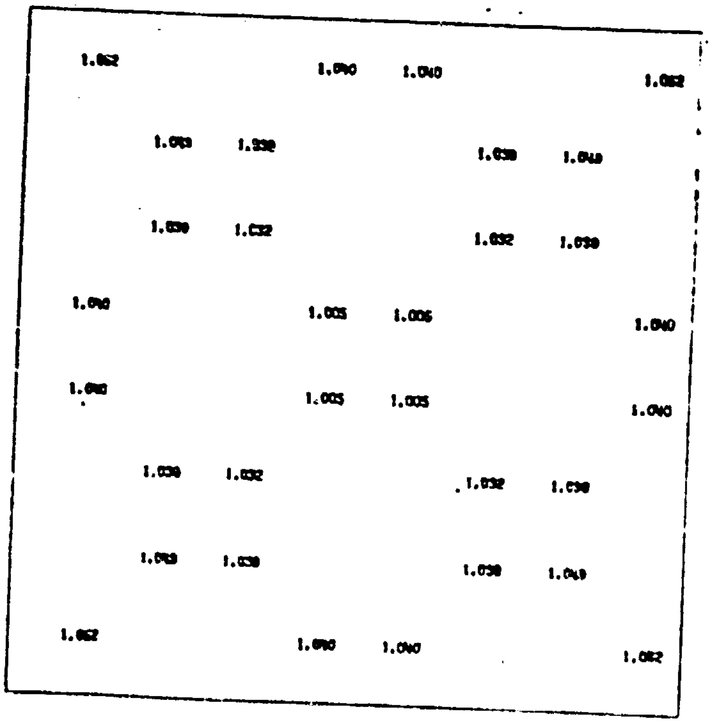

Fig. 86

SECTION N= 7 +

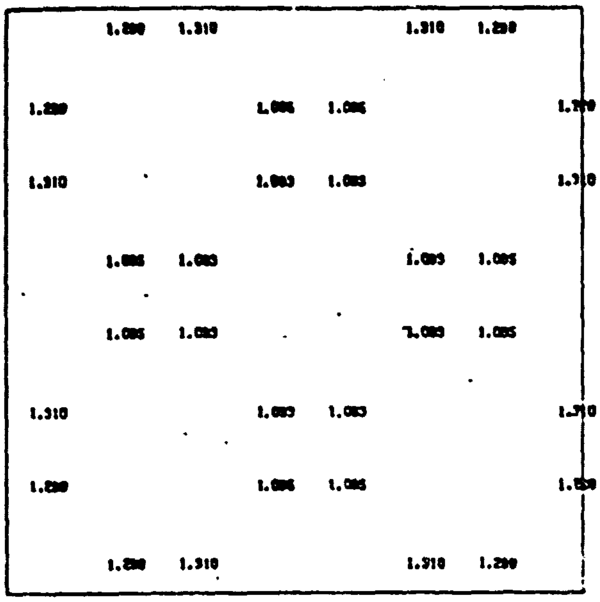

SECTION N= 8 -

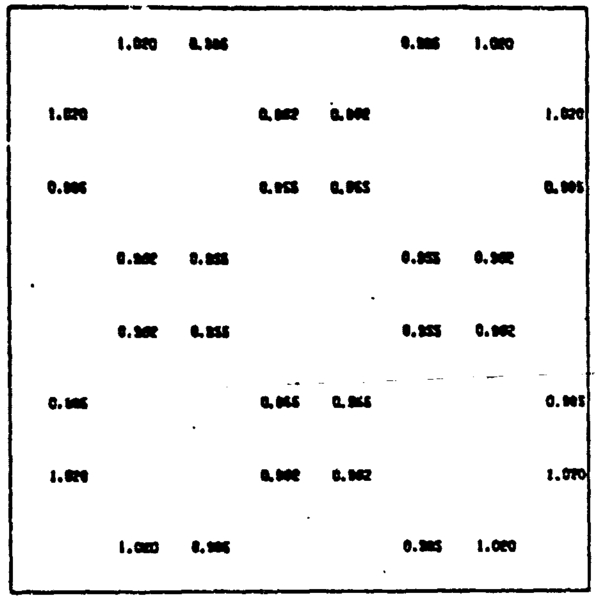

SECTION N= 8 +

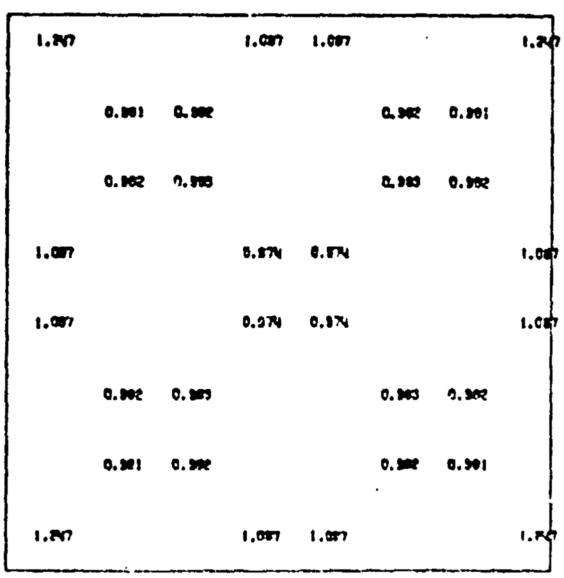

SECTION N= 9 -

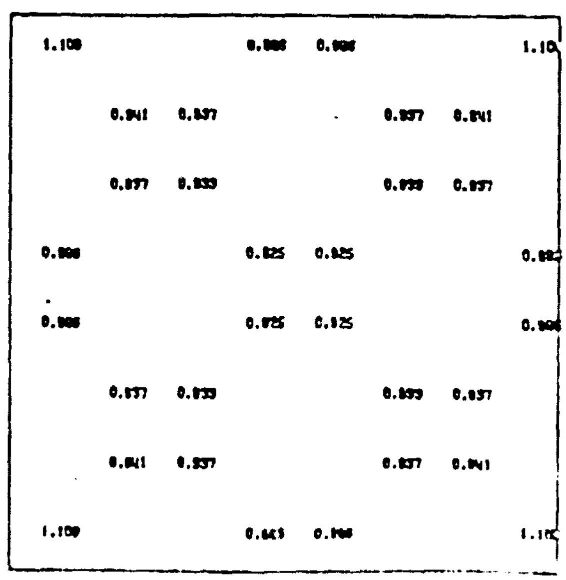

SECTION N= 17 -

1.120			1.116	1.116			1.120
	1.047	1.040			1.040	1.047	
	1.043	1.061			1.061	1.043	
1.110			1.020	1.020			1.110
1.110			1.020	1.020			1.110
	1.043	1.061			1.061	1.043	
	1.047	1.040			1.040	1.047	
1.120			1.116	1.116			1.120

SECTION N= 17 +

	1.102	1.102			1.102	1.102	
1.102			0.902	0.902			1.102
1.102			0.901	0.901			1.102
	0.902	0.901			0.901	0.902	
	0.902	0.901			0.901	0.902	
1.102			0.901	0.901			1.102
1.102			0.902	0.902			1.102
	1.102	1.102			1.102	1.102	

SECTION N= 18 -

	1.704	1.716			1.716	1.704	
1.704			1.272	1.272			1.704
1.716			1.282	1.282			1.716
	1.272	1.282			1.282	1.272	
	1.272	1.282			1.282	1.272	
1.716			1.282	1.282			1.716
1.704			1.272	1.272			1.704
	1.704	1.716			1.716	1.704	

SECTION N= 18 +

1.073			1.011	1.011			1.073
	1.433	1.425			1.425	1.433	
	1.425	1.417			1.417	1.425	
1.011			1.243	1.243			1.011
1.011			1.243	1.243			1.011
	1.425	1.417			1.417	1.425	
	1.433	1.425			1.425	1.433	
1.073			1.011	1.011			1.073

SECTION N= 19 -

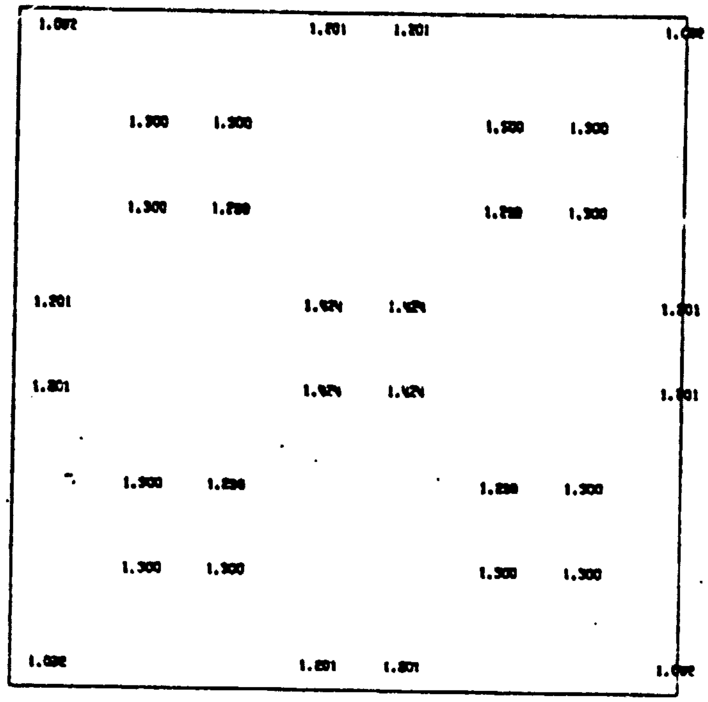

SECTION N= 19 +

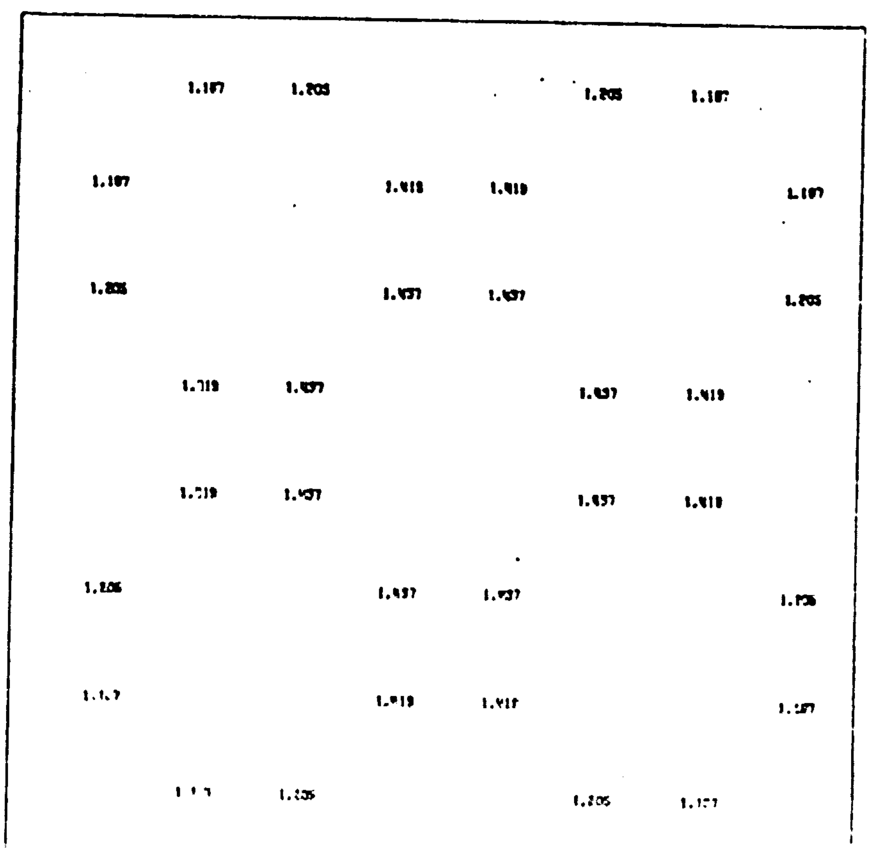

SECTION N= 20 -

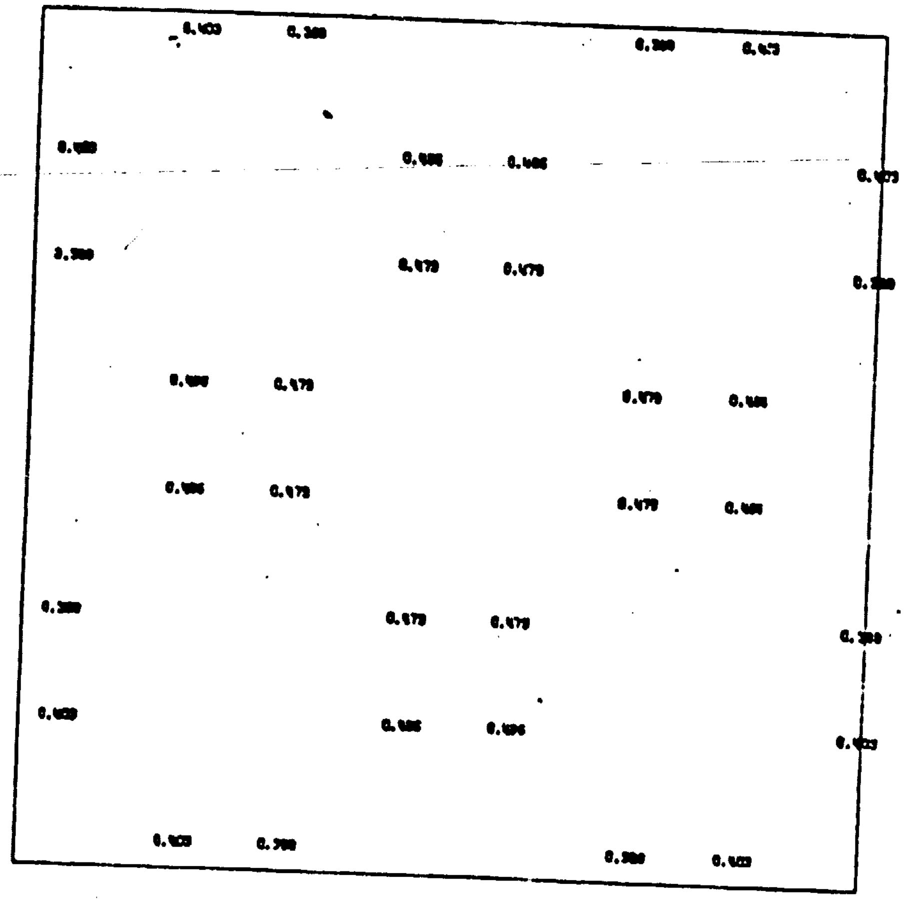

Fig. 90

12.2.8. The 3-D Air Inlet

/175

This is an industrial application. Figure 84 shows a detailing of the TETRAHEDRONIZATION (see J.G. NAVES (52)) near the air inlet in a vertical plane, whereas on figure 91 there is shown the geometry of the air inlet together with one part of the tetrahedronization (fronts of the tetrahedrons attached to the air inlet) used for a piece-wise linear approximation of the potential.

The external and internal domains of the air inlet are made up of 25664 tetrahedrons corresponding to 5732 Nodes. To give an idea of the complexity of the problem, one may observe that the Cholevski matrix $L(A=LL^t)$ (of the discrete Dirichlet operator) is made up of about 2 million coefficients and that its factorization requires 15 mn of process time.

REGULATION has been used to treat the condition of entropy.

The computation test case (M_∞ = .8 ; M_{motor} = .55 ; INC = 6°, DERAP = 0°) has required 40 iterations corresponding to 60 mn of process time.

Figure 92 gives the Machs internal and external surface distribution on the tetrahedrons ADJACENT (in the direction of one front) at the air inlet and shows the narrow supersonic band on the upper external part of the air inlet.

The long computer usage time, due to inputs-outputs of the factorized matrix L, is the reason for the incomplete numerical factorization tests $\tilde{L}$ presented in paragraph 12.4.

12.3.0. Characteristics of an Incompressible Viscous Calculation

/178

The Inputs

In the velocity-pressure formulation, a Navier-Stokes calculation required of boundary conditions on $\vec{u}$ and sometimes on p. Three situ tions are encountered in the applications.

1. Dirichlet conditions on the entire boundary Γ, $\vec{u}|_\Gamma = \vec{z}$
2. Neumann conditions on one part Γ_s of Γ, $\frac{\partial \vec{u}}{\partial n}|_{\Gamma_s} = 0$ + Dirichelt condition on the pressure $p|_{\Gamma_s} = q$
3. Mixed conditions on the components of velocity : $u_i|_{\Gamma_s} = z_i$; $\frac{\partial u_j}{\partial n}|_{\Gamma_s} = 0 \; j \neq i$

but such that $\int_\Gamma \vec{u}\cdot\vec{n}\, d\Gamma = 0$, constraint required by the condition of $\vec{\nabla}\cdot\vec{u} = 0$ in Ω. compressibility.

As the equations are without dimensions $|\vec{u}_\infty| = 1$, an external calculation around an obstacle (airfoil section - air inlet) requires the assumption of an incidence and of the Reynolds number $Re = \frac{1}{\nu}$, with ν fluid viscosity.

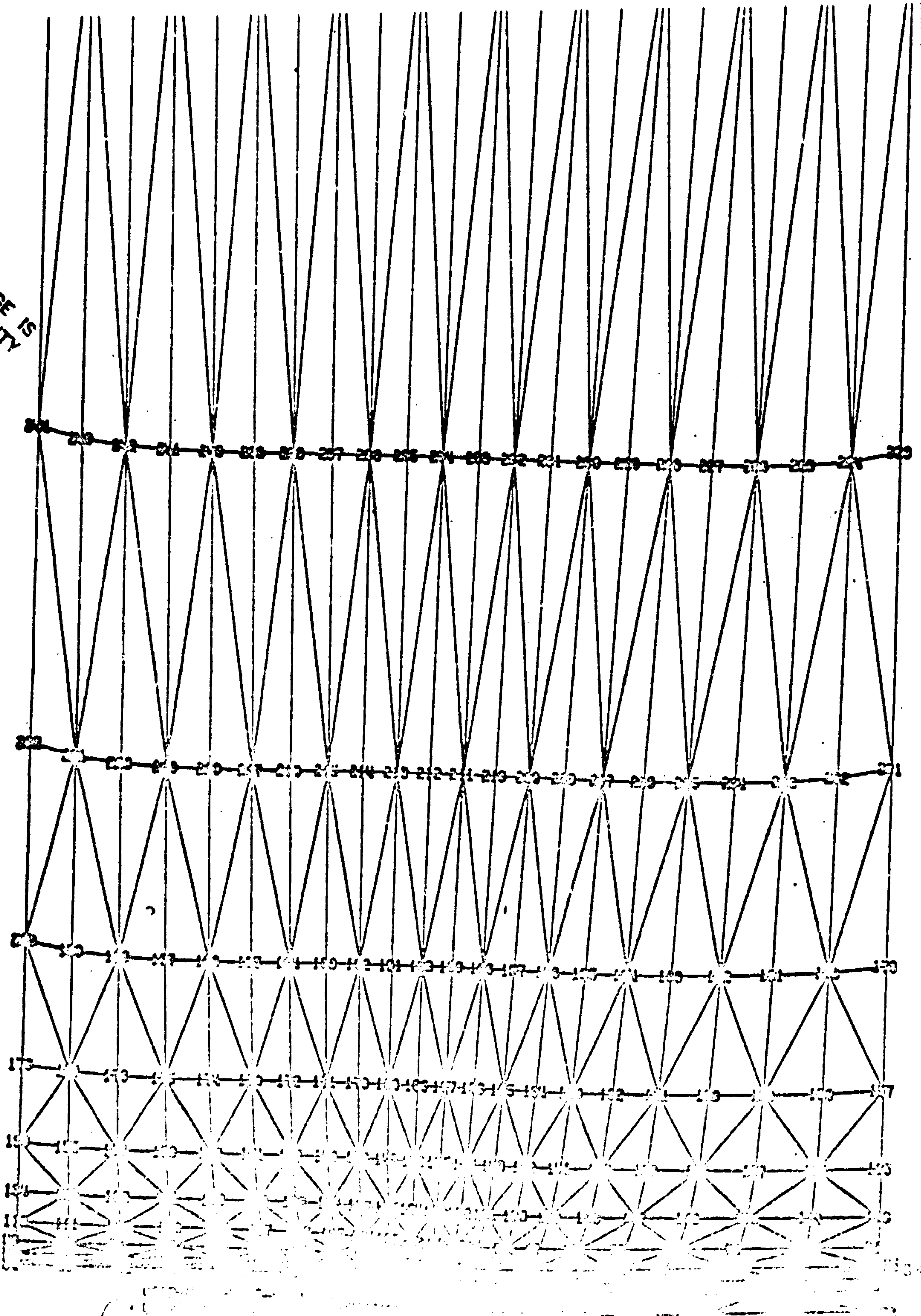

$M_\infty = .8 \quad M_M = .55 \quad \alpha = 6°$

9732
25664 elements
70954 coefficients
1854432 Cholesky coefficients

AIR INLET

60mn CPU (IBM 370-168)

SUPERSONIC ZONE

/117

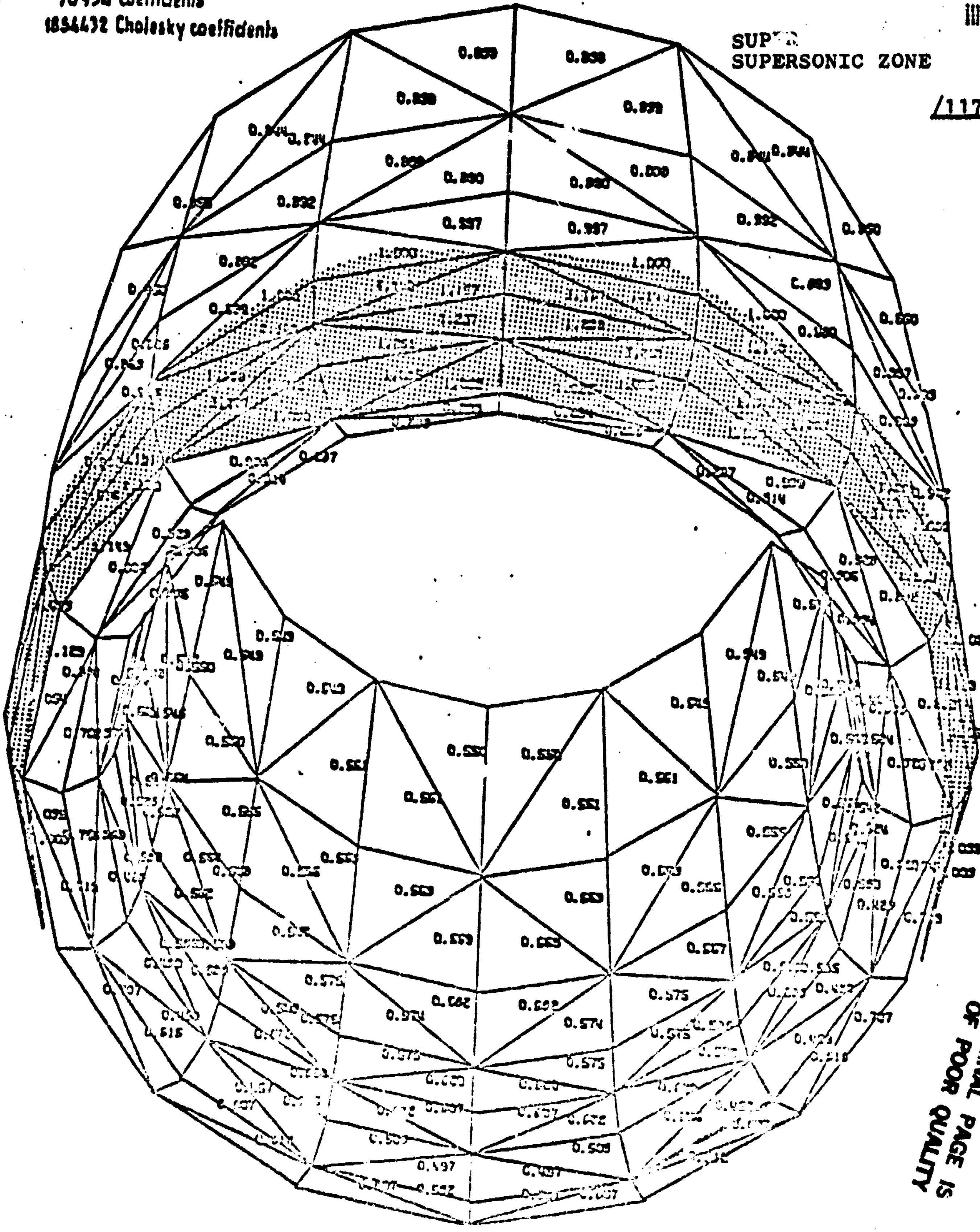

The Reynolds is reduced to a characteristic lenght L, which in the example shall always be the unit (cavity 1 x 1, diameter circle d=1 ; chord profile $\ell=1$, air inlet deviation h=1).

As the velocity and pressure approximations may vary (figure 93)
(1) pressure P1 - velocity P1
(2) pressure P1 - velocity P1 SIO P2
(3) pressure P1 - velocity P2

one computation requires the simultaneous presence of two card indices in the computer corresponding to two triangulations $(\mathcal{T}_h, \tilde{\mathcal{T}}_{h/2})$ for example. The discrete Dirichlet operator A is therefore constructed twice, depending on whether it is applied to the pressure $(\mathcal{T}_h)$ or to the velocity $(\tilde{\mathcal{T}}_{h/2})$. Furthermore, it may be observed, in the unsteady case, that it depends on the time step Δt and on the Reynolds number Re, since in this case the metric of the generalized Stokes algorithm is expressed

$$(\psi, A_k^{\nu}\phi) = \psi^t(kId-\nu A)\phi \quad (339)$$ /179

The two triangulations $\mathcal{T}_h$ and $\tilde{\mathcal{T}}_{h/2}$ are therefore numbered twice by the Cuthill-MacKee algorithm in order to obtain band widths m_1 and m_2 at minimum

The Outputs

The (velocity-pressure) formulation permits direct acces to the fields of velocities (1) and pressures (2) and to the vorticity intensity (3) $\vec{\nabla}\wedge\vec{u}$ constant on each element if $\vec{u}$ is P1, piece-wise linear when $\vec{u}$ is P2. The streamlines (4) are obtained by solving a Dirichlet problem (340) at a given field of velocity

$$\begin{aligned} -\Delta\psi &= \vec{\nabla}\wedge\vec{u} \quad (\Omega) \\ \psi|_{\Gamma} &= g \quad (\Gamma) \end{aligned} \quad (340)$$

The visualizations of magnitudes (1) (2) (3) (4) in the form of plottings at various time cycles Δt make it possible to follow the evolution of the flow in time (origine of eddies, appearance of spearated zone, alternating emission of eddies in the fluid, corresponding pressure fluctuation on the bodies).

The plotting of the iso-streamlines, the iso-pressures and the iso-vorticities is ensured by the TRACO modulus (refer to MARROCCO - INTERLIB (42)).

As the values ψ_{MIN} and ψ_{MAX} are determined after solving (340), N desired values of $(\psi_{D_i}$ i=1,N, with possible cubical concentrations on particular $(\psi_{D*} = 0)$ values ... (change of sign marking the eddies in the fluid) are marked geometrically (x,y) on the bars of triangulations $\mathcal{T}_h$ $\tilde{\mathcal{T}}_{h/2}$, with a linear connection from one bar to another on each element.

The convergence of the schemes of approximation is verified during N control iterations by plotting

- the evolution of criterion $(C^{\circ}, C^1, \ldots, C^N)$
- the evolution of gradient $(G^{\circ}, G^1, \ldots, G^N)$; $G^N = (g^N, g^N)^{1/2}$
- the values of constraint $\vec{\nabla} \cdot \vec{u} = 0$.

The control $\vec{w}$ is initializd following the applications either by the solution of the Stokes algorithm, or by the idealized fluid solution. In external flows, the Stokes solution proves to be a poor predictor. /180

In the unsteady case, the sequence of optimal control problems is initialized at the solution of the preceding time cycle, each problem requiring a few control iterations if the time steps are not too large.

Finally, industrial applications require numerically high laminar Reynolds (Re = 1000), a climb in Reynolds by a parabolic law of type $|\vec{u}_\infty| = \sqrt{\frac{11k-10}{100}}$; (k=1,10) shown on figure 94 makes it possible to simulate in a wind tunnel the transitory phase of determining the solution by Reynolds calculations.

For each value ν_i of the viscosity, the matrix $A_K^{\nu_i}$ is not reconstructed (which would be a penalty in computer time), but is substituted by an equivalent modification of the velocity boundary conditions expressed in figure 94.

Most of the following results are shown in R. GLOWINSKI-B. MANTEL - J. PERIAUX-O. PIRONNEAU (43), in IRIA/LABORIA-DRET (19), AMD/BA-DRET (44).

12.3.1. The 2-D Test Cavity

The Stokes flow in a cavity (1 x 1) was tested to verify the error estimates of schemes $O(h^\alpha)$ of BERCOVIER-PIRONNEAU (45) for three approximations (P1/P1) (P1/P1 ISO P2) (P1/P2) of the (pressure-velocity) formulation.

The characteristics of the 3 triangulations studied $\mathcal{T}_h^G$, $\mathcal{T}_h^M$, $\mathcal{T}_h^P$ corresponding respectively to the values $h_G = .125$, $h_M = .1$, $h_P = .5$ are defined in (341)

$$\mathcal{C}_h^G = \{145 \text{ nodes, } 256 \text{ éléments}\}$$
$$\mathcal{C}_h^M = \{221 \text{ nodes, } 400 \text{ éléments}\} \qquad (341)$$
$$\mathcal{C}_h^P = \{841 \text{ nodes, } 1600 \text{ éléments}\}$$

The calculation of α defining the convergence of the scheme is obtained to satisfy the constraint $\vec{\nabla}\cdot\vec{u} = 0$ evaluated numerically in (342) and (343).

$$\text{DIVGLO} = \sum_{T \in \mathcal{C}_h} \int_\Omega |\vec{\nabla}\cdot\vec{u}|^2 dx \qquad (342)$$ /181

$$\text{DIV MAX} = \sup_{T \in \mathcal{C}_h} (|\vec{\nabla}\cdot\vec{u}|_T) \qquad (343)$$

For each approximation, α is defined for the possible couples (G,M), (G,P), (M,P) by the formulas (344) (345) (346)

$$\alpha(G,M) = \frac{\text{Log} \dfrac{\text{DIVGLO (G)}}{\text{DIVGLO (M)}}}{\text{Log } 1.25} \qquad (344)$$

$$\alpha(G,P) = \frac{\text{Log} \dfrac{\text{DIVGLO (G)}}{\text{DIVGLO (P)}}}{\text{Log } 2.5} \qquad (345)$$

$$\alpha(M,P) = \frac{\text{Log} \dfrac{\text{DIVGLO (M)}}{\text{DIVGLO (P)}}}{\text{Log } 2.} \qquad (346)$$

For data C^1 on the edge of the cavity ($u = 16\, x^2(1-x)^2$, $v=0$), we have plotted on figures 95 and 96 a Log-Log scale, the slope of α of the straight line Log Divglo = α Log h. characterizing the scheme $O(h^\alpha)$ depending on the approximation chosen for the GLOWINSKI-PIRONNEAU Stokes algorithm and the optimal control Na r-Stokes method at Re = 100, after 30 control iterations. Sche $O(h)$ is verified approximately for the case P1/P1 ISO P2 and $O(h^2)$ for the case P1/P2. For more details, (46) may be consulted.

APPROXIMATION P1 / P1 iso P2

/182

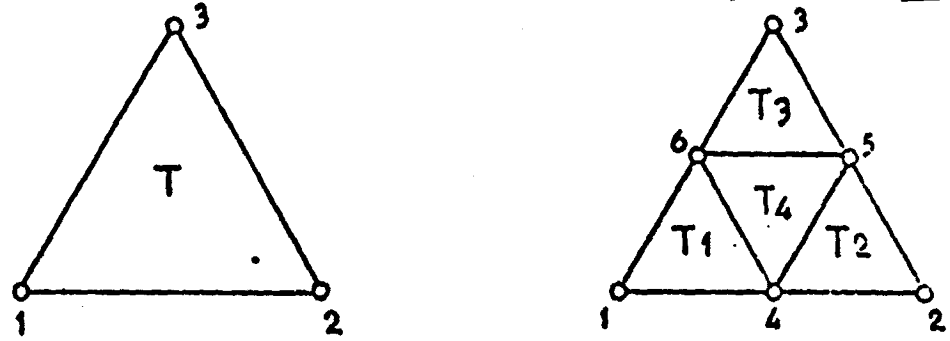

$\mathcal{C}_h$ PRESSURE P_1 $\qquad$ $\widetilde{\mathcal{C}}_{h/2}$ VELOCITY P_1

$$p = \sum_{i=1}^{3} \underline{p}_i L_i \qquad u = \sum_{i=1}^{3} \vec{\underline{u}}_i L_i$$

APPROXIMATION P1 / P2

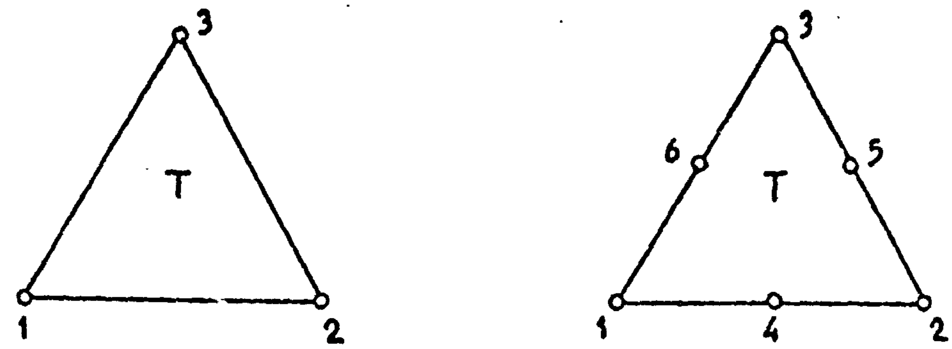

$\mathcal{C}_h$ PRESSURE P_1 $\qquad$ $\mathcal{C}_h$ VELOCITY P_2

$$p = \sum_{i=1}^{3} \underline{p}_i L_i \qquad \vec{u} = \sum_{j=1}^{6} \vec{\underline{u}}_j N_j(L_i)$$

Figure 93

— NAVIER-STOKES —

REYNOLDS CLIMB VIA BOUNDARY CONDITIONS

$$|\vec{U}_\infty| = \sqrt{\frac{11 * K - 10}{100}}$$

Re = 750

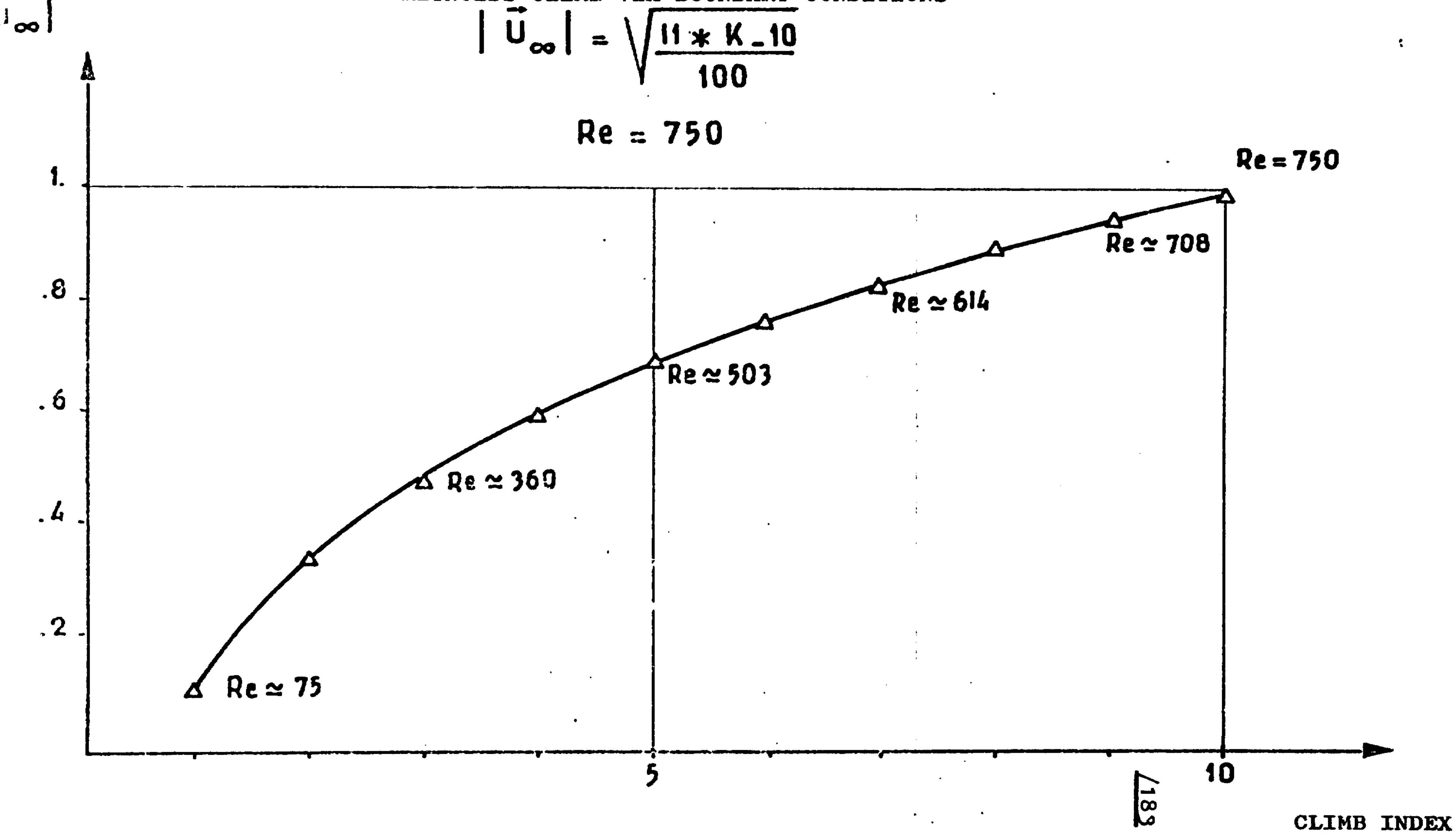

/183

STOKES

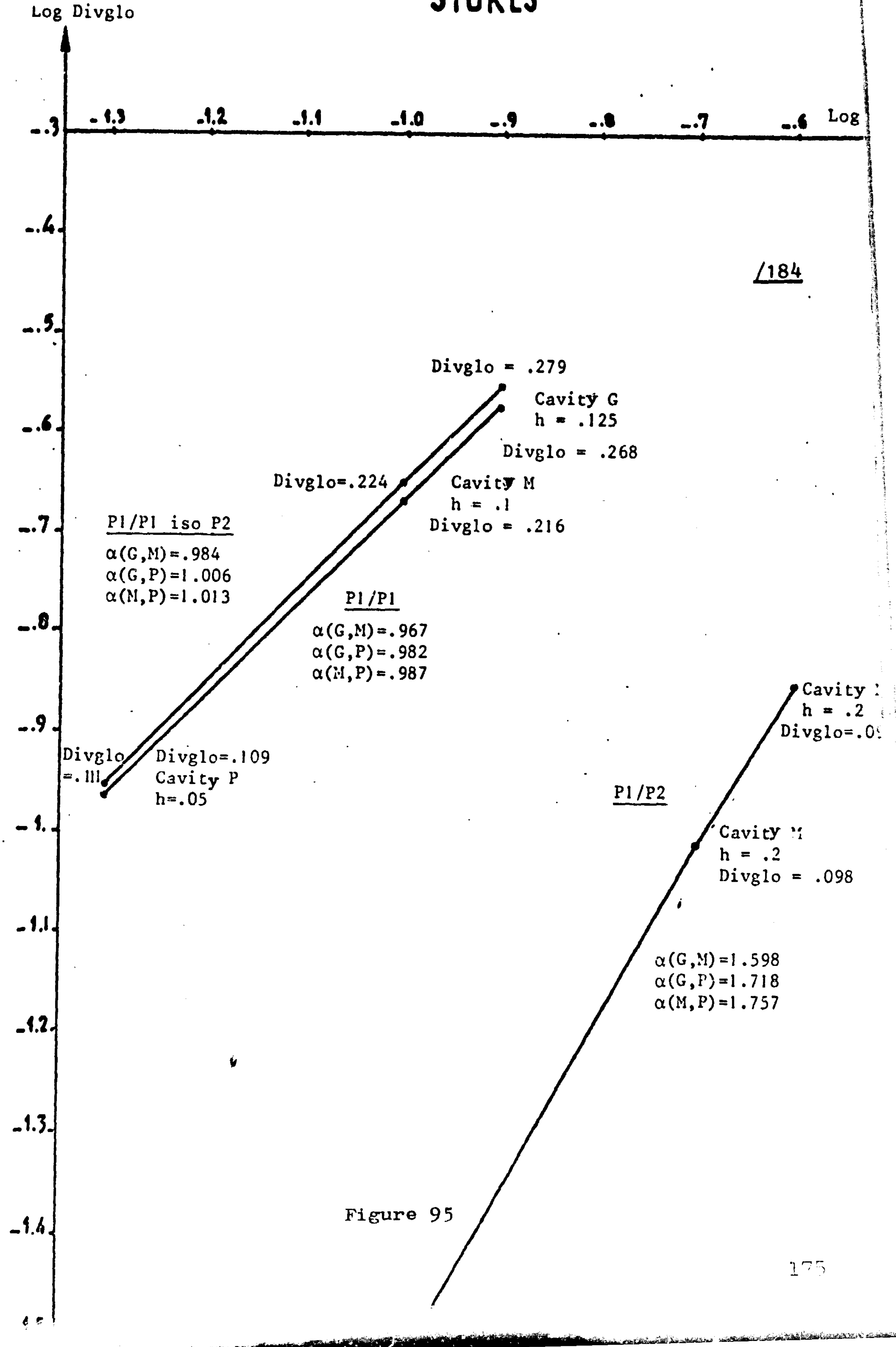

/184

Figure 95

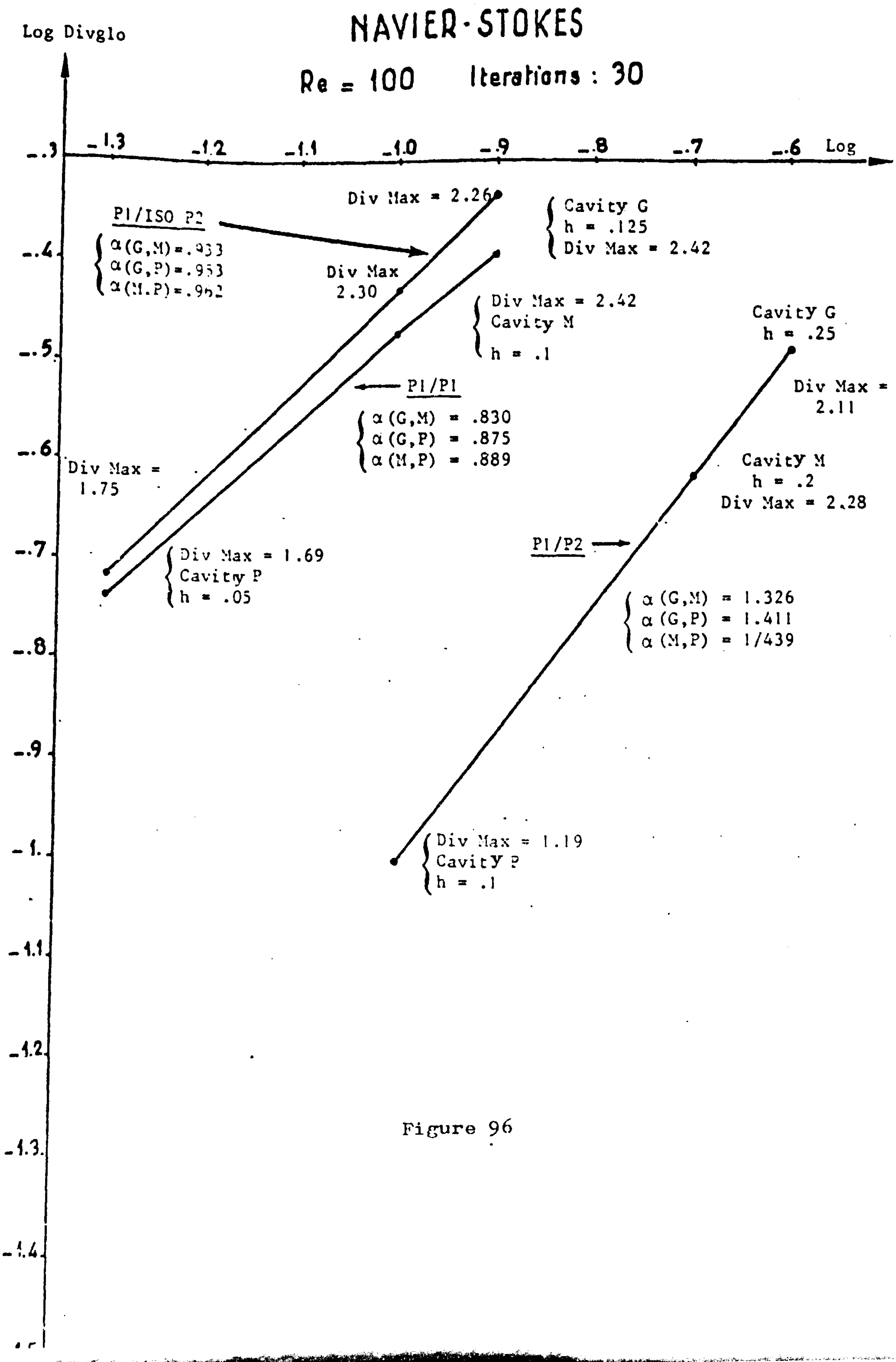
NAVIER-STOKES
Re = 100 Iterations : 30
Log Divglo
h
Log
-1.3
-1.2
-1.1
-1.0
-.9
-.8
-.7
-.6
-.3
-.4
-.5
-.6
-.7
-.8
-.9
-1.
-1.1
-1.2
-1.3
-1.4
Div Max = 2.26
Cavity G
h = .125
Div Max = 2.42
PI/ISO P2
α(G,M) = .933
α(G,P) = .953
α(M,P) = .962
Div Max
2.30
Div Max = 2.42
Cavity M
h = .1
Cavity G
h = .25
PI/PI
Div Max =
2.11
α (G,M) = .830
α (G,P) = .875
α (M,P) = .889
Div Max =
1.75
Cavity M
h = .2
Div Max = 2.28
Div Max = 1.69
Cavity P
h = .05
PI/P2
α (G,M) = 1.326
α (G,P) = 1.411
α (M,P) = 1/439
Div Max = 1.19
Cavity P
h = .1

Figure 96

12.3.2. The 2-D Conduit With Sudden Enlargment

The characteristics of triangulations $\mathcal{T}_h$ & $\tilde{\mathcal{T}}_{h/2}$, brought /186
about by MODULEF (35), are given on figure 97.

It may be observed that there is a concentration of elements in the recirculation zone. The calculation domain ($\delta x >> \delta y$), the boundary conditions ($u = z_1(y)$; $v=0$) and the Reynolds number are proposed by A.G. HUTTON (47). Two cases Re = 100, Re = 191 are obtained by making the unsteady code steady P1/P1 ISO P2 in 180 iterations corresponding to one time step Δt and requiring 3h. of process time.

Superposing the streamlines with those of theHUTTON code (figure 98) shows a good agreement along the length of the blister (if $\delta \ell = |x$ enlargement $- x$ point of connection and h designates the height of the enlargement $\delta \ell = 6 \times h$ à Re = 100, $\delta \ell = 8 \times h$ Re = 191).

The appearance and the developement of the separated zone throug through various time cycles Δt at Reynolds 100 are shown on figure

On figures 99 through 102, the field of pressures and streamlines of the flow at the two Reynolds numbers under consideration may be compared.

12.3.3. The Alternating Eddies Behind the Circle /193

The The triangulation $\mathcal{T}_h$(resp. $\mathcal{T}_{h/2}$) is composed of 144 elements and 84 nodes (resp. 576 triangles and 312 nodes), the solution $(\vec{u}_h, p_h)$ looked for is composed f 708 degrees of freedom.

At Reynolds 50, the Navier-Stokes solution is steady, as the streamlines show on figure 103, after 40 time cycles. Nevertheless, with this Reynolds, the Stokes solution is <u>already</u> a poor predictor on figure 104 at time cycle 1.

At Reynolds numbers above 80, the steady solutions of Navier-Stokes equations being unstable, we consider the unsteady case, as the flow is initialized at t=0 by the incompressible idealized flow. Since the approximation keeps the symmetry and the triangulations $\mathcal{T}_h$, $\mathcal{T}_{h/2}$ are also symmetrical, the solution $(\vec{u}_h^{10}, p_h^{10})$ as shown on figure 105 (a) corresponding to K=10 ($t = 10\,\Delta t$) is symmetrical and must therefore be perturbed at a point of fluid not found on the axis. Accordingly, we may observe behind the circle the formation of a Karman path. The results presented on figure 105 (a)-(f) correspond to Reynolds Re = 200 and are obtained by an implicit Crank-Nicholson type scheme with a time step $\Delta t = .1$. The process computation time is about 1 hour. We have verified the good agreement of the results obtained by FORTIN-THMASSET (48) by using a different unconform mixed finite elements method.

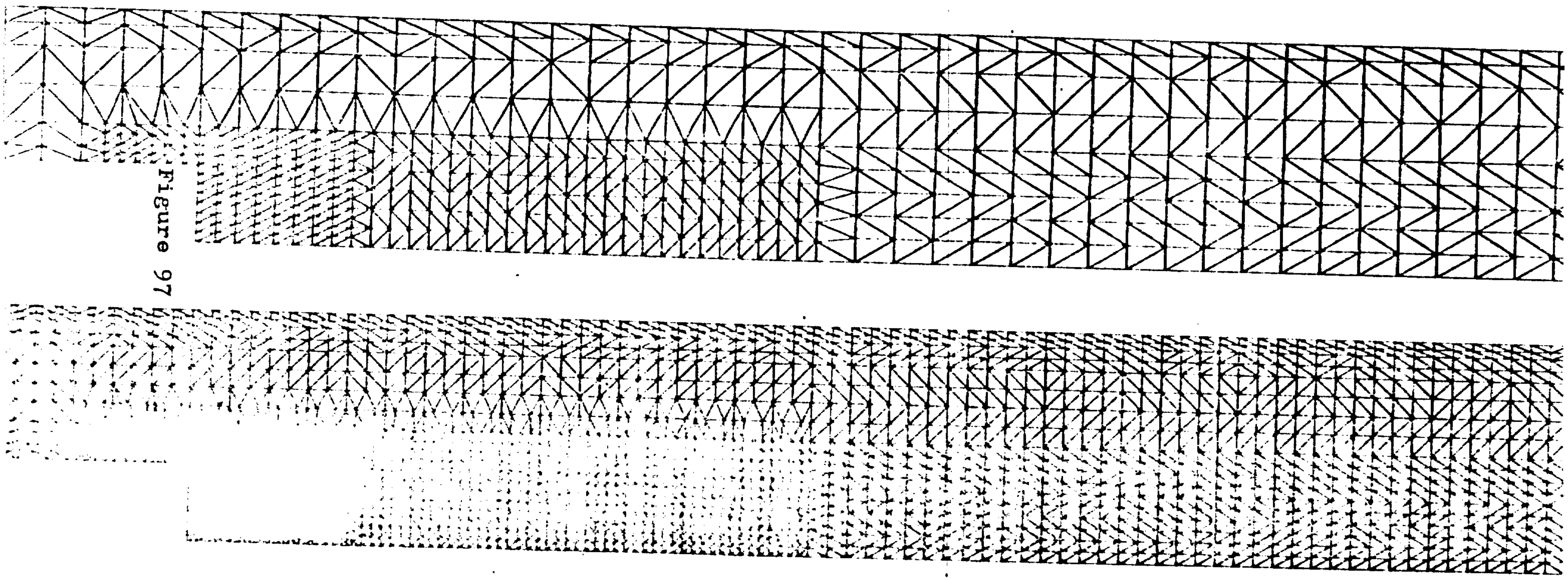

Figure 97

/187

TRIANGULATIONS $\mathcal{C}_h$ et $\tilde{\mathcal{C}}_h$

	$\mathcal{C}_h$	$\tilde{\mathcal{C}}_h$
NODES :	619	2346
ELEMENTS :	1109	4436
COEF. CHOL :	21654	154971

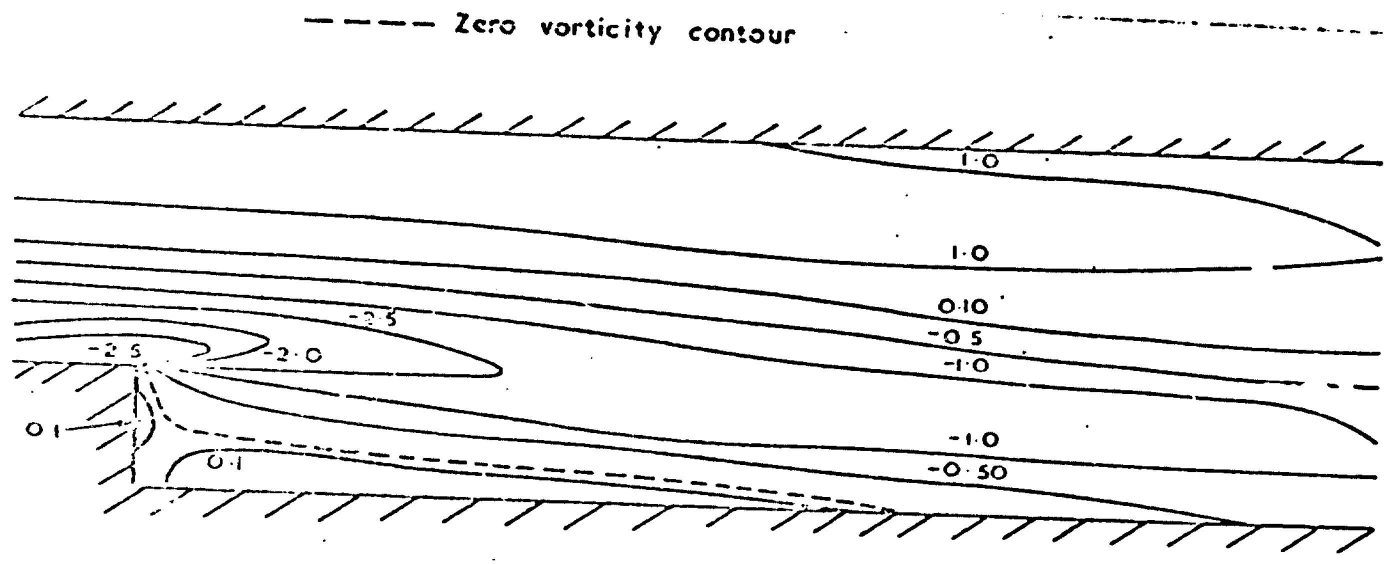

FIG. 7. Vorticity Contours Re = 100.

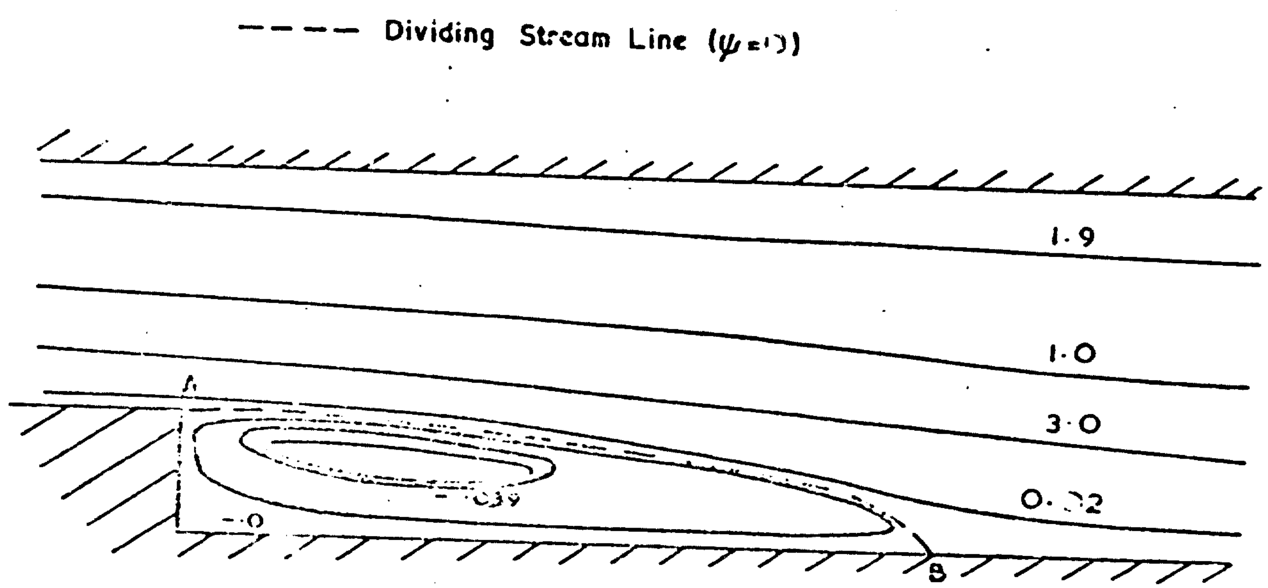

FIG. 6. Stream Function Contours Re = 100

Fig. 6

VELOCITIES STREAMLINES

/189

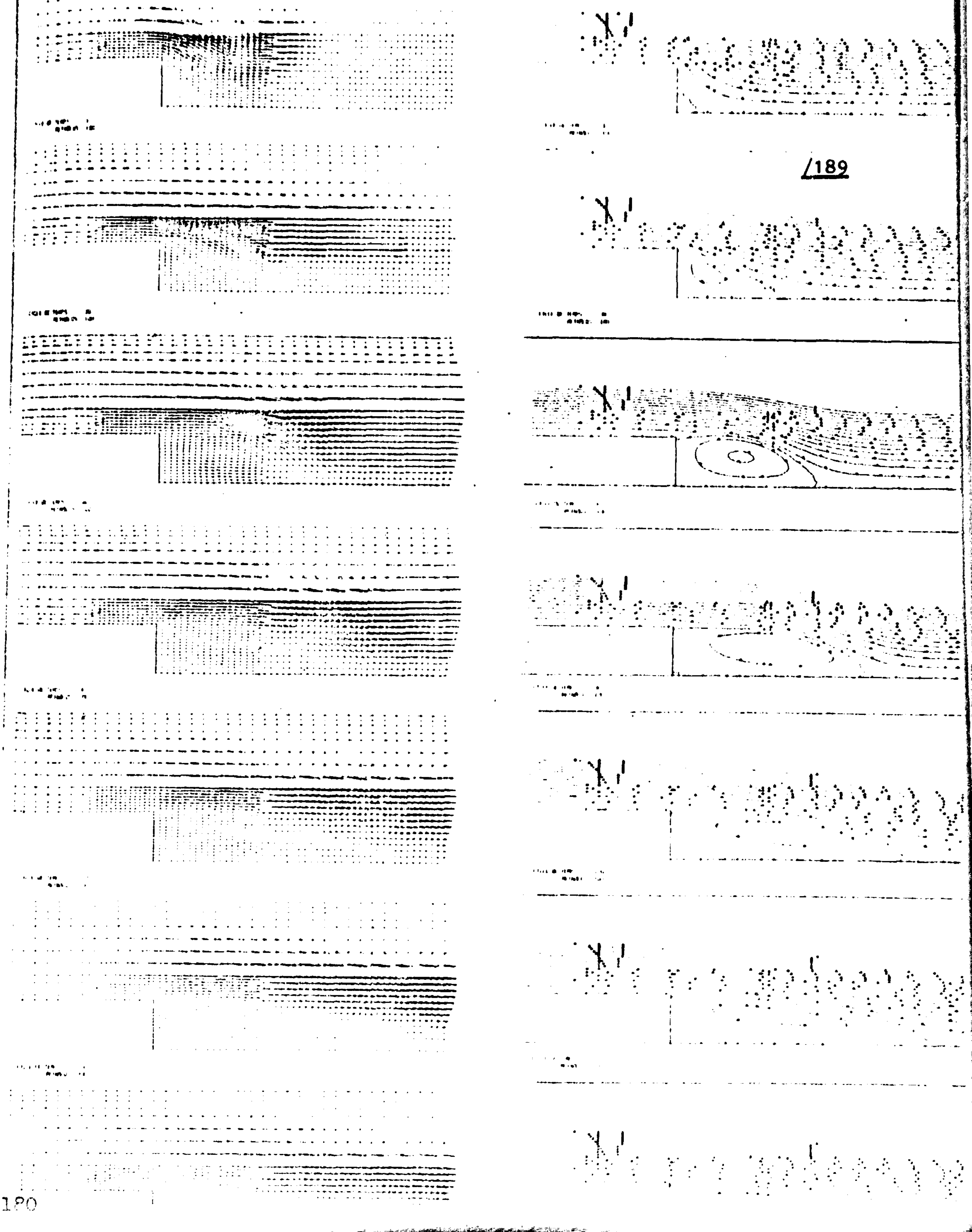

Time cycle

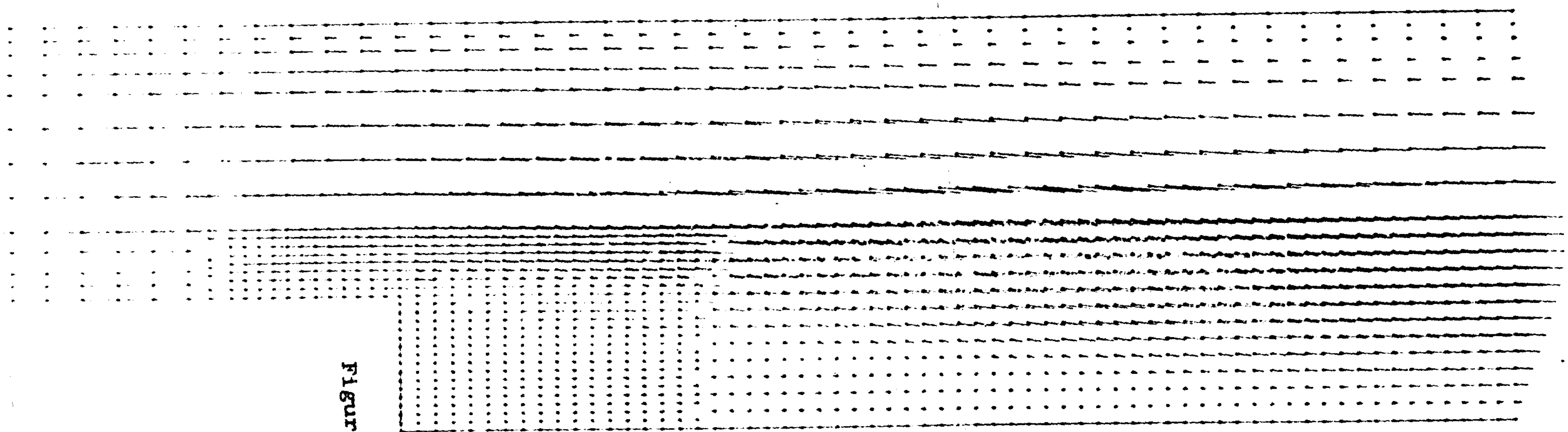

Figure 100

NCIDENCE DEGREE 0.

Time cycle
180
REYNOLDS 191.

I - FIELDS OF VELOCITIES IN A CONDUIT WITH SUDDEN ENLARGEMENT

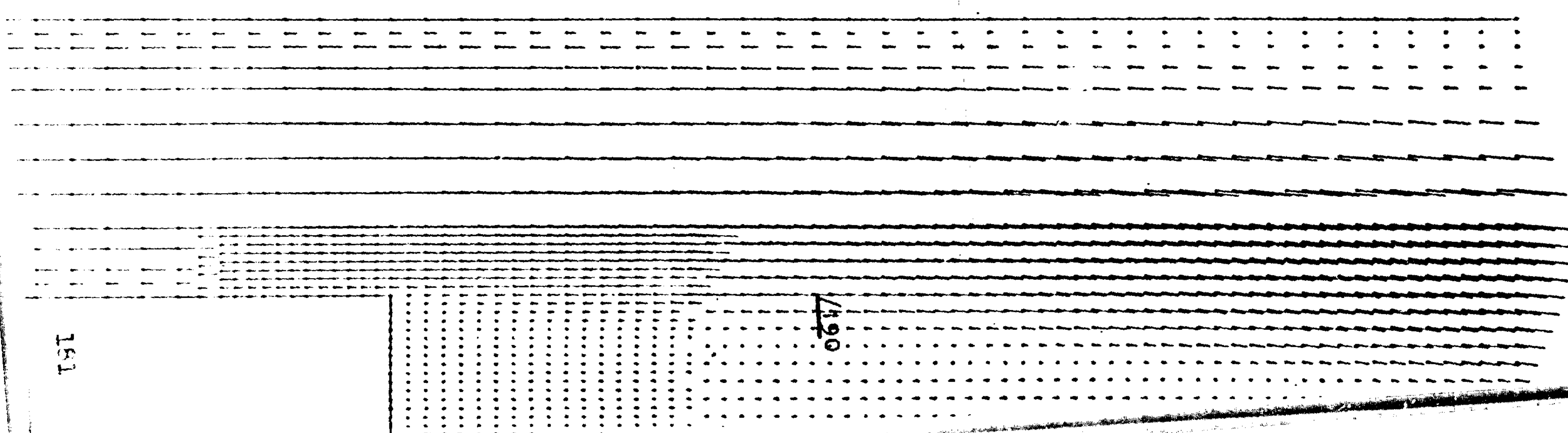

/190

180 Time cycle
100. Reynolds

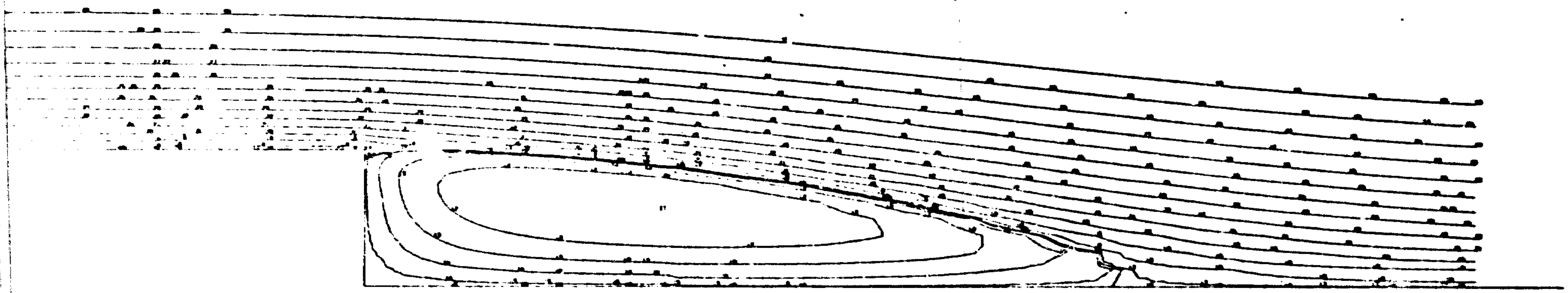

0. Incidence degree

II - STREAMLINES

180 Time cycle
191. Reynolds

Fig.101

P1/P1 ISO P2

180 Time cycle
100. Reynolds

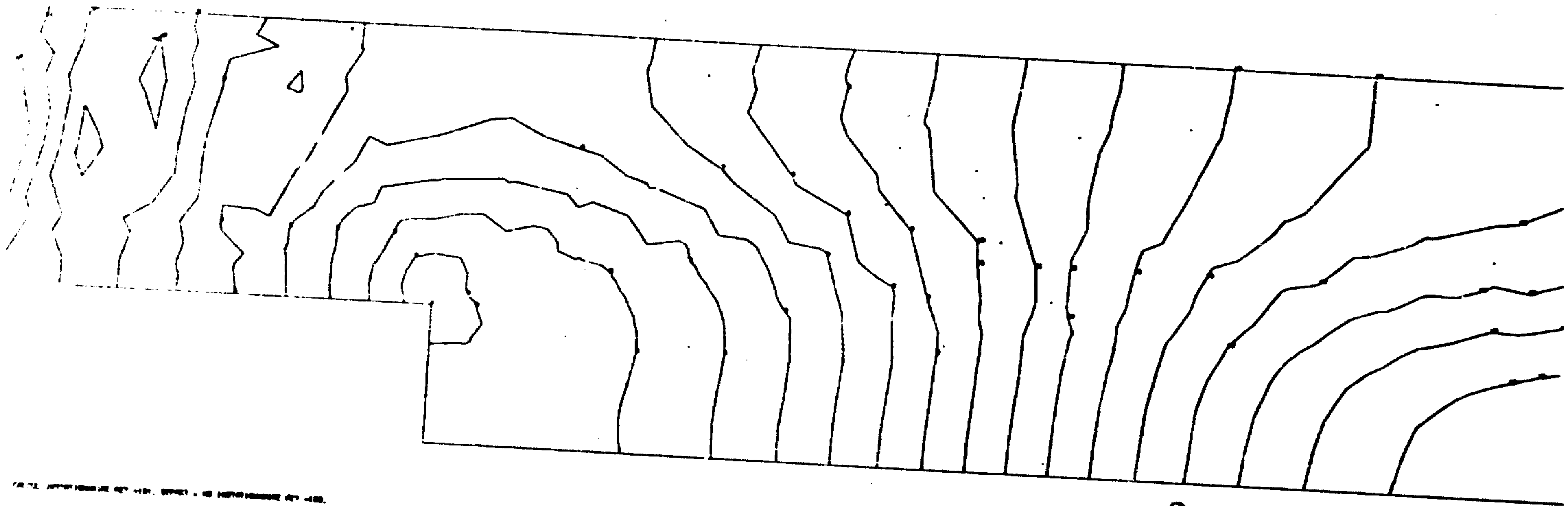

0. INCIDENCE DEGREE

P1/P1 ISO P2

180 Time cycle
191. Reynolds

III-ISO-PRESSURES

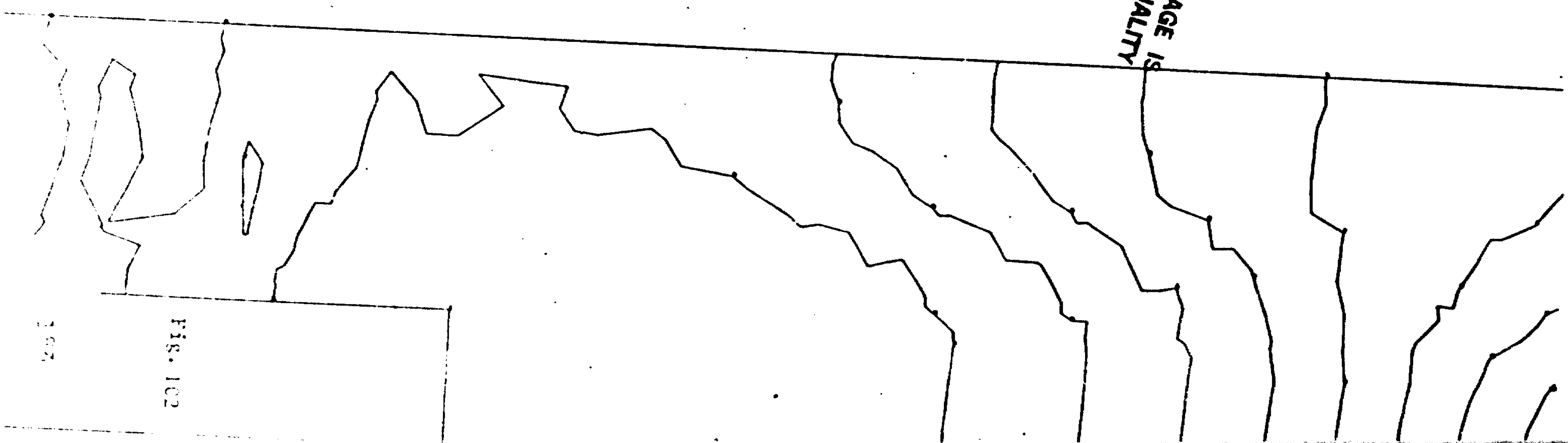

Fig. 102

Figures 106-107-108-109-110 show a flow Re = 200, with Nemann condition behind the circle, which is <u>inadequately</u> perturbed to provoke alternating eddies in 50 time cycles. /193

12.3.4. Separated Flow At Extrados of Airfoil Section In Incidence /202

We are taking into consideration an unsteady flow around an airfoil with Reynolds 200, placed at 30° incidence.

The calculation domain is substituted by a triangulated bound domain by MODULEF ($\mathcal{T}_h$: 412 triangles, 221 nodes ; $\tilde{\mathcal{T}}_{h/2}$: 1648 triangles, 854 nodes). The solution looked for $(\vec{u}_h, p)$ is composed of 1929 degrees of freedom. The quantification in time is accomplished by a completely implicit Gear scheme with two steps, with one time step $\Delta t = .1$. The predictor $\vec{u}_h^{\,0}$ is the solution of the incompressible idealized fluid.

80 time cycles (corresponding to a period of 8 seconds) have required 90 mn of process time and a core space of 1500 k octets. The number of control iterations per cycle of time is 4.

The velocity distribution and streamlines on figures 111 (a)-(f) and 112 (a)-(f) show the formation of eddie extrados of the airfoil which alternately expand and escape in the fluid to be finally absorbed by the downstream boundary conditions.

12.3.5.1. The Air Inlet In Incidence /207

The mixed flow around inside an idealized air inlet with high incidence is a typical example of a separated viscous flow. In a first phase, the air inlet is placed at an incidence of 30° as is shown on figure 113.

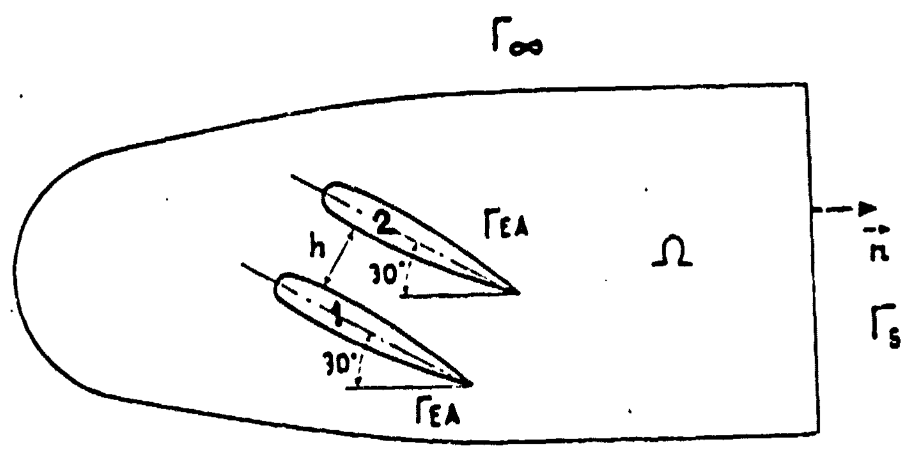

Figure 113

Steady NAVIER - STOKES- FLOW - simulation past a cylinder

CYCLE DE TEMPS 41
REYNOLDS 50.

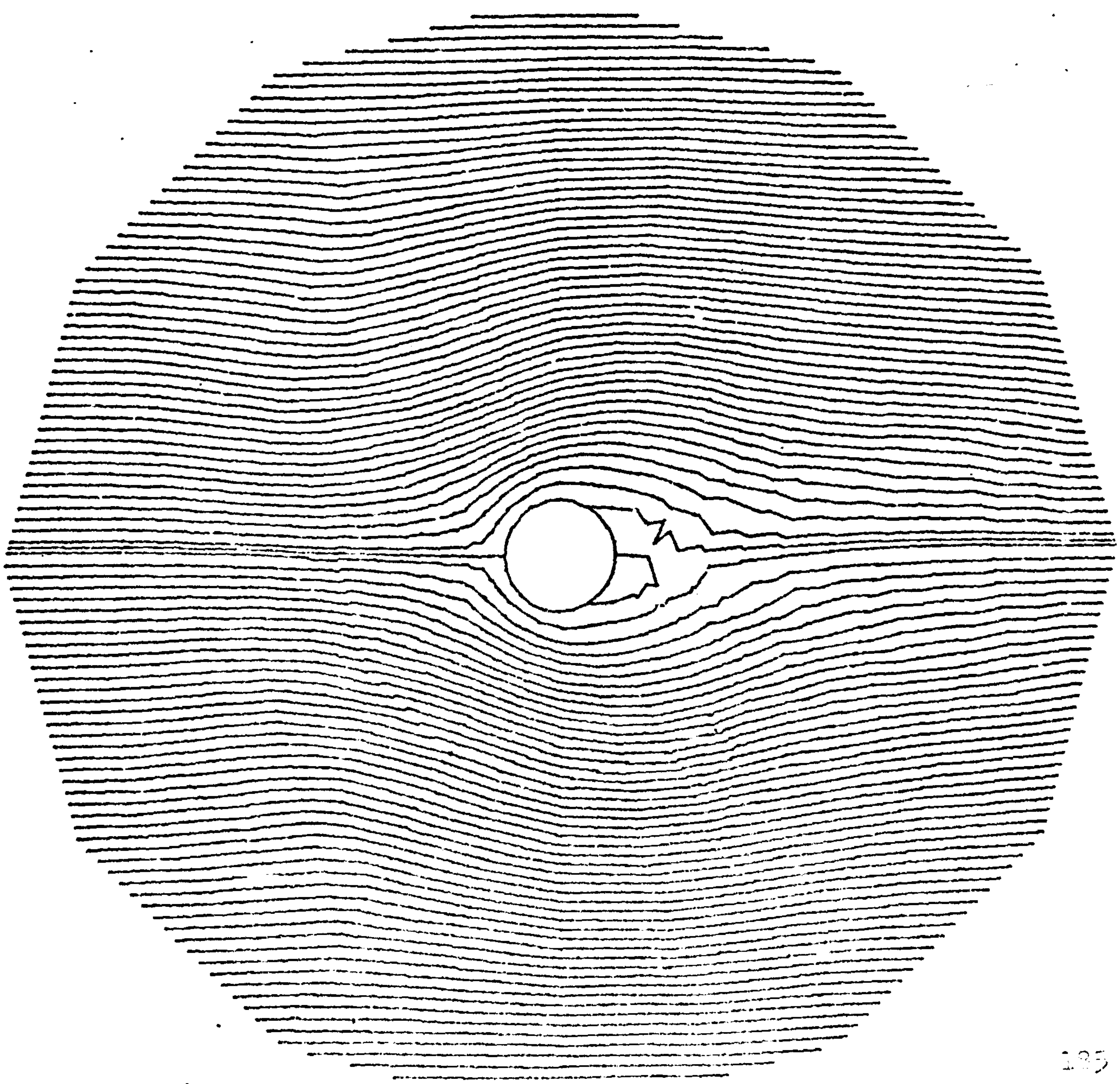

C-3

Steady NAVIER - STOKES - FLOW simulation past a cylinder Initial guess : STOKES solution

FLOW AROUND A CYLINDER

a) Time cycle 10
200.

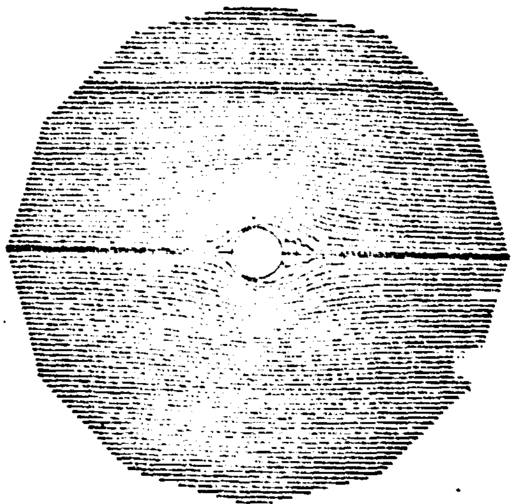

b) Time Cycle 20
REYNOLDS 200.

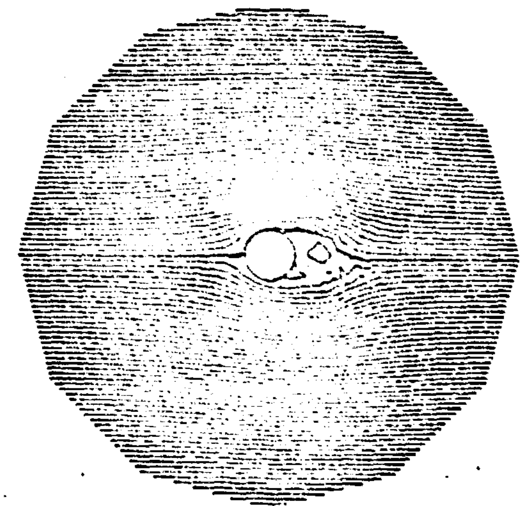

c) Time cycle 30
REYNOLDS 200.

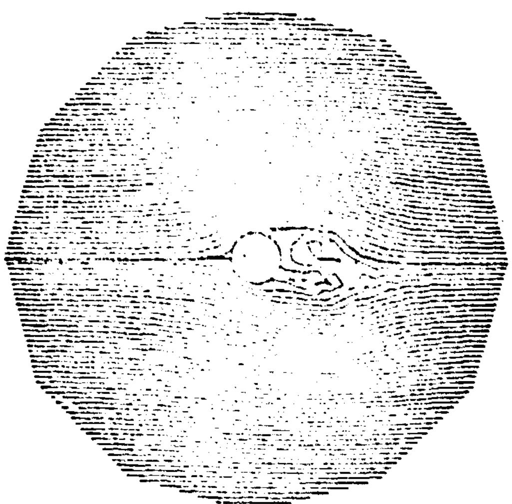

d) Time cycle 40
REYNOLDS 200.

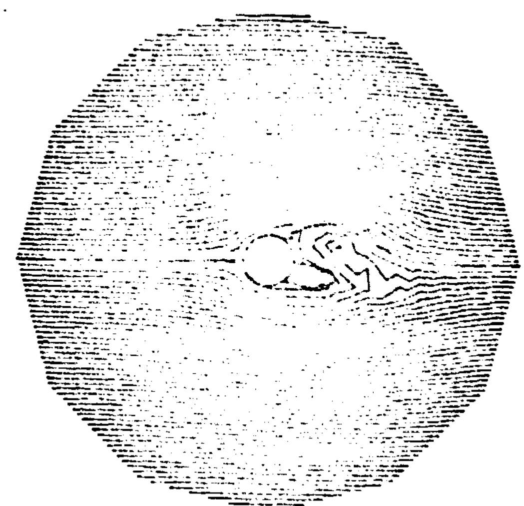

e) Time cycle 50
REYNOLDS 200.

f) Time cycle 60
REYNOLDS 200.

/197

Origin of eddies behind a cylinder

INCIDENCE DEGREE 0.
P1/P1 ISO P2
TIME CYCLE 20
REYNOLDS 200.

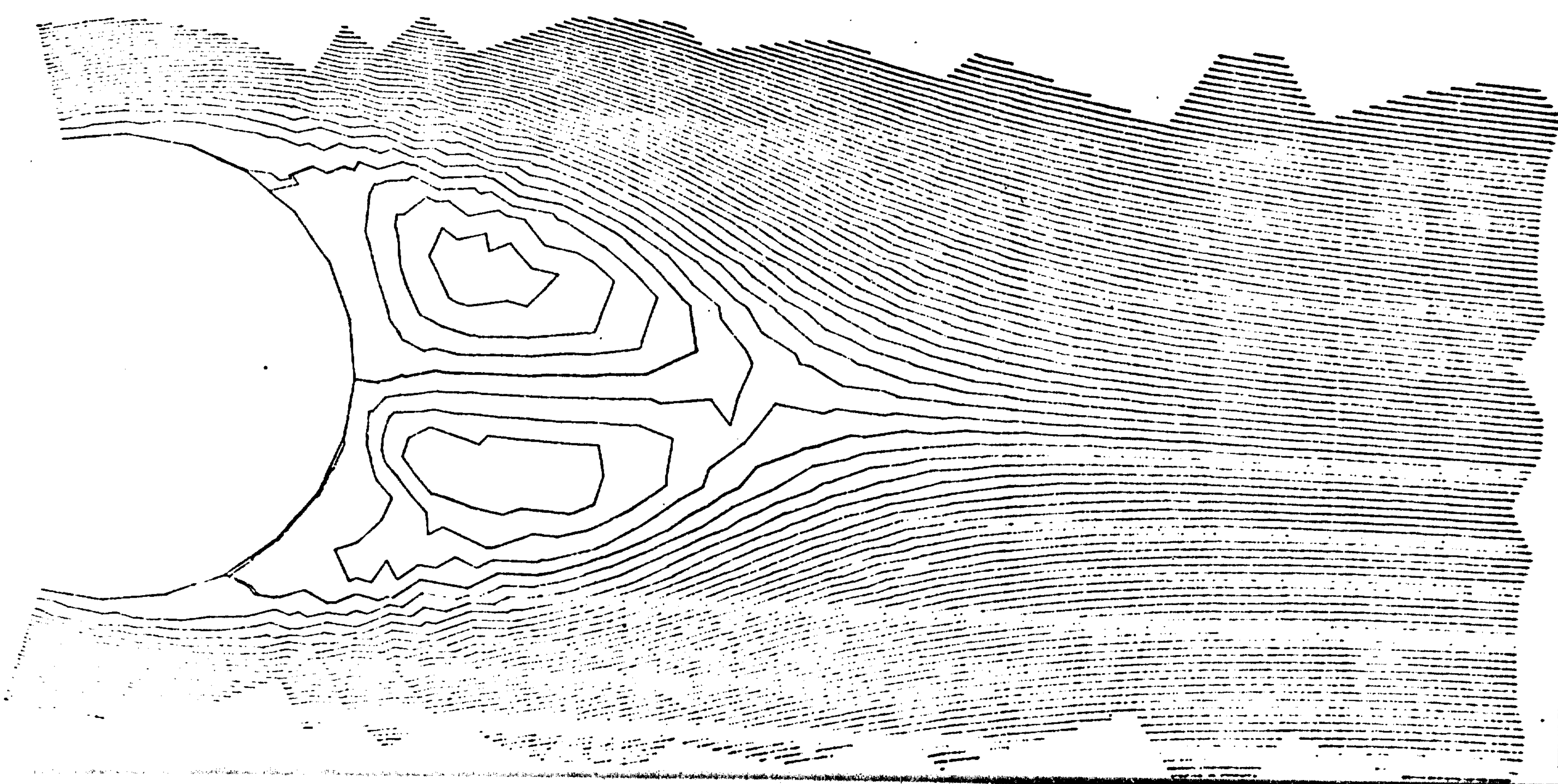

Fig. 106

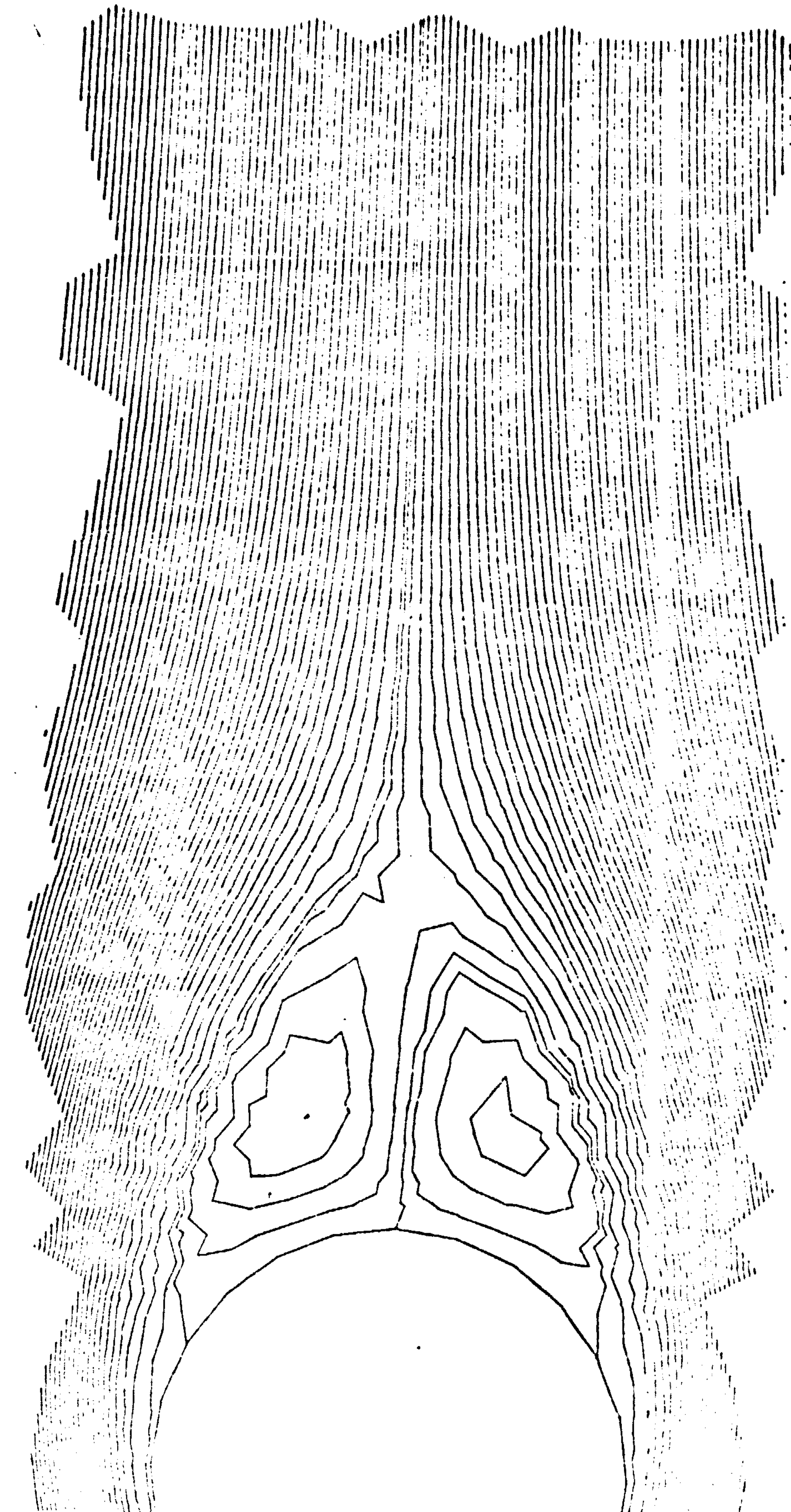

Origin of eddies behind a cylinder

Fig. 107

Origin of eddies behind a cyclinder

0. INCIDENCE DEGREE

P1/P1 ISO P2

24 TIME CYCLE

200. REYNOLDS

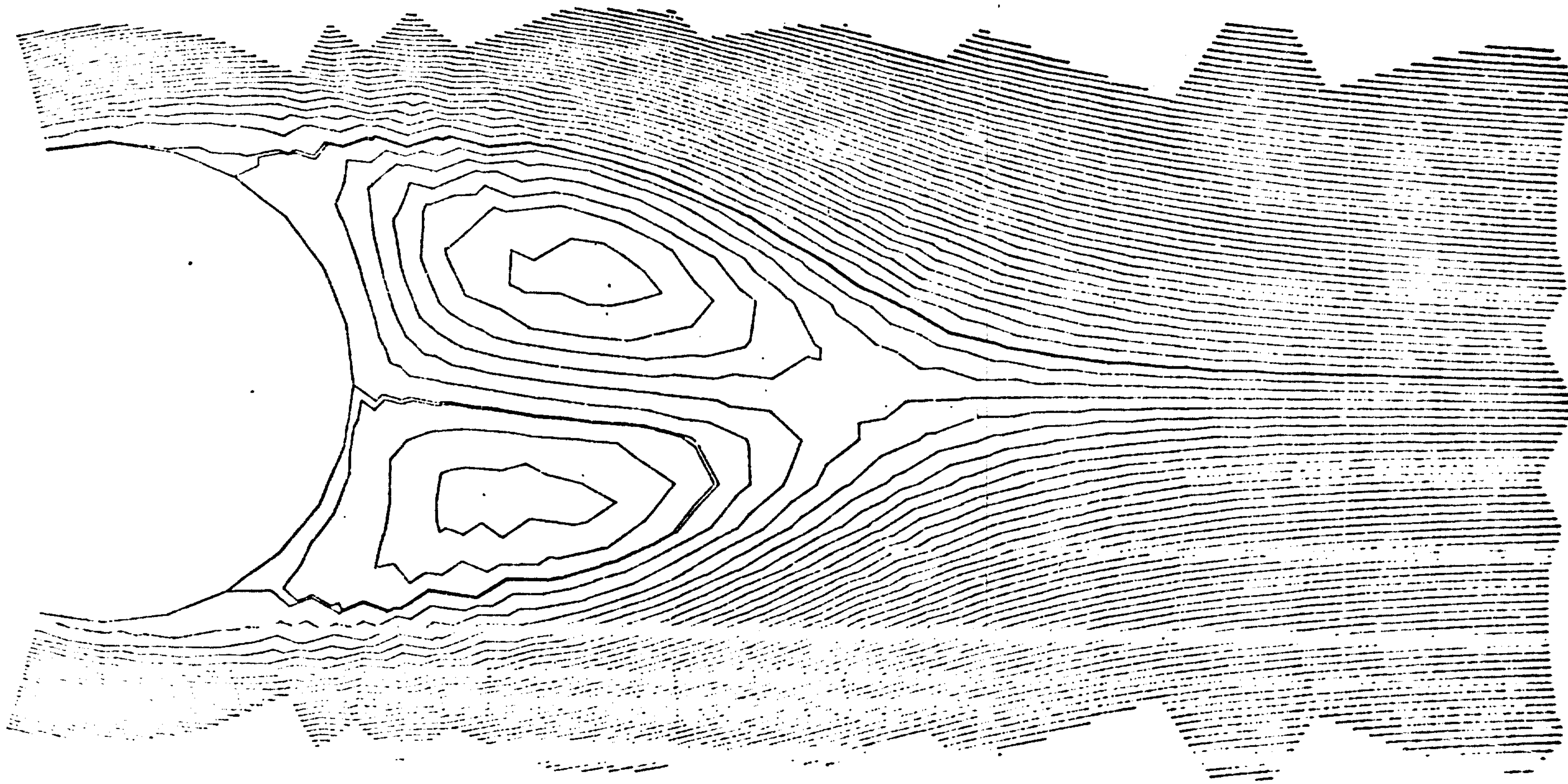

Fig. 10

50 TIME CYCLE
200. REYNOLDS

/200

P1 / P1 iso P2

PRESSURES Neuman Avel

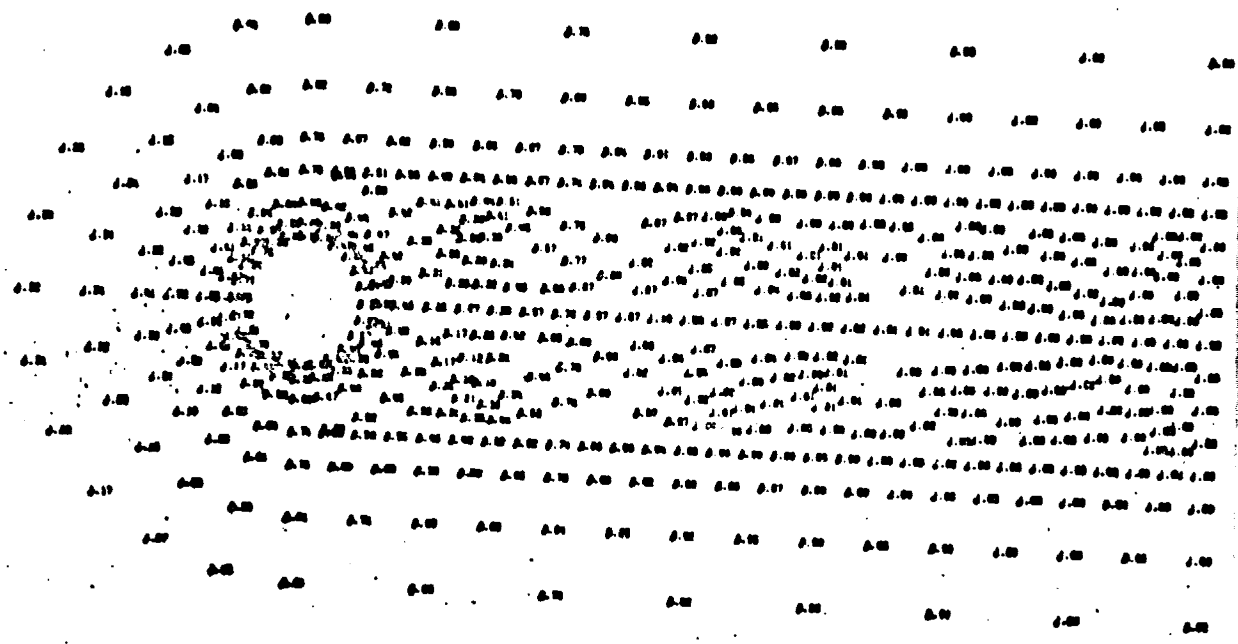

P1 / P1 iso P2

ISO-PRESSURES Neuman Downstream

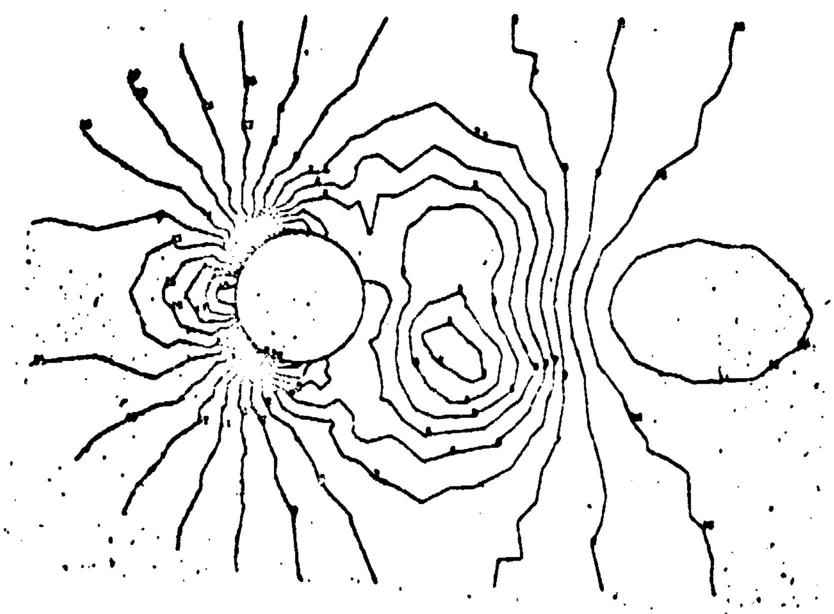

Fig. 109

TIME CYCLE 50
REYNOLDS 200

VELOCITY FIELDS Neuman Downstream

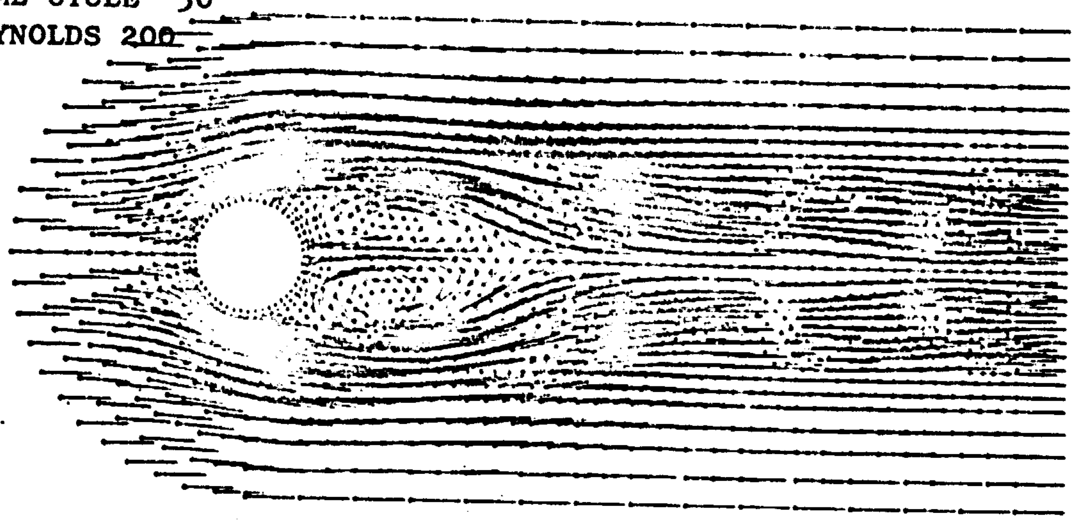

STREAMLINES Neuman Downstream

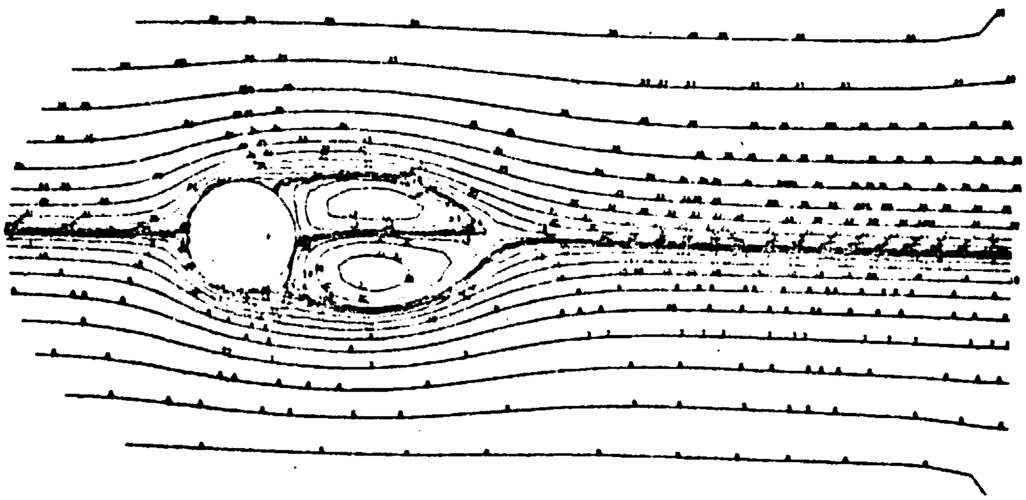

Iso-Vorticities Neuman Downstream

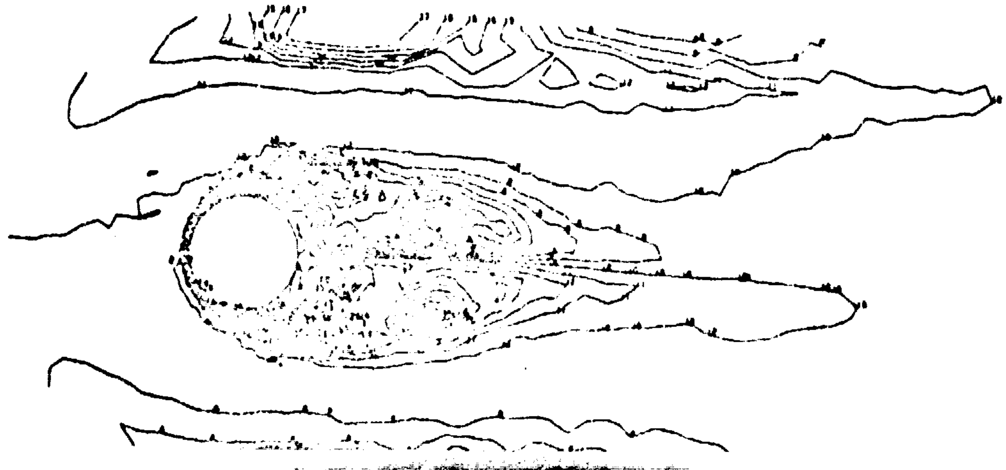

Fig. 110

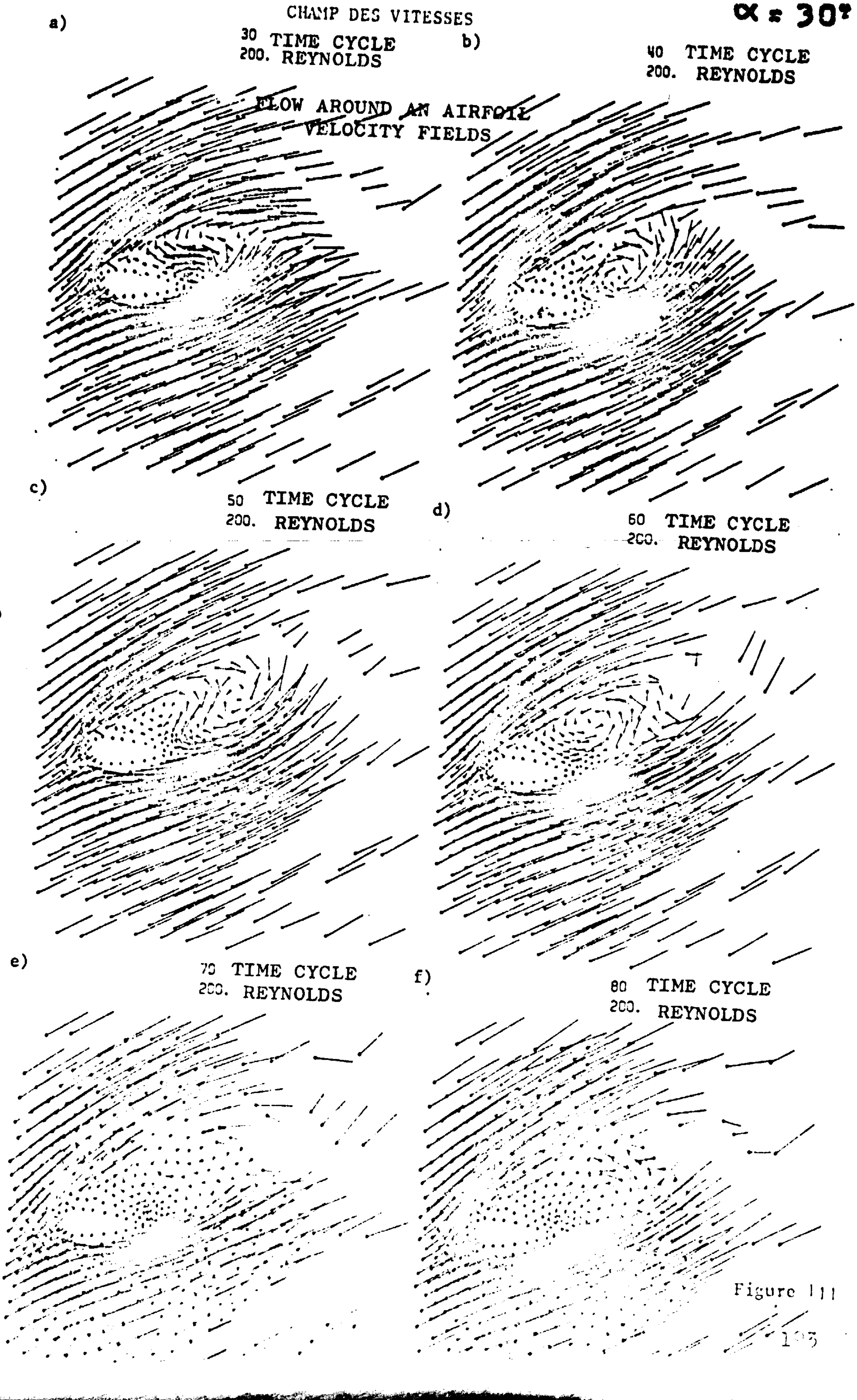
CHAMP DES VITESSES
α = 30°
FLOW AROUND AN AIRFOIL
VELOCITY FIELDS
a)
30 TIME CYCLE
200. REYNOLDS
b)
40 TIME CYCLE
200. REYNOLDS
c)
50 TIME CYCLE
200. REYNOLDS
d)
60 TIME CYCLE
200. REYNOLDS
e)
70 TIME CYCLE
200. REYNOLDS
f)
80 TIME CYCLE
200. REYNOLDS

Figure 111

a)

VISCOUS SEPARATED FLOW AROUND AN AIRFOIL

Streamlines _ Gear scheme , $\Delta t = .1$ _ Incidence 30°

P1/P1 ISO P2

30 TIME CYCLE

200. REYNOLDS

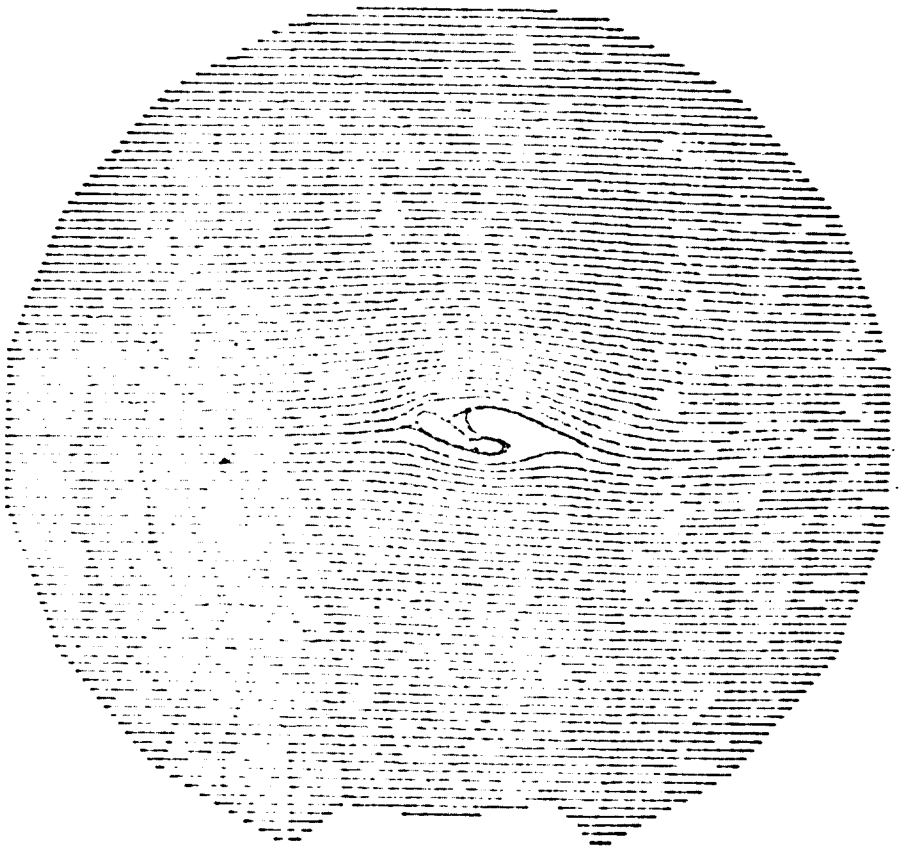

b)

VISCOUS SEPARATED FLOW AROUND AN AIRFOIL

Streamlines _ Gear scheme , $\Delta t = .1$ _ Incidence 30°

P1/P1 ISO P2

40 TIME CYCLE

200. REYNOLDS

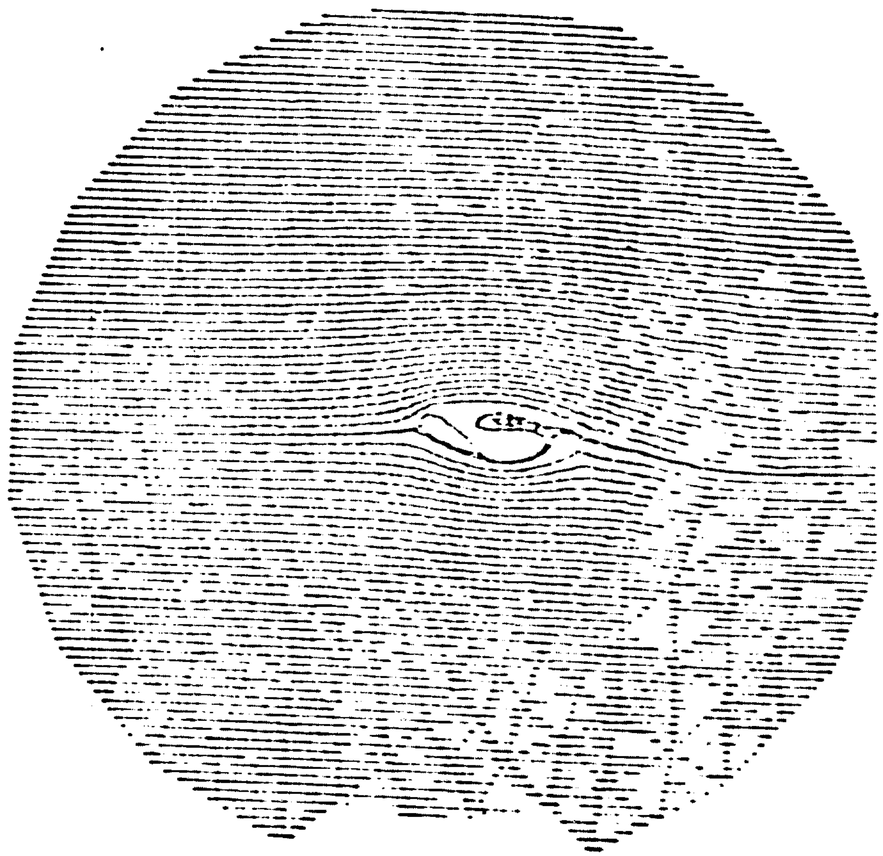

/204

Fig. 112 a)b)

c)

VISCOUS SEPARATED FLOW AROUND AN AIRFOIL

Streamlines _ Gear scheme, $\Delta t = .1$ _ Incidence 30°

P1/P1 ISO P2

50 TIME CYCLE

200. REYNOLDS

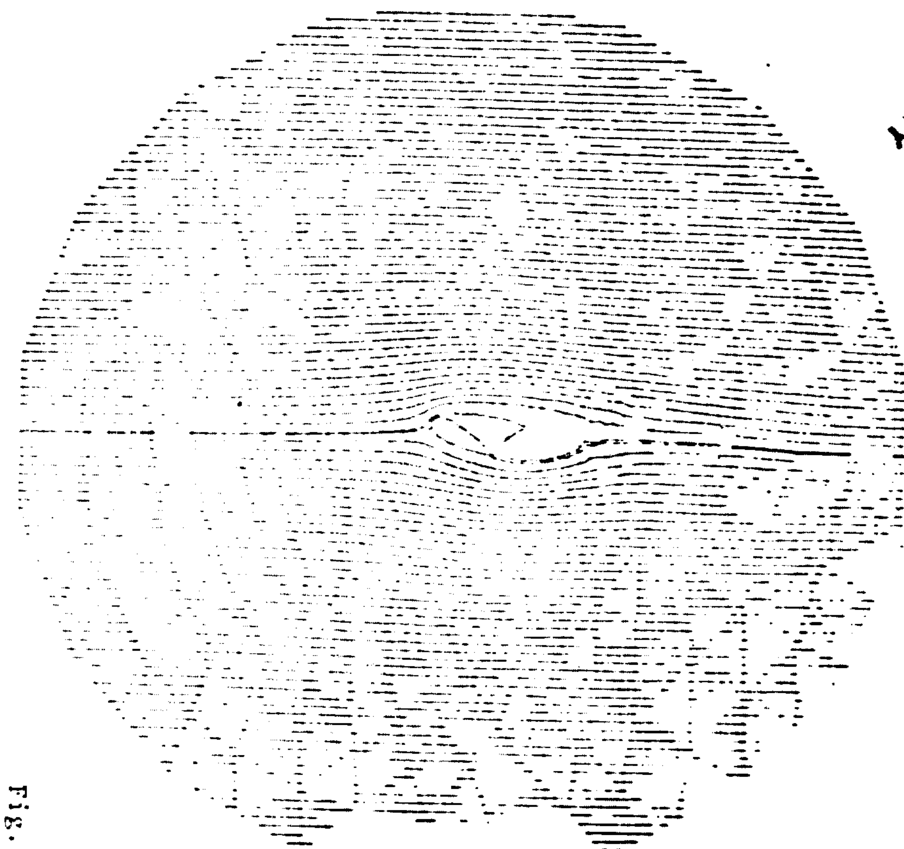

d)

VISCOUS SEPARATED FLOW AROUND AN AIRFOIL

Streamlines _ Gear scheme, $\Delta t = .1$ _ Incidence 30°

P1/P1 ISO P2

60 TIME CYCLE

200. REYNOLDS

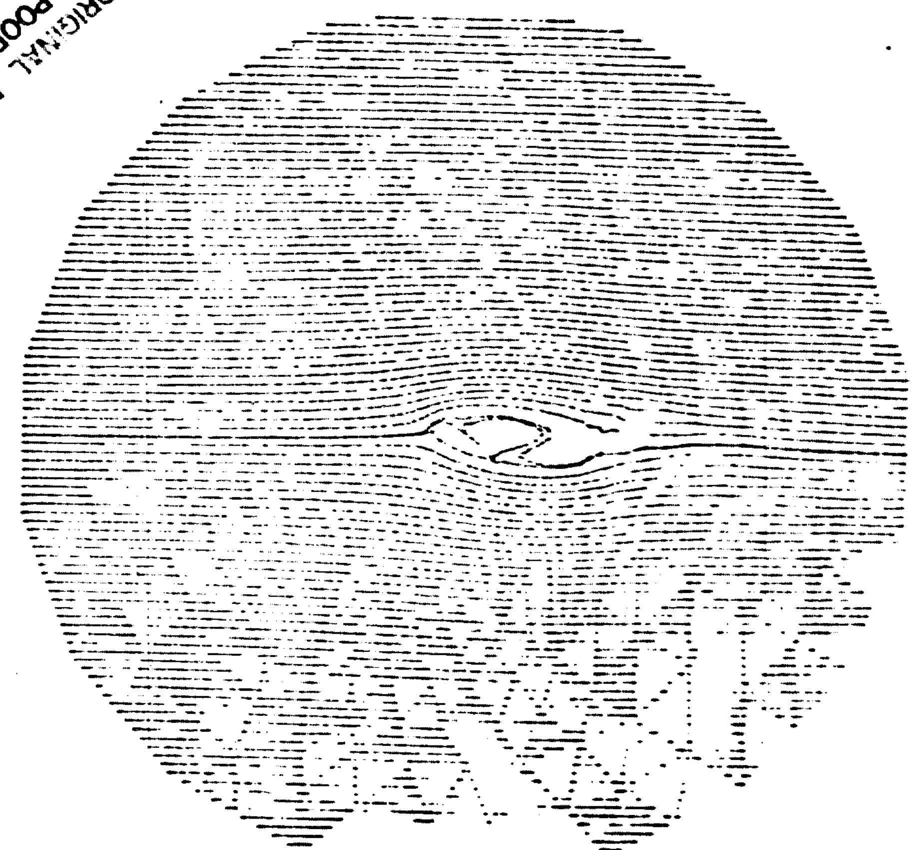

Fig. II2 c)d)

VISCOUS SEPARATED FLOW AROUND AN AIRFOIL

Streamlines _ Gear scheme, $\Delta t = .1$ _ Incidence 30°

P1/P1 ISO P2

e)

70 TIME CYCLE

200. REYNOLDS

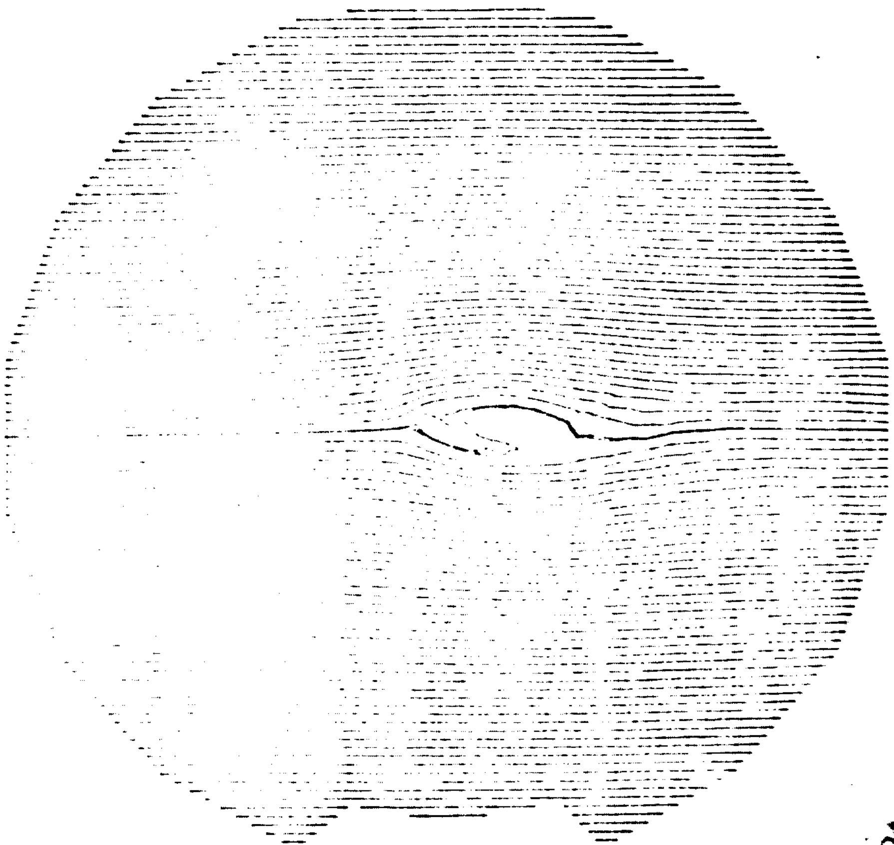

VISCOUS SEPARATED FLOW AROUND AN AIRFOIL

Streamlines _ Gear scheme, $\Delta t = .1$ _ Incidence 30°

P1/P1 ISO P2

f)

80 TIME CYCLE

200. REYNOLDS

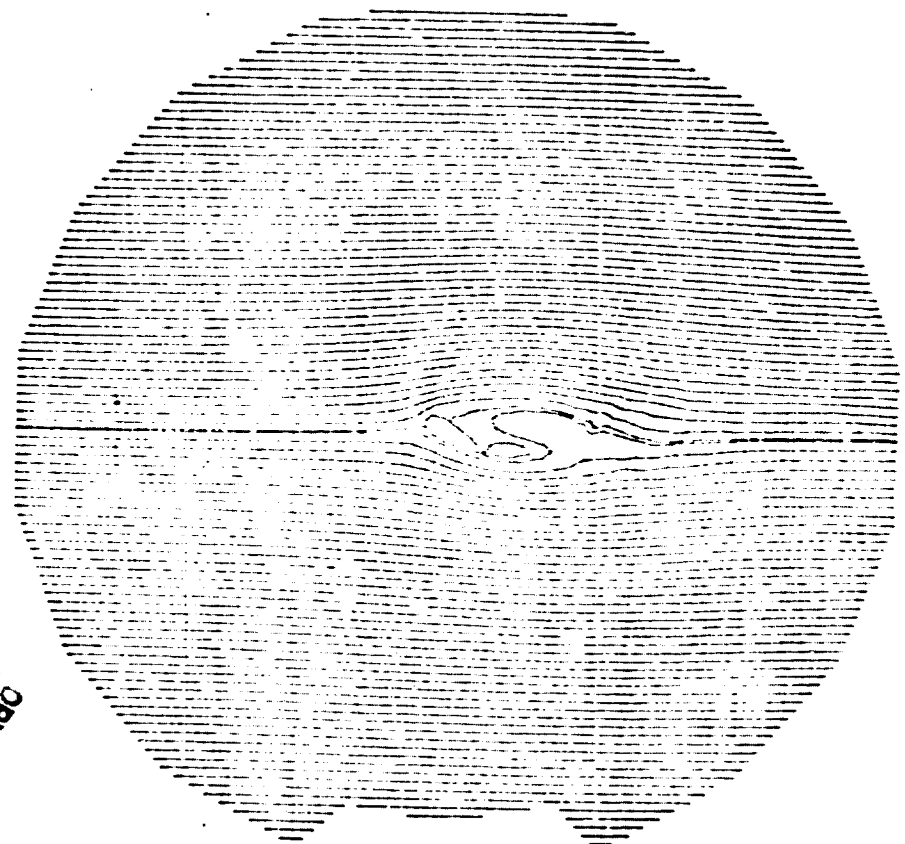

There are two types of boundary conditions verified by the /207 velocity :

-Dirichlet on $\Gamma_\infty \cup \Gamma_{EA}$, $\vec{u} = \{{1 \atop 0}\}$
-mixed Dirichlet-Neumann on Γ_s $\left\{ \begin{array}{l} u = 1 \\ \frac{\partial v}{\partial n} = 0 \end{array} \right.$

Thus we define the velocity satisfying the constraint

$$\int_{\Gamma = \Gamma_{EA} \cup \Gamma_\infty \cup \Gamma_s} \vec{u} \cdot \vec{n} \, d\Gamma = 0$$

where $\vec{n}$ designates the external perpendicular to Γ.

The domain Ω is triangulated by the MODULEF techniques (35). Th The triangulations $\mathcal{C}_h$ and $\tilde{\mathcal{C}}_{h/2}$ the characteristics of which are given on figures 114-115, are relatively rough, but on the other hand, they cannot sustain a large Reynolds number ($Re \leq 100$, Re reduced to h, distance of the 2 airfoil sections 1 - 2).

12.3.5.2. Solution of the Stokes Algorithm /208

In a first phase, we have compared from the point of view of informatics (calculation time) and of theory (accuracy of the scheme) the solution of the Stokes algorithm either by mixed formulation $(\vec{u},\phi)$ FLOWINSKI-PIRONNEAU, or by the TAYLOR-HOOD formulation $(\vec{u},0)$. The first approach relates the the numerical solution of (E_h) expanded in 10.6.5.3. by a conjugate gradient iterative method on the pressure trace λ on Γ , whereas in the second one, the conjugate gradient algorithm is used on pressure p in Ω , described in R. GLOWINSKI-O. PIRONNEAU (49).

The two algorithms converge for a same approximation P1/P2 toward a pressure distribution in Ω which is very similar, on figures 116-121 after satisfaction fot the stop test on g^n :
$g^n : (g^n,g^n)^{1/2} < \varepsilon$, in 30 iterations. ($\varepsilon = .1D-6$)

The conditioning S_h occurring in the solution (342) (343) is taken in L^2, optimal choice in the TAYLOR-HOOD approach, since

$$S_h\lambda^{n+1} = S_h\lambda^n - \rho A_h z^h \quad \text{with } A_{h\lambda}\phi_h = \frac{d\phi_{h\lambda}}{dn} \tag{342}$$

$$S_h p^{n+1} = S_h p^n - \rho A_h z^n \text{ with } A_h q = \vec{\nabla}\cdot\vec{u}_{hq} \tag{343}$$

but not in the GLOWINSKI-PIRONNEAU one, since $\lambda \in H^{-1/2}(\Gamma)$. We can therefore expect to improve the convergence speed of (342).

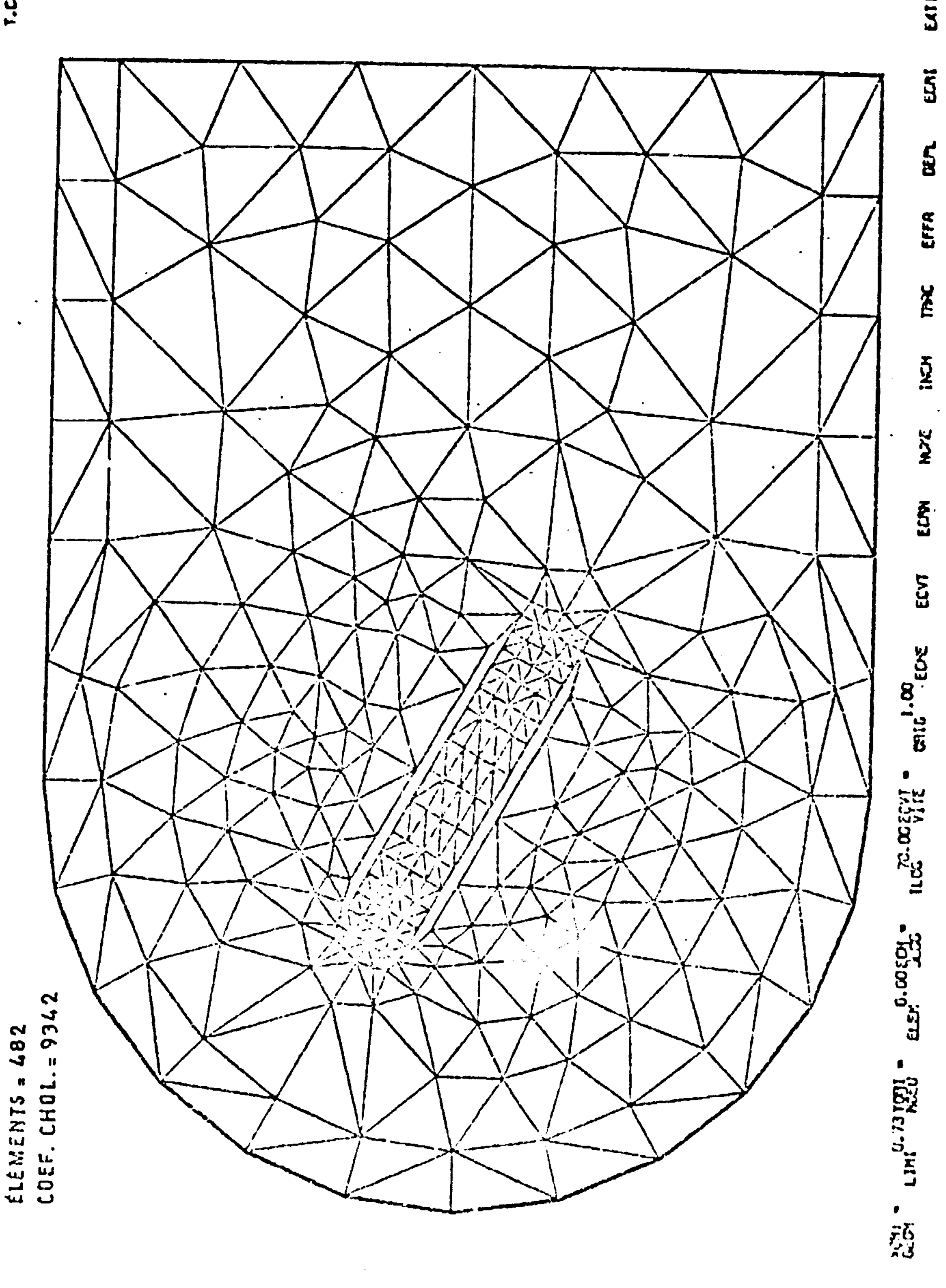

Fig. 114

ORIGINAL PAGE IS
OF POOR QUALITY

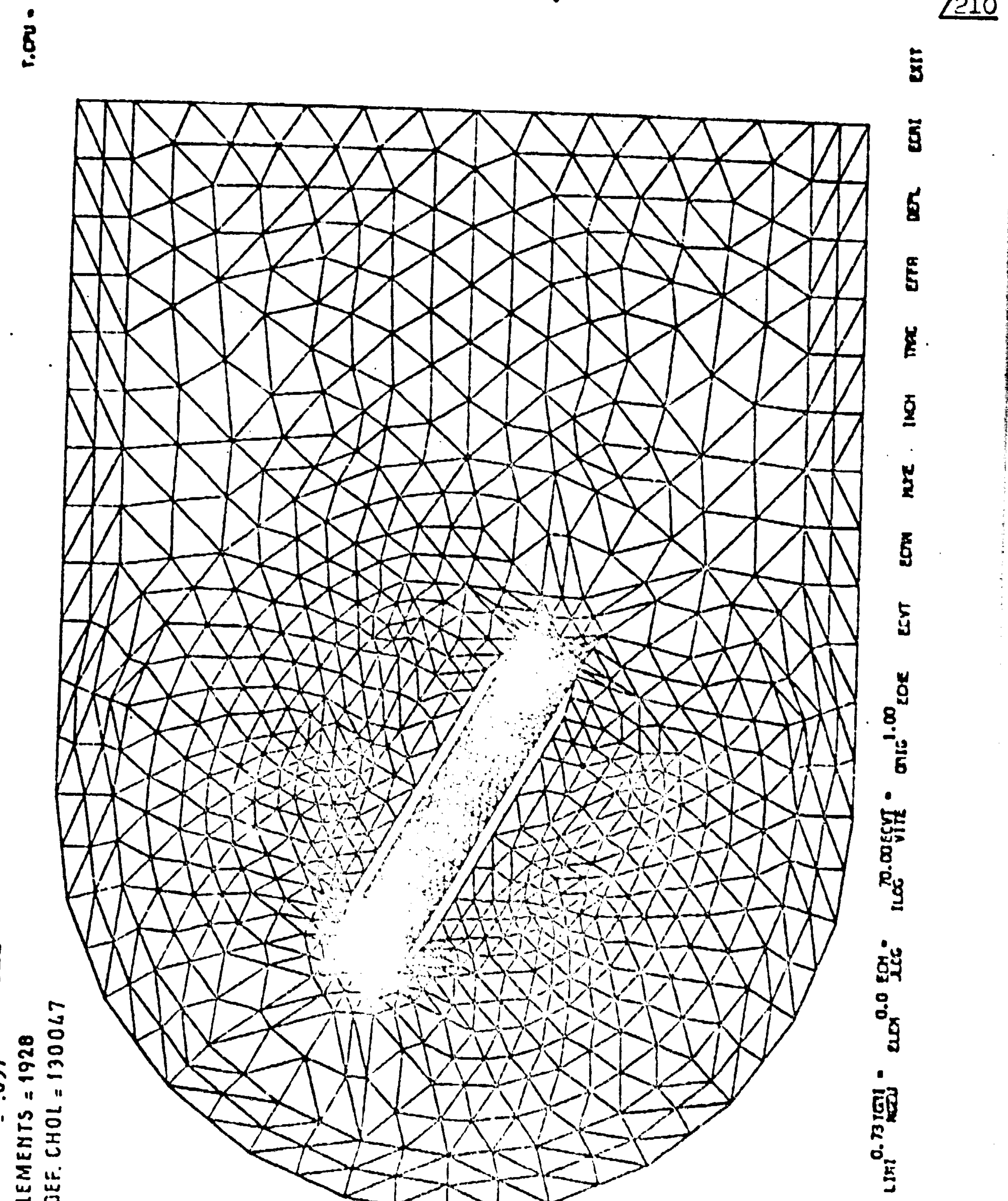

Fig. 115

GP

P1/P2 STOKES ALGORITHM - GLOWINSKI-PIRONNEAU ELEMENT

0. INCIDENCE DEGREE

0 TIME CYCLE

1. REYNOLDS

PRESSURE ON THE BODY AND IN THE FLUID

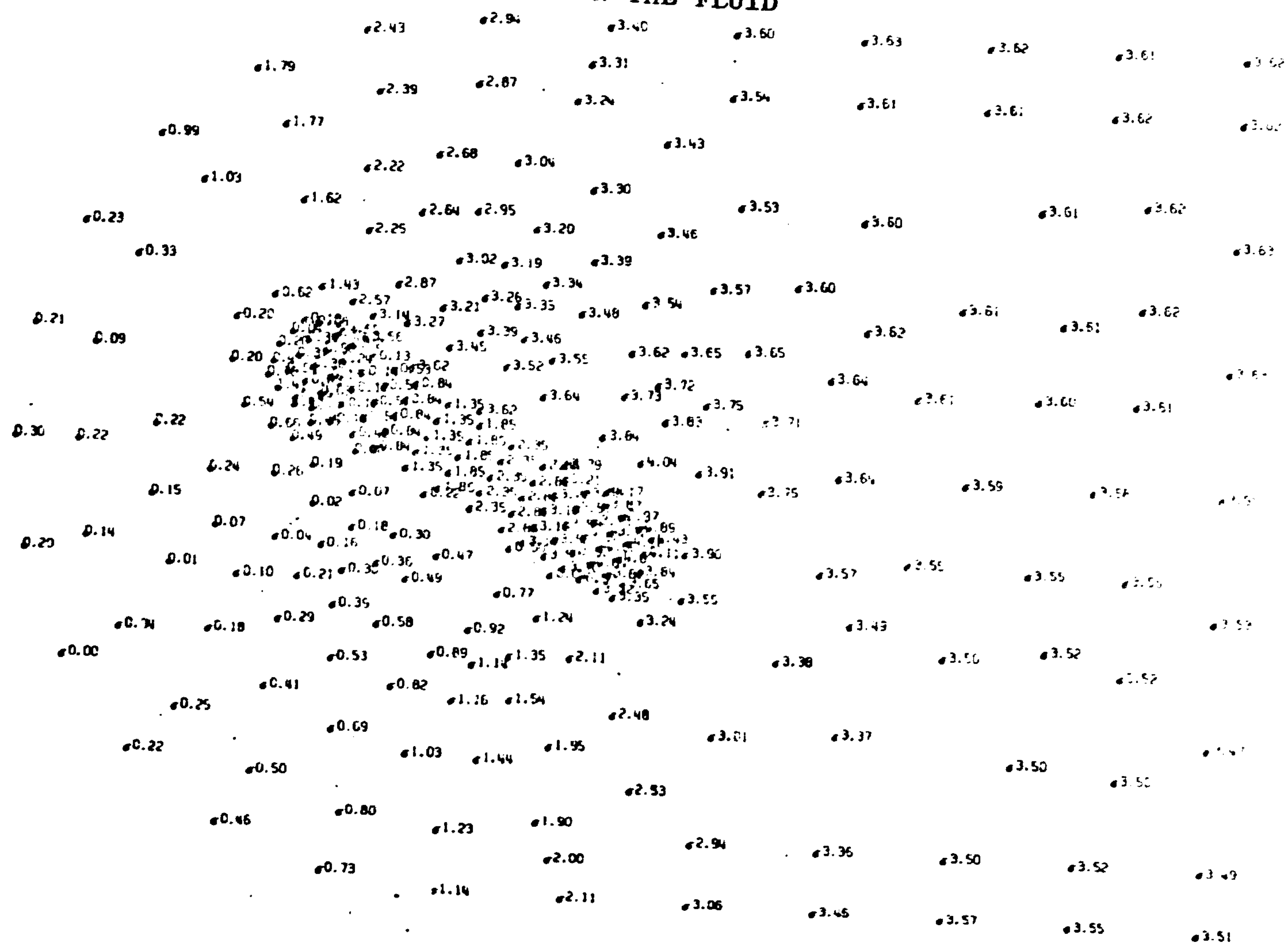

Fig. 116

ITER OF N STOKES - 5

P1/P2 STOKES ALGORITHM - GLOWINSKI-PIRONNEAU ELEMENT

TIME STEP 0.1

TIME CYCLE 0 ISO-PRESSURES

REYNOLDS 1.

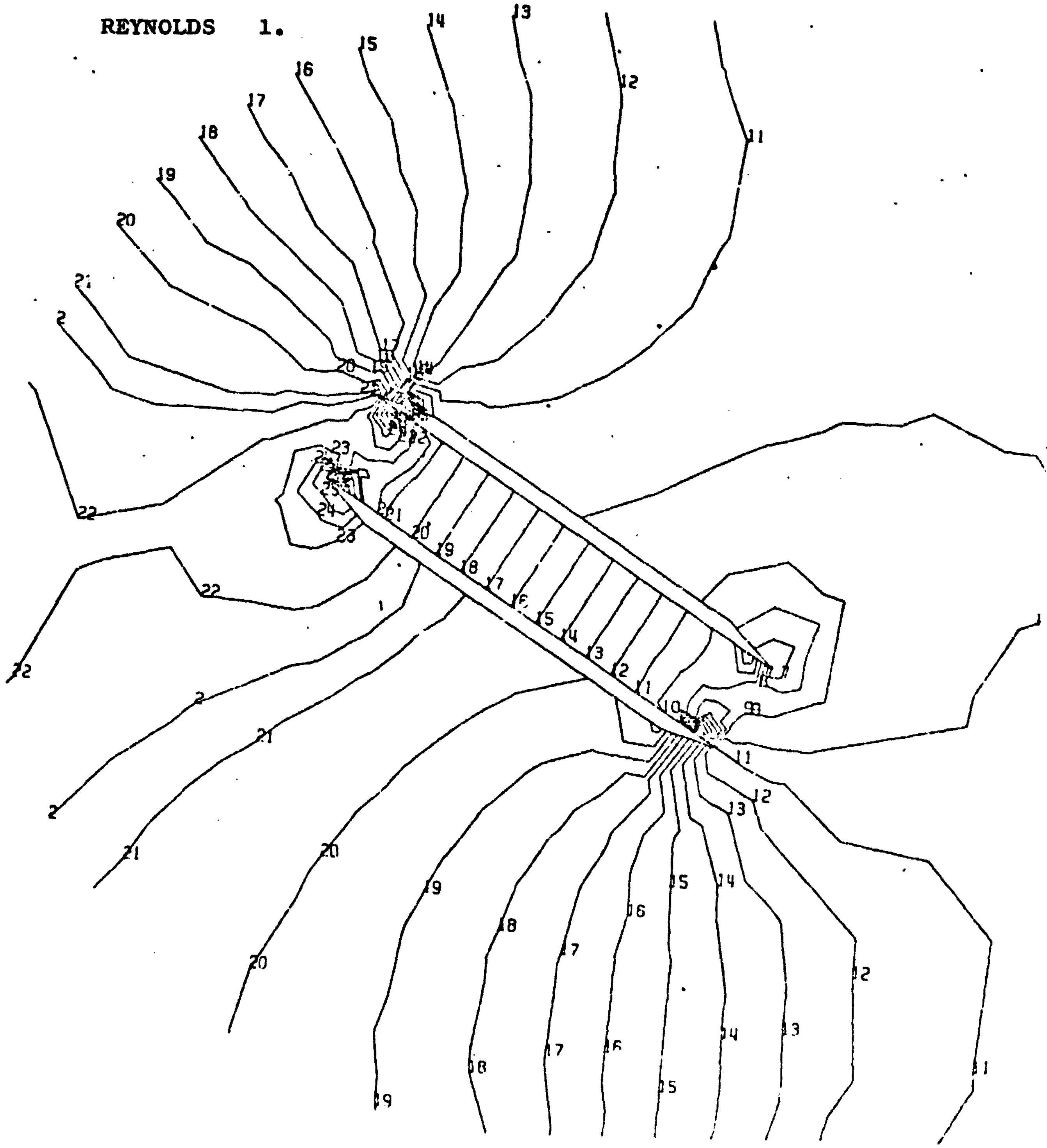

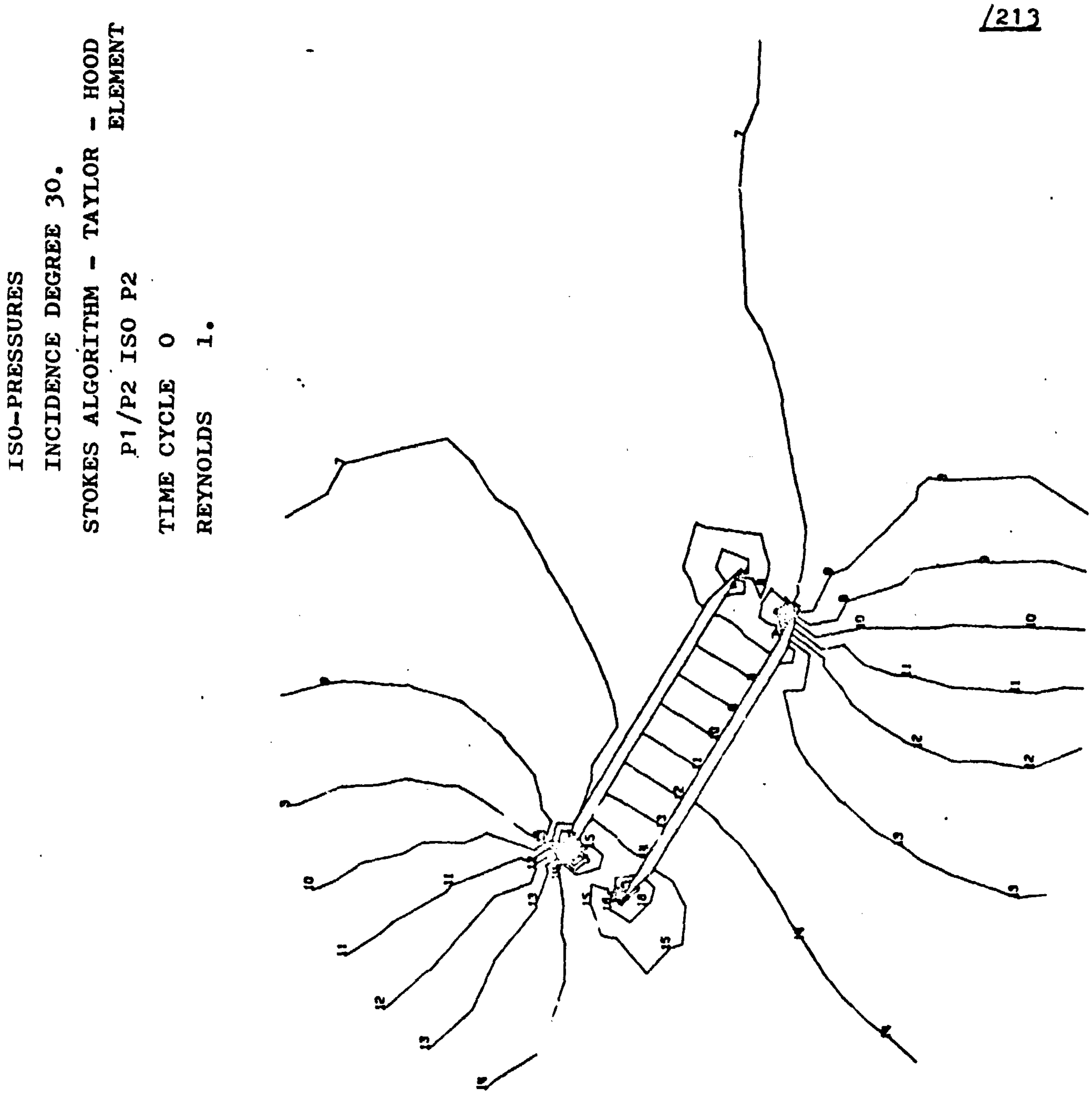
ISO-PRESSURES
INCIDENCE DEGREE 30.
STOKES ALGORITHM - TAYLOR - HOOD ELEMENT
P1/P2 ISO P2
TIME CYCLE 0
REYNOLDS 1.

Figure 118

P1/P1 ISO P2

TH

STOKES ALGORITHM -TAYLOR-HOOD ELEMENT
PRESSUR ON THE BODY AND IN THE FLUID

INCIDENCE DEGREE 30.
TIME CYCLE 0
REYNOLDS 1.

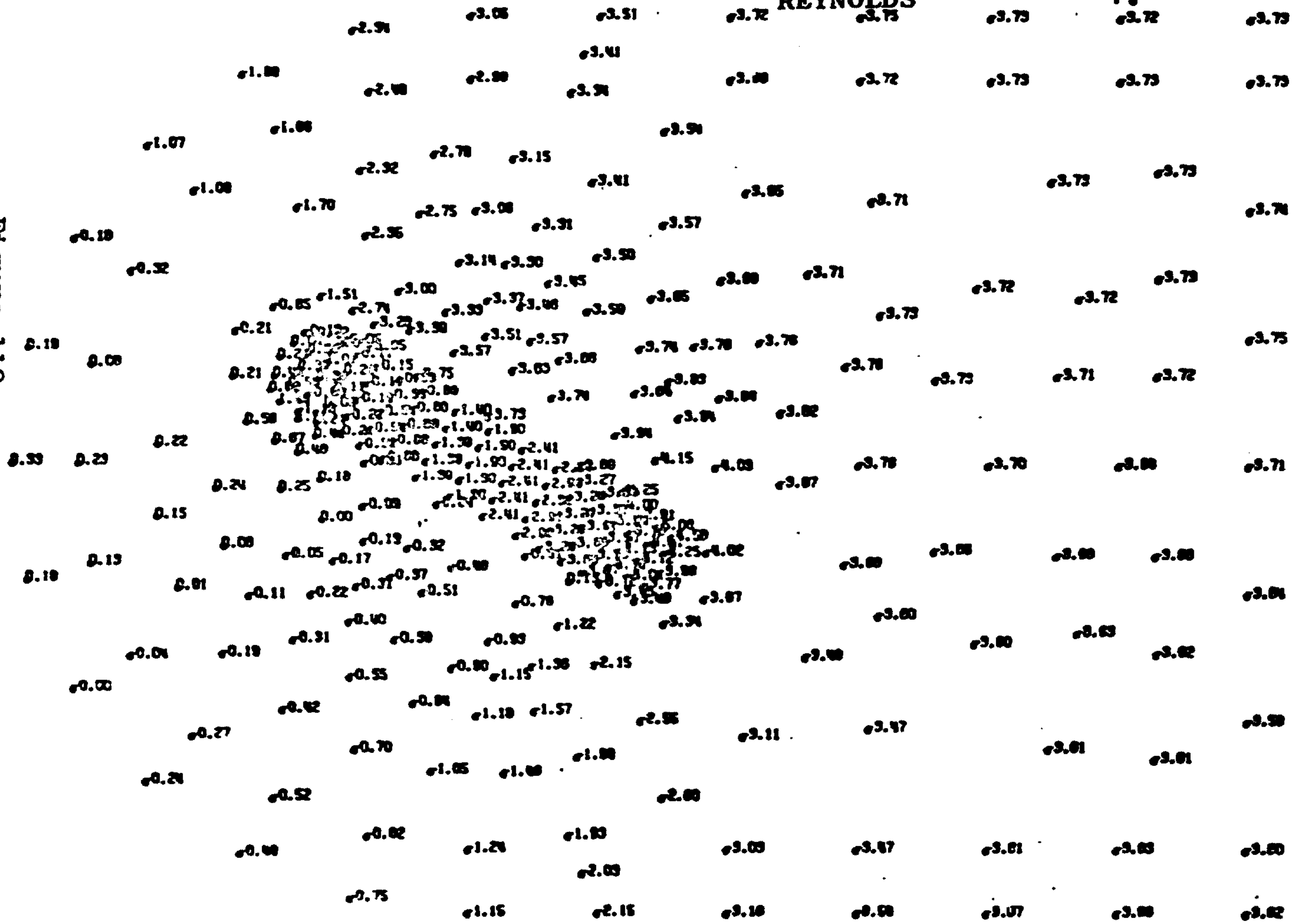

Figure 119

P1/P2 - STOKES ALGORITHM
TAYLOR-HOOD ELEMENT
PRESSURE ON THE BODY
INCIDENCE DEGREE O.
TIME CYCLE O.
REYNOLDS 100.

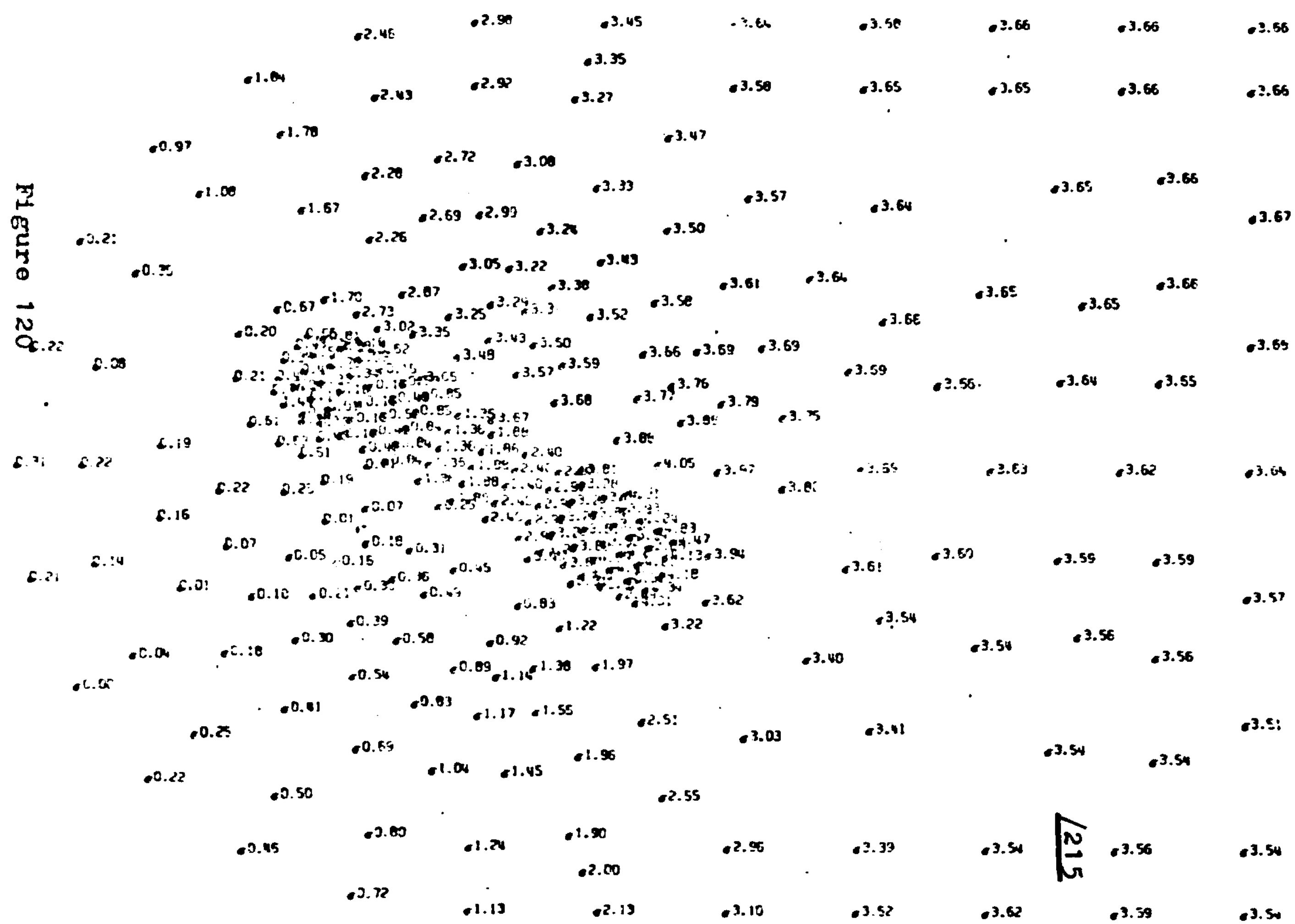

Figure 120

Fig. 120

UNSTEADY STOKES P1

ITER OF N STOKES 0

P1-P2 STOKES ALGORITHM

TAYLOR-HOOD ELEMENT

TIME STEP 0.0

TIME CYCLE 0 ISO PRESSURES

REYNOLDS 100.

ISO-PRESSIONS

41 ETAEA100 PL 3 03 MAI 1979 20.37.59

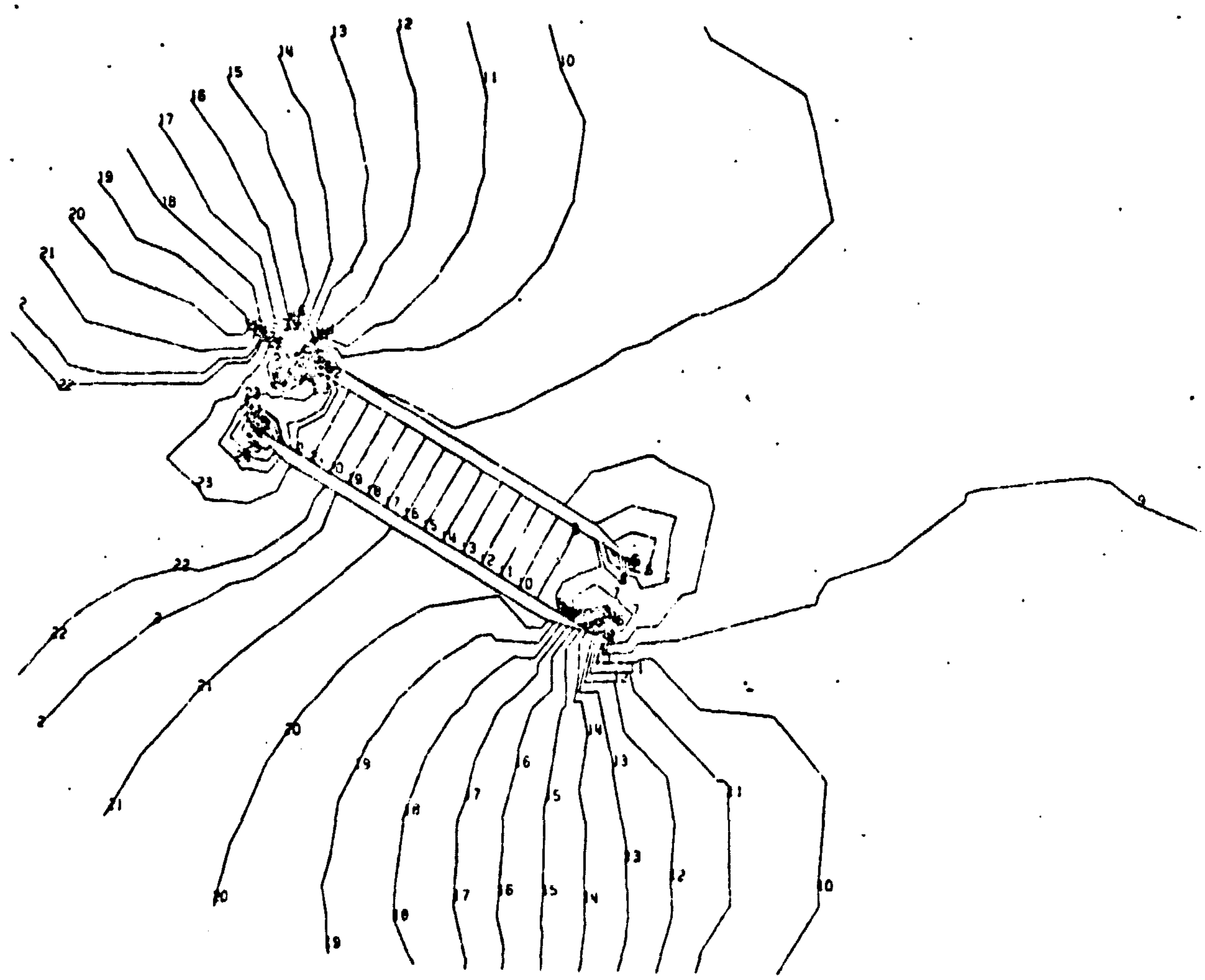

TH

Fig. 121

12.3.5.3. Comparisons of Codes P1/P1 ISO P2 and P1/P2 /217

Comparisons of the two codes are based on the following case :

-unsteady Navier-Stokes flows with Dirichlet or Neumann condition downstream.

Two cases have been calculated if $i = 30°$, $Re = 100$. The time step selected is $\Delta t = .2$,, the number of time cycles selected is 100, the number of control iterations at each Δt is 6. The process computation time is about 100' in the P1/P2 case, 55' in the P1/P1 ISO P2 case.

It may be stated that on the whole the numerical simulation of the flow obtained by one or the other code is very similar.

Figures (122) (123) (124) show through the means of streamlines at Re = 100, the appearance, the development and the discharge of large structures on the upper external part of the air inlet and in the internal part, the formation of a quasi-steady eddy, which remains attached to the lower side.

Since the domain of calculation is voluntarily selected to be small, the boundary conditions downstream interfere considerably with the entire flow as soon as the ejected eddies reach the downstream boundary, which is shown by the gobal flow at time cycle 100 (velocities, streamlines and pressure of figures 125-127 (resp. 128-130) for Dirichlet type conditions (resp. of Neumann type).

Interpretation of the results confirms the choice of Neumann type downstream boundary conditions for larger Reynolds.

It is interesting to observe the numerical operation of the two codes by following the evolution of values of criteria and gradients through time cycles and within one of them. It may be observed that when the Reynolds number increases, it takes longer for the convergence of the optimal control problem to be obtained (3 to 4 iterations for Re = 50, whereas 6 to 8 iterations on the average for Re = 100).

Figures 131 through 133 show the evolution of the criterion and /218 of the gradient within a time cycle without much alteration in the flow. The following 134 through 136 figures relate to a time cycle (75) close the the emission of a new eddy.

It may be observed that code P1/P2 absorbs "better" the alteration in configuration, whereas code P1/P1 ISO P2 shows more resistance (jump of criteria and of gradients) and requires more iterations to control the new fluid state.

P_1 / P_1 iso P_2

20 Time Cylcle
100. Reynolds

30 Time Cycle
100. Reynolds

STREAMLINES

NEUMAN DOWNSTREAM

/219

40 Time Cylce
100. Reynolds

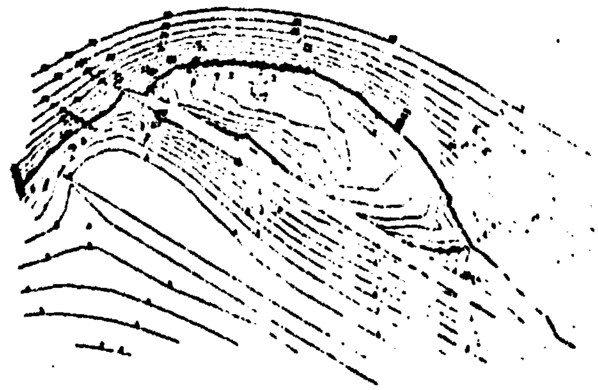

50 Time Cylce
100. Reynolds

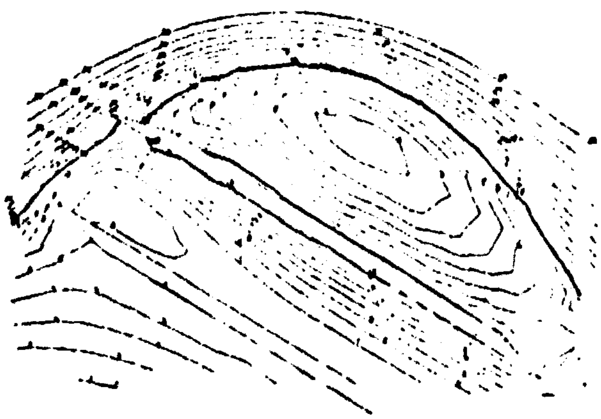

75 Time Cycle
100. Reynolds

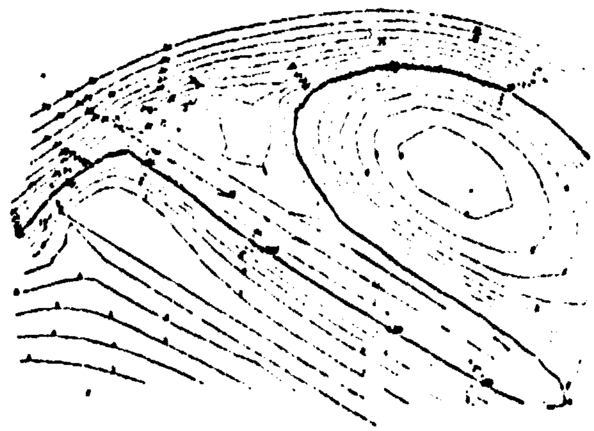

100 Time Cycle
100. Reynolds

Figure 122

P_1 / P_1 iso P_2

STREAMLINES DIRICHLET DOWNSTREAM

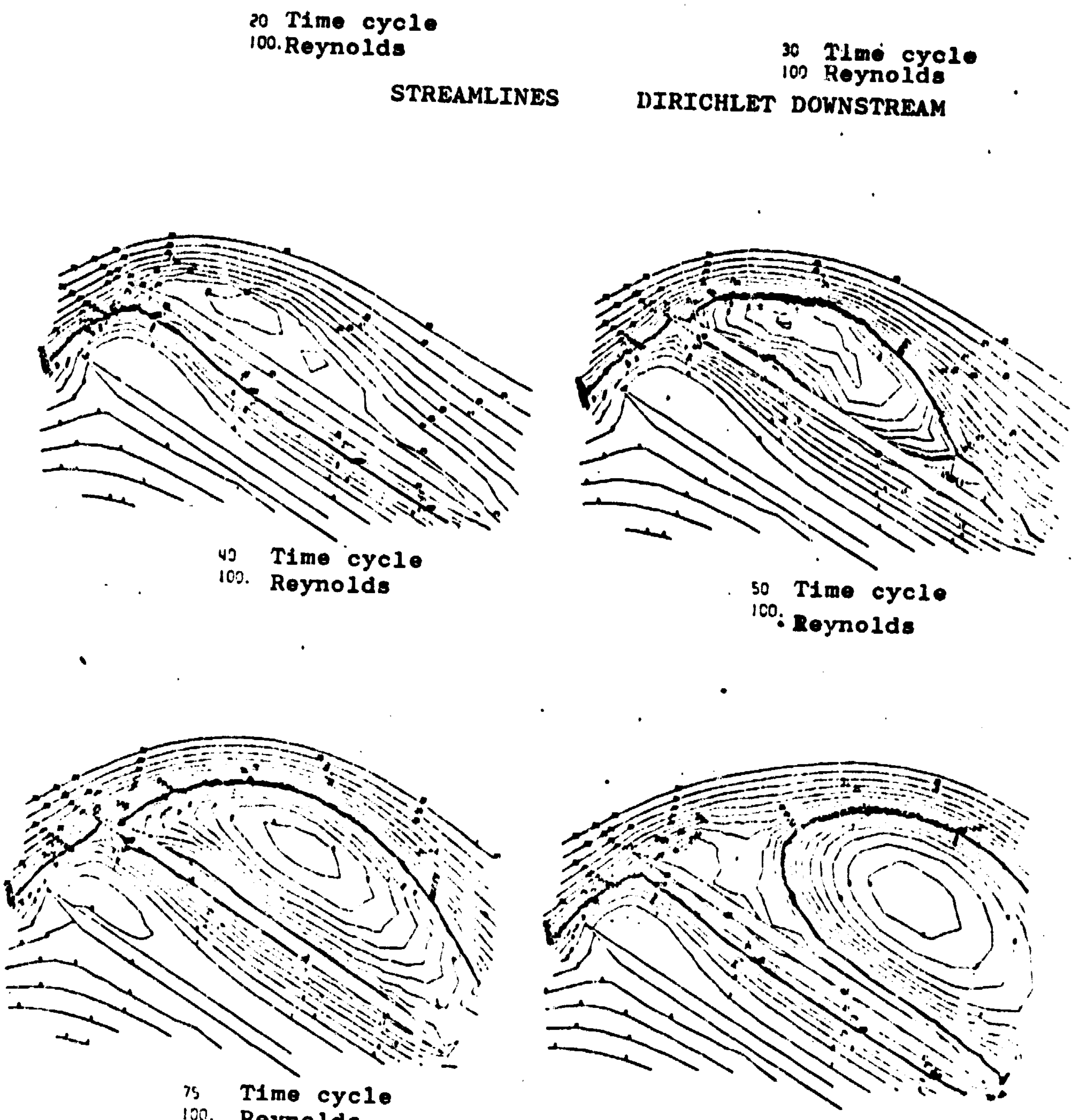

Figure 123

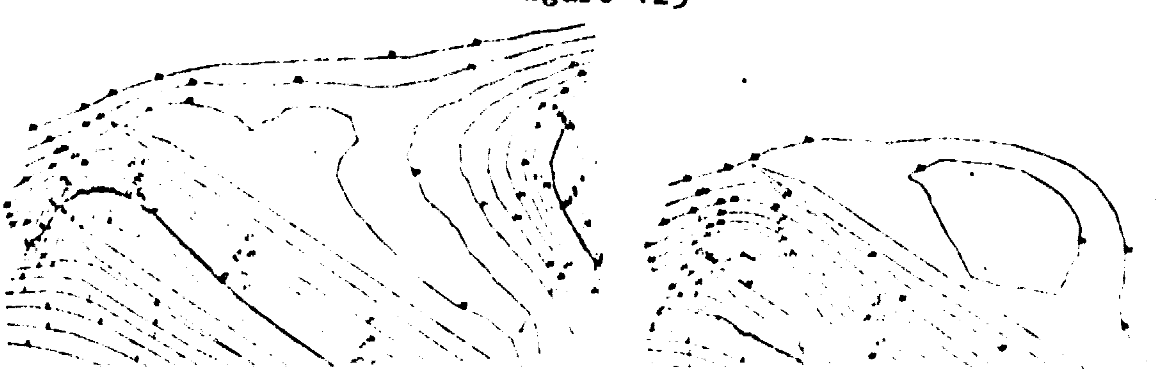

P_1/P_2

20 Time cycle
100. Reynolds

30 Time cycle
100. Reynolds

STREAMLINES DIRICHLET DOWNSTREAM

/221

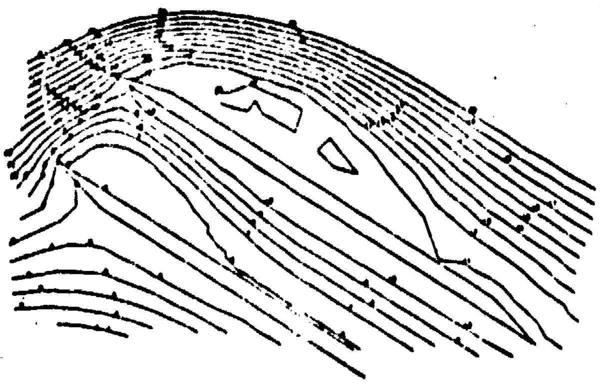

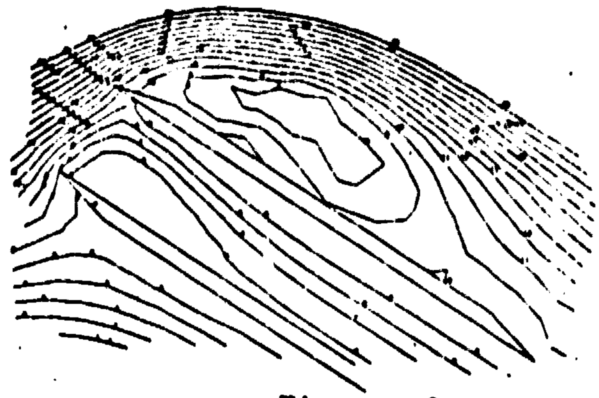

40 Time cycle
100. Reynolds

50 Time cycle
100. Reynolds

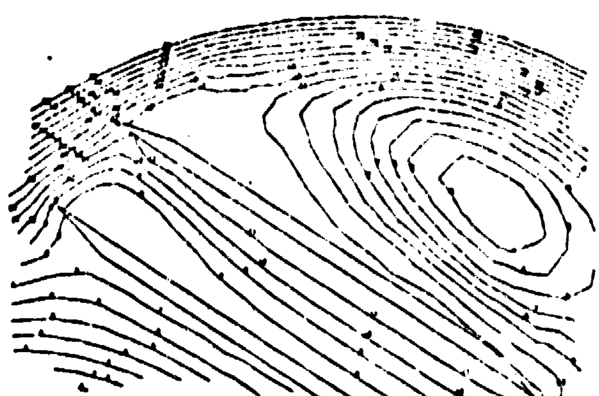

75 Time cycle
100. Reynolds

100 Time cycle
100. Reynolds

Figure 124

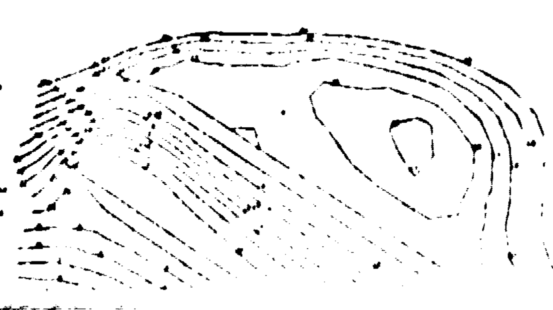

222

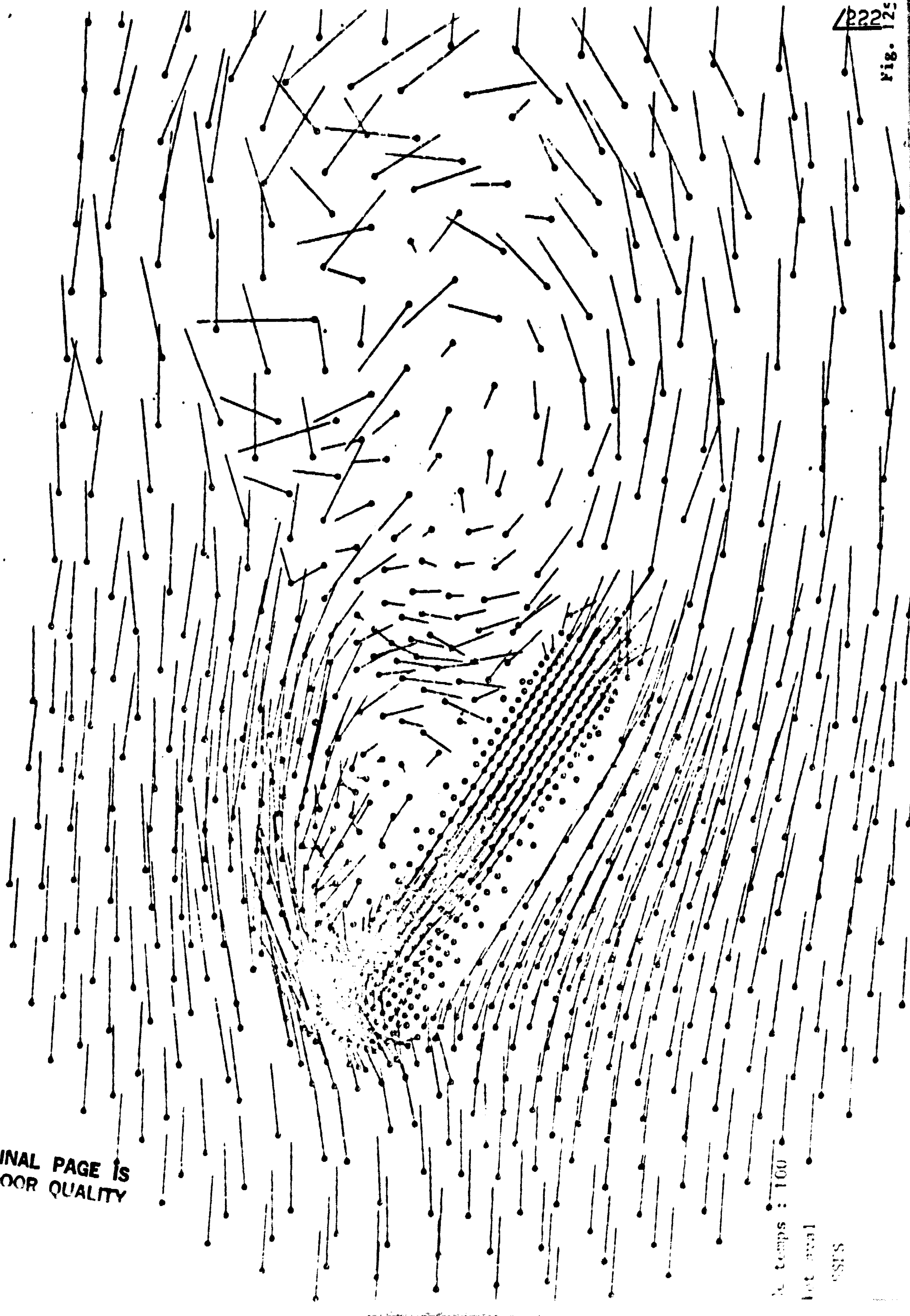

Fig. 125

temps : 100

0.2 TIME STEP

100 TIME CYCLE

100. REYNOLDS

P1/P2

G-P

DIRICHLET DOWNSTREAM

II - STREAMLINES

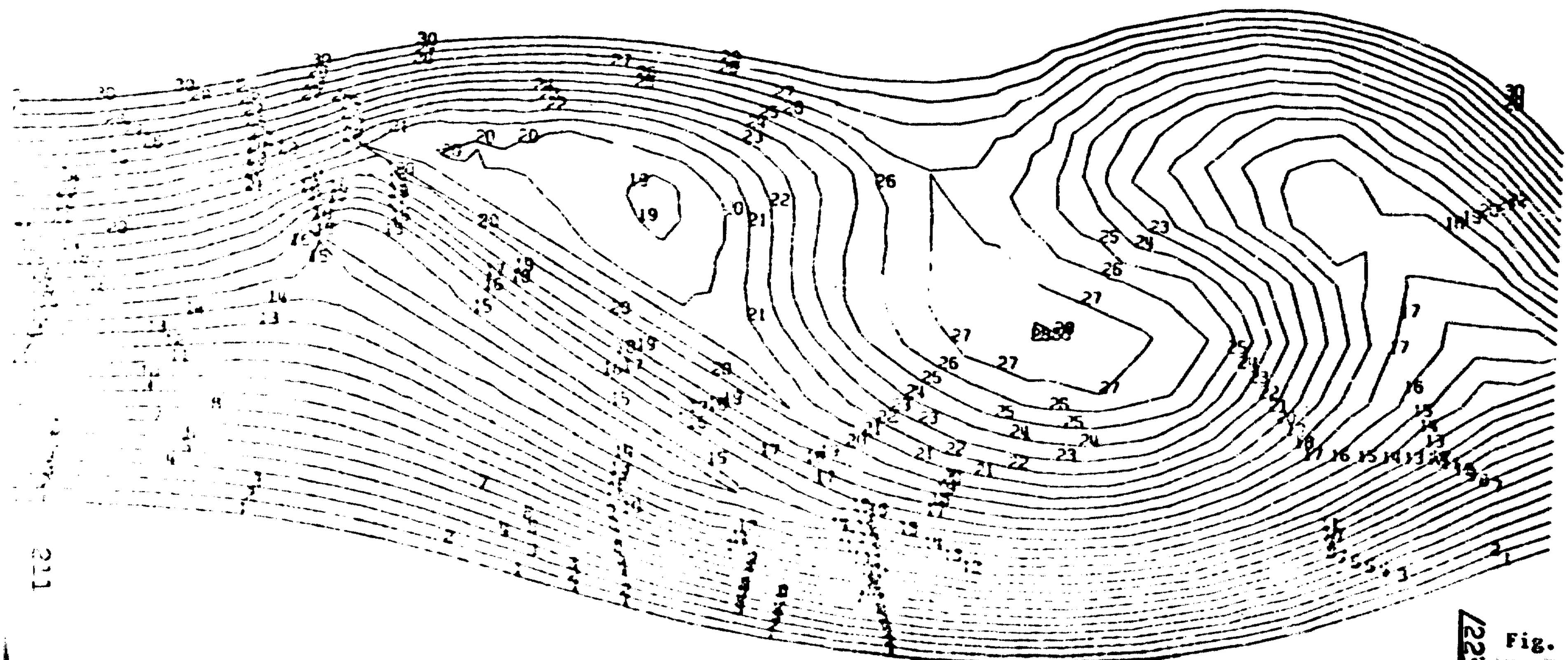

/223 Fig. 126

0.2 TIME STEP

100 TIME CYCLE

100. REYNOLDS

P1/P2

G-P

DIRICHLET DOWNSTREAM

III - PRESSURES

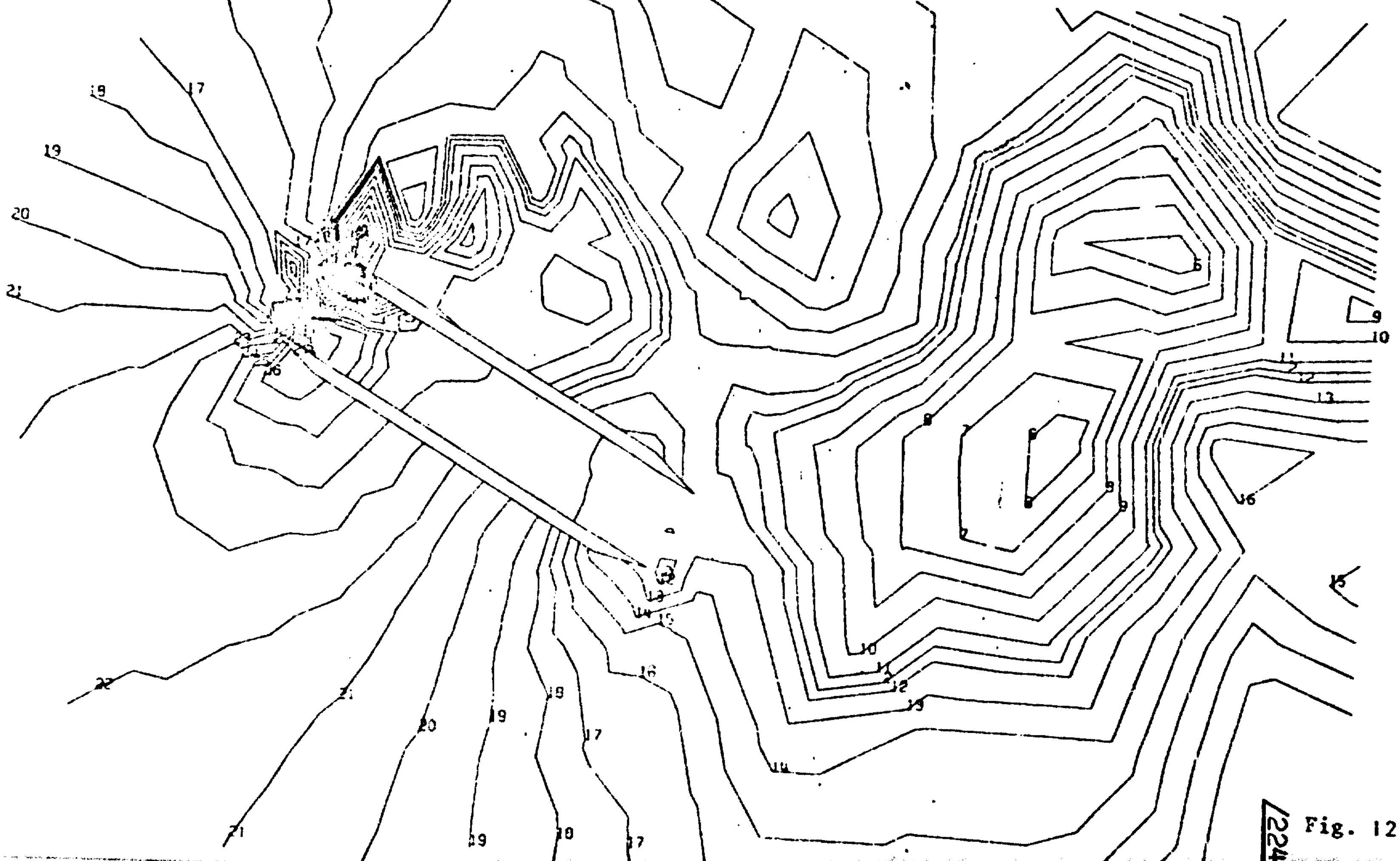

/224 Fig. 127

ORIGINAL PAGE IS
OF POOR QUALITY

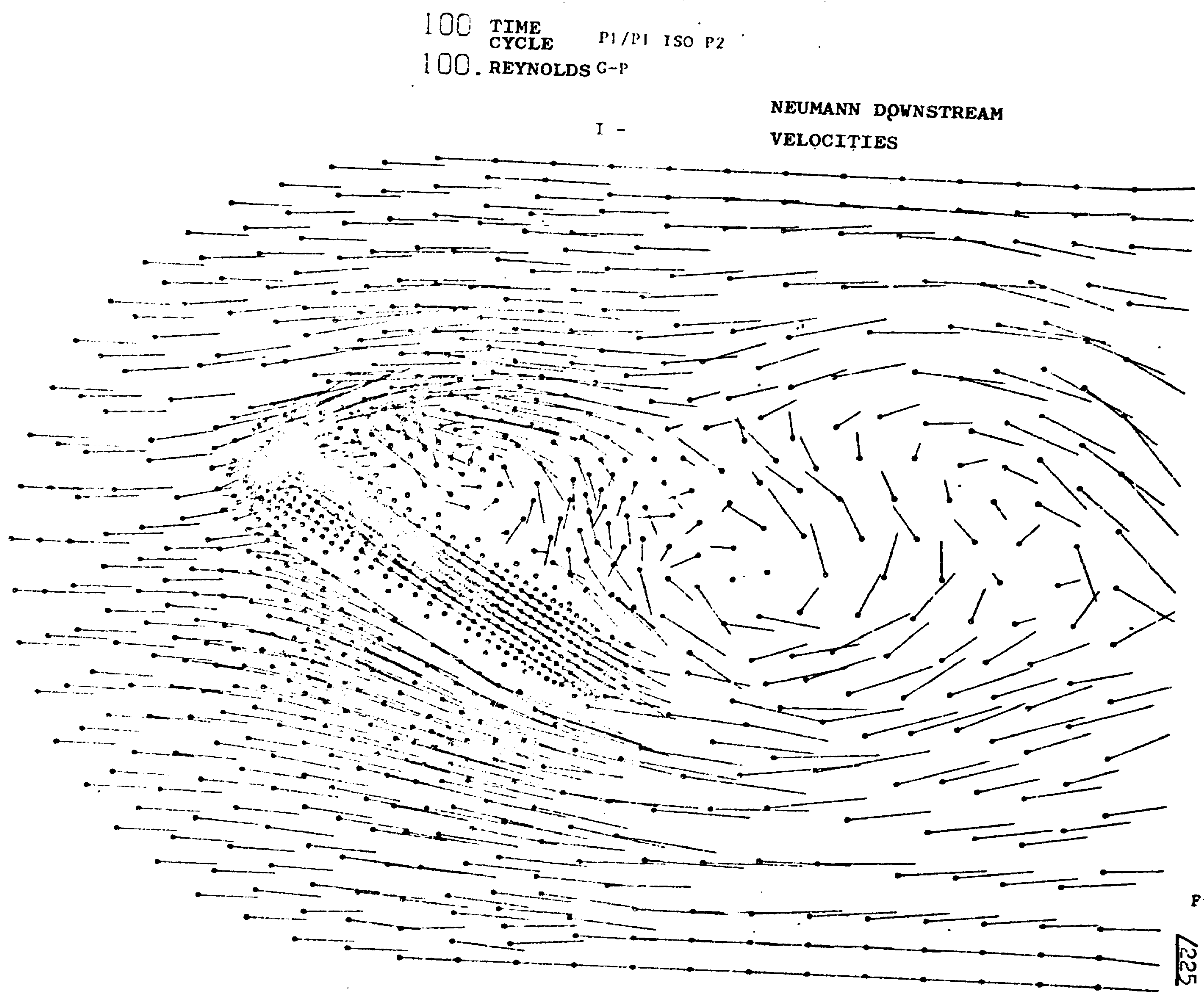
100 TIME
CYCLE
P1/P1 ISO P2
100. REYNOLDS G-P
NEUMANN DOWNSTREAM
VELOCITIES
I -

Fig. 128

/225

P1/P1 ISO P2

100 TIME CYCLE

100. G-P REYNOLDS

NEUMANN DOWNSTREAM

STREAMLINES - II

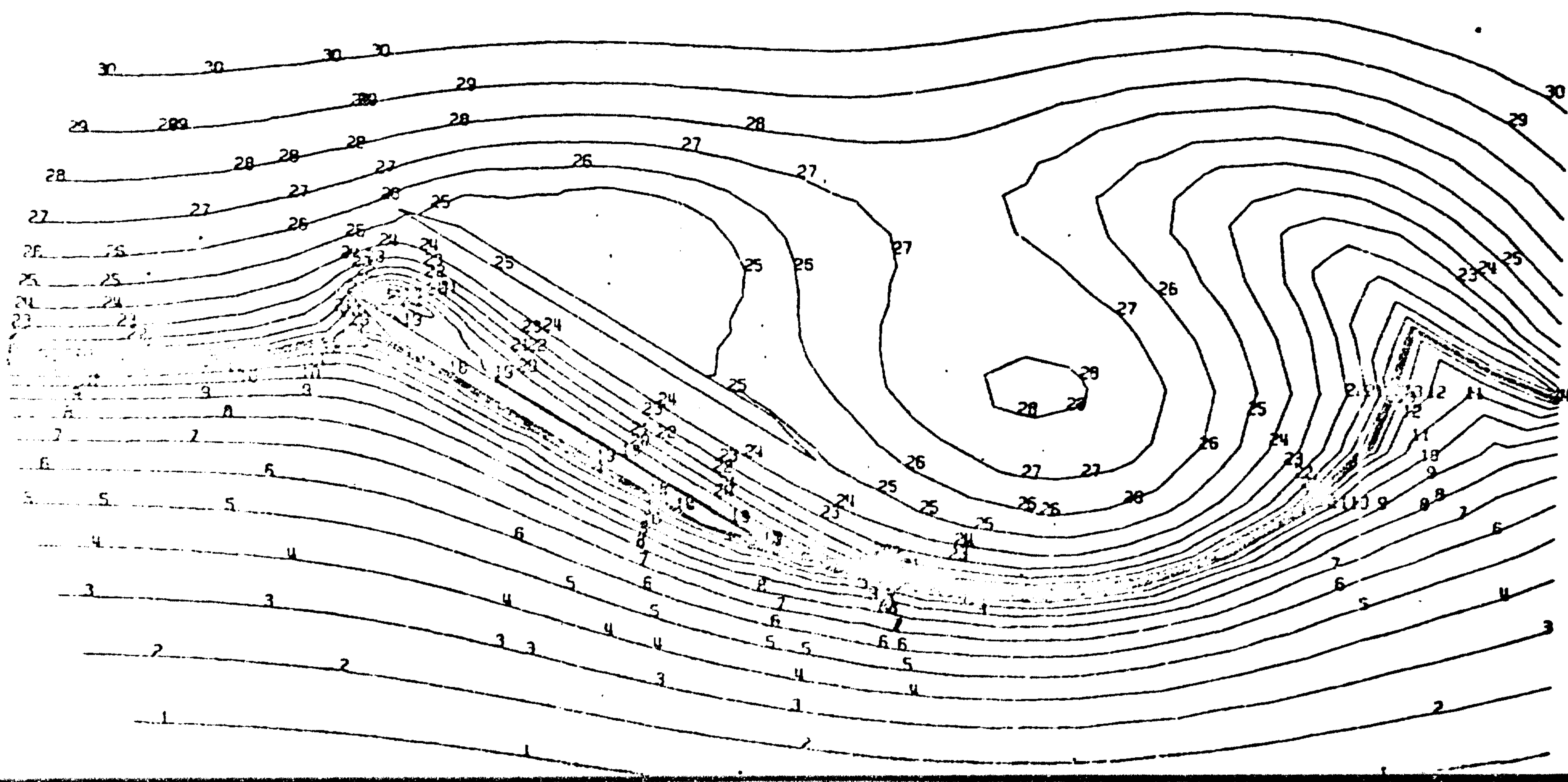

/226

Fig. 1:

P1/P1 ISO P2

100 TIME CYCLE

100. REYNOLDS

G-P

NEUMANN DOWNSTREAM

ISO-PRESSURES - III

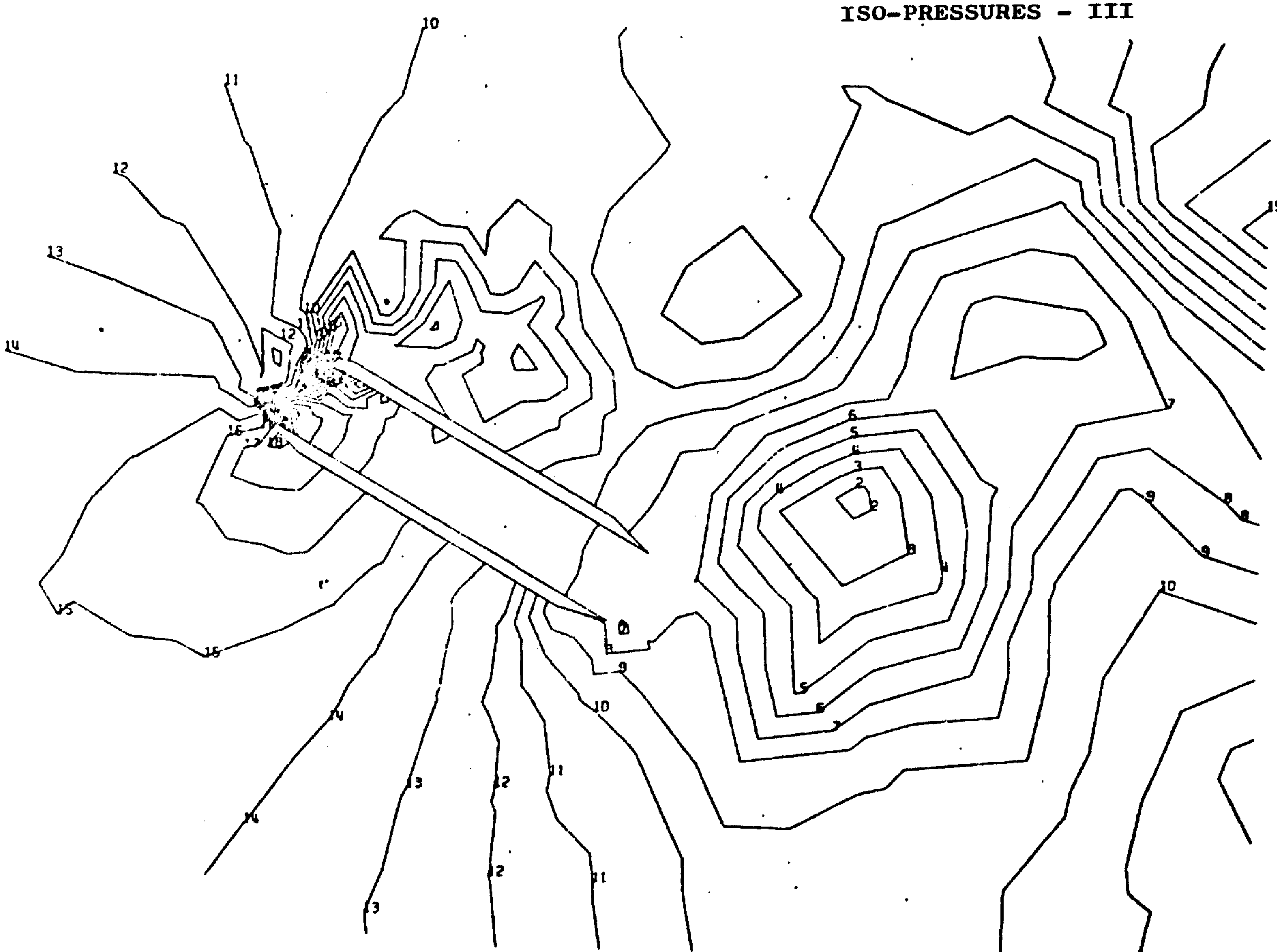

Fig. 130

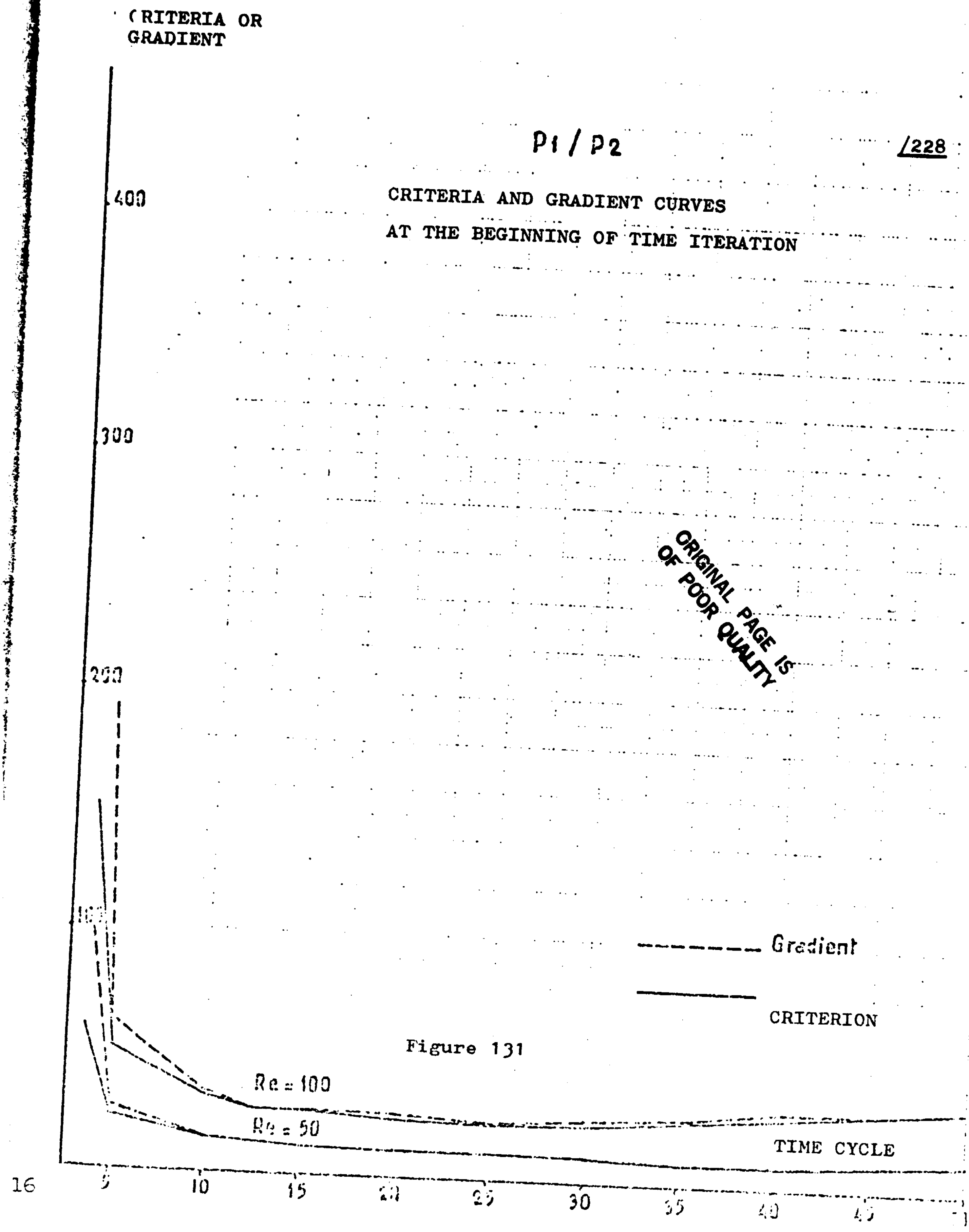

CRITERIA AND GRADIENT CURVES
AT THE BEGINNING OF TIME ITERATION

Figure 131

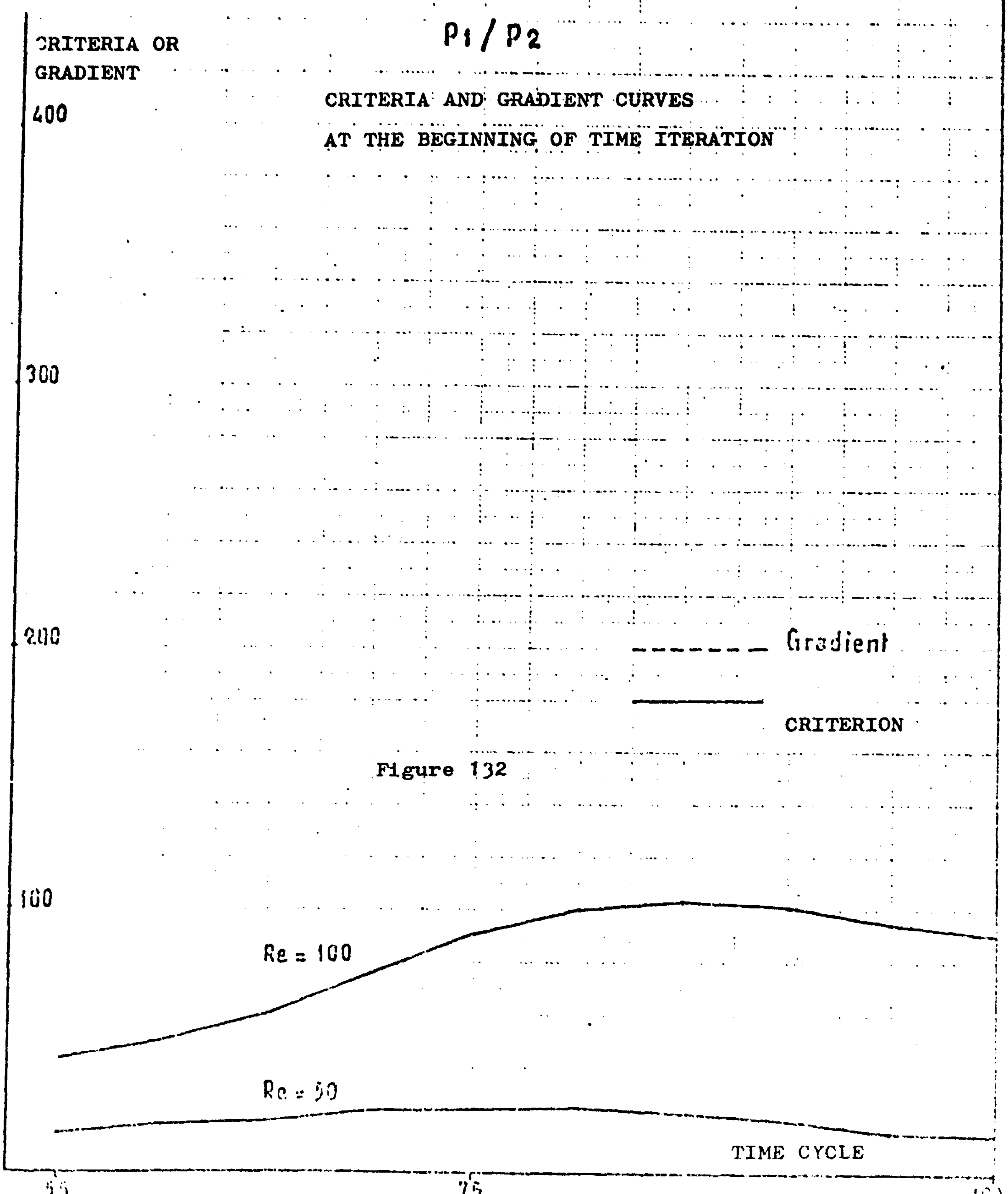

CRITERIA OR GRADIENT
400
300
200
100
p_1/p_2
CRITERIA AND GRADIENT CURVES
AT THE BEGINNING OF TIME ITERATION
Gradient
CRITERION
Re = 100
Re = 50
TIME CYCLE
55
75
100

Figure 132

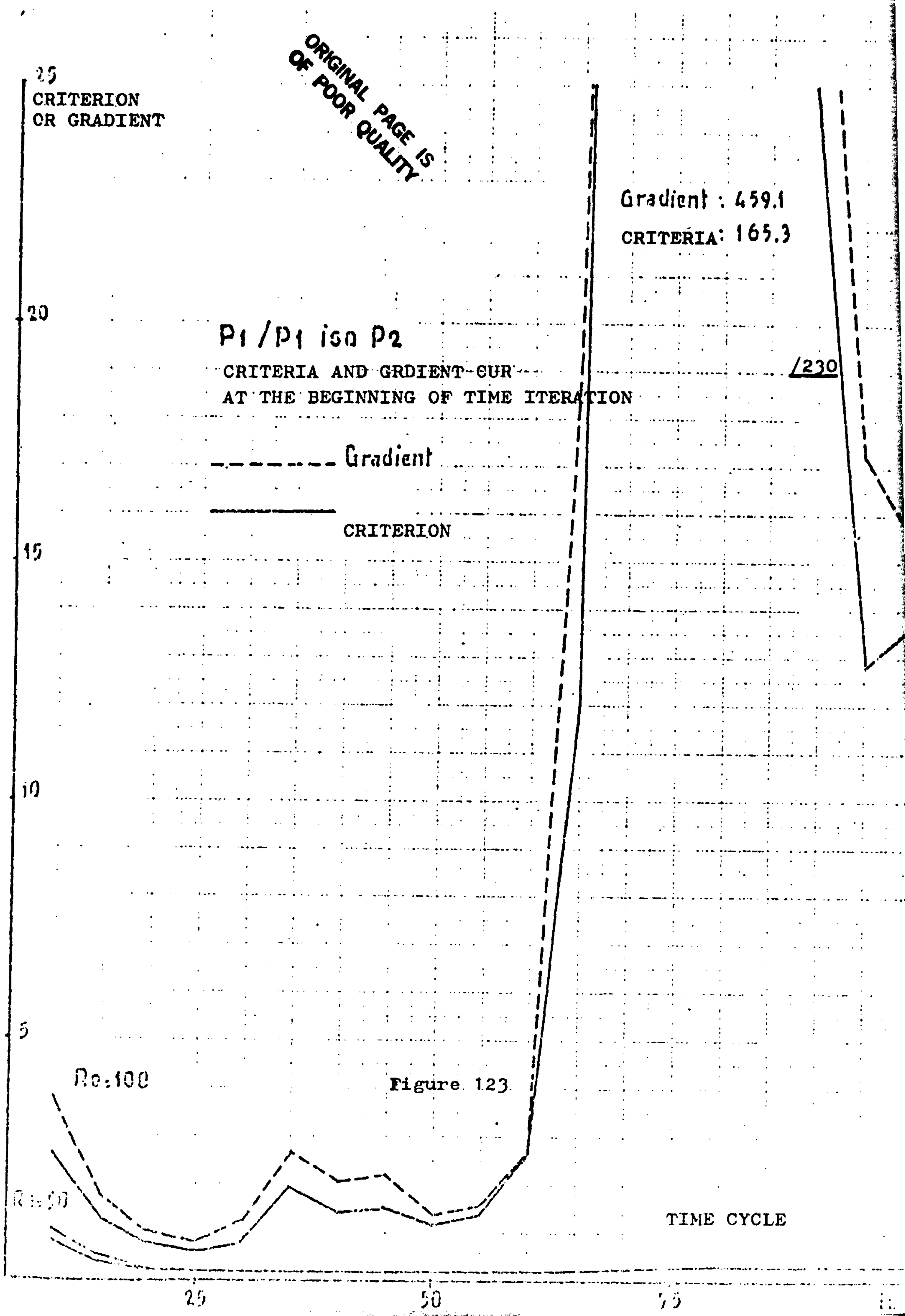
25
CRITERION
OR GRADIENT
Gradient : 459.1
CRITERIA: 165.3
20
P1 /P1 iso P2
CRITERIA AND GRDIENT CUR
AT THE BEGINNING OF TIME ITERATION
/230
Gradient
CRITERION
15
10
5
Re:100
TIME CYCLE
25
50

Figure 123

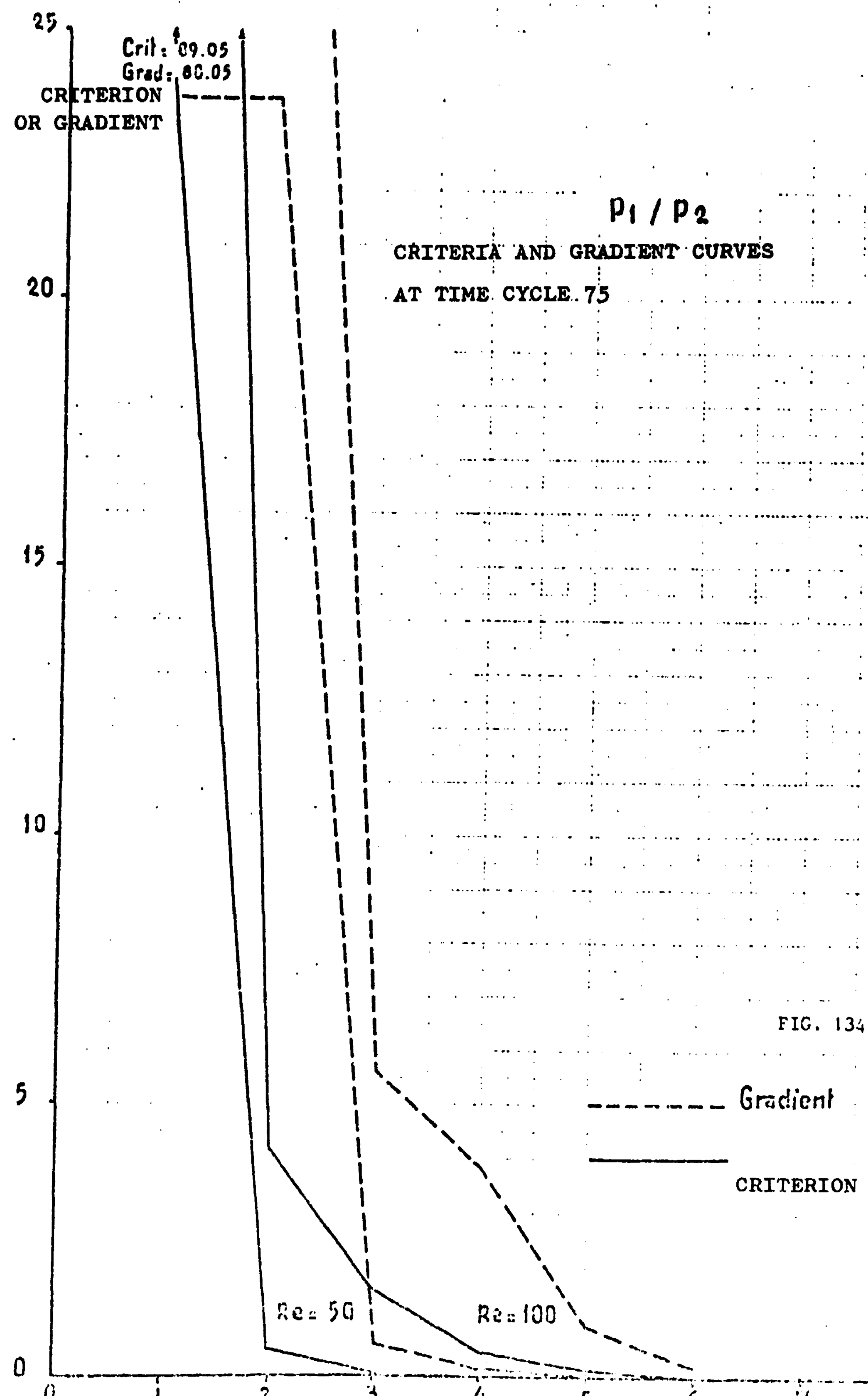

P_1 / P_2

CRITERIA AND GRADIENT CURVES AT TIME CYCLE 75

/231

FIG. 134

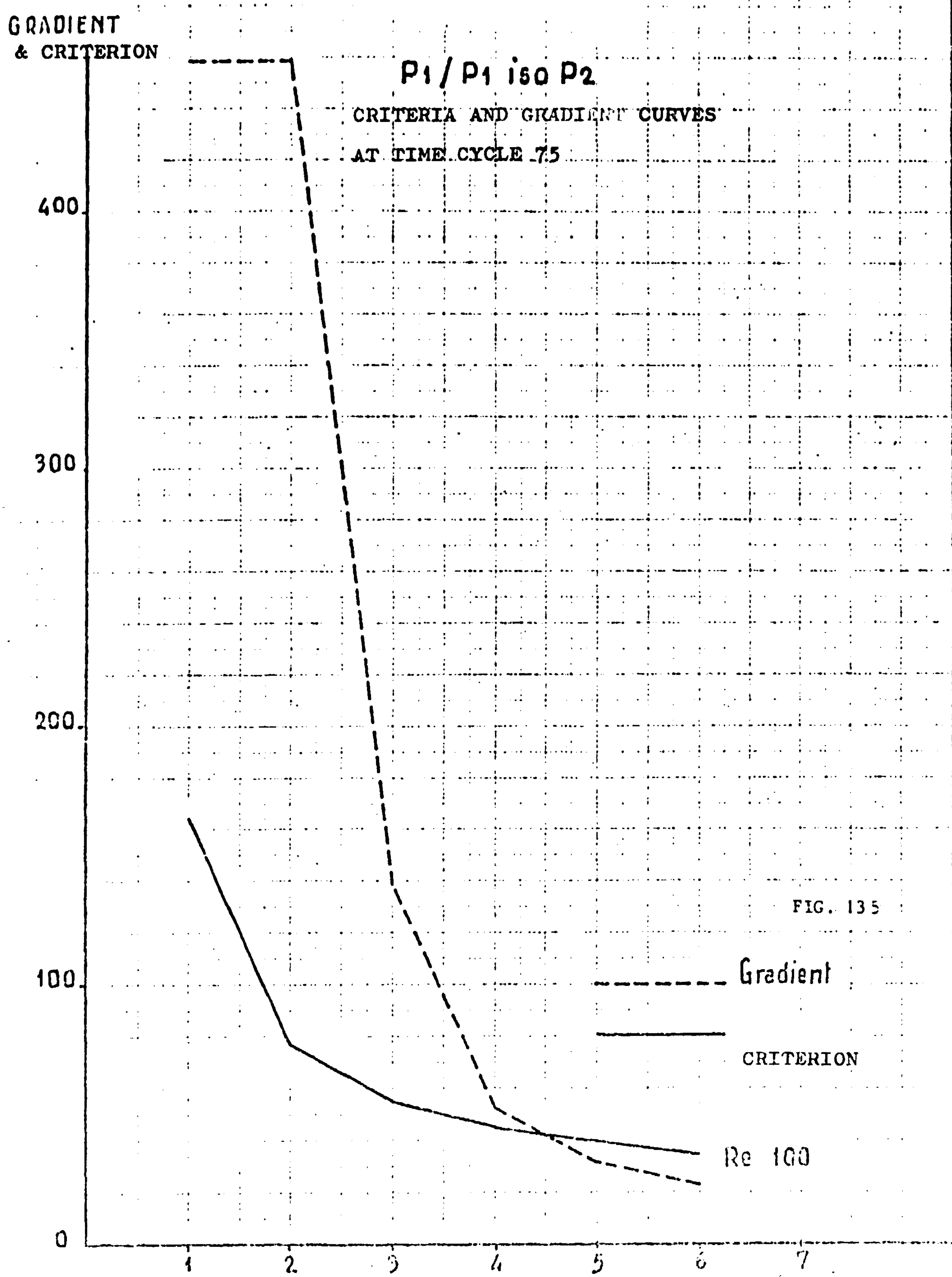
GRADIENT
& CRITERION
400
300
200
100
0
1
2
3
4
5
6
7
P1 / P1 iso P2
CRITERIA AND GRADIENT CURVES
AT TIME CYCLE 75
Gradient
CRITERION
Re 100

FIG. 135

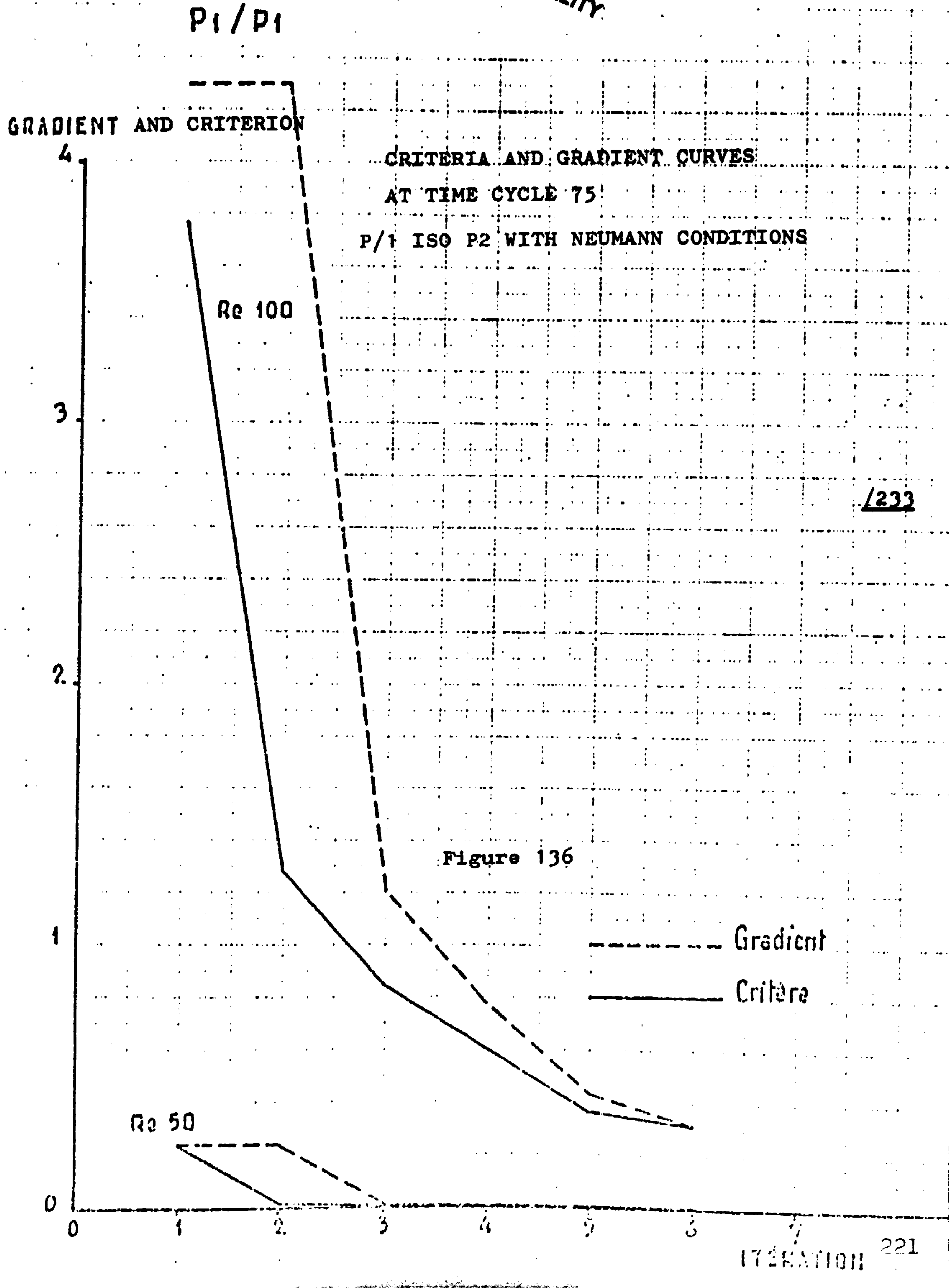

Figure 136

/233

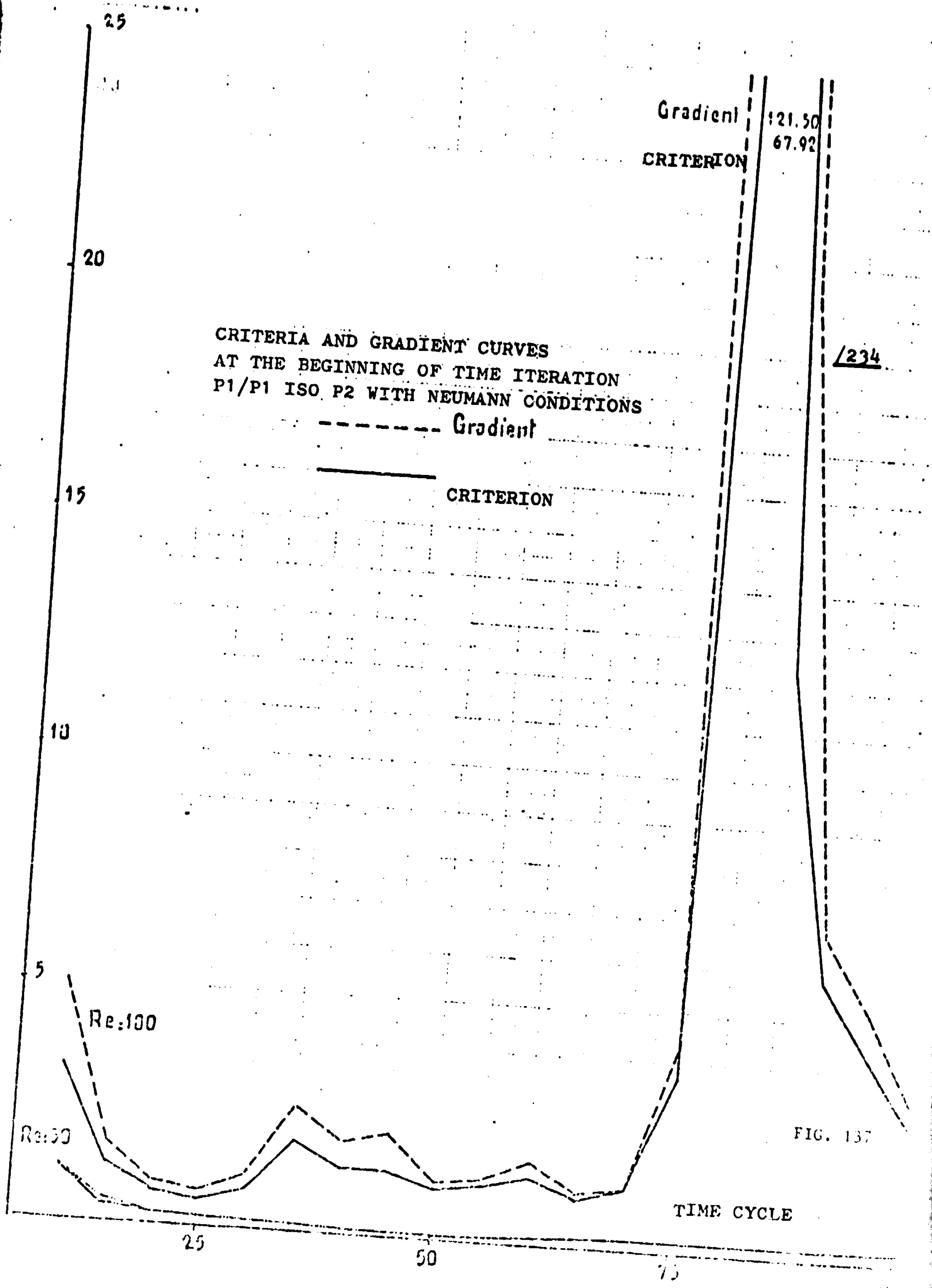
25
20
15
10
5
Gradient
CRITERION
121.50
67.92
/234
CRITERIA AND GRADIENT CURVES
AT THE BEGINNING OF TIME ITERATION
P1/P1 ISO P2 WITH NEUMANN CONDITIONS
Gradient
CRITERION
Re:100
TIME CYCLE
25
50

FIG. 137

Finally, it may be observed on figure 137 that, in code P1P1 ISO P2, the Neumann type condition downstream facilitates the measurement of the alteration in configuration (smaller jumps of criteria and of gradients). /_8

The comparison of the process computation times between the two codes, brings to light a ratio of 2 in favor of P1/P1 ISO P2, this figure is directly related to the amount of calculation for the creation of various second members according to the approximation P_k, k=1 or 2 through time cycles and especially to the amount of quantified Laplacien Choleski coefficients (as the band width m2 of P2 is about 2 times higher than for band width m2 of P1/P1 ISO P2. In the case under consideration m2 = 129, m1 = 68, the corresponding core space is 987 K for the case P2 and 540 for the case P1.

We shall see that, given the Reynolds range considered in industrial applications, the compromise P1/P1 ISO P2 is a sensible choice.

12.3.5.4. The Industrial Configuration i=40°, Re = 250 /235

The operation of the air inlet, proposed by ONERA (refer to H. WERLE (503) around/in which is simulated the separated flow, has been studied experimentally in the form of visualizations with Reynolds $\simeq .10^4$ The case computed (Re = 250) ; i=40°) is composed of 6893 degrees of freedom. Triangulations $\mathcal{T}_h$, $\mathcal{T}_{h/2}$ created automatically by MODULEF (35) are shown on figures 138-139. The density of the nodes near the air inlet is shown on enlargements 140-141. The large amounts of factorized discrete Dirichlet matrices requires the use of auxiliary disks with a Choleski "shyline" FLIP-FLOP method escribed in MODULEF (35).

Due to the high incidence, a parabolical flow $\varepsilon = .6$ inside the air inlet (percentage of $|\vec{u}_\infty|$) applied in order to prevent a possible blocking and to suck the eddies formed at the air suction inlet.

100 time cycles calculated with a time step $\Delta t = .05$ have required several hours of process time.

Figures 142 (a)-(f) (velocities), 143 (a)-(f) (iso-pressures) show the formation, the development and the ejection of several eddies inside and outside the air inlet. It may be seen on figure 144 (f), which represents the streamlines, the existance of 5 eddies with alternating signs, of which 2 are inside the air inlet spreading along the entire height and sliding slowly toward the aspirator ! It may also be observed that the streamlines in front of the air inlet are drawing closer together, which will effect the quality of the approximation, (density of nodes) the more the Reynolds is higher.

One may have a better idea of the complexity of the flow by looking on figure 146 at the superposing of the time cycle 100 of 142-f, 143-f, 144-f.

$\mathcal{C}_h$ TRIANGULATION AROUND AN INLET AT LARGE INCIDENCE

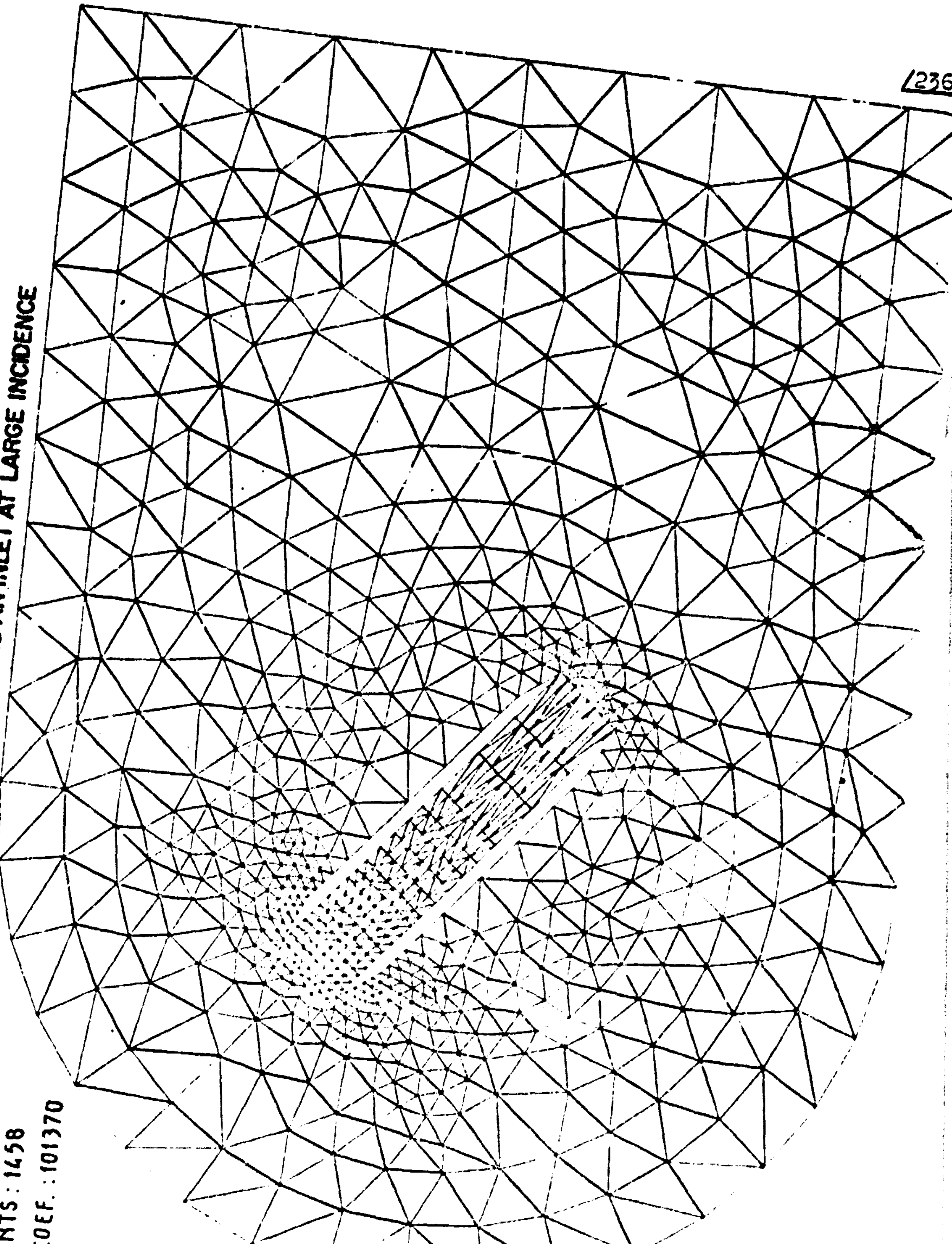

795 NODES
ELEMENTS : 1458
CHOL. COEF. : 101370

Figure 138

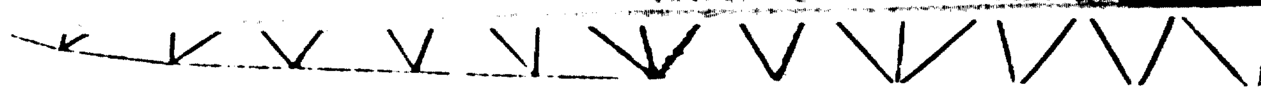

ℭh TRIANGULATICN AROUND AN INLET AT LARGE INCIDENCE

ɜDES : 3049
EMENTS : 5832
IOL COEF. : 314685

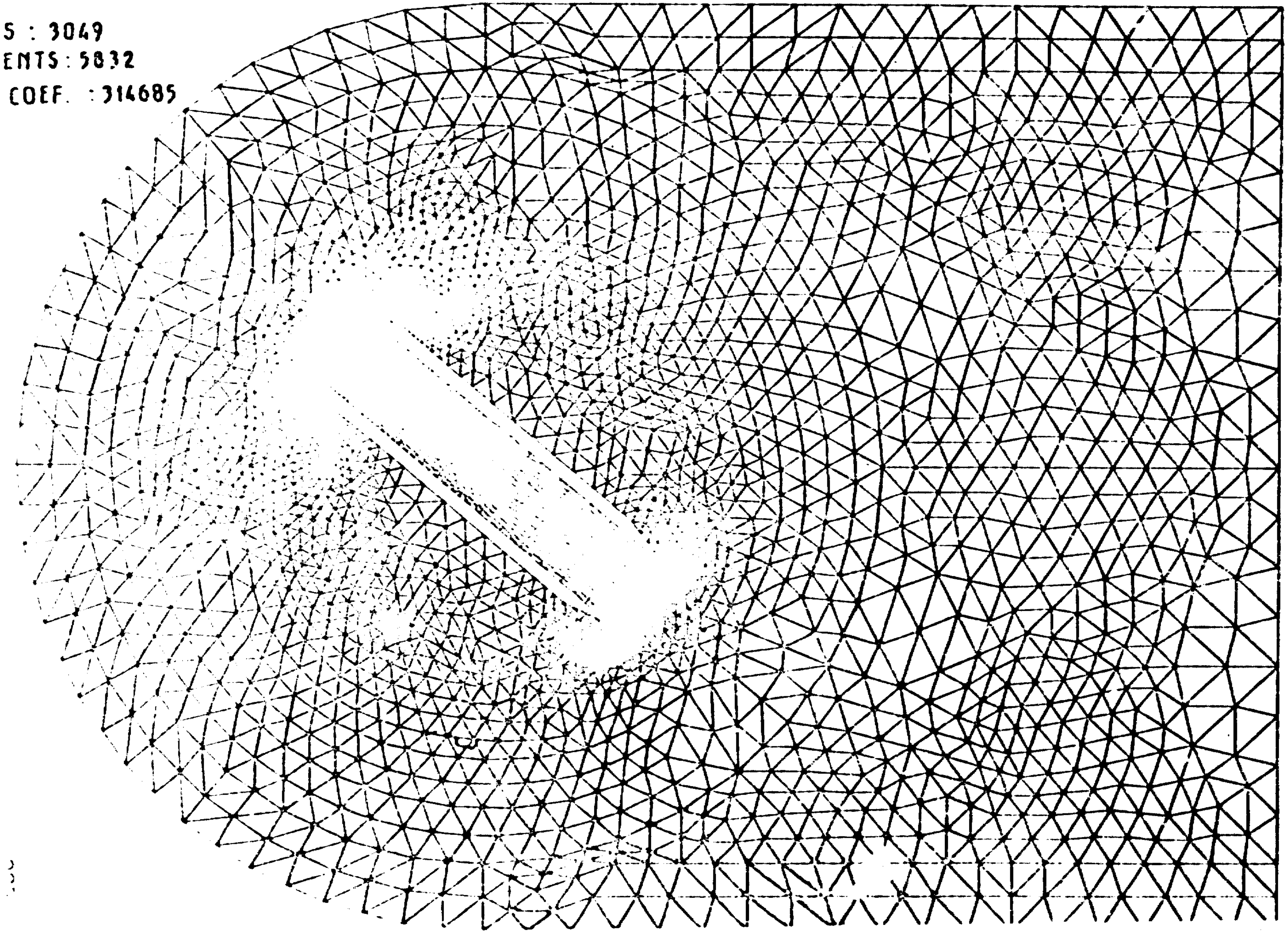

$\mathcal{C}_h$ ENLARGEMENT AROUND AN INLET

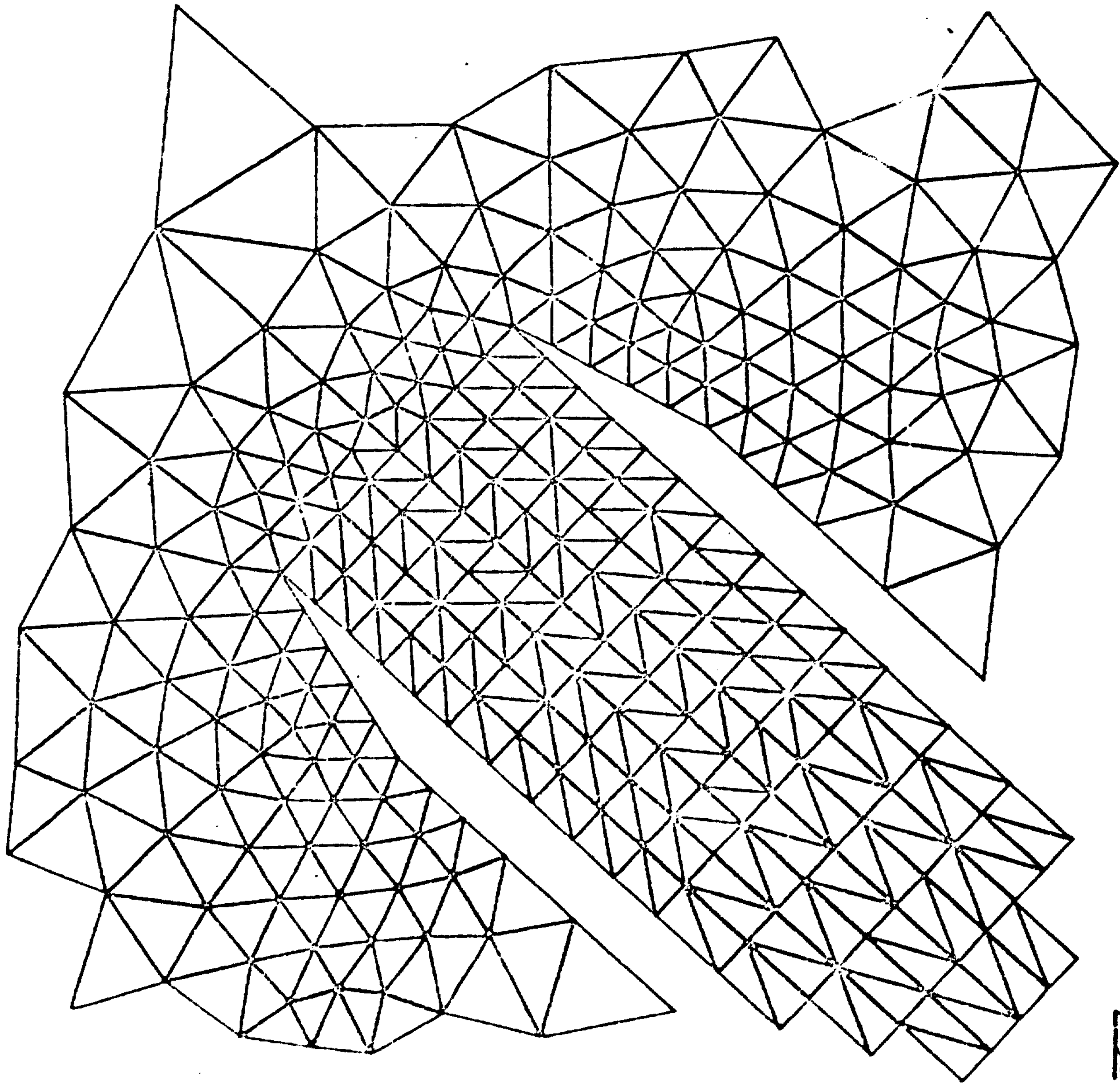

/239

$\tilde{\mathcal{C}}_h$ ENLARGEMENT AROUND AN INLET

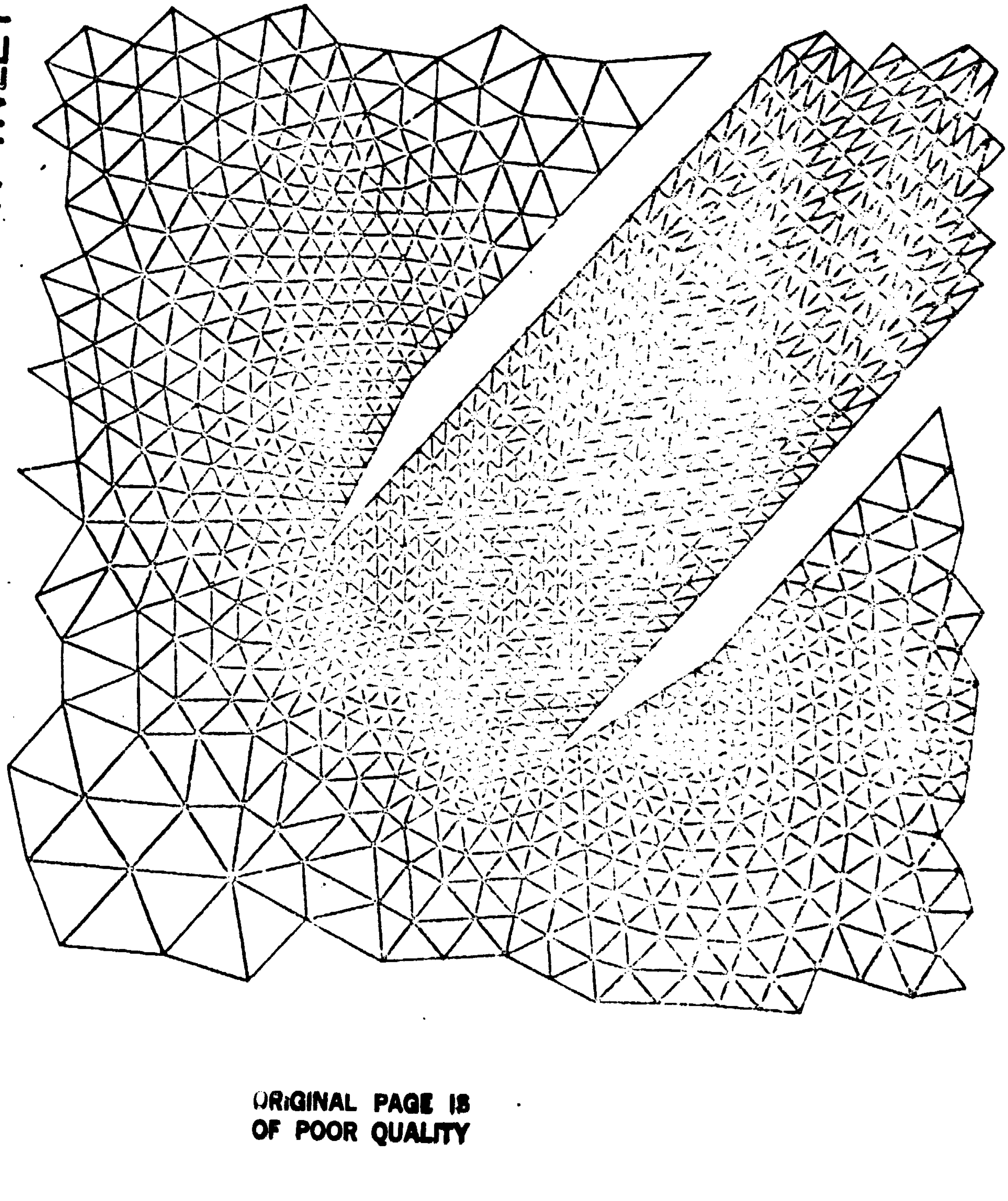

$\alpha = 40°$

FLOW AROUND AN AIR INLET - FIELDS OF VELOCITIES

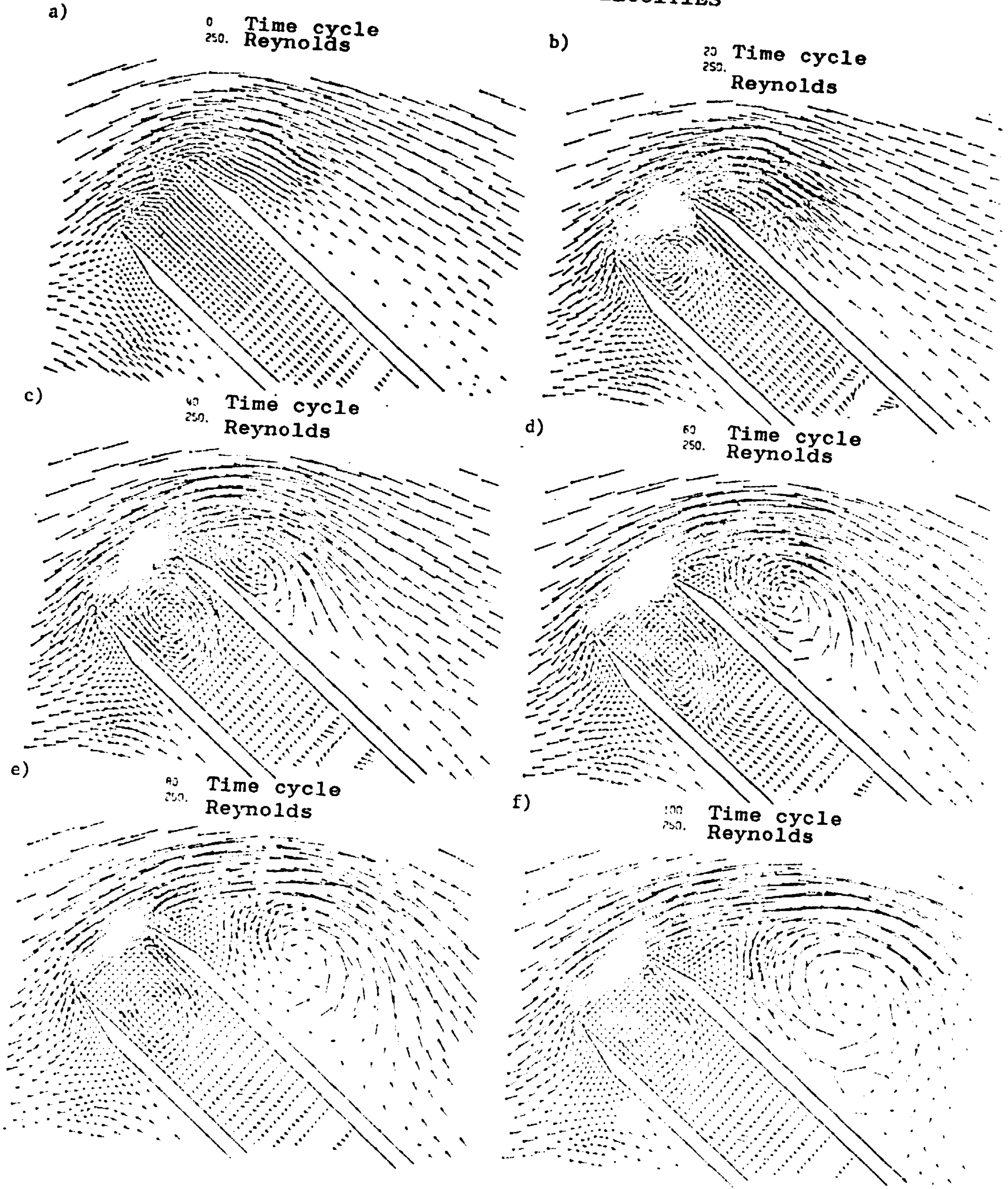

ORIGINAL PAGE IS
OF POOR QUALITY

Figure

α = 40°

FLOW AROUND AN AIR INLET - ISO-EDDY /241

a)

0 Time cycle
250. Reynolds

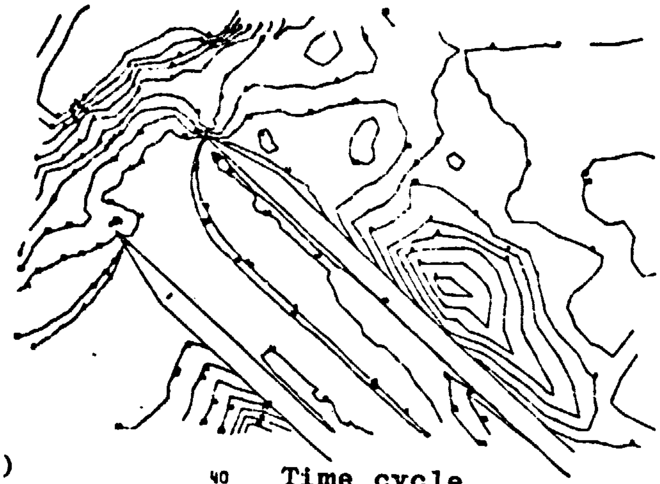

b)

20 Time cycle
250. Reynolds

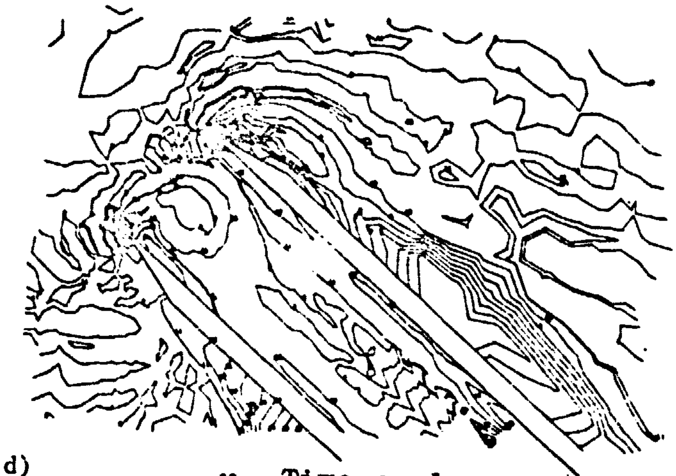

c)

40 Time cycle
250. Reynolds

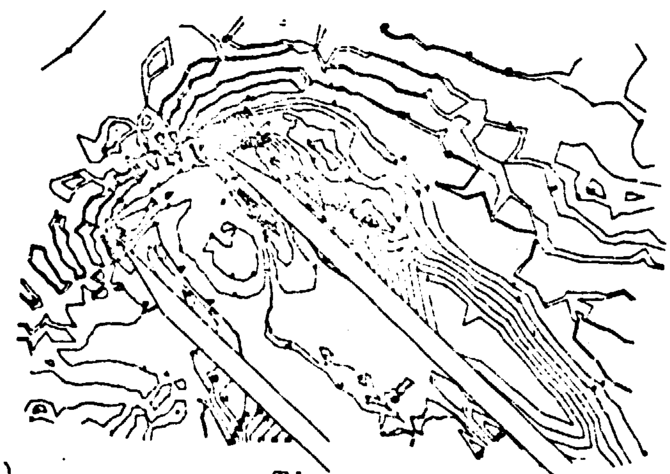

d)

60 Time cycle
250 Reynolds

e)

80 Time cycle
250. Reynolds

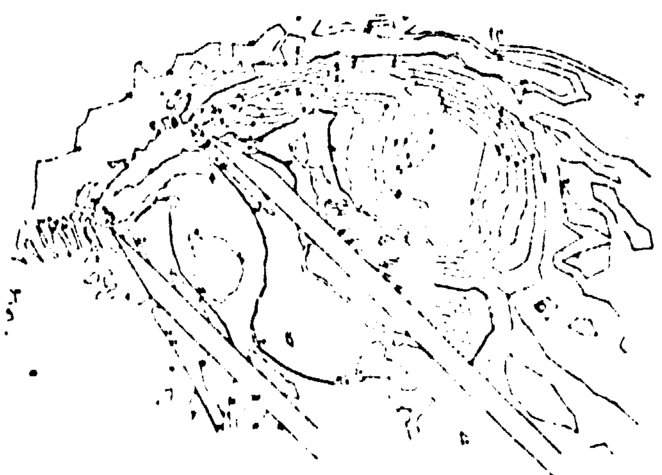

f)

100 Time cycle
250. Reynolds

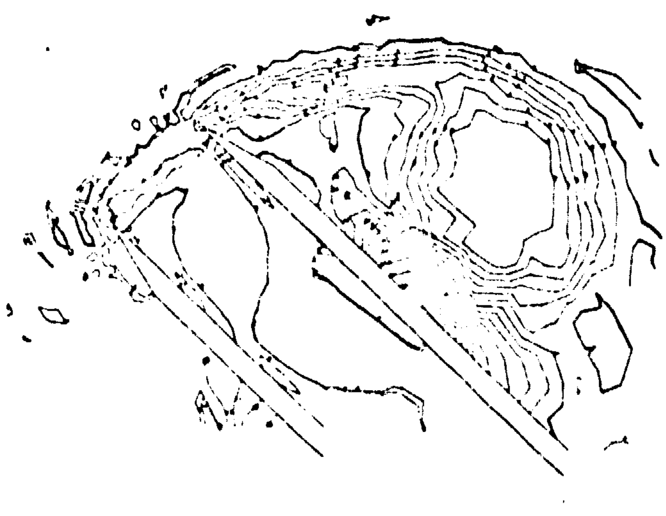

/242

$\alpha = 40°$

FLOW AROUND AN AIR INLET - STREAMLINES

a) 0 Time cycle
250. Reynolds

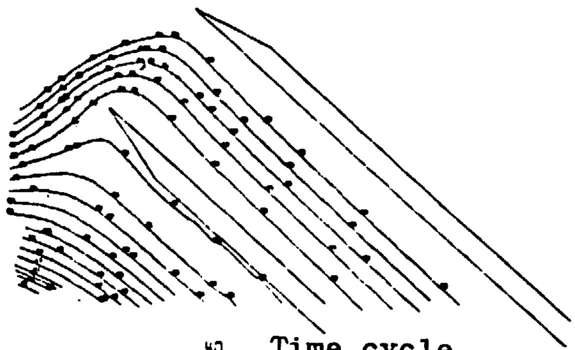

b) 20 Time cycle
250. Reynolds

c) 40 Time cycle
250. Reynolds

d) 60 Time cycle
250. Reynolds

e) 80 Time cycle
250. Reynodls

f) 100 Time cycle
250. Reynolds

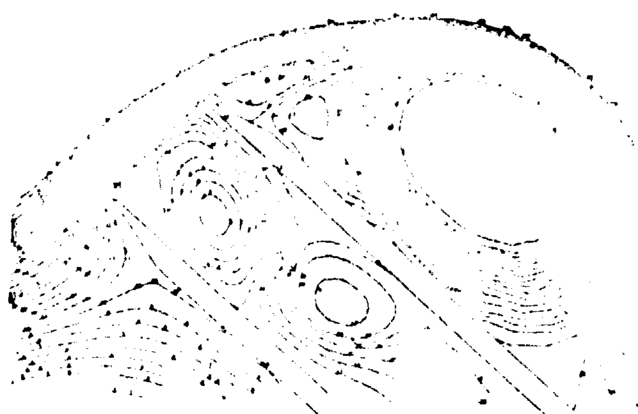

$\alpha = 40°$

FLOW AROUND AN AIRIINLET - ISO-PRESSURE

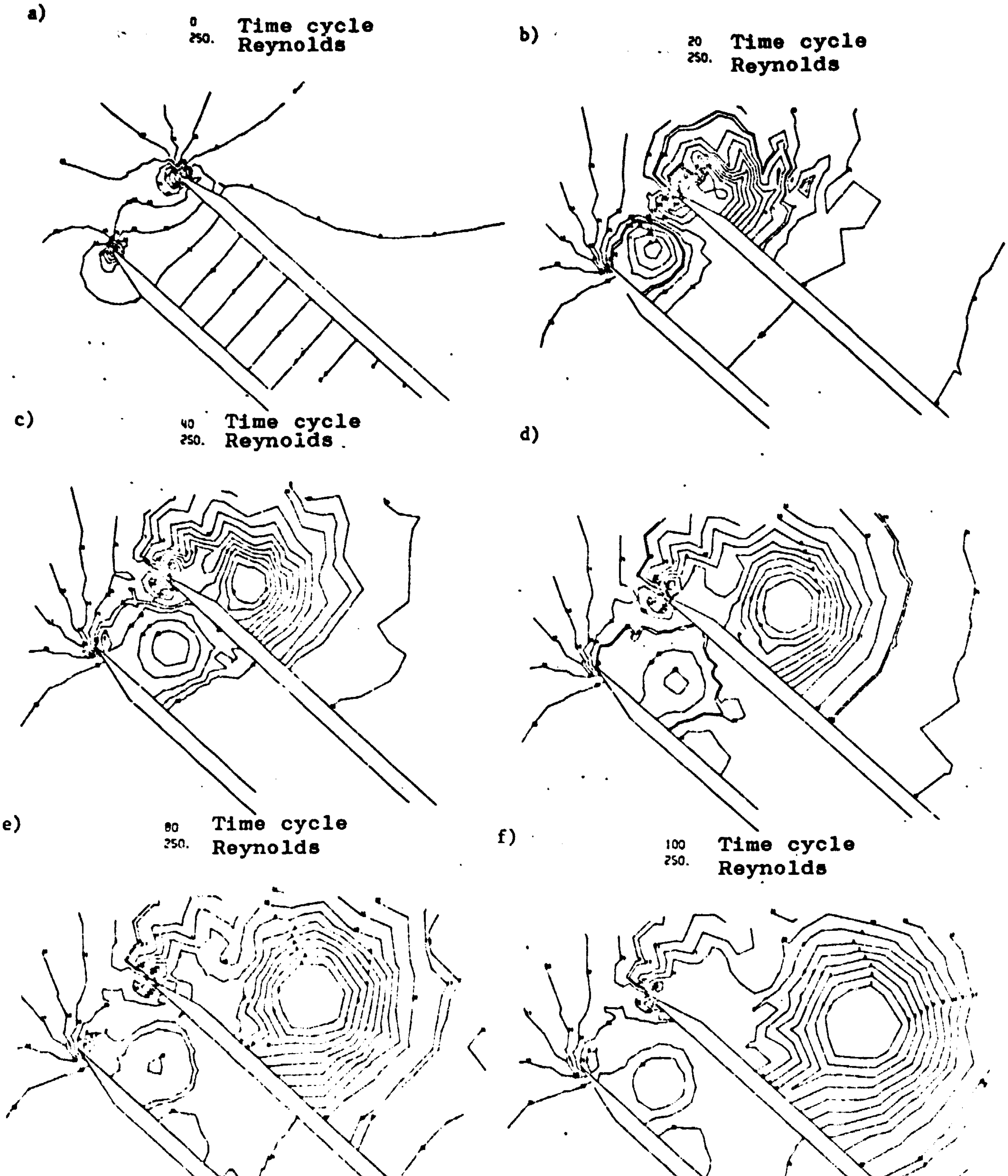

Figure 145

/244

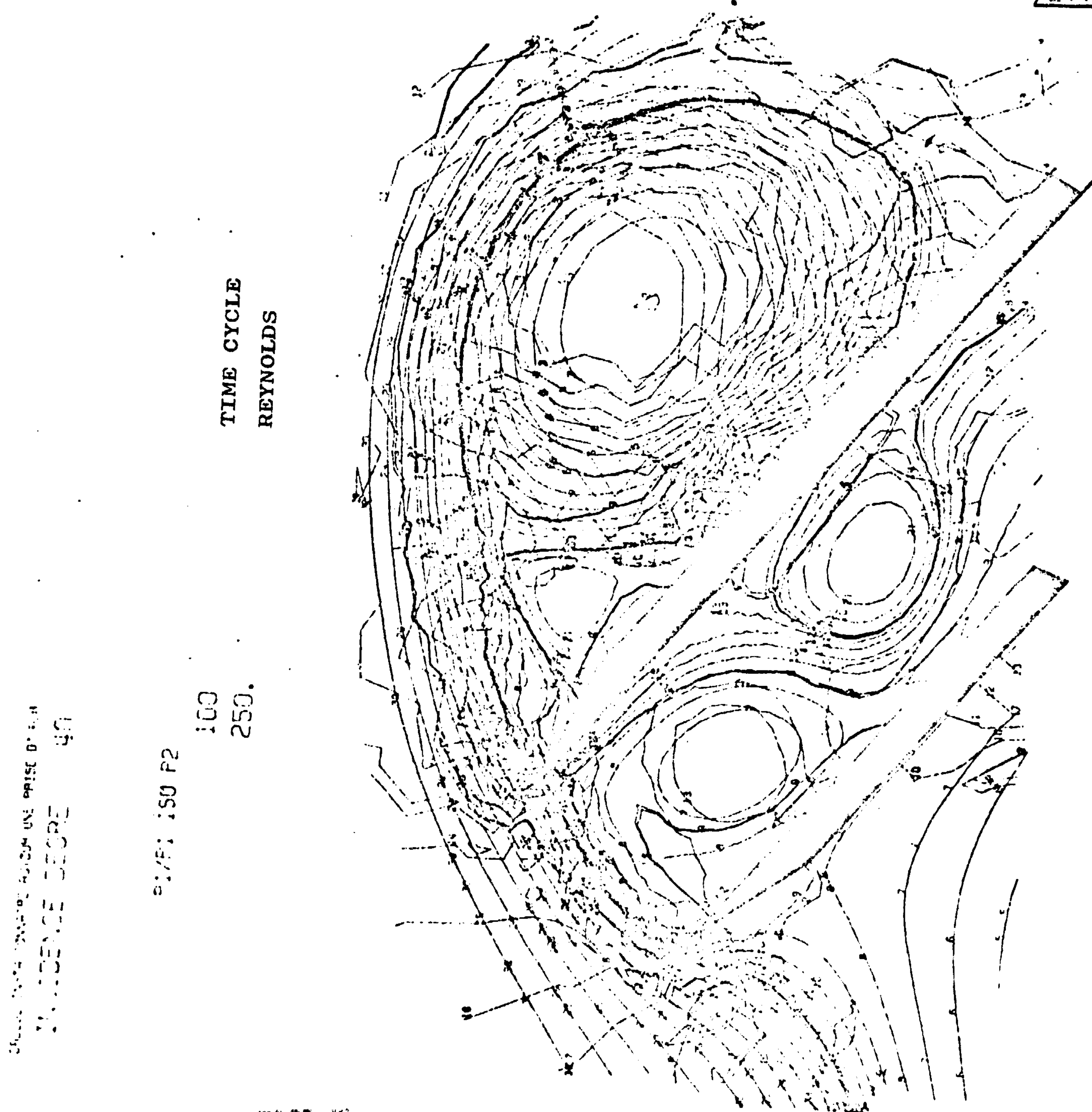

ORIGINAL PAGE IS
OF POOR QUALITY

Fig. 146

12.3.6. The 3-D Sphere /245

The incompressible viscous fluid flow around a sphere with diameter 1 proves to be an interesting informatics test to check the satisfactory operation of a 3-D Navier-Stokes code from the symmetry properties of the flow, the obstacle and the tetrahedron formation.

The conditions applied to the boundaries are the Dirichlet type

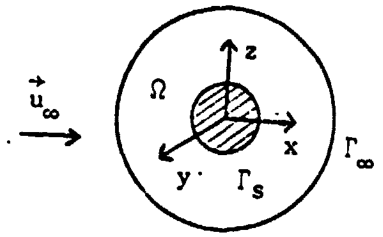

$$\vec{u}|_{\Gamma_\infty} = \begin{vmatrix} 1 \\ 0 \\ 0 \end{vmatrix} \; ; \; \vec{u}|_{\Gamma_s} = \begin{vmatrix} 0 \\ 0 \\ 0 \end{vmatrix}$$

Informatics problems due to the 3-D and to the analysis of results on this example are immediatly sufficient. The domain of computation Ω is formed into a tetrahedron containing $\sim$624 elements and 154 nodes in P1 ($\mathcal{C}_h$), , decomposing in P1/ISO P2 ($\mathcal{C}_{h/2}$, into 4992 elements as on figure 147 and into 970 nodes (reaching thus 2000 degrees of freedom the solution $(\vec{u}_h, p_h)$ obtained by the optimal control.

Minimization of the band width proves to be an essential preliminary step if we want to work with factorized Dirichlet matrices having a size acceptable in the main core, requiring 60' process and 1900 K of core space.

Since the time step is $\Delta t = .1$, 40 time cycles at Re = 100 is sufficient to induce behind the sphere a <u>separated</u> zone shown on figure 148.

Visualization of the return velocities is shown from the side and globally by hachuring the tetrahedrons, of which the component of the velocity $\vec{V}$ is negative.

12.3.7. Swept-back Wing at Large Incidence /248

In this <u>industrial</u> example, we have taken into consideration the 3-D flow of an incompressible viscous fluid at Re = 200, around a complete left-right idealized wing, placed at 30° incidence.

The triangulation $\mathcal{C}_h$ consists of 2060 tetrahedrons and 560 nodes. Due to the importance of the factorized Dirichlet A matrix ($A = LL^t$, A constructed from an approximation in P_1), 74562 coefficients, we are focusing in a first phase on a linear approximation of the velocity $\vec{u}$ on $\mathcal{C}_h$.(A_k^V constructed like A). We are assuming that there are enough nodes in $\mathring{\Omega}_h$ for us to solve (E_h).

The calculation (70' process) consists of 40 time cycles, with the time step being $\Delta t = .1$, the number of control iterations at

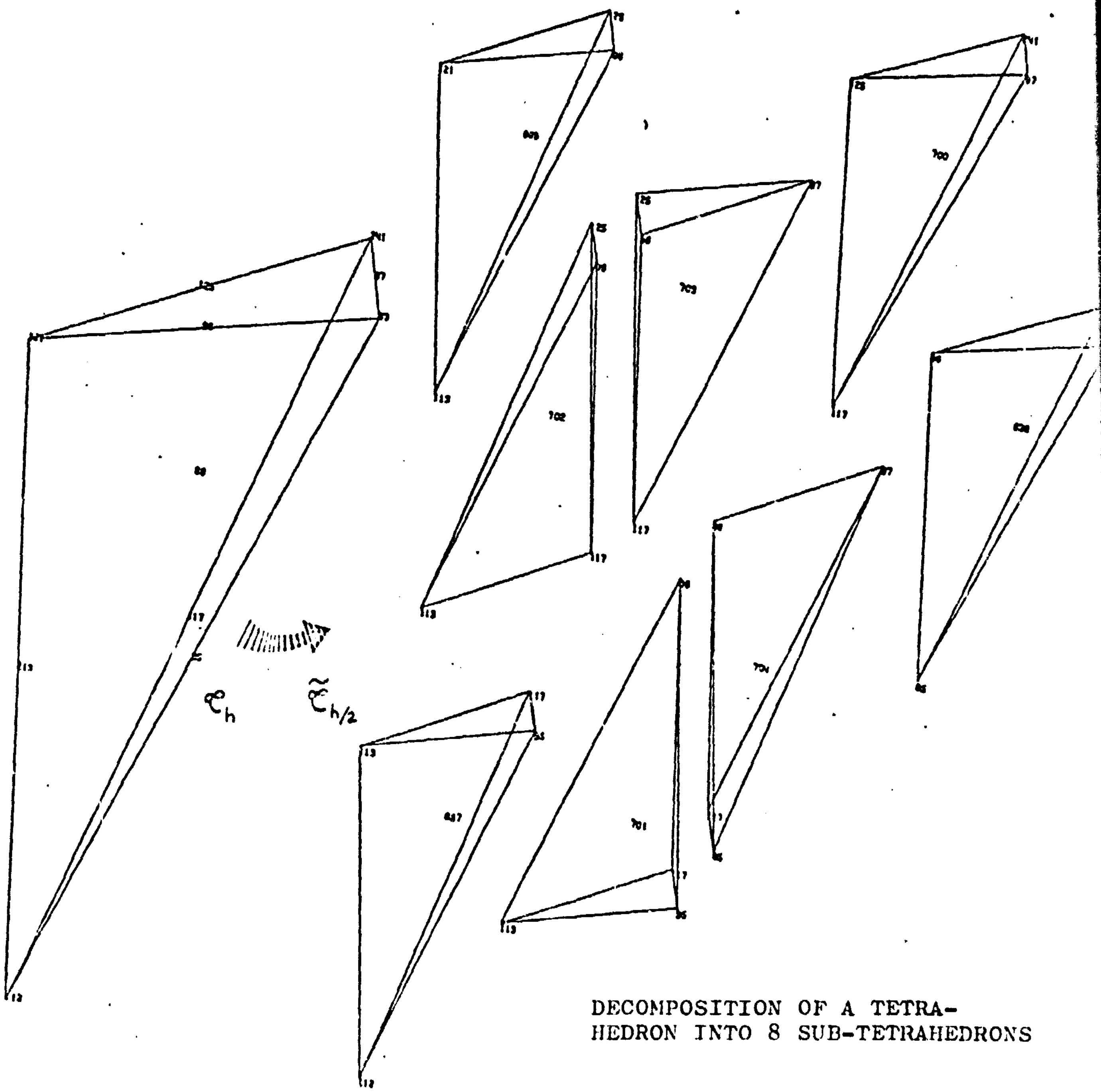

DECOMPOSITION OF A TETRA-
HEDRON INTO 8 SUB-TETRAHEDRONS

Fig. 147

SEPARATED FLOW AROUND A SPHERE FINITE ISO P2 ELEMENT METHOD WITH OPTIMAL CONTROL THEORY

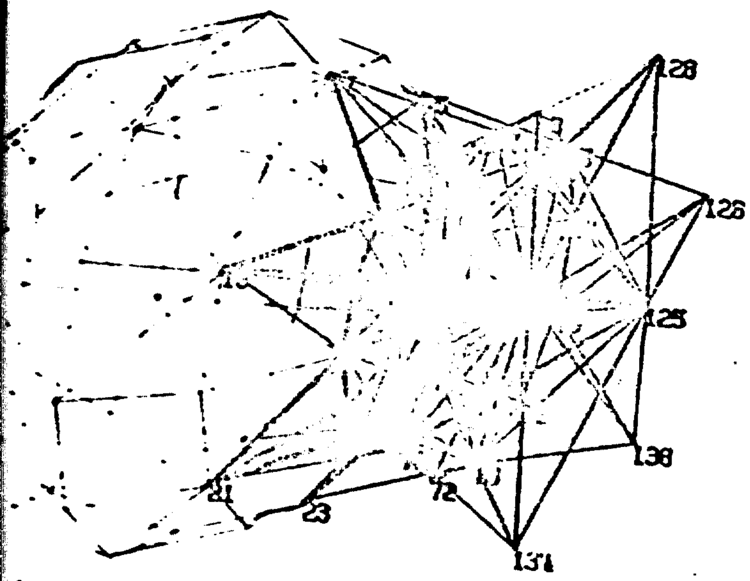

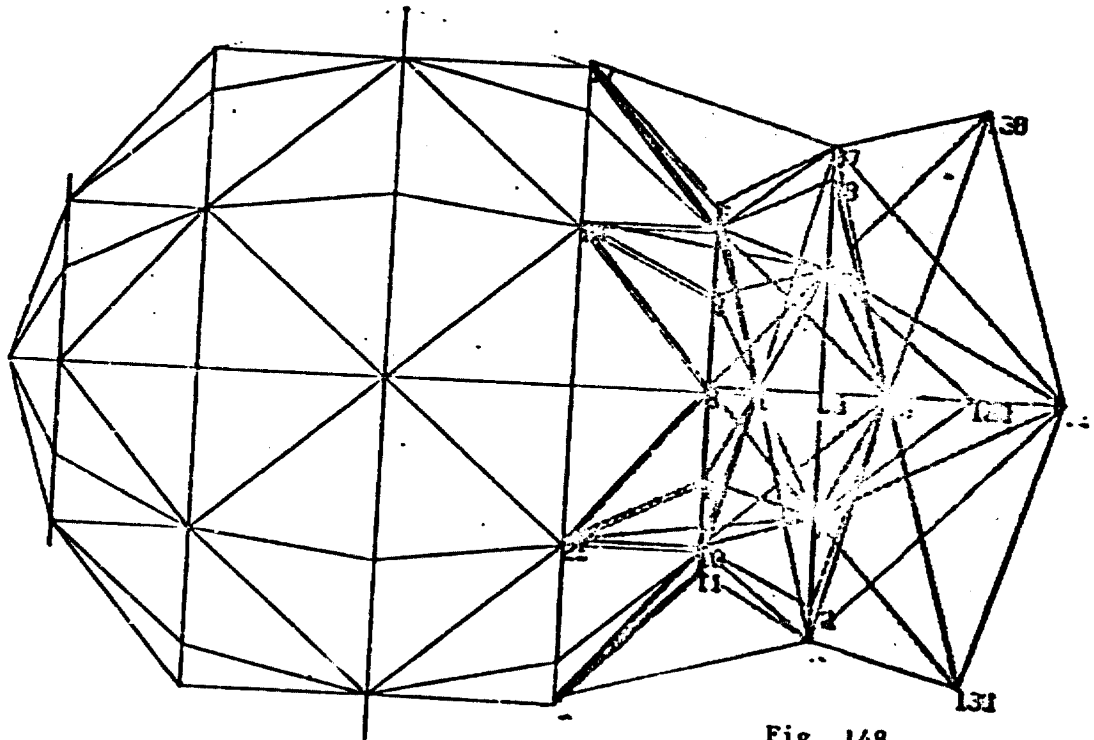

Fig. 148

/24

each cycle being 4. The use of auxiliary disks for solutions $AX = b$ brings us to consider two different computer times : one time t_1 of process for the computation volume itself and one time t_2 machine space due to external transfers to the main core $t_2 = nt_1$ with $1 \leq n \leq 10$, highly dependent on the informatics environment at the moment of computations. /248

The solutions $(\vec{u},p)$ at various time cycles are registered on disk to be analyzed after the computation. Visualizations make it possible to identify the separated zones which are obtained in the following manner.

1. Several angles are plotted (views from the front, side, rear from above, below, in perspective) at various time cycles, the set of tetrahedrons $T \in \mathcal{T}_h$ in which the component u of velocity $V = (u,v,w)$ is negative. The support of the entire wing is represented by a plotting with a different color, making it possible to locate the separated zones and to evaluate the intensity of them (figure 149 (a) (b) (c)).

2. From a separated zone, we can plot the lines upon which the vorticity is applied (vorticity tube lines) to visualize the eddy intensity (A. MARROCCO (51)).

Depending on the starting point (end of the wing, for example), we may represent, in the separated zone, the complex path of the fluid particles. /249

Various views of the three dimensional eddies are shown on figures 150 (a)-(d), 151 (a) (c) corresponding to two integrations with different initial conditions.

On figure 150 (a)-(d), we are focusing on eddies which escape at the end of the wing (left or right), whereas on figure 151 (a)-(c), we are placed initially in a less turbulent separated zone. It may be stated that the two separated zones interact, since the integration of the vorticities from the wing-right provides trajectories leading to the separated zone of the wing-left via the socket.

The numerical integration of the lines is obtained by the following process : given a point Z_o of the separated zone $Z_o \in T_o$ of $\mathcal{T}_h$ we calculate the vorticity $\vec{\omega} = \nabla \wedge \vec{u}$ constant in T_o, the velocity $\vec{u}$ being P_1. Since we are looking for the geometrical intersection Z_1 of $\vec{\omega}$ with fronts $(F_i^{T_o})_{i=1,4}$ of T and a point Z_o at Z_1. The front F_k found gives a new tetrahedron $T_1 \in \mathcal{T}_h$ (close to T_o in the direction of F_k). We calculate the new vorticity $\vec{\omega}_1$ of element T_1 and so forth...

3D NUMERICAL SIMULATION OF VISCOUS SEPARATED FLOW AROUND A IDEALIZED WING

Reynolds 200 - Incidence 30°

/25

The triangles show the domain where the u-component of the velocity is negative.

a)

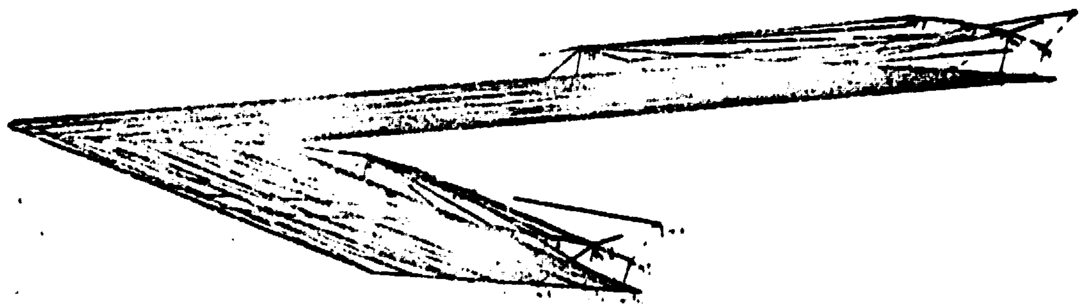

Time cycle: 20

b)

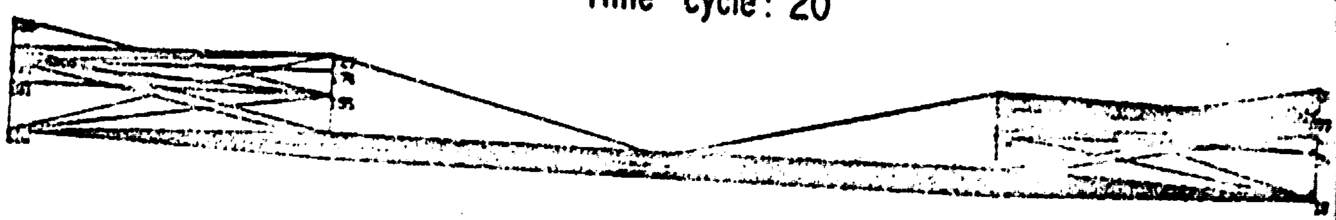

Time cycle: 40

c)

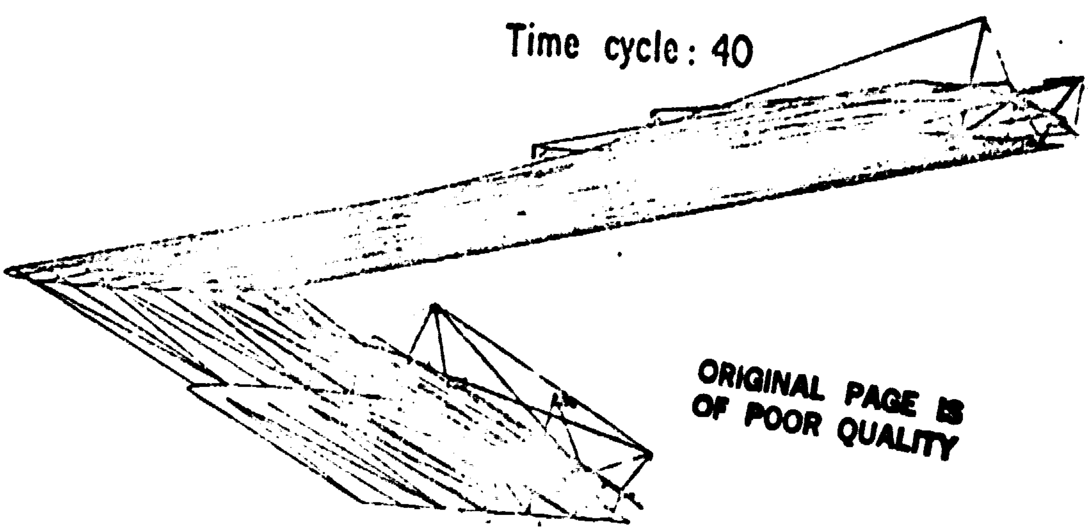

Fig. 149

VORTICITY TUBE LINES IN THE REVERSE DOMAIN

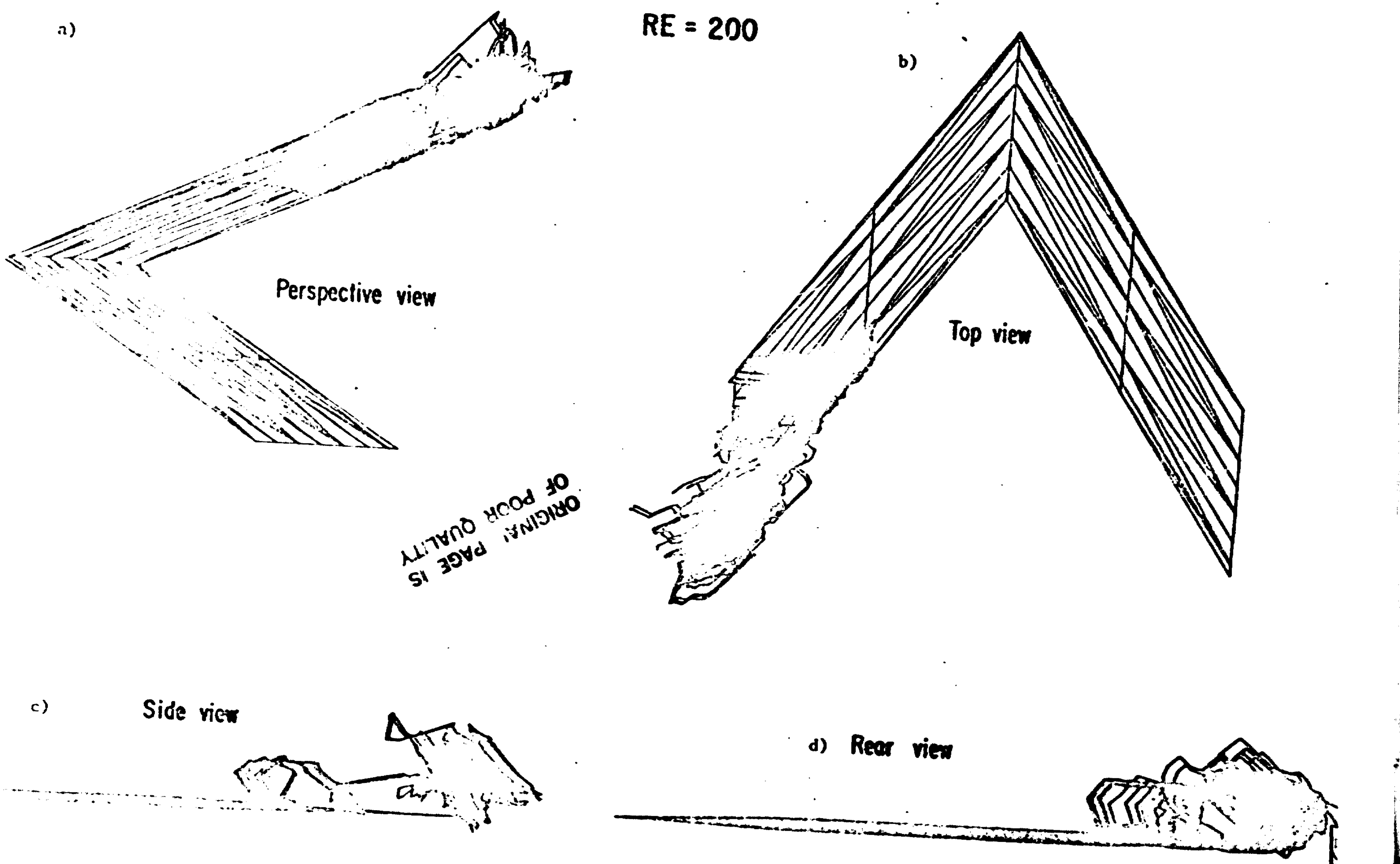

Figure

DIFFERENT VIEWS OF VORTICITY LINES IN THE REVERSE DOMAIN

a)

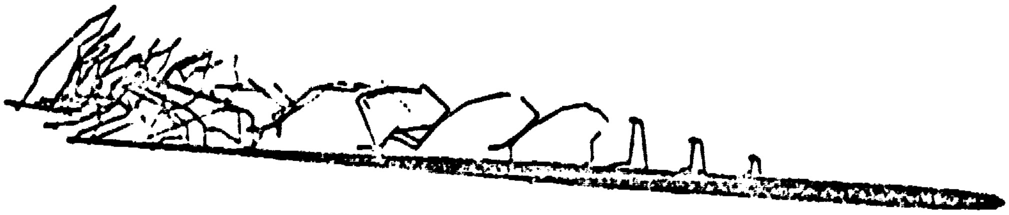

Side view

b)

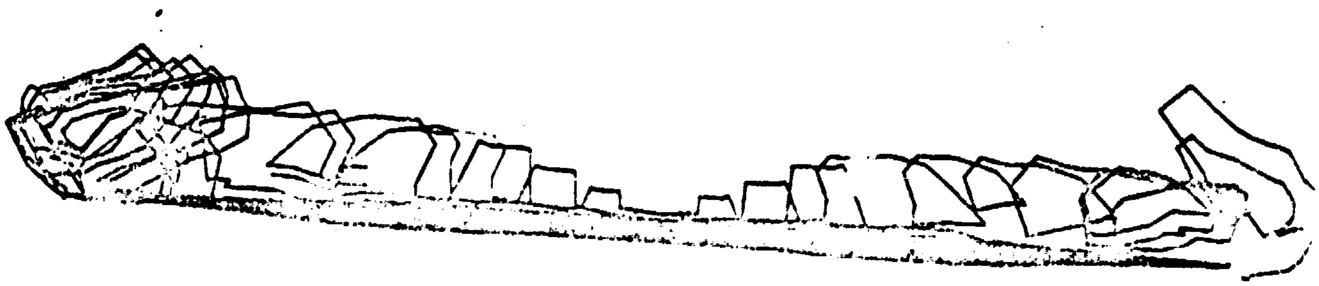

Rear view

c)

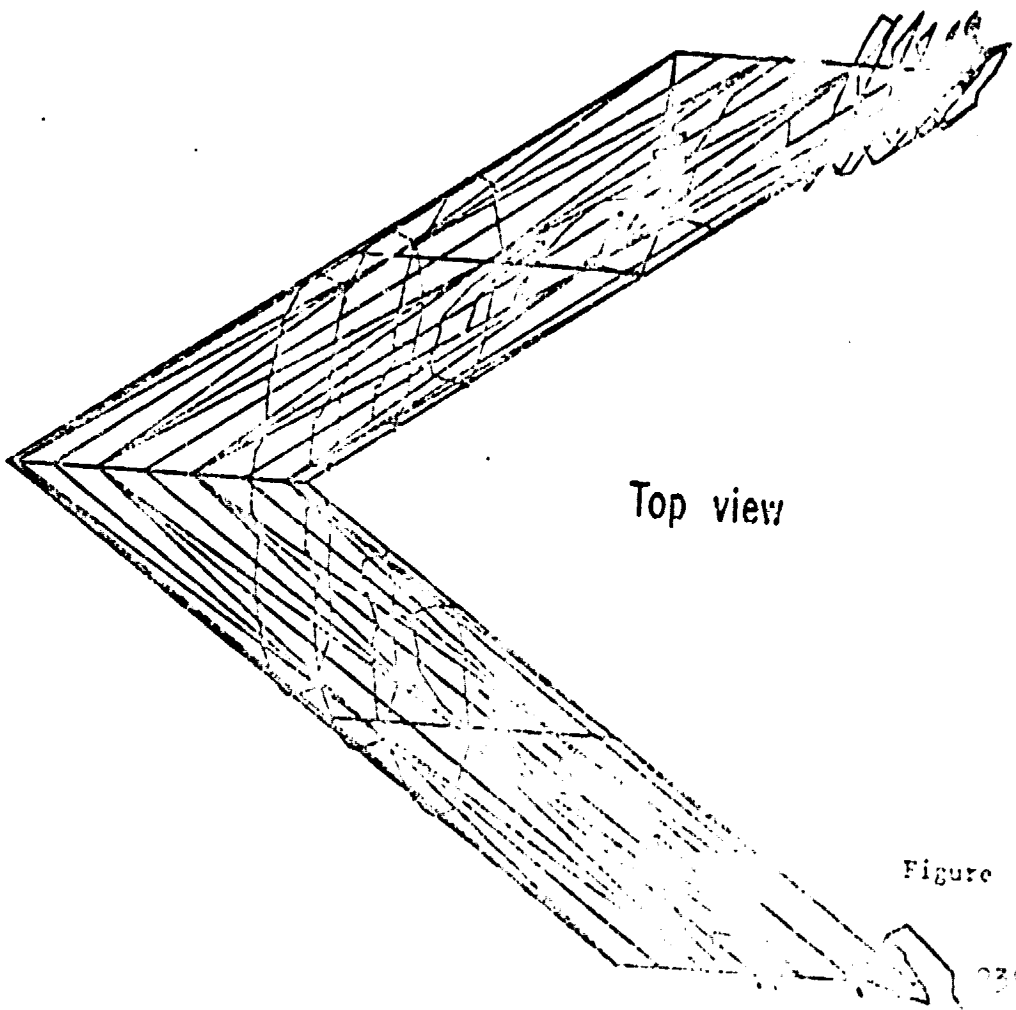

Top view

Figure [illegible]

12.4 Data Processing Efficiency for Functional Least Squares Algorithms Using Auxiliary Operators or Metrics /253

12.4.0. Characteristics of a Preconditioned Computation

The examples of 3-D transonic and incompressible viscous flows have demonstrated the need for auxiliary disks which serve to memorize the factorized Dirichlet matrices L ($\simeq 5.10^6$ coefficients). These matrices are read numerous times during the descent-climbs of a solution $LL^tX = B$ and result in excessive memory use time (5 times more than process time).

It may be recalled that one optimal control iteration requires 5 Dirichlet solutions in the transonic case and 35 Dirichlet solutions in the Navier-Stokes case.

The objective of these examples is to show that preconditioning operators $L_{d/100}$, constructed in chapter 11, make it possible to solve entirely in main core a problem which initially exceeds the computer capacity. We present two ways to use conditioning operators in an optimal control problem.

1) The matrix H^1 is kept in the penalty (344) or B plays the role of the discrete Laplacien

$$\min_{\Phi \in R^n} \{E^t BE \mid \underset{(*)}{BE = R(\Phi)}\} \tag{344}$$

but, $\tilde{B}_{d/100} = \tilde{L}_{d/100}\, \tilde{L}^t_{d/100}$ is used as auxiliary operator of Laplacien in the sense of O. Axelson to solve (*). In this case, the convergence speed of the algorithm is not slowed down.

2) The metric H^1 is approached in formulation (345) by $\tilde{B}$, $\tilde{B}$ plays, then, the role of the auxiliary metric.

$$\min_{\Phi \in R^n} \{E^t \tilde{B} E \mid \underset{(**)}{\tilde{B}E = R(\Phi)}\} \tag{345}$$

but in this case, it shall be fair to choose percentages of $\tilde{B}_{d/100}$ such that $d/100 \geq d^o/100$ & so the algorithm does not slow down excessively. It may be pointed out, on the other hand, that (**) has an extremely fast solution : a descent-climb of one operator $L_{d/100}\tilde{L}^t_{d/100}$ representing, for example, 20 of the Laplacien if d=20. The choice of d in case 2 is the better compromise between (345) and the possible size of the computer. Examples of $\tilde{L}_{d/100}$ are shown on figure 152. Attention shall be brought to the proximity of non zero coefficients of $\tilde{L}$ d-100 kept to those of A.

12.4.1. Auxiliary Operators and Metrics in Transonic

/254

12.4.1.1. 2-D Laplaciens Preconditioned by $\tilde{L}\tilde{L}^t$

In a first phase, it is worthwhile to test a conjugate gradient algorithm to solve the problem (346) by the finite elements method.

$$\min_{\phi \in R^N} \{\frac{1}{2} \phi^t A \phi - F\phi\} \tag{346}$$

in which $\tilde{A} = \tilde{L}\tilde{L}^t$ is introduced as an auxiliary operator of the Laplacien operator A in the sense of O AXELSSON (32).

is constructed from the factorization L (11267 coefficients of A and $L_{d/100}$ represents various percentages of $\tilde{L}$ constructed in accordance with the procedure described in 11.

We have plotted on figure 153 the number of iterations required to solve (346) with a specified accuracy $\varepsilon = .10-6$, by using $L_{d/100}$ and $\tilde{L}'_{d'/100}$ constructed in (324) (325) for different d's. We may note the interest of the interval (5%, 25%) for memory decrease, and compare the convergence velocity with other auxiliary operators such as the Van der Vorst operator $\tilde{L}_{VDV}$, which does not require factorization L or still $\tilde{L}_{...}$ constructed by keeping only the coefficients very close to L and representing a small percentage (20%) in 2-D. At both ends of the curve, we find the solution of (346) in one iteration for $\tilde{L}_{100/100}$ and the standard conjugate gradient, without preconditioning.

On figure 154, we have superposed two curves $\tilde{L}_{d/100}$ $\tilde{L}'_{d/100}$ as a function of the number of iterations with $\tilde{L}$ and $\tilde{L}'$ constructed in (324), but from two different renumberings of the Cuthill-McKee algorithm : L contains 11267 non zero coefficients and L' 13569. The agreement of the two curves may be verified when working with iso-percentages on the two auxiliary operators.

12.4.1.2. 3-D Laplacien Preconditioned by

The solution of (345) has been also found on an industrial configuration with 5328 degrees of freedom, of which the Choleski matrix L contains 1.5 D^6 coefficients and could not be held in the main store.

Figure 155 describes the number of reasonable iterations when operators $L_{d/100}$, with $d/100 < 20/100$ are used in the main store of the computer. We may note the number of excessive iteratio (1462) of the standard conjuage gradient when (346) must be sol several hundreds of times.

12.4.1.3. Transonic Optimal Control 2-D With Metric H^1 and Auxiliary Operator $\tilde{\tilde{L}}L^t$.

The approach 12.4.1.1 is used to solve the state equation (*) of (344)

$$BE = R(\phi) \qquad (*)$$

by preconditioning the conjugate gradient algorithm by $\tilde{B}_{d/100}$. We shall point out the safety of the algorithm (344) which converges in N iterations regardless of the conditioning $L_{d/100}$ selected to solve (*). We have shown on figure 156 the process computation time to perform a transonic computation on a NACA 0012 at (M_∞ = .8 ; i=0°) by using $L_{d/100}$ for several values of d. We shall bring our attention to the interest of the pointss of the curve in the interval 5%, 25% producing about the same process times as those using high percentages. The optimal control formulation using the standard conjugate gradient as Laplacien algorithm is very costly. The curve stability is kept by working on another numbering of the triangulation $\mathcal{T}_h$.

12.4.1.4. Transonic Optimal Control 2-D With Auxiliary Metric $\tilde{\tilde{L}}L^t$.

When the metric attached to the solution of the transonic operator is perturbed in the sense of (345), N iterations required for a transonic computation may increase if the metric $B = \tilde{\tilde{L}}L^t$ is too weak (percentages too low of d/100 comparing the initial metric H^1 with the metric L^2).

Figure 157 shows for various choices of d/100 the evolution of the error $\tilde{\varepsilon}$, taken in the good standard $\tilde{\varepsilon}^t B \tilde{\varepsilon}$, committed to solve the equation $R(\phi) = 0$ in the functional space H^{-1}, as a function of the control iterations. /256

When the metric $\tilde{L}_{d/100}$ is acceptable in the sense of the convergence, the solutions of (345) prove to be faster and more econical in store than the standard solution.

It may be observed that the Van der Vorst operator used as auxiliary metric to solve an optimal control problem via(345) is inadequate. On the other hand, the metric L_{VV}, composed of very close coefficients and representing in 2-D about 20% of the coefficients of L, appears to be an acceptable auxiliary metric on figure 157.

The quality of the transonic solution as a function of the various auxiliary metrics (various percentages d/100, Van der Vorst after 80 control iterations is represented by shock restoration on the airfoil section, on figure 158. It may be concluded that 15% is the minimum allowable percentage for an auxiliary metric. It still represents a considerable gain in memory for industrial applications.

12.4.1.5. 3-D Transonic Optimal Control With Metric H^1 and Auxiliary Operator $\tilde{L}\tilde{L}^t$. /256

The solution of (344) using the preconditioning $\tilde{L}_{d/100}$ of (*) has been tested on an industrial type air inlet configuration composed of 1.5 10^6 Choleski coefficients and 5328 degrees of freedom, at $M_\infty = .8$.

The curve of figure 159 represents the process time of N=10 control iterations for percentages d/100 of $L_{d/100}$ entirely in the main store. We may note the vertical slope of the curve as soon as $d/100 > 5\%$, , expressed by the constant number of iterations required to solve (*) AS LONG AS $L_{d/100}$ is in THE MAIN CORE. The point obtained with $L_{100/100}$ and an auxiliary disk depend on the working configuration of the computer at the moment the computation is performed. Fluctuating usage times may be obtained for the same calculation at various phases.

12.4.1.6. 3-D Transonic Optimal Control With Auxiliary Metric $\tilde{L}\tilde{L}^t$. /257

The same industrial configuration has been tested by solving (344) via (345). The error evolution for various auxiliary metrics $B_{d/100}$ is shown on figure 160 during the control iterations. It may be seen that $\tilde{B}_{15/100}$ is the minimum metric leading to an allowable error curve compared to reference $\tilde{B}_{100/100}$.

Since the Van der Vorst metric $\tilde{B}_{VDV}$ is too far from the factorized L of the Laplacien, it is poorly suited for the solution of (345) and leads to an insufficient convergence velocity.

It may be concluded, after examining figure 160, that d/100 = 20% is an auxiliary metric making it possible to treat (345) entirely in the main core and to ensure the convergence of the preconditioned algorithm with a sufficient safety margin.

OF THE INCOMPLETE CHOLEVSKY FACTORIZATION

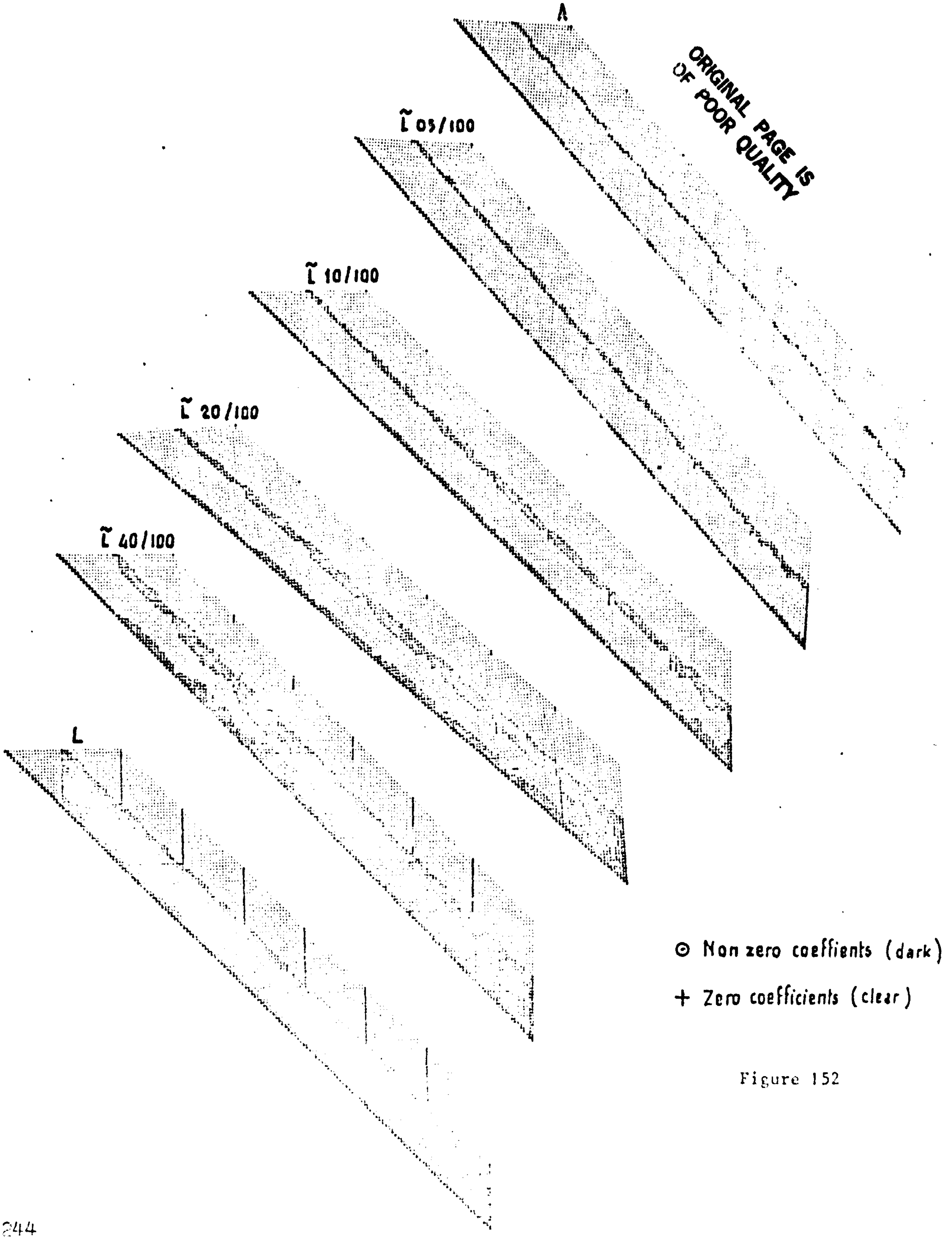

Figure 152

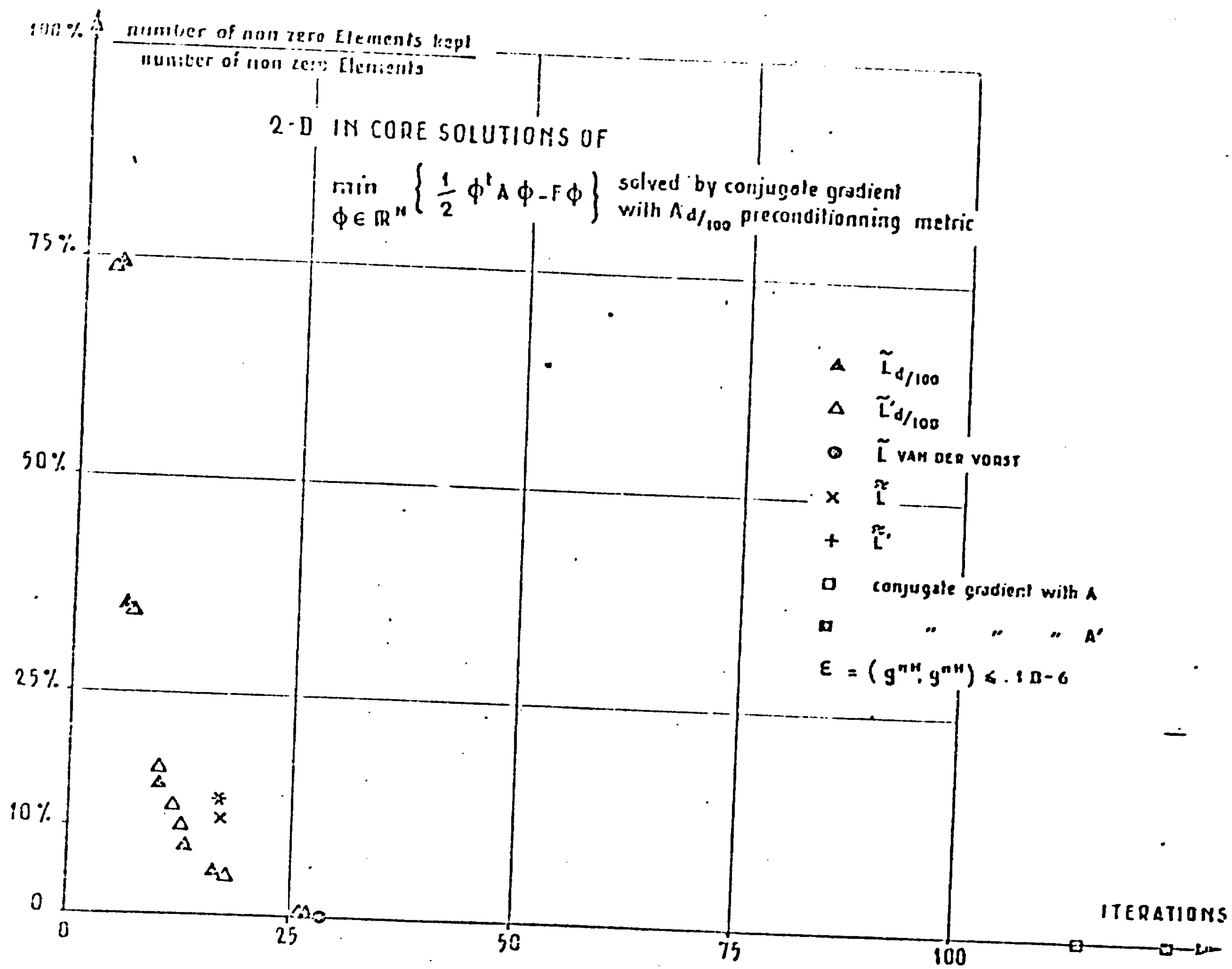

2-D IN CORE SOLUTIONS OF
$\min_{\phi \in \mathbb{R}^N} \left\{ \frac{1}{2} \phi^t A \phi - F\phi \right\}$ solved by conjugate gradient with $A_{d/100}$ preconditionning metric
number of non zero Elements kept / number of non zero Elements
100 %
75 %
50 %
25 %
10 %
0
25
50
75
100
ITERATIONS
$\tilde{L}_{d/100}$
$\tilde{L}'_{d/100}$
$\tilde{L}$ VAN DER VORST
$\tilde{\tilde{L}}$
$\tilde{\tilde{L}}'$
conjugate gradient with A
" " " A'
$\varepsilon = (g^{nH}, g^{nH}) \leq .1\,D-6$

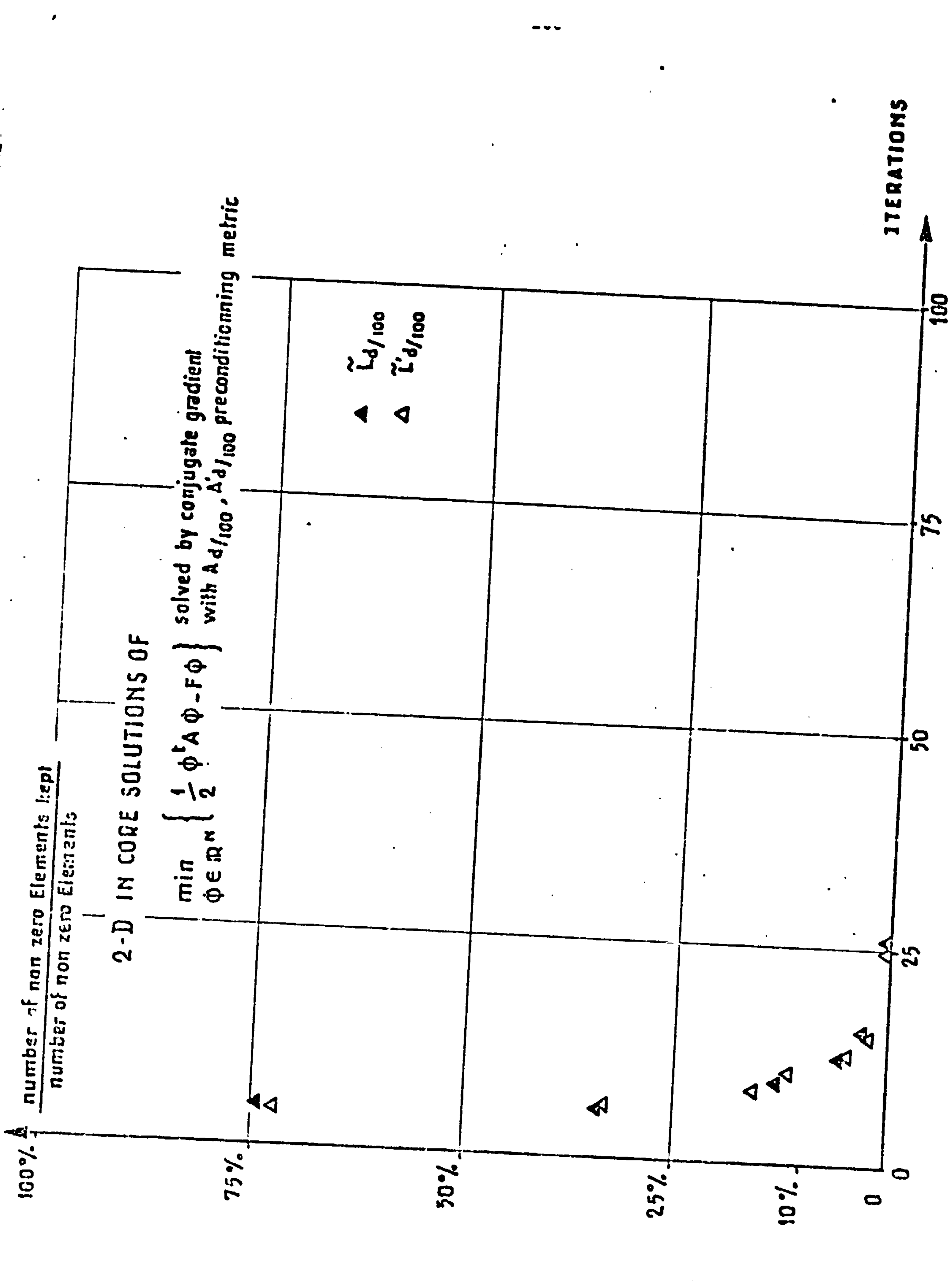

number of non zero Elements kept / number of non zero Elements
100%
75%
50%
25%
10%
0
2-D IN CORE SOLUTIONS OF
$\min_{\phi \in \mathbb{R}^N} \left\{ \frac{1}{2} \phi^t A \phi - F\phi \right\}$ solved by conjugate gradient with $A_{d/100}$, $A'_{d/100}$ preconditioning metric
$\tilde{L}_{d/100}$
$\tilde{L}'_{d/100}$
0
25
50
75
100
ITERATIONS

Figure 154

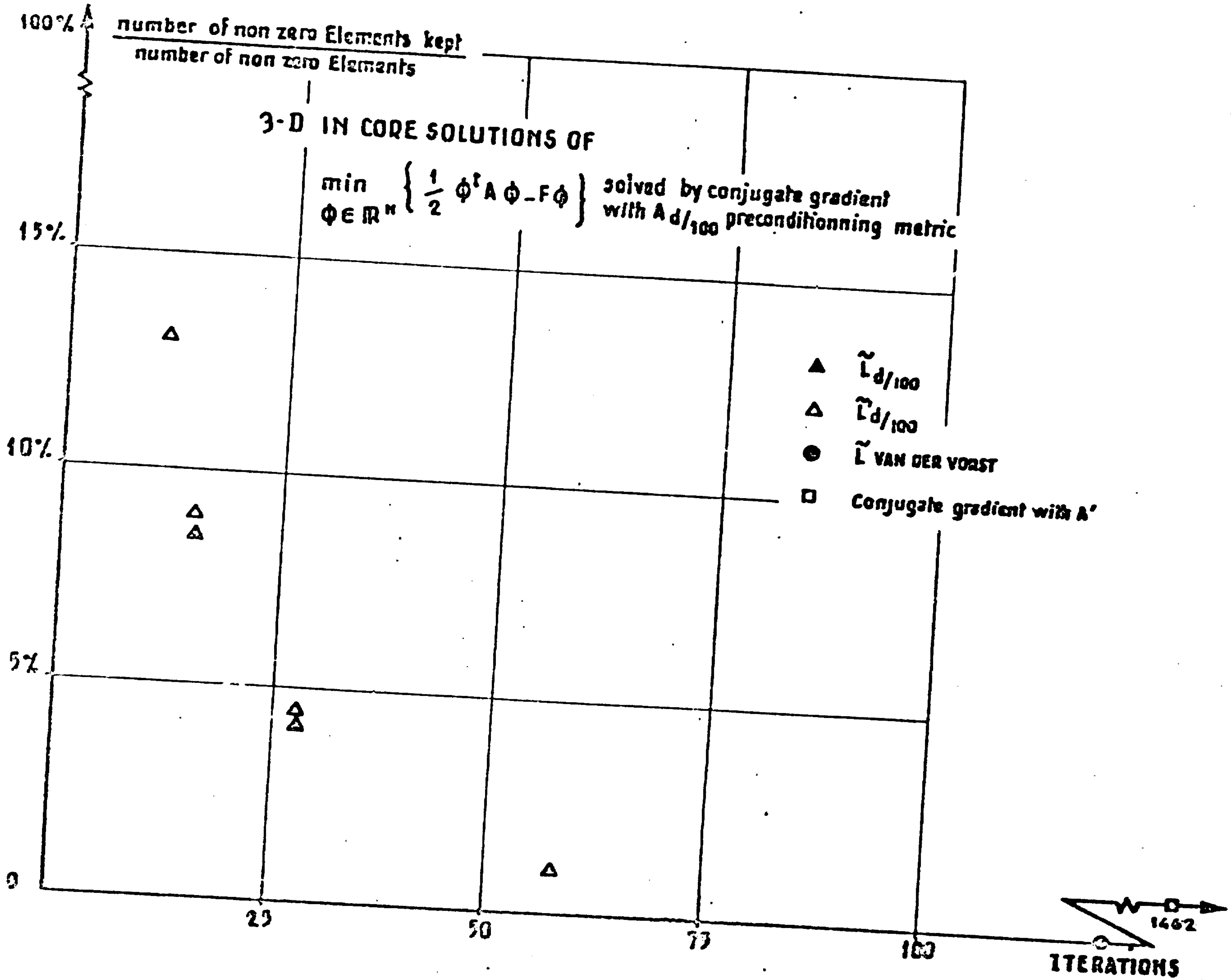
100%
number of non zero Elements kept
number of non zero Elements
3-D IN CORE SOLUTIONS OF
$\min_{\phi \in \mathbb{R}^n} \left\{ \frac{1}{2} \phi^t A \phi - F\phi \right\}$ solved by conjugate gradient with $A_{d/100}$ preconditionning metric
15%
10%
5%
0
25
50
75
100
1462
ITERATIONS
$\tilde{L}_{d/100}$
$\tilde{L}_{d/100}$
$\tilde{L}$ VAN DER VORST
Conjugate gradient with A'

Figure 155

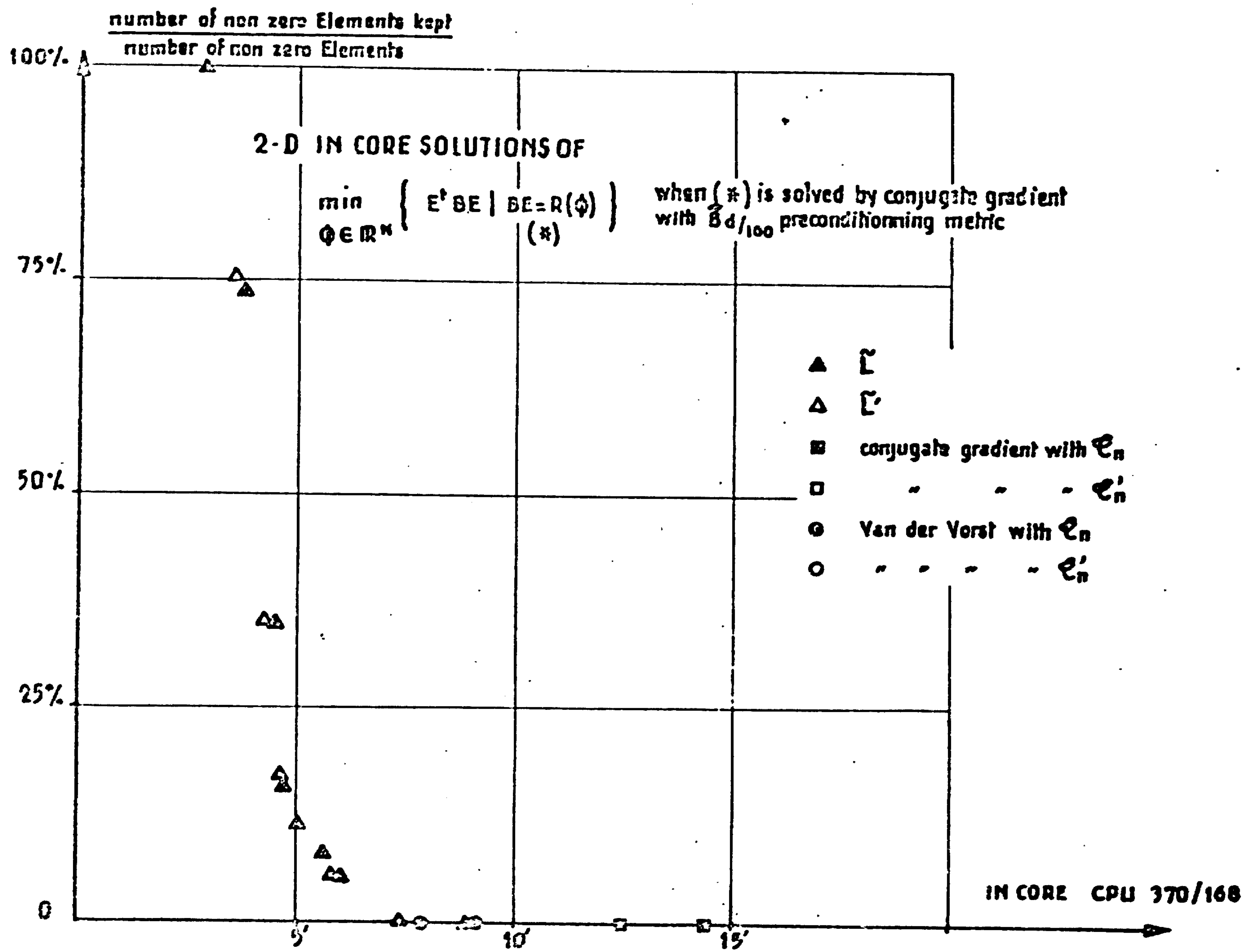
number of non zero Elements kept
number of non zero Elements
100%
75%
50%
25%
0
2-D IN CORE SOLUTIONS OF
min $\Phi \in \mathbb{R}^N$ { $E^t BE$ | $BE = R(\Phi)$ (*) }
when (*) is solved by conjugate gradient with $\tilde{B}_{d/100}$ preconditionning metric
conjugate gradient with $\mathcal{C}_n$
" " " $\mathcal{C}'_n$
Van der Vorst with $\mathcal{C}_n$
" " " " $\mathcal{C}'_n$
IN CORE CPU 370/168
5'
10'
15'

Figure 156

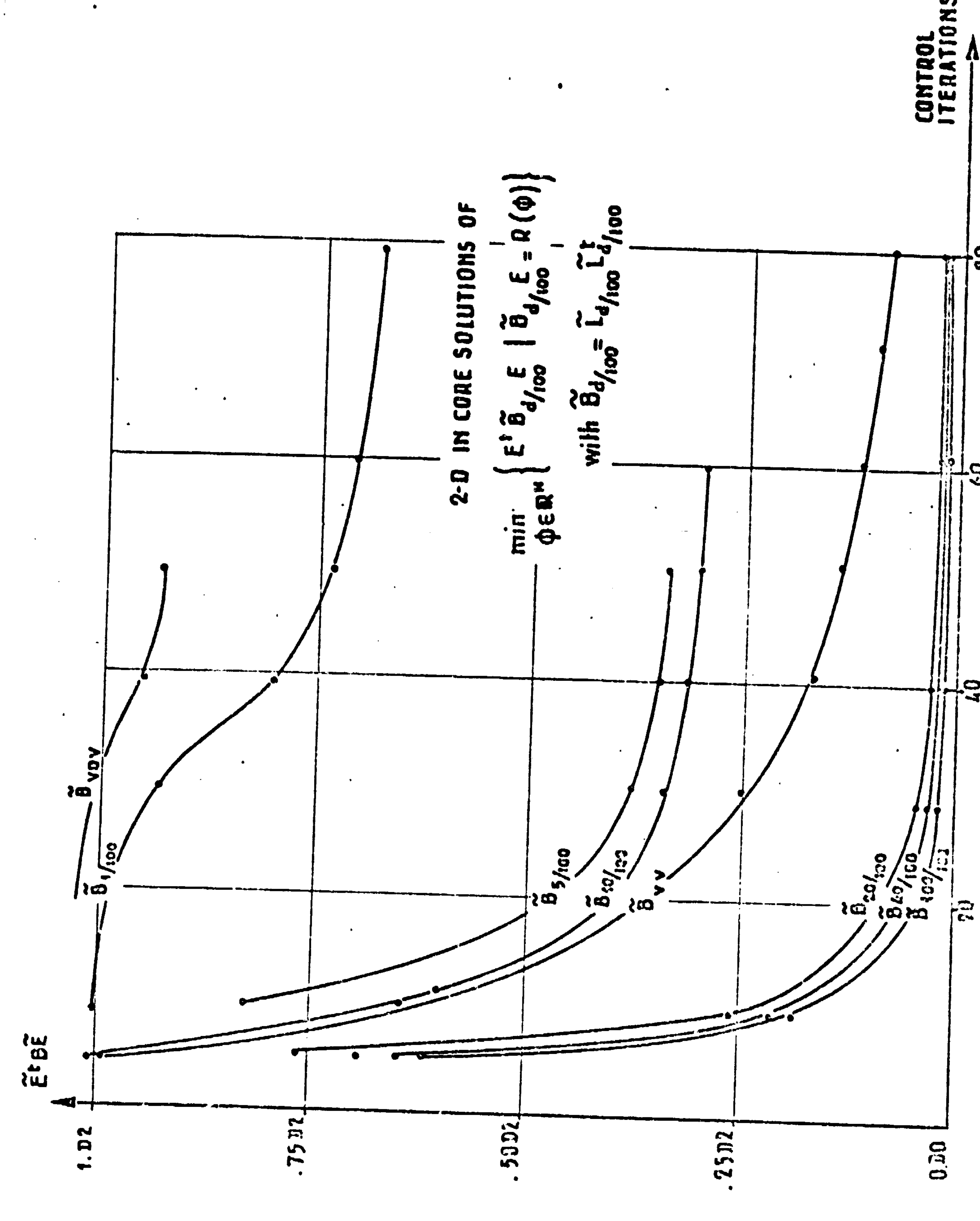
2-D IN CORE SOLUTIONS OF
CONTROL ITERATIONS
1.D2
.75D2
.50D2
.25D2
0.D0
20
40
60
80

Figure 157

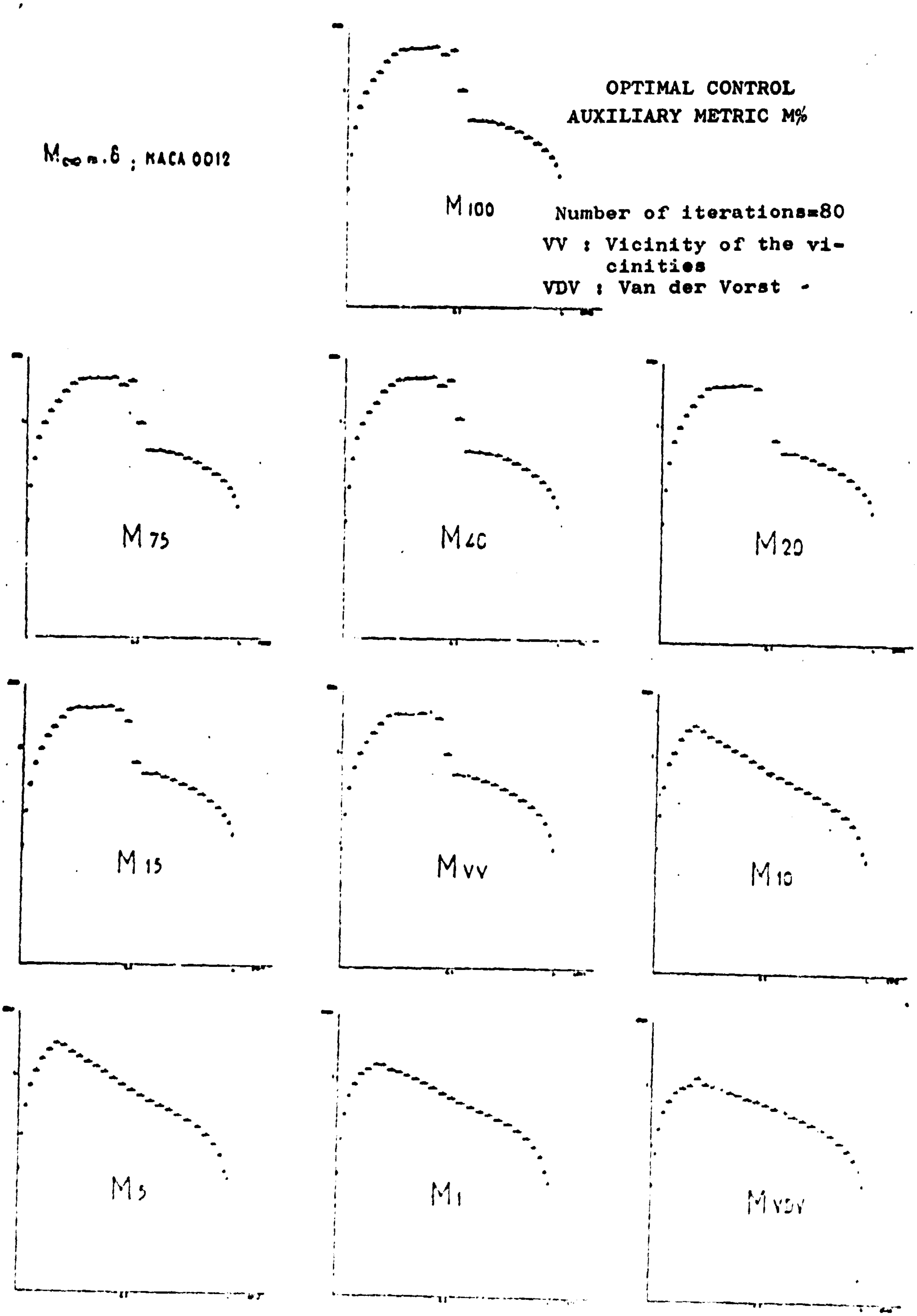
OPTIMAL CONTROL
AUXILIARY METRIC M%
M∞ = .8 ; NACA 0012
M 100
Number of iterations=80
VV : Vicinity of the vicinities
VDV : Van der Vorst
M 75
M 40
M 20
M 15
M VV
M 10
M 5
M 1
M VDV

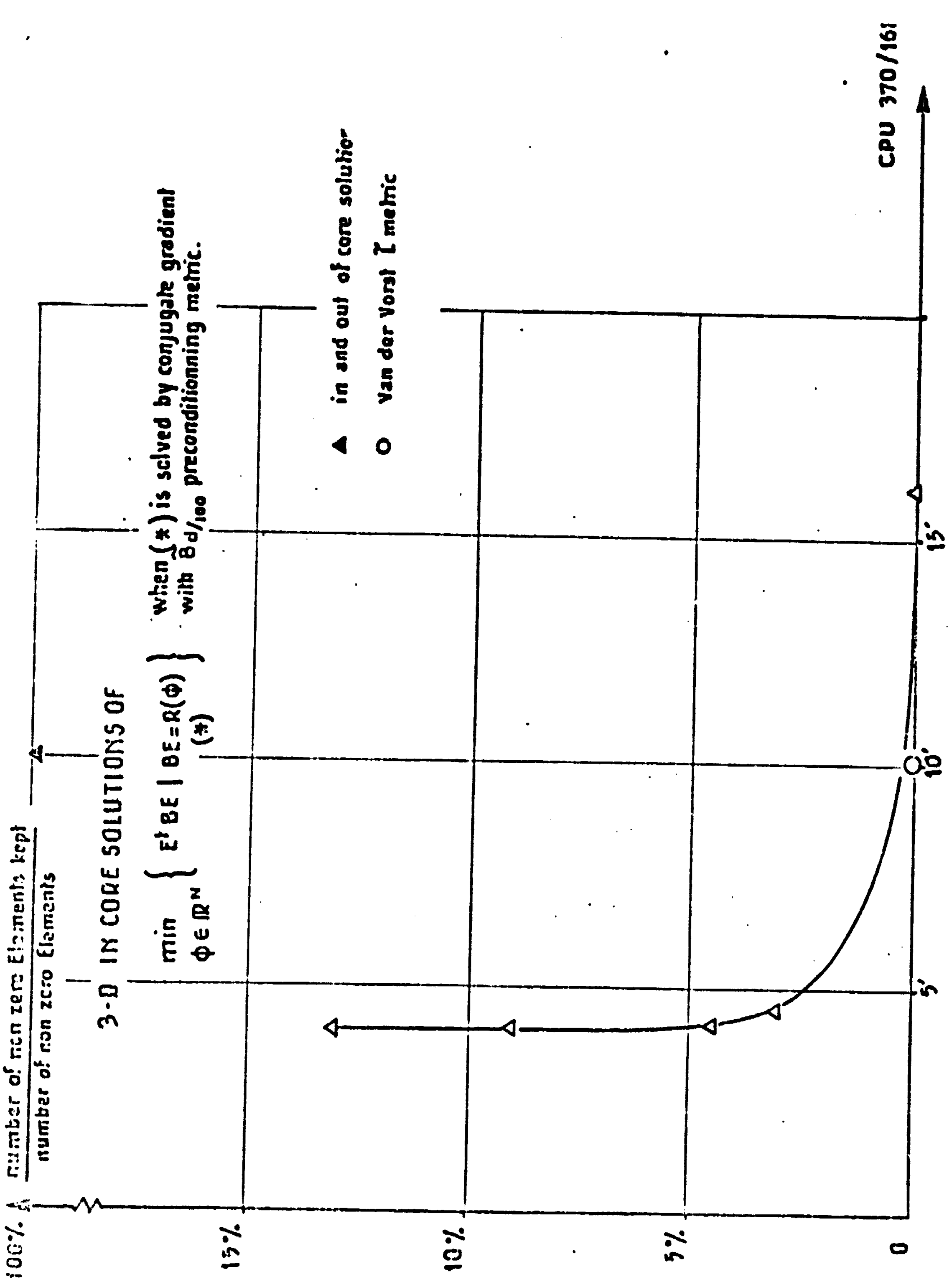

100%
15%
10%
5%
0
number of non zero Elements kept / number of non zero Elements
3-D IN CORE SOLUTIONS OF
$\min_{\phi \in \mathbb{R}^N} \left\{ E^t BE \mid BE = R(\phi) \right\}$ (*)
when (*) is solved by conjugate gradient with $B_{d/100}$ preconditionning metric.
in and out of core solution
Van der Vorst τ metric
5'
10'
15'
CPU 370/161

Figure 159

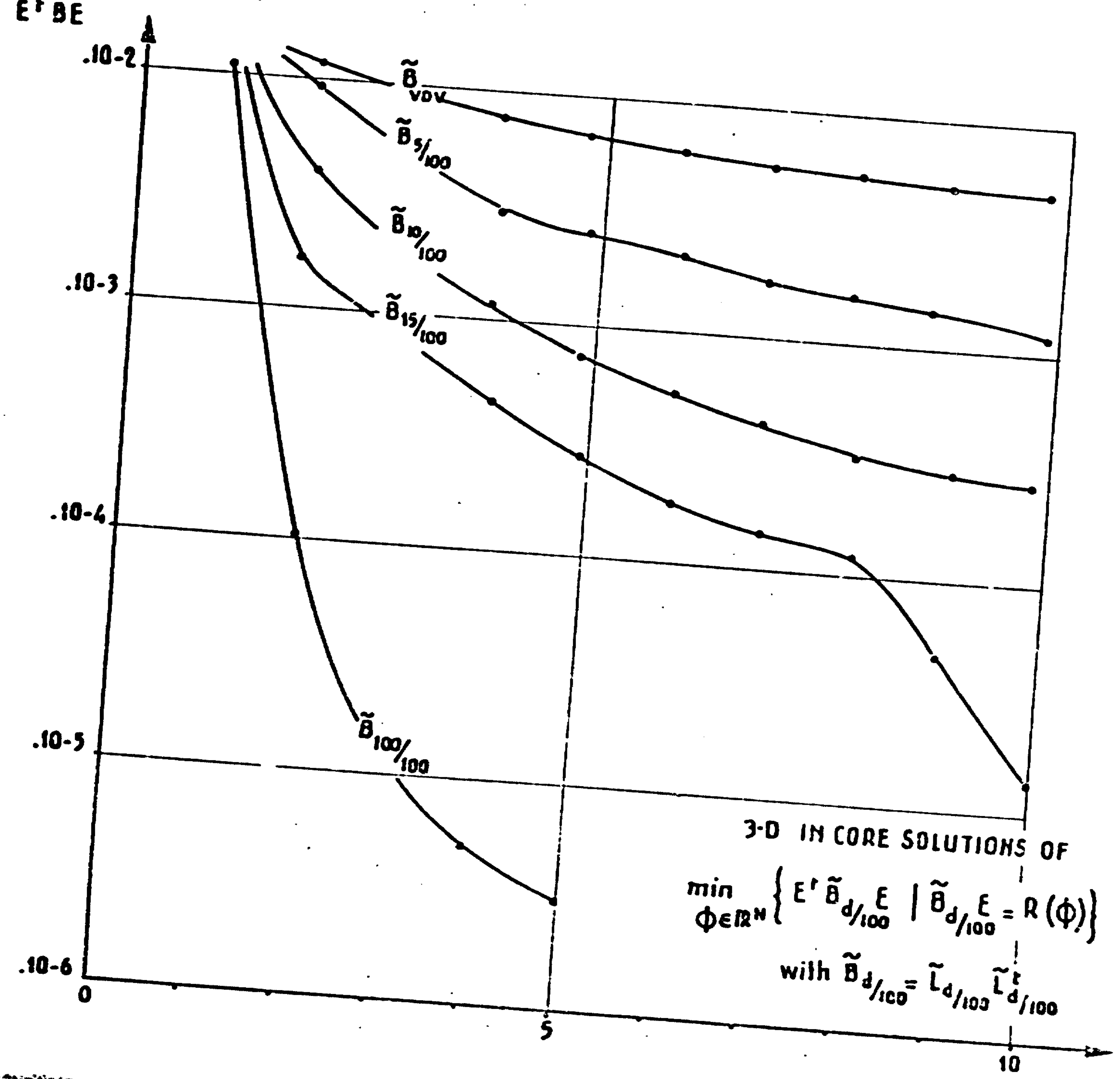

$\tilde{E}^t B \tilde{E}$
.10-2
.10-3
.10-4
.10-5
.10-6
0
5
10
CONTROL ITERATIONS
$\tilde{B}_{VDV}$
$\tilde{B}_{5/100}$
$\tilde{B}_{10/100}$
$\tilde{B}_{15/100}$
$\tilde{B}_{100/100}$
3-D IN CORE SOLUTIONS OF
$\min_{\phi \in \mathbb{R}^N} \left\{ E^t \tilde{B}_{d/100} E \mid \tilde{B}_{d/100} E = R(\phi) \right\}$
with $\tilde{B}_{d/100} = \tilde{L}_{d/100} \tilde{L}^t_{d/100}$

Figure 160

12.4.2. Navier-Stokes Case Around/In an Air Inlet (2-D) and Around A 3-D Wing /267

12.4.2.1. The Stokes Algorithms (T-H) and (G-P)

12.4.2.1.1. Preconditioning of the Laplacien in the Iterative Stokes Algorithm (T-H)

We have introduced in the iterative algorithm of Flow Chart 4 (see Chapter 11), a preconditioning $\tilde{L}\tilde{L}^t$ in the solutions in 2-D and 3-D of the Dlreichlet problems. Figures 161 and 162 show the evolution of calcluation time for solving the Stokes algorithm (T-H) with accuracy $\varepsilon = .10^{-6}$ given on the pressure, for various preconditioning percentages $L_{d/100}$. It may be pointed out that the optimal working zone, hachurated on the figures, the economy $5/100 < d/100 < 20/100$ of memory ($\approx$ 90%) does not penalize at all the computer process time ! The 2-D example (resp. 3-D on the shpere) was initially composed of 9342 (resp.149734) Choleski coefficients on the air inlet for the factorized matrix L. Algorithm 4 does not call for preconditioning on the pressure, since the conditioning L^2 in the Taylor-Hood ap proach is optimal.

12.4.2.1.2. Preconditioning $\tilde{L}\tilde{L}^t$ of the Laplacien and $\tilde{S}\tilde{S}^t$ of the Pressure Trace in the Iterative Stokes Algorithm (G-P)

We have introduced in the iterative algorithm of Flow Chart 5 (see Chapter 11), first, a preconditioning $\tilde{A} = \tilde{L}\tilde{L}^t$ in the solution of Dirichlet problems, second, a preconditioning $\tilde{A} = \tilde{S}\tilde{S}^t$ on the pressure trace, since the conditioning L^2 in the Glowinski-Pironneau approach is not optimal.

Figures 163, 164 show in 2-D and 3-D the eveolution of calculation time for solving the Stokes algorithm (G-P) with accuracy $\varepsilon = .10^{-6}$ given on the pressure trace, for various preconditioning percentages $\tilde{L}_{d/100}$ and $\tilde{S}_{d/100}$. Since matrix A is complete $\tilde{A}_{d/100}$ is obtained by a test, absolute in 2-D, and relative in 3-D, on the amount of coefficients of factorized A.

Figure 163 shows the optimal working zone, hachurated, corresponding to $L_{24/100 < d < 8/100}$ and $\tilde{S}_{34/100}$. It may be observed that the preconditioning L^2 $(\tilde{S}_v)$ is inadequate. Figure 164 shows the fast decline in computation time in 3-D, as soon as percentage of $\tilde{S}$ which is too small, is used.

If a comparison is made of the calculation time of the two approaches (T-H) and (G-P), it comes to light that it is better to work on the pressure trace (factor 3 to 4).

In any case, the numerical tests shown on figures 160 through 163 clearly show that the preconditioning problem of a Dirichlet operator in Ω is perfectly solved, whereas the problem of a trace operator on Γ remains open. /268

2-D TAYLOR-HOOD STOKES ALGORITHM-PRECONDITIONED CONJUGATE GRADIENT + AUXILIARY OPERATOR

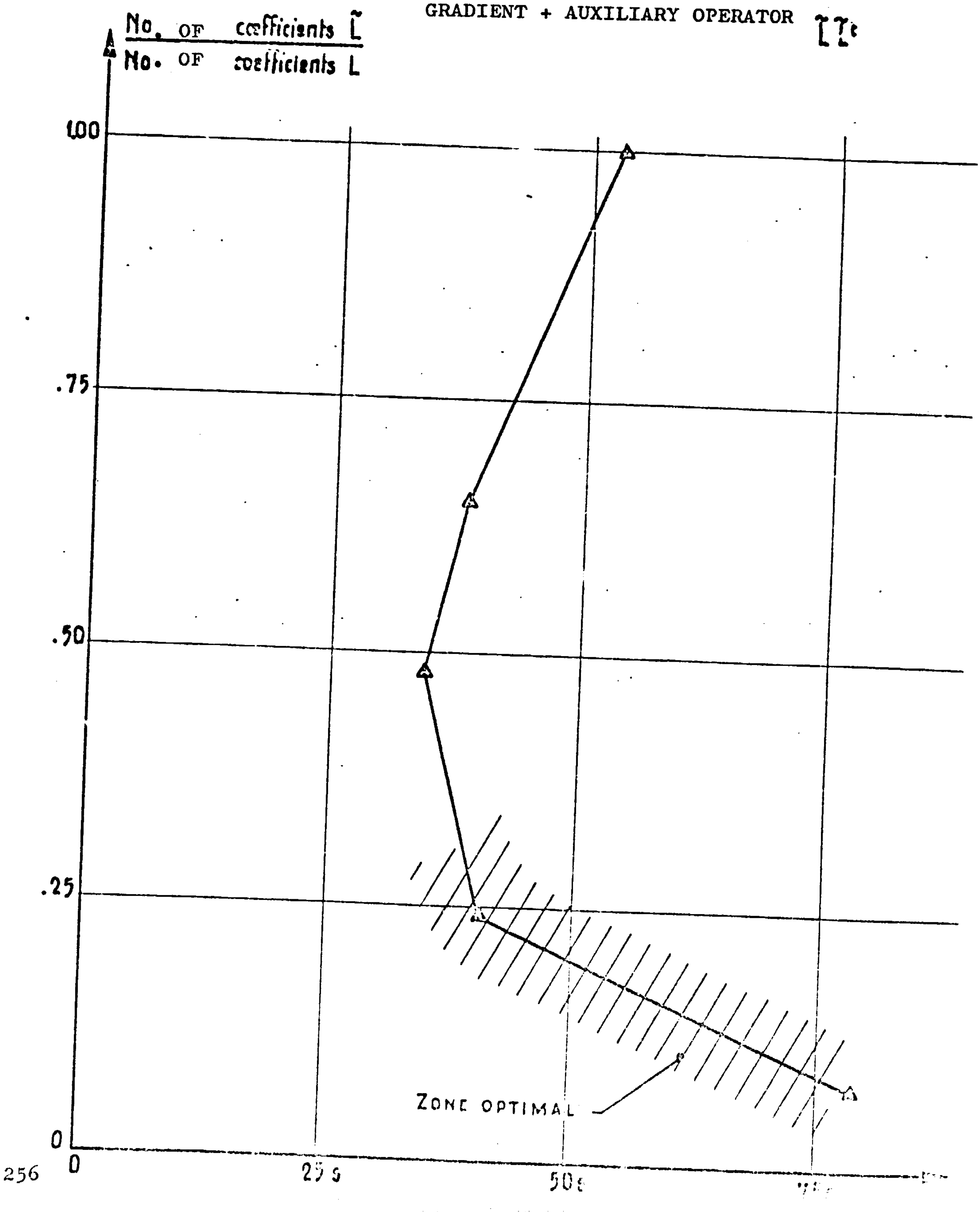

3-D TAYLOR-HOOD STOKES ALGORITHM PRECONDITIONED CONJUGATE GRADIENT + AUXILIARY OPERATOR $\tilde{L}\tilde{L}^t$

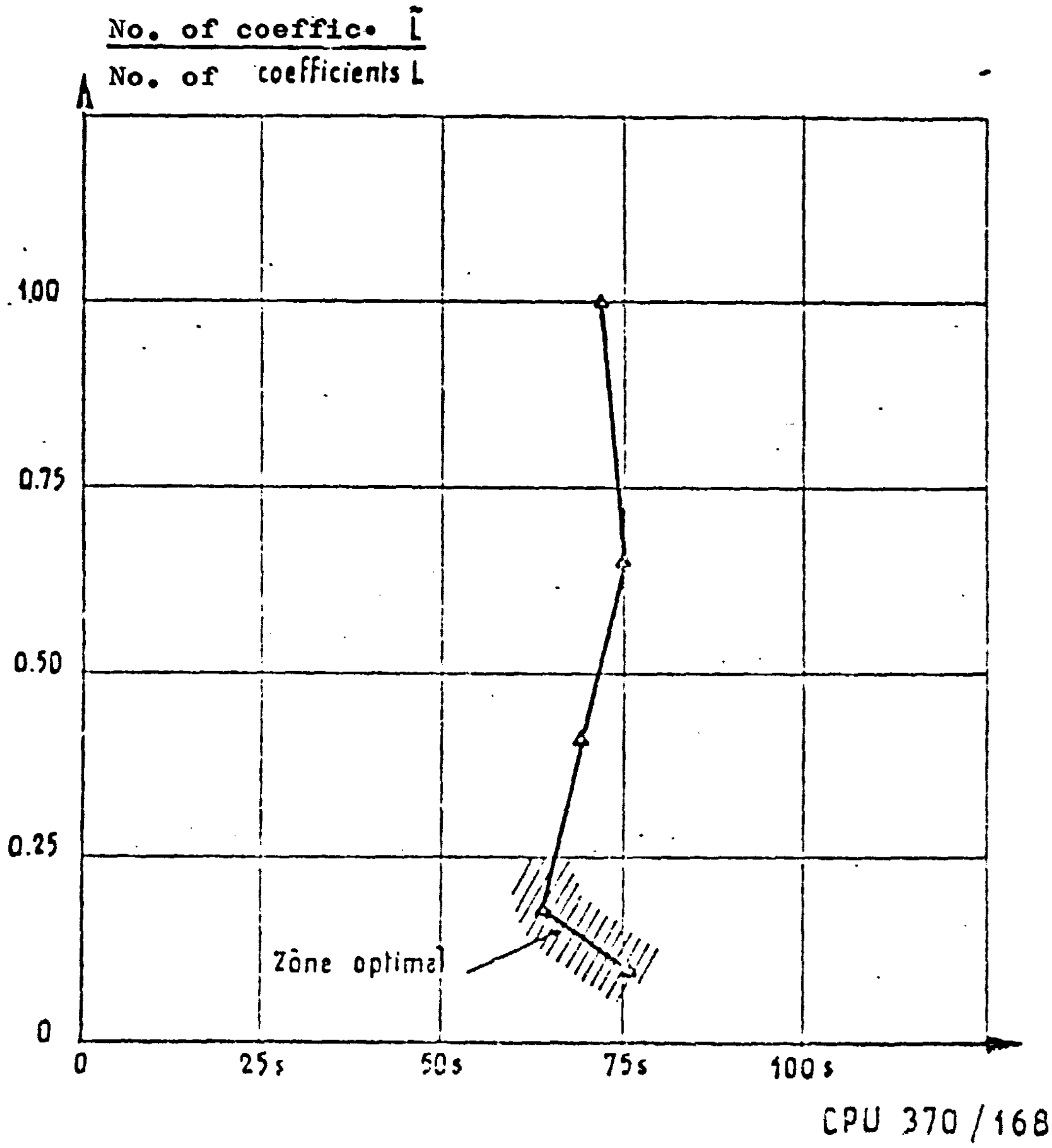

Figure 162

2-D GLOWINSKI-PIRONNEAU (E_h) STOKES ALGORITHM

CONJUGATE GRADIENT + AUXILIARY

OPERATORS $\tilde{L}\tilde{L}^t - \tilde{S}\tilde{S}^t$

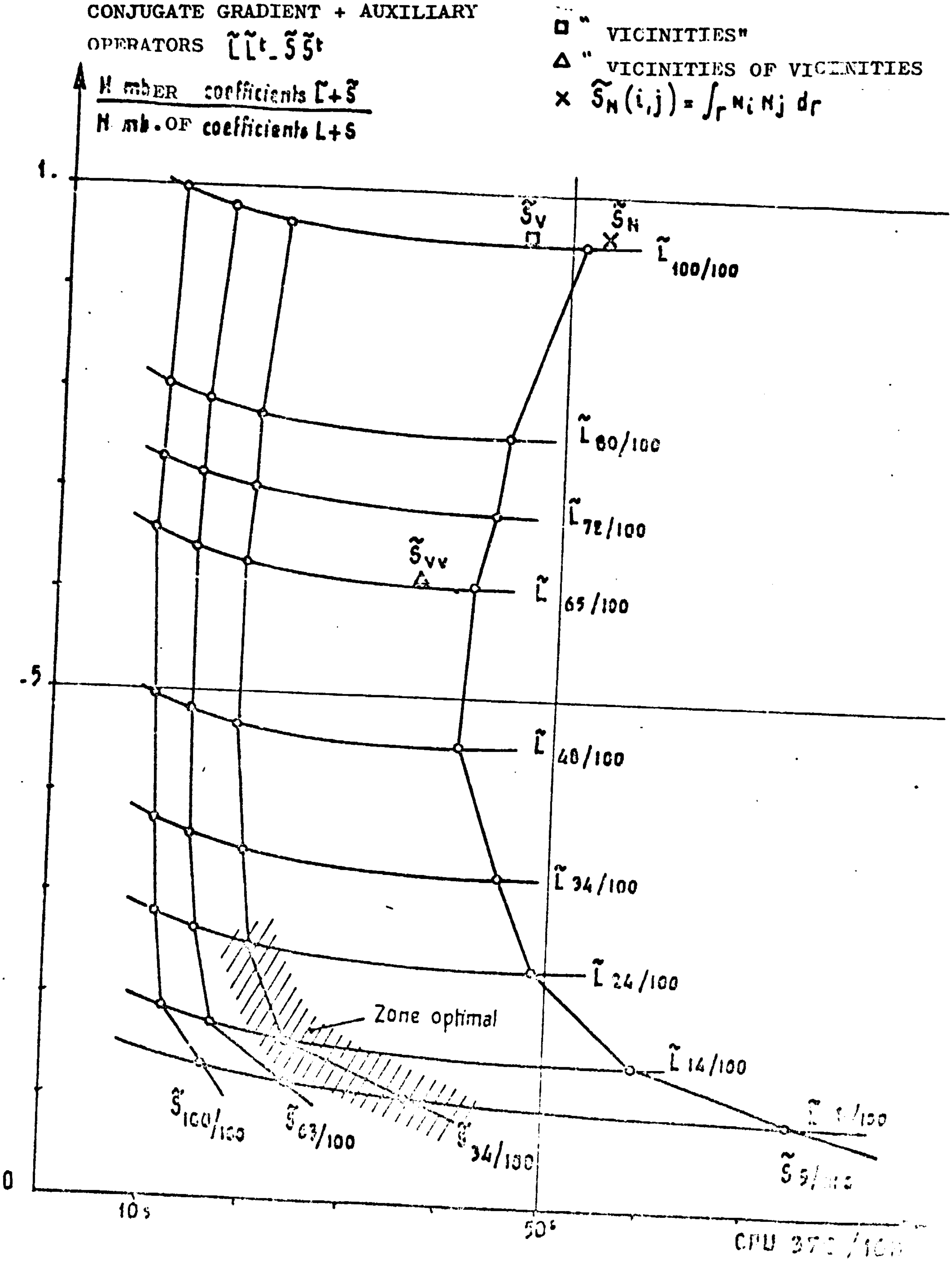

3-D STOKES ALGORITHM GLOWINSKI-PIRONNEAU (E_h)

CONJUGATE GRADIENT + AUXILIEARY OPERATORS

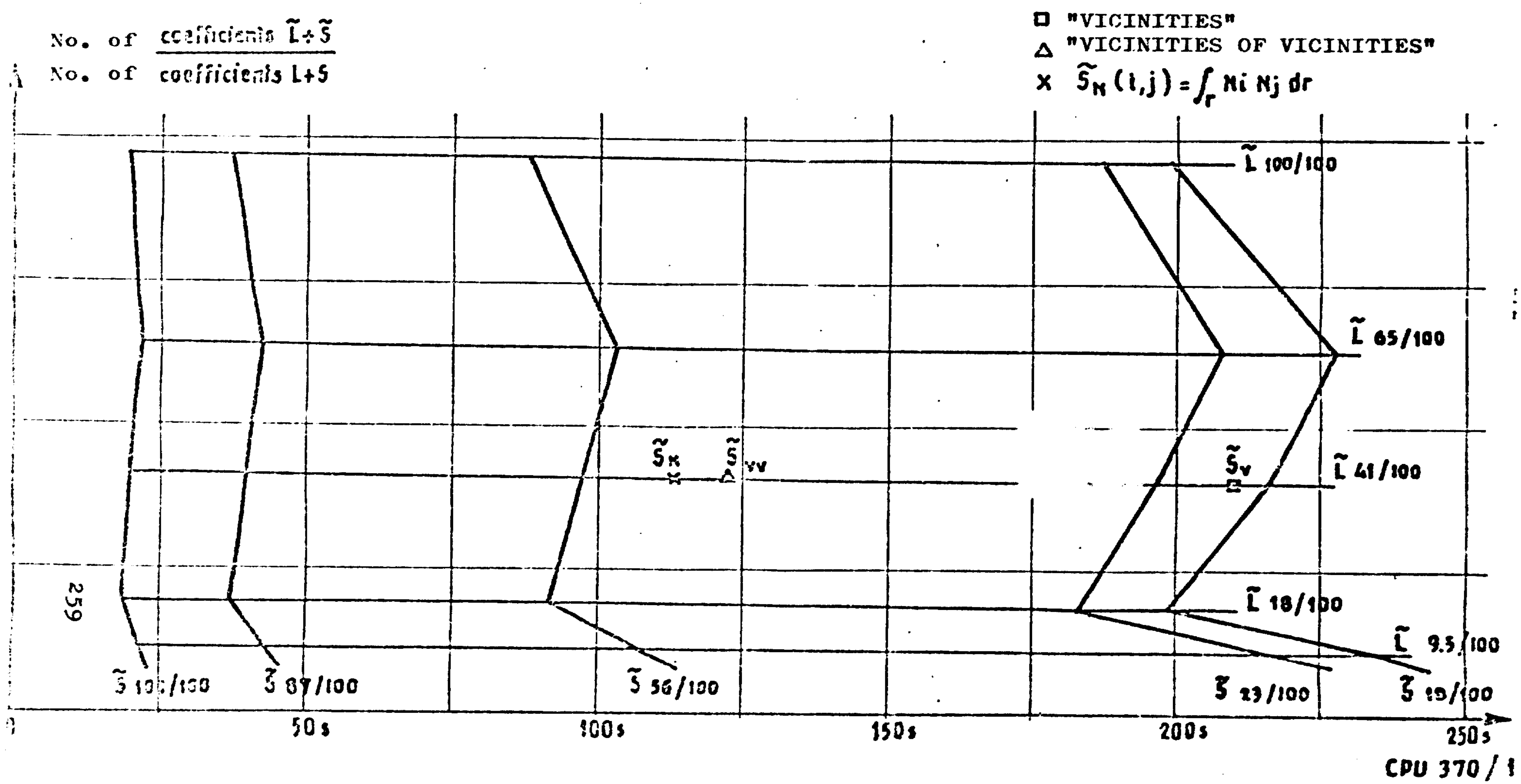

12.4.2.2. Optimal Control (2-D)(3-D) Navier Stokes metric H^1 - Auxiliary Operators $\tilde{L}\tilde{L}^t$, $\tilde{S}\tilde{S}^t$. /273

In industrial applications (2-D) (air-inlet) and 3-D (wing), the informatics memory problms are due to the storage of the Dirichlet operator $(\alpha Id - \nu\Delta)$, on the one hand and of the trace operator $\lambda \to A\lambda = \frac{\partial\phi_\lambda}{\partial n}\Big|_\Gamma$ on the other hand.

An alternative ① ② in order to gain is memory space is proposed for solving the Navier-Stokes equations via Flow Chart 1.

① Apply the direct algorithm of the Stokes algorithm (G-P)(Flow Chart 3) with preconditioning $\tilde{L}\tilde{L}^t$ to solve the sequence of Dirichlet problems. In this case, we must construct upstream of the optimal control loop the trace operator $\lambda \to A\lambda$, symmetrical but complete, with the use of auxiliary operator $\tilde{L}\tilde{L}^t$, then factorize it ($A = SS^t$) and store S (flow chart 2). The importance of S may require auxiliary memories for direct solutions of $E_h : A\lambda = b$ with the auxiliary operator $\tilde{L}_{d/100}$ being completely stored in the main memory.

② Apply the iterative algorithm of the Sotkes algorithm (G-P) (Flow Chart 5) with preconditioning $\tilde{L}\tilde{L}^t$ to solve the sequence of Dirichlet problems. In this case, a preconditioning $\tilde{S}\tilde{S}^t$ of the trace A operator is necessary in order for the time required for solving, compared with the direct method, is still competitive. Nevertheless, making the choice remains delicate! Two auxiliary trace operators $\tilde{S}$ are suggested.

2.1. We use $\tilde{S}_N(\lambda) = \int_{i \in \Gamma} \lambda\, N_i \cdot d\Gamma$, conditioning L^2, restricted to the boundary node supports of figure 24. With this choice, operator A is never constructed. It may be observed that $\tilde{S}_N$ is sparse, its memorization presents no problem.

2.2. We use a percentage $\tilde{S}_{d/100}$ of the complete matrix $A = SS^t$ after constructing the latter upstream. For various percentages d/100 relating to the relative value of coefficients (S_{ij}) $(j > i)$, we obtain conditioning operators $S_{d/100}$ of which the efficiency is measured a posteriori by the convergence velocity.

The use of auxiliary operators $\tilde{L}\tilde{L}^t$ and $\tilde{S}\tilde{S}^t$ in a Navier-Stokes algorithm is presented on figures 165 (2-D) and 166 (3-D). We have set in a[illegible]ssa the process time for treating tho Navier-Stokes completely i[illegible] the main memory in 10 iterations with a small Reynolds number (Re = 50) a[illegible] a function of percentages d/100 and d'/100 of operators $\tilde{L}$ and $\tilde{S}$. Attention may be brought to the fast increase in calculation time for percentages d'/100 of $\tilde{S}$ which are insufficient ($d' \leq 50$). On the other hand, for a given S, the interest of operators $L_{d/100}$ $(5 \leq d \leq 20)$ may be pointed out, as they have very little effect on the process time, while representing a gain in memory space of about 90%! /274

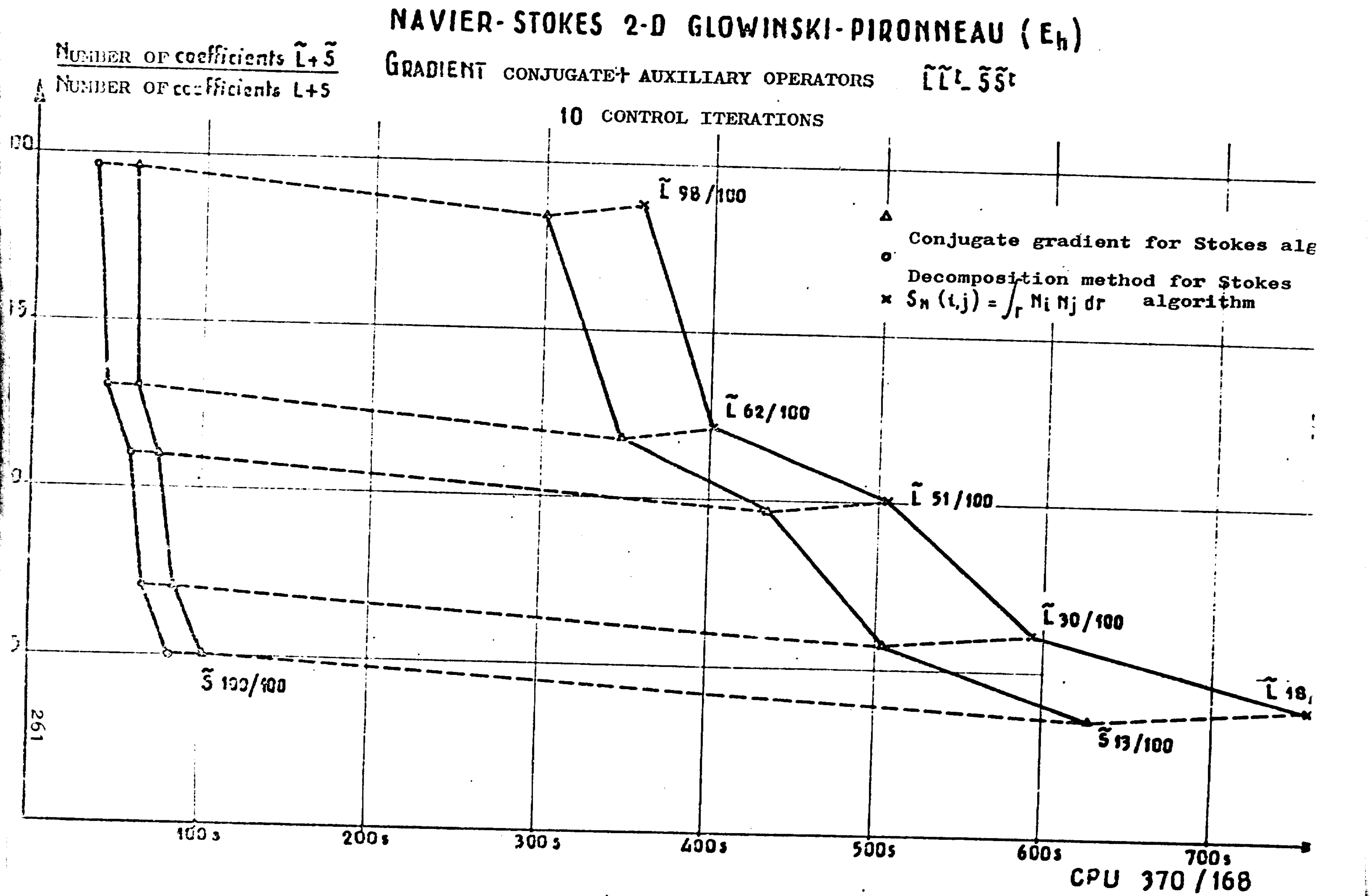
NAVIER-STOKES 2-D GLOWINSKI-PIRONNEAU (E_h)
GRADIENT CONJUGATE + AUXILIARY OPERATORS $\tilde{L}\tilde{L}^t - \tilde{S}\tilde{S}^t$
10 CONTROL ITERATIONS
NUMBER OF coefficients $\tilde{L}+\tilde{S}$
NUMBER OF coefficients L+S
$\tilde{L}$ 98/100
$\tilde{L}$ 62/100
$\tilde{L}$ 51/100
$\tilde{L}$ 30/100
$\tilde{L}$ 18
$\tilde{S}$ 100/100
$\tilde{S}$ 13/100
Conjugate gradient for Stokes alg
Decomposition method for Stokes algorithm
$S_H(i,j) = \int_\Gamma N_i N_j \, d\Gamma$
100s
200s
300s
400s
500s
600s
700s
CPU 370/168

NAVIER-STOKES 3D (GLOWINSKI-PIRONNEAU)

GRADIENT CONJUGATE + AUXILIARY OPERATORS $\tilde{L}\tilde{L}^t$

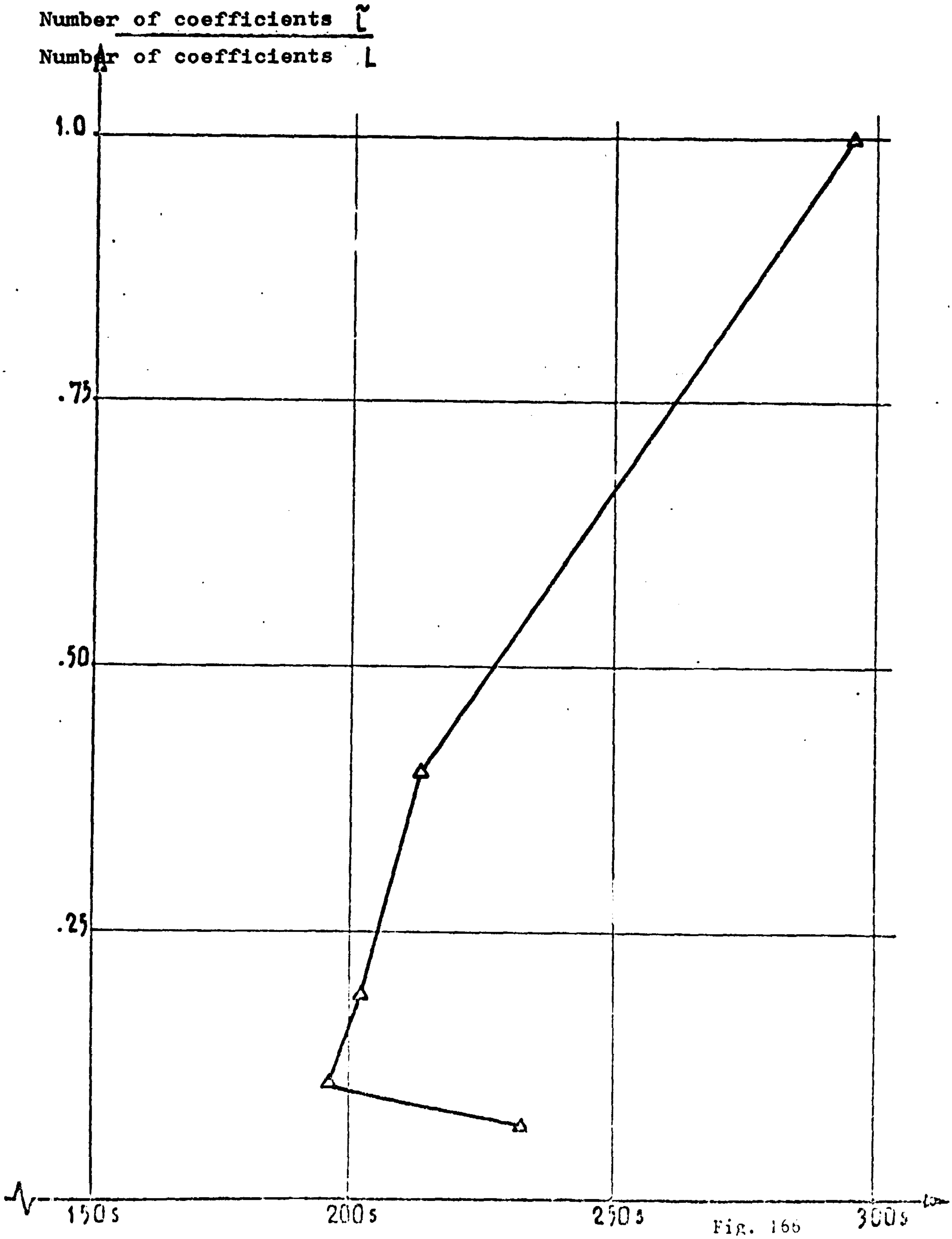

Fig. 166

CONCLUSION

The quality of the numerical results of this study confirm that /277 the functional least squares methods coupled with preconditioned conjugate gradient algorithms proves to be a tool which is particularly suited for multiple industrial configurations. The possibility of treating correctly the boundary conditions of any complex geometry by a finite elements method, gives to the codes obtained from the method presented, a flexibility which is indispensable to the three dimensional aerodynamics of today and of the future (optimum design).

In the case of transonic flows, it appears that Lagrange P_1 approximation by conform finite elements (resp. mixed) of the related optimal control problem, including the condition of entropy treated by penalty (resp. artificial viscosity), is of sufficient accuracy, after comparison with results derived from the A. JAMESON finite differences codes.

With respect ot the incompressible viscous fluid flows, the complexity of the Navier-Stokes equations suggests the use of quantification schemes of lower order, P_1 for velocity and P_1 for pressure. The convergence, however, is ensured only if the triangulation of the domain used for the velocity is twice as fine as the one required for the pressure.

In the two flow families considered, the approximation by mixed finite elements (artificial viscosity in idealized fluid, Stokes algorithm in viscous fluid), as presented in P.G. CIARLET-P.A. RAVIART (54), R. GLOWINSKI (55), GLOWINSKI-LIONS-TREMOLIERES (56) and J.M. THOMAS (57) for the biharmonic problem and more recently in FORTIN-THOMASSET (48) by the Navier-Stokes equations, remains a very important point.

Sophisticated codes, obtained from the optimal control-Stokes algorithm combination, and the convergence of which is ensured by the absolutely stable CRANK-NICHOLSON implicit schemes, while being perhaps more costly in machine time and memory usage, are easier to use in industry (no convergence parameters to set !) than the traditional codes requiring domains of reduced stability.

The numerical simulation of three dimensional separated large structures, the dimension and location of which play a fundamental role in aerodynamics with large incidence (interaction of eddies emitted by several bodies, life-time of eddies in the air inlets) is a demonstration of feasibility of the optimal control tool, which is indispensable in the subsequent phase of combining Navier Stokes with turbulence models. In any case, calculations with a large Reynolds number is still prohibitive, if not impossible, with the size of computers currently available (sequential organization of computations), the memory capacity of which proves quickly to be inadequate for associated quantification (10^6 calculation points for 3-D applications is not an excessive number !).

The <u>incomplete</u> factorization methods presented in the <u>nonlinear</u> context (solution of the Dirichlet problem several hundreds of times) brings a gain in memory space of the order of a factor 10. Introduced in the conjugate gradient algorithms coupled with optimal control <u>in the form of auxiliary operators</u> (preconditioning - $\tilde{L}\tilde{L}^t$ of the Dirichlet problem $LL^t\phi = F$) or <u>auxiliary metrics</u> (minimization in $\tilde{H}^{-1}$ of $F(\phi) = 0$), they make it possible to solve entirely in the main memory 3-D configurations taken from the two flow families, and this is accomplished in <u>acceptable</u> machine times. /278

They represent, however, only an intermediary stage, if compared with the possibilities of parallel calculators of tomorrow.

REFERENCES

1. Germain, P., Mechanics of continuous mediums, Masson, 1962.

2. Landau L., Lifchitz E., Fluid Mechanics, Editions Mir, Moscow.

3. Murman E.M., Cole J.D., Calculation of plane steady transonic flows, AIAA Journal, Vol. 9, (1971), pp. 114-121.

4. Bauer F., Garabedian P., Korn D., Supercritical wing sections, Lecture Notes in Economics and Math. Systems, Vol. 66, Springer-Verlag, 1972.

5. Jameson A., Transonic flow calculations, V.K.I. Lecture Series : Computational Fluid Dynamics, Von Karman Institute for Fluid Dynamics, Rhode-St-Genèse, Belgium, March 15-19, 1976.

6. Bristeau M.O., Application of Optimal Control theory to transonic flow computations by finite element methods, in Proceedings of the Third IRIA Symposium on Computing Methods in Applied Sciences and Engineering, Versailles, France, December 5-9, 1977.

7. Gelder D., Solution of the compressible flow equation, Int. J. Num Num. Meth. Eng., Vol. 3, (1971), pp. 35-43.

8. Norries D.H., de Vries G., The finite element method - Fundamentals and Applications, Academic Press, New-York, 1973.

9. Periaux J., 3-D Analysis of Compressible potential flows with the finite element method, Int. J. Num. Meth. Eng., Vol. 9, (1975), pp. 775-831.

10. Vainberg M.M., Variational methods for the study of non linear operators Holden-Day, Inc. San Francisco, London, Amsterdam, 1964.

11. Polak E., Computational methods in optimization, Academic Press, New York, 1971.

12. Yoshihara H., A survey of Computational Methods for Two and Three-dimensional Transonic Flows with Shocks, Advances in Numerical Fluid Dynamics, AGARD LS64, VKI, Rhode-St-Genèse, 1973.

13. ESSERS J.A., Essers J.A., Fast unsteady techniques for the numerical simulation of permanent flows in all states, Publications de la Faculté des Sciences Appliquées de l'Université de Liège (No. 73), 1978.

14. Fortin M., Numerical calculation of Bingham fluid flows and Newtonian incompressible fluid flows by the finite elements method, Thesis, 1972.

15. Lions J.L., Optimal control of systems governed by equations with partial derivatives, Dunod, Paris, 1968.

16. Lions J.L., Magenes E., Problems with non homogenous boundaries, Vol. 1, Dunod, Paris, 1968.

17. Necas J., Theoretical direct methods of elliptical equations, Moscou, Paris, 1967.

18. Glowinski R., Pironneau O., Approximation by finite elements method of the Stokes problem in velocity-pressure formulation. Convergence and resolution of solutions approached, C.R.A.S. Paris, T.286A, (1978),pp.181-183, 225-228.

19. Laboria/Iria, Application of optimal control for the numerical solution of Navier-Stokes equations, Part 1 and 2, DRET Contract 77/213.

20. Bristeau M.O., Application of a finite element method to transonic flow problems using an optimal control approach, V.K.I. Lecture Series : Computational fluid dynamics, Von Karman Institute for Fluid Dynamics, Rhode-St-Genèse, Belgium, March 1978.

21. Glowinski R., Pironneau O., On the computation of transonic flows, in Proceedings of the 1st Frano-Japanese Colloquium of Functional Analysis and Numerical Analysis, Tokyo, Kyoto, September 1976.

22. Laplace A., Study, correction and development of a system to handle formally mathematical notations.(FORMAC), Convention D.R.M.E. 75/338.

23. Martin E.D., A split-recouples-semi direct computational technique applied to transonic flow over lifting airfoils, Paper 78-11, Proceedings of AIAA 16th Aerospace Sciences Meeting, Huntsville, Alabama, Jan. 16-18, 1978.

24. Zienkiewicz O.C., The Finite Element Method In Engineering Sciences, McGraw Hill, 1978.

25. Taylor C. - Hood P., A numerical solution of the Navier Stokes equations using the finite element technique, Comp. and Fluids, 1, 73-100 (1973).

26. Le Tallec P., Numerical Simulation of Incompressible Viscous Flows by the Mixed Finite Elements Methods, Doctorate Thesis, University of Paris VI, 1978.

27. Glowinski R.-Pironneau O., On a mixed finite approximation of the Stokes problem (I). Convergence of the approximate solution, Numerische Mathematik, 1979.

28. Glowinski R.-Pironneau O., On a mixed finite element approximation of the Stokes problem (II). Solution of the approximate problem (to appear).

29. Glowinski R; -Pironneau O., Numerical methods for the first biharmonic equation and for the two-dimensional Stokes problem, SIAM Review and Stanford Report STAN-CS-77-615, May 1977.

30. Meijerink J.A. Van Der Vorst H.A., An iterative solutionnmethod for linear systems of which the coefficient matrix is a symmetric matrix, Math. of Comp., 31, (1977), pp. 148-162.

31. Varga R., Matrix Iterative Analysis, Prentice-Hall, Englewood Cliffs, pp. 123-138.

32. Axelsson O., A class of iterative methods for finite element equations, Comp. Meth. Applied Mech. Eng., 9, (1976), 2, pp. 123-138.

33. Manteufel, The shifted Incomplete Cholesky Factorization, SAND 78-8226, May 1978, Sandia Laboratories, Livermore, Calif. 94550.

34. Kershaw D.S., The incomplete Cholesky-Conjugate Gradient Method for the iterative solution of systems of linear equations, J. of Comp. Physics, 26, (1978), pp. 43-65.

35. Perronnet A. The Club Modulef - A library of subroutines for finite element analysis, in Proceedings of the Third IRIA Symposium on Computing Methods in Applied Sciences and Engineering, Versailles, France, December 5-9, 1977.

36. Cuthill E.H., McKee J.M., Reducing the bandwidth of sparse symmetric matrices, in Sparse matrices and their applications, D.J. Rose and R.A. Willoughby Ed., Plenum Press, New-York, 1972, pp. 157-160.

37. Laboria/Iria GB4P, Application of optimal control and finite element methods to the calculation of transonic flows and incompressible viscous flows, Rapport de recherche No. 294.

38. Bristeau M.O., Glowinski R., Perrier P., Periaux J., Pironneau O. Poirier G., Contract Report DRME 77/011, Calculation of transonic flows by optimal control.

39. Winslow A.M Equipotential zoning for two dimensional meshes, University of California U.C.R.L. (1964).

40. Beranger P., Fil A., P1/P2 interpolation techniques in transonic finite elements, AMD/BA, rapport interne, June 1978.

41. Powell M.J.D., Restart procedure for the conjugate gradient method, Mathematical Programming, 12, (1977), pp. 241-254.

42. Marrocco A., Interlib, INF-LAB 7817, Ed. O. Pironneau

43. Glowinski R., Mantel B., Periaux J., Pironneau O., H^{-1} least squares method for the Navier-Stokes equations, Numerical methods in Laminar and turbulent flows, Swansea 17-21 July, 1978.

44. AMD/BA, Air inlets at large incidences, Part 1, DRET Contract 77/401.

45. Bercovier M., Pironneau O., Error estimates for the solution of Stokes problem in Conform finite elements of Lagrange, C.R.A.S. Paris, T. 285 A, 1085-1087 (1977).

46. Mantel B., Heber-Suffrin, Study of the convergence of schemes P1/P1 iso P2 by the Stokes algorithm, Internal Report AMD/BA DGT September 1977.

47. Hutton A.G., A general F.E.M. for vorticity and stream function applied to a laminar, separated flow. Central Electricity Generating Board. Research D partment, Berkeley Nuclear Laboratories, August 1975.

48. Fortin M., Thomasset F., Mixed finite element methods for incompressible flow problem, J. of Comp. Physics, Vol. 31, No. 1, April 1979.

49. Glowinski R., Pironneau O., On numerical methods for the Stokes problem, Chapter 13 of Energy Methods in Finite Element Analysis R. Glowinski, E.Y. Rodin, O.C. Zienkiewicz Eds., Wiley and Sons, London, 1979.

50. Werle H., Unsteady separation in a two dimensional air inlet, RT 62/2149 AN, Dec. 1976.

51. Marroccoo A., 3-D integration of vorticity tube lines, Restricted Memorandum.

52. Naves J.G. Problems arising for the application of the finite elements methods, AAF, 12ème colloque d'Aérodynamique appliquée, Poitier, 1975.

53. Dinh Q.V., Mantel B., Periaux J., Comparative study of the Stokes algorithm (TH Elements, GP Elements) by preconditioned conjugate gradient methods, AMD/BA, Restricted Memorandum, June 1979.

54. Ciarlet P.G., Raviart P.A., A mixed finite element method for the biharmonic equation in Mathematical aspects of finite elements in partial differential equations. C. de Boor Ed., Acad. Press. 1974 pp. 124-145.

55. Glowinski R., External approximation by finite elements of order one and two of the Dirichlet problem for . In Topics in Numerical Analysis, J.J.F. Miller Ed., Acad. Press, 1973, pp. 123-171.

56. Glowinski R., Lions J.L., Tremolieres R., Numerical Analysis of variational inequations, Dunod, 1976.

57. Thomas J.M., On the Numerical Analysis of hybrid finite elements methods, Thesis, University of Paris VI, 1977.